




京都大学化学研究所 国際共同利用・共同研究拠点

化学関連分野の深化・連携を基軸とする
先端・学際グローバル研究拠点

令和元年度
成果報告書

京都大学化学研究所 国際共同利用・共同研究拠点

化学関連分野の深化・連携を基軸とする
先端・学際グローバル研究拠点



令和元年度
成果報告書

まえがき

京都大学化学研究所は、平成22年度から「化学関連分野の深化・連携を基軸とする先端・学際研究拠点」（平成28年度から第二期）として国内外の共同利用・共同研究を推し進め、それを新たな糧としてより多様でグローバルな化学研究の展開と若手研究者の育成・輩出を図って参りました。特に本拠点では、化学関連コミュニティの研究者の皆様からの要請を踏まえながら、化学研究所の研究分野の広がりと深さに加えて、これまでの様々な連携実績を活かし、国内外の研究機関の相互協力を担保するハブ環境も提供しています。先端・学際的分野深耕にあたっては、関連コミュニティの研究者の皆様と化学研究所の教員が推進する分野選択型、課題提案型、施設・機器利用型、連携・融合促進型等の多彩な共同研究と、拠点として主催・共催する各種国際会議、シンポジウム、研究会等を通じて、多様性と先進性を担保し、さらに、国際的視点に基づいて次代の化学関連分野を担う若手研究者の育成にも注力しています。また、拠点運営では、所外、学外の関連分野有識者と化学研究所の教員を委員とする共同研究委員会および運営評議会を核として、共同研究課題の公募・採択などを戦略的に遂行しております。

このようなグローバルな拠点活動が評価され、化学研究所は、平成30年11月13日文部科学大臣から国際共同利用・共同研究拠点に認定され、「化学関連分野の深化・連携を基軸とする先端・学際グローバル研究拠点」として活動を強化しています。国際拠点活動の二年目にあたる令和元年度には、化学研究所教員が一丸となって、179件の応募の中から採択された122件の共同研究を遂行し、5件の国際シンポジウム・研究会を主催・共催致しました。また、グローバルな化学研究の展開と人材育成のため、令和元年度の国際共同研究枠を平成30年度の20件から55件（若手国際枠3件を含む）に増やしました。今後とも、国際的ハブ機能を活用し、国際共同利用・共同研究の一層の促進、国際学術ネットワークの充実、国際的・先進的視野をもつ若手研究者の育成に取り組むことで、化学を中心とする研究分野の深化と境界学術分野の新規開拓を一層推進して参ります。皆様にはさらなるご支援・ご協力のほどよろしくお願い申し上げます。

本報告書は、令和元年度の本拠点における研究成果をとりまとめたものです。本報告書をご一読頂き、今後の本拠点の目指すべき方向や活動の推進方法などに関する忌憚のないご意見・ご提案などをお聞かせ下されば幸甚に存じます。

化学研究所
所長 辻井 敬亘

令和元年度 共同利用・共同研究報告書 目次

1. 共同研究成果報告

分野選択型共同研究

ビーム科学分野

2019-1※	Advanced functionality on materials induced by Intense THz pulse irradiation Setsunan University Takeshi Nagashima	1
2019-2※	Ultra directional neutron beam generation by using laser driven x-ray and spin polarized deuterium target Osaka University Yasunobu Arikawa	2
2019-3※	Research on the high-performance superconducting cavity and the cost reduction by noble inner-surface processes KEK Takayuki Saeki	3
2019-4※	Study on magnification of the pulsed-neutron transmission image using the sextupole magnet, aimed at visualization of charge and discharge in the electrode materials of Li-ion batteries AIST Koichi Kino	4
2019-5	鏡像体過剰率による金ナノワイヤーのらせん構造制御 東京理科大学 河合 武司	5
2019-6	Crystal structure analysis of GraE protein from root-nodule-forming bacterium Kansai University Tadao Oikawa	6
2019-7	マルチピコ秒の相対論的放射圧で駆動される臨界面の超高速運動の観測 大阪大学 藤岡 慎介	7
2019-8	プリパルス付与による高変換TNSA イオン加速 大阪大学 砂原 淳	8
2019-9	レーザー吸収制御によるシリコンの微細加工に関する基礎研究 大阪産業大学 草場 光博	9
2019-10	カーボンナノチューブを用いたISOL 用標的の開発 理化学研究所 大西 哲哉	10
2019-11	Development of a fast and efficient neutron trigger device for electron-RI scattering experiments RIKEN Akitomo Enokizono	11
2019-12	化学反応の量子制御を目指したCEP安定化自由電子レーザーのための省電力型超伝導加速空洞の製作方法の高度化 量子科学技術研究開発機構 羽島 良一	12
2019-13	グラファイト化薄膜テープ標的を用いたレーザー駆動イオン加速実験 量子科学技術研究開発機構 近藤 康太郎	13

元素科学分野

2019-14※	High pressure approach to the synthesis of novel ferroelectric photovoltaic transition metal oxides National Taiwan University Wei-tin Chen	14
2019-15※	Catalysis research of transition metal oxides Ningbo Institute of Industrial Technology Haichuan Guo	15
2019-16※	“Small molecule activation using anionic crypto-FLPs” University of Bonn Rainer Streubel	16
2019-17※	Development of unsymmetrical π -electron systems of heavier main group elements and elucidation of their property Tohoku University Takeaki Iwamoto	17

2019-18※	Mechanistic studies of C-H bond functionalization reactions catalyzed by 3d transition metals	Nanyang Technological University Naohiko Yashikai	18
2019-19※	Development of iron-catalyzed strategies for diversity oriented synthesis of heterocycles and carbocycles	Visva-Bharati University Alakananda Hajra	19
2019-20※	Iron-catalyzed carbometalation of heterobicyclic alkenes: development of asymmetric reactions and application to synthesis of polycyclic aromatic hydrocarbons	Nanyang Technological University Shingo Ito	20
2019-21※	Open-cage fullerenes incorporating hydrogen as n-type composite materials for polymer solar cell applications	National Chiao Tung University Shih-Ching Chuang	21
2019-22	中赤外レーザー光源の開発とナノ物質科学への応用	東京大学 板谷 治郎	22
2019-23	Study on the mechanism for the stability of an In-doped novel Fe-Pd phase	Meio Unibersity Yasutomi Tatetsu	23
2019-24	ウルシオール金属錯体を構成要素とする新規機能性塗料の開発	京都市産業技術研究所 橘 洋一	24
2019-25	Study on nickelate complexes constructed by a monoanionic tridentate pincer-type ligand	Yokohama National University Yoshitaka Yamaguchi	25
2019-26	アクリロニトリル系ポリマー末端ラジカルの反応機構研究とその合成応用	物質・材料研究機構 中村 泰之	26
2019-27	高性能ペロブスカイト太陽電池作成を指向した高活性酸化スカベンジャーの開発	名古屋市立大学 笹森 貴裕	27
2019-28	ヘテロダイン干渉分光法を用いた鉛ペロブスカイト太陽電池の光電流の研究	上越教育大学 小川 佳宏	28
バイオ情報学分野			
2019-29※	Network analyses for data-driven exploration and hypothesis testing in microbial ecology	CNRS UMR6004 Samuel Chaffron	29
2019-30※	Distribution of prasinoviruses and their association with natural hosts in the global ocean	CNRS UMR 7232 Nigel Grimsley	30
2019-31※	Integrating omics data and module-based network with deep learning to develop cancer type predictive models	National Chiao Tung University Jinn-Moon Yang	31
2019-32※	Next-generation bioinformatics approaches for the accurate identification of protease-specific substrate cleavage sites	Monash University Jiangning Song	32
2019-33	Viral impacts on microbial ecosystems in the highly-enclosed inlet, Uranouchi Bay, Kochi	Kochi University Kenzo Nagasaki	33
2019-34	新規巨大ウイルスの単離とゲノム・トランスクリプトーム解析	東京理科大学 武村 政春	34
2019-35	環境サンプルからの赤潮藻類の濃縮とその藻類に感染するウイルスの同定	京都大学 吉田 天士	35

2019-36	生物ネットワーク構造の局所構造変化の網羅的解析	岐阜大学 志賀 元紀	36
2019-37	分子ネットワーク解析のための統計的機械学習法の開発と応用	帯広畜産大学 茅野 光範	37
2019-38	Control and analysis of complex networks via minimum dominating sets	Toho University Jose C. Nacher	38
物質合成分野			
2019-39※	Application of s-tetrazines in guanidine functionalization of fullerenes	Rudjer Boskovic Institute Davor Margetic	39
2019-40※	Coupling of planar and curved π -systems for the development of novel functional materials	Max Planck Institute for Polymer Research Akimitsu Narita	40
2019-41※	Design, synthesis, and characterization of charge transport materials for non-lead perovskite	Osaka University Akinori Saeki	41
2019-42	新規 π 共役系ポリマーの開発と有機薄膜太陽電池への応用	広島大学 尾坂 格	42
2019-43	Preparation of novel branched block copolymer with well-controlled stereoregularity and evaluation of its molecular aggregation state	Osaka Institute of Technology Tomoyasu Hirai	43
2019-44	キラルネマチック液晶のアンカリング挙動に関する研究	立命館大学 赤木 和夫	44
2019-45	Molecular engineering of organic semiconductors toward the control of molecular packing in thin films via a thermal precursor approach	Osaka University Mitsuharu Suzuki	45
2019-46	電子ドナー性アニオンと電子アクセプター性カチオンを連結した π 共役双性イオンの合成と物性	大阪大学 清水 章弘	46
現象解析分野			
2019-47※	The elemental and isotopic composition of particulate trace metals in the subarctic Pacific Ocean: sources and internal cycling	Academia Sinica Tung-Yuan Ho	47
2019-48※	Application of $\delta^{98/95}\text{Mo}$ and $\delta^{186/184}\text{W}$ isotopes ratios for the reconstruction of late miocene oxygenation in the Arabian sea	Birbal Sahni Institute of Palaeosciences Gurumurthy Gundiga Puttoji Rao	48
2019-49※	Investigation on the decay process of hot carriers in heavily doped semiconductor nanocrystals	University of Castilla-La Mancha Abderrazzak Douhal A.	49
2019-50※	Development of photocatalytic materials by quantitative charge carrier dynamics and structural analysis	RMIT University Yasuhiro Tachibana	50
2019-51※	High frequency rheological and dielectric response of polymeric liquids	Yamagata University Sathish K. Sukumaran	51
2019-52※	Elongational rheology of telechelic-type ionomers	Changchun Institute of Applied Chemistry Quan Chen	52
2019-53	都市大気エアロゾルの起源および発生メカニズム解明に関する研究	近畿大学 中口 譲	53

2019-54	Study on transportation and separation of metal ions through a liquid membrane using ionic liquid	Kyoto University of Education Hiroshi Mukai	54
2019-55	Study on gelation behaviors of polymer oleogels	Okayama University of Science Noboru Osaka	55
2019-56	機能性配位子保護量子ドットの緩和過程の解明	関西学院大学 玉井 尚登	56
2019-57	新規部分フッ素化リン脂質分子群の膜物性・構造のキャラクタリゼーション	群馬大学 園山 正史	57
2019-58	スチレン系ブロック共重合体をベースとした非共有結合性エラストマーの調製と力学特性	名古屋大学 野呂 篤史	58

課題提案型共同研究

2019-59※	Regulatory network of gene expression for plant cell morphogenesis	Peking University Li-Jia Qu	59
2019-60※	Role of PX-PH-type phospholipase Ds in plant intracellular membrane traffic	University of Cambridge Yohei Ohashi	60
2019-61※	Site-selective protein acetylation by a small molecule	Fudan University Lu Zhou	61
2019-62※	Proteomic approach to discovering specific inhibitors for bile-acid interacting enzymes	Peking University Xiaoguang Lei	62
2019-63※	Study of magnonic properties of ferrimagnets	KAIST Kab-Jin Kim	63
2019-64※	Development of highly efficient and stable blue organic light emitting diodes using thermally activated delayed fluorescent materials as sensitizer	Tsinghua University Dongdong Zhang	64
2019-65※	Highly efficient blue thermally activated delayed fluorescence emitters using sterically hindered donor skeleton	Kyung Hee University Jang Hyuk Kwon	65
2019-66※	Structural analysis of organic amorphous thin films using solid effect dynamic nuclear polarization NMR	U.S. Department of Energy Takeshi Kobayashi	66
2019-67※	Memory of chirality using flow electrochemistry	Cardiff University Thomas Wirth	67
2019-68※	Creation of functional molecules based on hydrogen bond networks	University of Bristol Jonathan Clayden	68
2019-69※	Micro- and nano-structural characterization by advanced transmission electron microscopy of novel functional materials for battery development	Chiang Mai University Torranin Chairuangstri	69
2019-70※	Structural and functional analysis of the surface components of bacterial outer membrane vesicles	University of Naples Federico II Maria Michela Corsaro	70
2019-71※	Construction of low-temperature protein expression system by using cold-adapted microorganisms	Southwest University Xianzhu Dai	71
2019-72※	Search for four-wave-mixing in the vacuum – Unveiling dark components in the Universe –	Hiroshima University Kensuke Homma	72

2019-73※	Development of biosensors by combining stimuli-responsive polymer brushes with electrochemical analysis	South China University of Technology Ying Ma	73
2019-74※	Exploring new polyether nanocomposite electrolytes to enhance energy storage of lithium ion batteries	Michigan State University Robert C. Ferrier, Jr.	74
2019-75※	Fluorinated polymer-brush-grafted nanoparticles: Precise synthesis and applications to membrane technology	University of Montpellier Vincent Ladmiral	75
2019-76※	Determine the three-dimensional structure of ^{13}C labeled α -synuclein(61-95) in the Langmuir-Blodgett film and supported phospholipids bilayers by p-MAIRS FT-IR	Middle Tennessee State University Chengshan Wang	76
2019-77※	Real-time imaging of single-molecule mRNA with different methylation states	Colorado State University Timothy J. Stasevich	77
2019-78※	Structural and functional analysis of curvature-inducing peptides	Karlsruhe Institute of Technology Anne S. Ulrich	78
2019-79※	Research of multi-qubit diamond quantum processors	Australian National University Marcus W. Doherty	79
2019-80※	Research on shallow NV center in diamond	Max-Planck Institute for Biophysical Chemistry Gopalakrishnan Balasubramanian	80
2019-81※	Effect of dipole alignment along chain backbone on dielectric relaxation of type-A polymers at association/dissociation equilibrium	Sungkyunkwan University Youngdon Kwon	81
2019-82	植物表皮細胞の分化における制御ネットワークの研究	広島大学 富永 るみ	82
2019-83	アシルドーパミンの新機能	東京薬科大学 伊藤 昭博	83
2019-84	ビタミンDの新機能の調節	東京農工大学 長澤 和夫	84
2019-85	高スピン偏極電流源の開発のためのコバルトフェライト薄膜の磁気・電氣的性質の評価	名古屋工業大学 田中 雅章	85
2019-86	Develop of the epitaxial thin film of Weyl semimetal Mn_3Sn	Hokkaido University Taro Nagahama	86
2019-87	Effect of microstructure on damping constant in polycrystalline Bi-YIG thin films prepared by sol-gel method	Gifu University Keisuke Yamada	87
2019-88	Giant isotope effects of deuterium atoms terminating on nanocrystalline silicon and their use	Nagoya City University Takahiro Matsumoto	88
2019-89	4-ピロリジン-ピリジン型分子触媒による化学選択的アシル化反応の理論的解析	立教大学 山中 正浩	89
2019-90	α -フッ素化アミノ酸を含む抗腫瘍性環状オクタデプシペプチドの合成と生物学的評価	岐阜薬科大学 永澤 秀子	90
2019-91	Studies on total synthesis of gonytolides	Kanazawa University Tomoyuki Yoshimura	91

2019-92	Analysis of the physiological functions of membrane vesicles produced by intestinal bacteria and fermented food-derived bacteria and their application	Kindai University Atsushi Kurata	92
2019-93	Studies on the physiological significance of two alanine dehydrogenases in <i>Geobacillus kaustophilus</i>	Osaka Institute of Technology Taketo Ohmori	93
2019-94	異常高原子価イオンを含む機能性酸化物合成とその構造物性研究	高エネルギー加速器研究機構 齊藤 高志	94
2019-95	溶媒含浸樹脂を用いた白金族元素抽出における界面活性剤の利用	大阪府立大学工業高等専門学校 倉橋 健介	95
2019-96	ポリマーブラシ付与強磁性ナノプレートの高精密合成による強磁性フォトニック液晶の実現	大阪大学 内田 幸明	96
2019-97	Additive Manufacturing による多孔性高分子複合材料の3次元構造制御	共立女子大学 村瀬 浩貴	97
2019-98	Ferromagnetic single-electron transistor	Tokyo Institute of Technology Yutaka Majima	98
2019-99	パーフルオロアルキル鎖とアミノ酸頭部基を有する新規な界面活性剤型防錆剤の探索	千葉大学 山田 哲弘	99
2019-100	NanoBRET 型CXCR4 結合解析によるペプチドリガンド評価系の構築	広島大学 野村 渉	100
2019-101	がん深部到達型修飾膜透過ペプチドの創出と大腸がん幹細胞効率的除去への展開	富山大学 大橋 若奈	101
2019-102	ダイヤモンド表面近傍のNV 中心作製	金沢大学 徳田 規夫	102
2019-103	ダイヤモンド中のNV 中心量子ビットの電氣的制御と電氣的検出	産業技術総合研究所 牧野 俊晴	103
2019-104	シクロパラフェニレンの励起ダイナミクスの環サイズ依存性	大阪大学 藤塚 守	104
2019-105	半屈曲性高分子溶液の非線形レオロジー	大阪大学 井上 正志	105
2019-106	Analysis of Soret effect for DNA in molecular-scale temperature gradient	Japan Women's University Ryoko Shimada	106
連携・融合促進型共同研究			
2019-107※	Fabrication of nanotopographical polymer surfaces with bactericidal properties	Stony Brook University Maya K. Endoh	107
2019-108※	Synthesis of structurally controlled polymers having green fluorescence protein chromophore and their photophysical properties in solution	National Taiwan University Jye-Shane Yang	109
2019-109※	Vinyl azides as new monomers of radical polymerization for the fabrication of green polymers having chemically- and biodegradable properties	Nanyang Technological University Shunsuke Chiba	111
2019-110※	The 15th International workshop for East Asian Young Rheologists	Osaka University Tadashi Inoue	113
2019-111	第8回日本-中国有機化学シンポジウム	静岡県立大学 濱島 義隆	115

2019-112 第26回酸化物エレクトロニクスに関する国際会議

大阪大学 松野 丈夫 117

施設・機器利用型共同研究

2019-113※ Atomic level analysis and fabrication of highly stable perovskite films and light emitting diodes

Tsinghua University Juan Qiao 119

2019-114※ High-pressure synthesis of potential multiferroic oxides

University of Edinburgh J. Paul Attfield 120

2019-115※ Synthesis and characterization of novel organoselenium and -tellurium compounds

Rikkyo University Mao Minoura 121

2019-116 核融合プラズマ対向材中の水素・ヘリウム挙動に関する電子分光学的研究

島根大学 宮本 光貴 122

2019-117 プラズモニック結晶上でのプラズモン-エキシトン結合

九州大学 斉藤 光 123

2019-118 完璧な π 共役二次元シートを持つフラットシリセンの設計

東北大学 高橋 まさえ 124

2019-119 Synthesis and structures of acene molecules bearing chalcogenopyrylium units

Fukuoka University Noriyoshi Nagahora 125

2019-120 Synthesis and structural characterization of divalent species of heavier group 14 elements

Kindai University Tsukasa Matsuo 126

2019-121 Elucidation of the fluorine interactions in the crystal structures of fluorine-containing conjugated molecules by the single-crystal X-ray structural analysis

Ibaraki University Tomohiro Agou 127

2019-122 生体組織由来のカルボニル化合物を標的とする高感度質量分析イメージング解析

奈良県立医科大学 秦野 修 128

2. 国際学会、シンポジウム・研究報告会

国際会議

- 9th Pacific Symposium on Radical Chemistry 129
- 19th Annual International Workshop on Bioinformatics and Systems Biology 130

シンポジウム・研究会

- 2019 年 日本分光学会年次講演会 132
- The 1st Germany–Japan–China Joint Workshop on Extremely Large π -Systems 133
- 第 12 回台湾－日本機能性有機分子構築に関する二国間シンポジウム 135

3. 成果発表論文 137

(令和 2 年 2 月までに刊行された論文で、平成 22–30 年度の成果報告書に掲載されていないもの)

紙数の都合により、*を付けた論文のみについて、別刷りを本報告書に記載する。

*Reversible Isomerizations between 1,4-Digermabenzenes and 1,4-Digerm-Dewar-benzenes: Air-stable Activators for Small Molecules, *J. Am. Chem. Soc.*, 141, 2263–2267 (2019).

*Probabilistic controllability approach to metabolic fluxes in normal and cancer tissues, *Nat. Commun.*, 10, 2725 (2019).

The Formation of a 1,4-Disilabenzene and its Isomerization into a Disilabenzvalene Derivative, *Dalton Trans.*, 48, 9053–9056 (2019).

A Mixed-Anion System Consisting of a Germyl Anion and Anions Delocalized on Conjugated Carbon Ring Skeletons, *Chem. Eur. J.*, 25, 6284–6289 (2019).

Synthesis and Properties of Perfluoroalkylated TIPS-pentacenes, *Tetrahedron*, 75, 130678 (2019).

Dibromometallyl-iron Complexes Generated by the Recombination of an Alumanyl-iron Complex with EBr (E = Al, Ga), *Heteroat. Chem.*, 29, e21465 (2018).

Syntheses and Structures of Novel λ^3, λ^3 -Phosphanylalumanes Fully Bearing Carbon Substituents and Their Substituent Effects, *Inorganics*, 7, 132–143 (2019).

H₂O/Olefinic- π Interaction inside a Carbon Nanocage, *J. Am. Chem. Soc.*, 141, 12928–12938 (2019).

Probing the Regioselectivity by Encapsulated H₂: Diels-Alder Reaction of a Cage-Opened C₆₀ Derivative with Anthracene, *Chem. Eur. J.*, 25, 2482–2485 (2019).

pMAIRS Analysis on Chain-End Functionalization of Densely Grafted, Concentrated Polymer Brushes, *Macromolecules*, 52, 6673–6682 (2019).

The Effect of Viscosity on the Diffusion and Termination Reaction of Organic Radical Pairs, *Chem. Eur. J.*, 25, 9846–9850 (2019).

Multifunctionalization of Cells with a Self-Assembling Molecule to Enhance Cell Engraftment, *ACS Chem. Biol.*, 14, 775–783 (2019).

Nutrient-Based Chemical Library as a Source of Energy Metabolism Modulators, *ACS Chem. Biol.*, 14, 1860–1865 (2019).

Synthetic Chemical Probes That Dissect Vitamin D Activities, *ACS Chem. Biol.*, 14, 2851–2858 (2019).

Raman Optical Activity on Solid Sample: Identification of Atropisomers of Perfluoroalkyl Chains Having a Helical Conformation and No Chiral Center, *J. Phys. Chem. A*, 18, 3985–3991 (2019).

Determination of pH Dependent Structures of Thymol Blue Revealed by Cooperative Analytical Method of Quantum Chemistry and Multivariate Analysis of Electronic Absorption Spectra, *Bull. Chem. Soc. Jpn.*, 92, 1759–1766 (2019).

Dielectric Relaxation of Type-A Chains Undergoing Head-to-Tail Association/Dissociation: Difference from Head-to-Head Case and Correlation with Viscoelastic Relaxation, *Macromolecules*, 52, 8484–8502 (2019).

Increased energy of THz waves from a cluster plasma by optimizing laser pulse duration, *AIP Adv.*, 9, [015134-1]–[015134-4] (2019).

Detection of alpha particles from ${}^7\text{Li}(\text{p},\alpha){}^4\text{He}$ and ${}^{19}\text{F}(\text{p},\alpha){}^{16}\text{O}$ reactions induced by laser-accelerated protons using CR-39 with potassium hydroxide–ethanol–water etching solution., *Rev. Sci. Instrum.*, 90, 83307 (2019).

Ablation suppression of a titanium surface interacting with a two-color double-pulse femtosecond laser beam, *Appl. Surf. Sci.*, 478, 882–886 (2019).

Dynamic Behavior of Helium Bubbles at High Temperature in Si Studied by in-situ TEM, STEM-EELS and TDS, *J. Appl. Phys.*, 126, [131504-1]–[131504-11] (2019).

Bulk Dzyaloshinskii–Moriya Interaction in Amorphous Ferrimagnetic Alloys, *Nat. Mater.*, 18, 685–690 (2019).

Recognition Behavior of a Porphyrin Heterodimer Self-Assembled through an Amidinium-Carboxylate Salt Bridge, *Asian J. Org. Chem.*, 7, 2087–2093 (2018).

Iron-Catalysed Enantioselective Suzuki–Miyaura Coupling of Racemic Alkyl Bromides, *Chem. Commun.*, 55, 1128–1131 (2019).

Iron-Catalyzed Cross Coupling of Aryl Chlorides with Alkyl Grignard Reagents: Synthetic Scope and $\text{Fe}^{\text{II}}/\text{Fe}^{\text{IV}}$ Mechanism Supported by X-ray Absorption Spectroscopy and Density Functional Theory Calculations, *Bull. Chem. Soc. Jpn.*, 92, 381–390 (2019).

Iron-catalyzed Alkyl–Alkyl Negishi Coupling of Organoaluminum Reagents, *Chem. Lett.*, 48, 238–241 (2019).

Ligand-Free Iron-Catalyzed C–F Amination of Diarylamines: A One-Pot Regioselective Synthesis of Diaryl Dihydrophenazines, *Org. Lett.*, 21, 461–464 (2019).

Endergonic addition of N-methylamines to aromatic ketones driven by photochemical offset of the entropic cost, *Chem. Commun.*, 55, 11683–11686 (2019).

KofamKOALA: KEGG Ortholog Assignment Based on Profile HMM and Adaptive Score Threshold, *Bioinformatics*, 36, 2251–2252 (2019).

Fifteen Marseilleviruses Newly Isolated from Three Water Samples in Japan Reveal a Local Diversity of Marseilleviridae, *Front. Microbiol.*, 24, 1152 (2019).

The Earth is Small for “Leviathans”: Long Distance Dispersal of Giant Viruses Across Aquatic Environments, *Microbes Environ.*, 34, 334–339 (2019).

Medusavirus, a Novel Large DNA Virus Discovered from Hot Spring Water, *J. Virol.*, 93, (2019).

Finding and Analysing the Minimum Set of Driver Nodes Required to Control Multilayer Networks, *Sci. Rep.*, 9, [576-1]–[576-12] (2019).

Network Controllability Analysis of Intracellular Signalling Reveals Viruses are Actively Controlling Molecular Systems, *Sci. Rep.*, 9, [2066-1]–[2066-11] (2019).

Bastion3: a Two-layer Ensemble Predictor of Type III Secreted Effectors, *Bioinformatics*, 35, 2017–2028 (2019).

Deep Learning with Evolutionary and Genomic Profiles for Identifying Cancer Subtypes, *J. Bioinform. Comput. Biol.*, 17, [1940005-1]–[1940005-15] (2019).

4. 参考資料

4-1.令和元年度公募要領	151
4-2.令和元年度採択課題一覧	155

1. 共同研究成果報告

Advanced functionality on materials induced by Intense THz pulse irradiation

Takeshi Nagashima Setsunan University

Recently, generation of intense terahertz (THz) wave in the $\sim 100 \mu\text{m}$ wavelength region has rapidly progressed. Since the intense THz wave can apply high electric field to materials in picosecond time duration, it allows non-thermal material processing that would induce a ultra-fine structuring and creation of novel functionalities on various material surfaces. The purposes of this study are as follows: 1. development of intense THz pulse sources and 2. observations of material processing and nonlinear optical effects by irradiating various materials (Si wafer and water film) with the intense THz pulses.

Developments of intense THz pulse sources

Two types of THz pulse sources utilizing the tilted pulse front scheme with T^6 laser in Sakabe lab. that generates fs optical pulses with a pulse energy of 500 mJ at maximum were developed. In both setups, large LiNbO_3 (LN) crystals (up to $40 \times 25 \text{ mm}^2$) were used for obtaining greater THz pulse energy. One of the setups was constructed in ambient air. This setup in which the available energy of the excitation optical pulses was less than 40 mJ generated THz pulses with a THz pulse energy of 120 μJ at maximum. To further gain the THz pulse energy, another setup was developed in a vacuum chamber allowing the use of the full laser pulse energy. We obtained 1.6 mJ THz pulses when the energy of the excitation optical pulses was greater than 200 mJ.

Experiments of irradiation with intense THz pulses

The THz pulses from the setup in the air were focused on a Si wafer, but there was no damage on the surface of the wafer. We conducted the THz pulse irradiation experiments using THz-FEL at Osaka Univ. and found that the damage threshold for Si was 13 J/cm^2 that corresponds to a THz pulse energy of 1.8 mJ, which confirms that the THz pulse source in the air was unable to damage the surface of Si wafer. In addition, we conducted z-scan experiments for semiconductors and a water film, however no effect caused by nonlinear refraction was observed because of the lack of the THz pulse fluence. The water film was prepared by Prof. Hatanaka and Huang from Academia Sinica, Taiwan as the international collaborators. Spectra of the THz pulses measured at a position just after the LN crystal show that the central frequency of the dominant component is $\sim 0.1 \text{ THz}$. One of the reasons of the lack of higher frequency components would be absorption of the THz pulse by the thick LN crystal used in this study. The experiments of the surface processing and nonlinear optical effects with the THz source in the vacuum chamber and mid-infrared FEL are to be conducted.

Publications and presentations

- [1] C. Hosokawa, M. Hashida, T. Nagashima *et al.*, “Development of Intense Terahertz Light Source for Forming Periodic Structures on Material Surface,” The Papers of Technical Meeting, IEE Japan, LAV-19-018(2019).
- [2] H.-H. Huang, T. Nagashima, K. Hatanaka *et al.*, “Giant enhancement of THz wave emission under double pulse excitation of thin water flow,” arXiv2001.11753 (2020).

Ultra directional neutron beam generation by using laser driven x-ray and spin polarized deuterium target

Yasunobu Arikawa Osaka University

Neutron is a unique particle source having numerous application capabilities in scientific researches, industrial applications, and medical applications. Neutron sources such as large scale accelerator J-PARC, nuclear reactors, compact accelerators have been widely used for these purposes. Laser driven neutron sources have been recently recognized as an alternative neutron source having a point source, and ultra-short pulse and thus effective for the applications. The directionality of neutron beams has not able to be controlled in present technologies unfortunately. If we could generate a highly directional neutron beams like electrons or protons we can realize various neutron sciences which have been expected. We have been proposing highly directional neutron beam might be generated by using a spin-polarized deuterium and laser. Since a small target can generate neutrons in laser neutron sources, such a new neutron generation method can be easily innovated. In this study we aimed the potentially highly directional neutron generation from spin-polarized deuterium target by using ultra-short pulse laser.

At present, the Spin-Polarizer for deuterium has not been completed which is unexpectedly. In our latest test, only a few % of the deuterium in the target was polarized which is not sufficient for our neutron generation experiment. We are ongoing on this work.

On the other hands, an ultra-fast, high efficient, and Polarization-sensitive neutron detector is required for demonstrating our scheme for generating ultra-short directional neutron beam. We developed an such neutron detector based on Pockels effect. Small Pockels (ZnTe) crystal was attached to a single-mode optical fiber, and the tip of the fiber will be placed very close to the neutron generation target (~2mm away from target).

T6 laser system. Kyoto-Univ T6 laser has been used to generate neutrons (for the first time experiment we use electron alternative to the neutrons because it is much easier to generate). The probe laser was picked up from the second stage T6 laser amplifier. The preparation of the system has been almost completed and the timing between the T6 laser and the probe laser was adjusted at the same time. The electron generation experiment has been still going and will be completed within 2020 March. This work has been supported by Dr. Inoue, Prof. Sakabe, Prof. Hashida, Kyoto Univ.

Research on the high-performance superconducting cavity and the cost reduction by noble inner-surface processes

Takayuki Saeki KEK

(1) Objectives: Realization of compact and efficiency Superconducting Radio-Frequency (SRF) particle-accelerators by the accelerating cavities with thin-film inner-surface coating of various new SRF materials like NbN, Nb₃Sn and so on. The thin-film coating technology might achieve drastically higher accelerating gradient and lower power consumption than the conventional bulk-Nb accelerating cavity.

(2) Experimental methods: The team of ICR (Y. Iwashita, H. Tongu), CEA-Saclay (C. Antoine), KEK (T. Saeki, T. Kubo, R. Katayama) and QST (R. Hajima, M. Sawamura) studies on this subject. At KEK, the resonant frequency of accelerating cavity is normally set at 1.3 GHz. The team fabricates several elliptical-shaped single-cell Copper (Cu) and Niobium (Nb) cavities at the resonant frequency of 3 GHz, whose dimension/size is smaller by about half than that of 1.3-GHz cavity. Such small-sized and high-frequency cavities are important for the realization of compact and efficient accelerators. The thin-film creation on the inner surface of cavities and coupon-samples are performed by KEK in collaboration with industry. The SRF characteristics of the coupon-samples with NbN/SiO₂ thin-film structure on pure Nb substrate is measured at ICR by using the third-harmonic voltage method.

(3) Experimental results: Nine 3.0-GHz single-cell Copper (Cu) cavities and six 3.0-GHz single-cell Niobium (Nb) cavities were fabricated for the studies of thin-film technology [1]. It was proven that an optimum film-thickness of the NbN layer exists for the maximum effective critical magnetic-field (H_{c1} -effective) of NbN/SiO₂/Nb multilayer sample. The corresponding coupon-sample results in the increase of H_{c1} -effective by 23.8%, being compared to that of bulk-Nb [2]. The principle of measurement method and the experiments at CEA-Saclay are described in [3].

(4) Discussions: Theoretical calculations were compared to experimental results. We confirmed that the experimental results are qualitatively consistent with the theoretical prediction. The results imply the possibility that the acceleration gradient of SRF cavities might be effectively enhanced by controlling the multilayer thin-film structure, and the possibility to realize high-performance SRF cavities with thin-film technology in mass-production consistently.

(5) Publications: [1] T. Saeki et al., Proc. of SRF2020 in Dresden/Germany, 30 June – 5 July 2019, Paper ID: MOP054. [2] R. Katayama et al., Proc. of SRF2020 in Dresden/Germany, 30 June – 5 July 2019, Paper ID: THFUA2. [3] “Optimization of tailored multilayer superconductors for RF application and protection against premature vortex penetration”, C Z Antoine, M Aburas, A Four, F Weiss, Y Iwashita, H Hayano, S Kato, T Kubo and T Saeki, Published on 5 July 2019, Superconductor Science and Technology, Volume 32, Number 8.

Study on magnification of the pulsed-neutron transmission image using the sextupole magnet, aimed at visualization of charge and discharge in the electrode materials of Li-ion batteries

Koichi Kino AIST

We are studying on magnification of the pulsed neutron transmission image for non-destructive analysis of charge/discharge distributions in the electrode of the lithium ion battery (LIB). The pulsed neutron beam is irradiated on a sample and the transmitted neutron image is magnified by the modulated-Permanent Magnet Sextupole (mod-PMSx) and observed by a 2D neutron detector. We have already succeeded in a magnification of an image of a cadmium mask sample using the mod-PMSx with a bore radius of 15 mm for a neutron wavelength longer than 8 Å. However, we have to shorten the lower limit of the neutron wavelength since the Bragg cut off of the 002 reflection of graphite, which is a negative electrode of LIBs, is 6.7 Å. For the shorter wavelength, the magnetic field has to be increased and it is inversely proportional to the square of the bore radius. On the other hand, a neutron yield becomes smaller as the bore radius becomes smaller. Therefore, we calculated with a bore radius of 7 mm taking into account a balance of them.

Distances from a neutron source to a sample, mod-PMSx, and focal plane are 1.35 m, 3.9 m, and 9.0 m, respectively. The magnification percentage was set to be 2 due to the limitation of the size of an experimental facility. By the calculation, we found that the magnetic field has to be modulated twice faster than our previous experiments in order to keep the magnification percentage constant in the required wavelength region. The relation of the required relative strength of the magnetic field to focus neutron images and relative mod-PMSx modulation is shown in Fig. 1. They are almost synchronizing. Calculated neutron tracks are shown in Fig. 2. The neutrons emitted from different positions of the sample are bent in the magnetic field at 3.9 m and make an inverted image at 9.0 m of magnification percentage of 2. From these calculation results, we could make a magnet with a 7 mm bore radius.

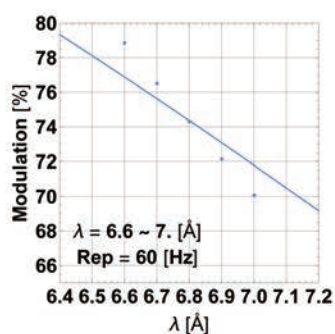


Fig. 1 Synchronization of the new mod-PMSx. Data points are relative strength required to focus neutrons. Solid line shows the relative mod-PMSx modulation.

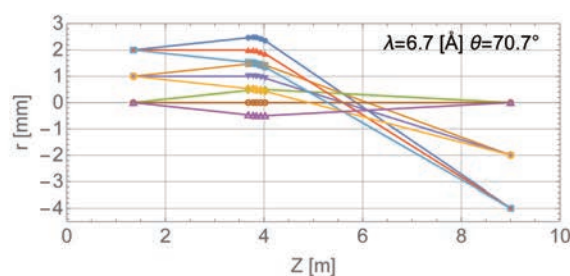


Fig. 2 Neutron tracks of a 6.7 Å wavelength from the sample to the focal plane.

鏡像体過剰率による金ナノワイヤーのらせん構造制御

河合武司 東京理科大学

[目的] 無機ナノワイヤーの研究は現在精力的に行われているが、次にチャレンジングな課題は高機能化を目指した二次構造の自在制御技術の開拓である。最近我々は、キラル源としてひまし油から得られる D 体の 12-ヒドロキシステアリン酸 (D-HSA) と長鎖アミドアミン誘導体(C18AA)とが形成するゲルファイバー (右巻きのらせん状分子集合体)を鋳型に用いると、らせん状極細金ナノワイヤーが合成できることを報告した。さらに、らせん状金ナノワイヤーは、鋳型 (HSA+C18AA) を取り除いても形態を保持することや可視から近赤外領域に特徴的な円偏光二色性(CD)ピークを与えることを明らかにした。ごく最近、キラルな HSA 分子の鏡像体過剰率によって鋳型のらせん構造が制御できことがわかった。そこで本研究では、分子集合体およびらせん状金ナノワイヤーに及ぼす鏡像体過剰率の影響について検討した。

[実験] D-HSA および L-HSA のメタノール溶液を混合し、メタノールを蒸発させることで様々な割合の D-HSA/L-HSA 混合物を調製した。D-HSA を用いたとき鏡像異性体過剰率 (ee) = 100%、L-HSA を当量混合したとき ee = 0%とした。D-HSA/L-HSA と C18AA を組み合わせてらせん状のハイドロゲルを調製した後、塩化金酸と還元剤を添加してらせん状金ナノワイヤー (Au NWs) を合成した。

[結果と考察] D-HSA の ee が 100, 80, 60, 40, 20, 0%のゲル化能を調べた結果、ee = 100%または 0%ではゲル化し、80%では一部がゲル化、60、40、20%では沈殿が生じた。これらの溶液に含まれる分子集合体および Au NWs の TEM 像 (共同研究者の倉田教授担当) を観察したところ、それぞれの溶液からは ee = 100%のときに形成したナノリボンの他に、チューブ状の分子集合体や板状の分子集合体が観察された。また、ee = 60, 40%ではケーブル状、ee = 20, 0%ではコイル状の分子集合体もわずかに観察された (Fig.1)。興味深いことに、チューブ状および板状分子集合体上でも、らせん状および直線状 Au NWs がそれぞれ形成した。さらに興味深いことに、ee = 80%ではねじれたナノリボンのみが生成したのに対し、ee = 40%ではチューブ状の分子集合体、ee = 0%では板状の分子集合体が選択的に生成した。すなわち、HSA と C18AA の分子集合体は HSA の鏡像体過剰率によって、ねじれたリボン状、チューブ状、板状という 3 つの形態を

取り、ee が 100%付近ではねじれたナノリボン、ee が 40%付近ではナノチューブ、ee が 0%付近では板状の分子集合体が形成されることが明らかになった。また、3 種類の分子集合体の形態の中でナノチューブが最も強いコットン効果を示し、CD シグナルの強さは ee=40%で最大となり、ee = 0%ではほぼゼロであることも明らかとなった。

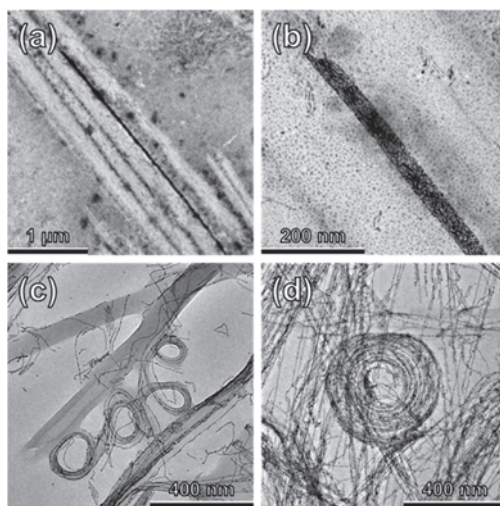


Fig.1 (a, b) ee = 60%で観察されたナノチューブおよびケーブル状 Au NWs の低倍率および高倍率の TEM 像. (c, d) ee = 20%のコイル状分子集合体およびコイル状 Au NWs.

Crystal structure analysis of GraE protein from root-nodule-forming bacterium

Tadao Oikawa Kansai University

Rhizobium is a genus of tubercle-forming bacteria. It grows in the root of a plant in symbiosis with other bacteria to fix nitrogen from the air. Although considerable attention has been paid to *Rhizobium* genes and gene products, there is still little information available regarding the molecular structure, function, and detailed properties of the enzymes involved in its metabolic pathways. In the course of a screening experiment, *Rhizobium* sp. strain MTP-10005 was isolated from natural river water. Enzymological and genetic studies showed that the translational products of the gene cluster *graDAFCBEK* in the bacterium (GraR, GraD, GraA, GraF, GraC, GraB, GraE, and GraK, respectively) were probably involved in the degradation pathway of γ -resorcylyate. To reveal the structure and function of all these proteins, I have collaborated with Dr. Tomomi Fujii and Prof. emeritus Dr. Yasuo Hata, Institute for Chemical Research, Kyoto University, and have performed already X-ray structural studies of GraA, GraC, and GraD. In this study, we focused on GraE, whose function and role in the degradation pathway of γ -resorcylyate are currently unknown. The X-ray crystal structure of GraE is expected to reveal its function and role *in vivo*.

N-terminal His-tagged GraE was overexpressed in *Escherichia coli* BL21 (DE3), purified, and used for crystallization. The protein solution consisted of 5 mg/ml GraE, 150 mM NaCl, and 50 mM Tris-HCl pH 8.0. Initial crystallization experiments were performed by the sitting-drop vapor-diffusion method using several screening kits. Thin plate-shaped adequately sized crystals for X-ray diffraction experiments were obtained using a reservoir solution consisting of 3 M NaCl and 0.1 M citric acid buffer pH 3.5. Diffraction experiments were performed on beamline BL-5A, Photon Factory, KEK, Japan. A crystal was soaked in a cryoprotectant solution consisting of 23% (v/v) glycerol, 3 M NaCl, and 0.1 M citric acid buffer pH 3.5. The crystal was mounted with a cryoloop and cooled with a cold stream of nitrogen. Diffraction data were collected up to 1.8 Å resolution. The crystal belonged to space group $P2_1$, with unit-cell parameters of $a = 34.31$ Å, $b = 80.90$ Å, $c = 43.38$ Å, and $\beta = 107.36^\circ$.

The collected diffraction data have been improved, in terms of diffraction quality, compared to the data of crystals from other crystallization conditions. The diffraction limit of the collected data has been extended from 3.0 Å to 1.8 Å resolution. Based on the molecular mass of the protein and unit-cell volume, the existence of two subunits in the asymmetric unit gave a Matthews coefficient (V_M) of 2.02 Å³/Da and solvent content of 39%, each of which was within a range of values frequently found in protein crystals. This case appeared to be more likely than other cases, wherein V_M values of 4.03 and 1.34 Å³/Da for one and three subunits per asymmetric unit were obtained, respectively. Structure determination trials utilizing the molecular-replacement method using homologous models of monomers/dimers are currently carrying out. Moreover, crystallization of seleno-methionine-labelled GraE for the multiple anomalous dispersion method and the preparation of heavy-atom derivative crystals for the isomorphous replacement method are presently under way.

マルチピコ秒の相対論的放射圧で駆動される臨界面の 超高速運動の観測

藤岡慎介 大阪大学

マルチ ps に及ぶ高強度レーザーとプラズマ相互作用ではレーザーにより加熱されたプラズマの圧力がレーザーの光圧を上回り、プラズマの運動がホールボーリングからプラズマ膨張へ遷移する現象が現れると予測されている。プラズマは膨張と付随して準静的な電磁場の急激な成長を引き起こし、レーザー電磁場との間の相乗効果により、相対論的電子加速の高効率な加速を引き起こす。このようにプラズマ膨張はマルチ ps 高強度レーザー・プラズマ相互作用で起きる特異な電子加速の発端となるため、観測およびその物理の理解は非常に重要である。

我々の研究ではこの相対論的臨界密度面の高速運動を観測するために相対論的臨界密度面からの反射光を FROG (Frequency-Resolved Optical Gating) 法により観測する方法を選択した。反射光は移動する相対論的臨界密度面を光源として発生するため、その移動速度はドップラー効果により波長シフトとして現れる。本研究では偏光ゲートと呼ばれるタイプの FROG の観測時間領域をマルチ ps に拡大する設計を行い、その較正実験を京都大学化学研究所の T⁶ レーザーを用いて行った (図 1)。偏光ゲート FROG は入射に角度をつけた 2 つのビームが非線形媒質中で起こす光カー効果を用いて時間分解に利用する。これまでに非線形媒質として 500 μm 厚の SF-11 ガラスを用いて 121 fs の時間分解能、600 本/mm の回折格子を用いた分光器を用いて波長分解能 0.5 nm を実現した。

また、FROG 開発では FROG を動作させるレーザー強度が自己位相変調によるスペクトル変調に注意が払われ最適化された。スペクトル変調の B 積分しきい値は、繰り返し率が高い T⁶ レーザーシステムを使用して実験的に調べられ、スペクトル変調の所定のしきい値は、厚さ 500 μm の SF-11 ガラスで 18 GW/cm² であり、B 積分値に対応して 0.14 rad ($\pi/22$) であると導かれた。反射光学系を含むエネルギー減衰器が低繰り返し LFEX レーザーのフルパワーショット用に設計され、レーザー強度はスペクトル変調を防ぐために適切に調整された。

マルチ ps 高強度レーザーの照射中に起きるプラズマの高速運動を観測する実験は大阪大学レーザー科学研究所の LFEX レーザーで行い、エネルギー：161 J、パルス幅：3.3 ps (FWHM) の LFEX レーザーパルスを実験室ターゲットへ照射し反射光を FROG によって計測した (図 2)。観測されたドップラーシフトの時間発展から LFEX レーザーが相互作用したプラズマのスケール長及び電離度を推定した。今回の計測によりフットパルス・ペデスタルの寄与によりメインパルスの到着時点で発生するプリプラズマのスケール長が 4~5 μm と実験的に計測された。また電離度は 6 価に達し over-barrier-ionization を仮定した場合の集光強度 10¹⁸ W/cm² に一致した。このことから電離はなく、フットパルス・ペデスタルではなく、強度が上がったメインパルスの初期の数 100 fs で進行したものと結論付けた。

研究成果は光・量子ビーム科学合同シンポジウム 2019 において発表し、ベストポスター賞を受賞した。また同成果は、第 11 回慣性核融合とその応用に関する国際会議 (IFSA2019) においても発表を行った。現在、Elsevier 社が発刊する High Energy Density Physics 誌に論文を投稿しており、査読審査が行われている。

プリパルス付与による高変換 TNSA イオン加速

砂原 淳 大阪大学

高強度フェムト秒レーザーと物質の相互作用は電子やイオンの加速を通じ、多様かつ魅力的な工学的応用につながることに加え、素過程の機構解明が未だ途上であるため、世界中で精力的な研究が行われている。特に、Target Sheath Normal Acceleration(TNSA)と呼ばれるイオン加速機構は高強度レーザーを用いたレーザー加速の基本となっており、 $10^{18}\text{W}/\text{cm}^2$ 以上の高強度レーザーをターゲット物質に照射することで相対論的領域まで加速される電子がターゲット周りに静電場を励起し、最終的にイオンを MeV 領域まで加速させることが出来る。我々は時間的に同期させたナノ秒レーザーを適切なタイミングで予めターゲットに照射することでターゲット表面の初期プラズマ状態を制御し、効率的な TNSA イオン加速が実現できることを理論的に見出しており、本アイデアの実験的実証を目的として、京都大学化学研究所共同研究（受け入れ：井上助教，参加機関：京都大学、大阪大学、光産業創成大学院大学、東北大学）としてレーザー施設において実験を行った。本実験ではナノ秒レーザーと高強度フェムト秒レーザーを適切な時間差でくり返し照射する必要があり、図 1 のように高強度($10^{18}\text{W}/\text{cm}^2$)フェムト秒レーザーと比較的低強度($\sim 10^{12}\text{W}/\text{cm}^2$)のナノ秒レーザーを時間的に同期させて厚さ $10\mu\text{m}$ のプラスチックターゲットに照射し、ターゲット裏面から TNSA 加速されるプロトン数、エネルギー及び角度広がり

を CR-39 により観測した。昨年度（1 年目）の実験ではナノ秒レーザー照射により、高強度フェムト秒レーザー照射時に発生する MeV 級の高速電子の発生がナノ秒レーザーを照射しない場合に比べ、5～10 倍と飛躍的に増大することを確認した。このことは TNSA 加速を駆動する電場が 5～10 倍増強され得ることを示して

いる。この実験結果を受け、本年度は加速プロトン発生数の観測を行い、ナノ秒照射時にプロトン数が増大する条件を確認した。しかし、期待した 5～10 倍のプロトン数発生には至らず、その原因として(1)ナノ秒レーザーが照射開始初期に透明ターゲットを透過し、ターゲット裏面をプラズマ化することによる加速電場抑制と(2)ナノ秒レーザーの照射不均一性に起因するターゲットの歪みが発生プロトンの加速方向に影響を及ぼす効果がそれぞれ実験的に見出された。得られた実験結果は加速プロトン発生数の飛躍的増大に直接的につながる鍵となるものであり、ターゲットのセットアップ及びレーザー照射条件、プロトンの観測位置の変更に知見を活かすことで(1)と(2)を回避することで、加速プロトン発生数の飛躍的増大の実現への具体的パスが見出されたと言える。今後(1)と(2)の効果を数値シミュレーションにフィードバックすることで計算精度を高めるとともに実験条件を改良し、加速プロトン発生数の飛躍的増大を目指す。

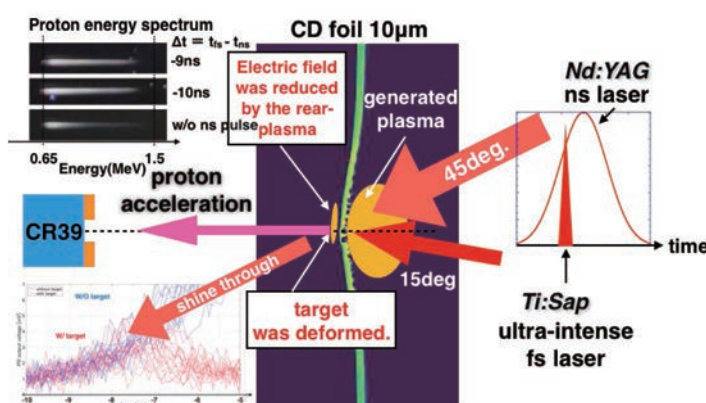


図 1 実験配置及び結果概要

レーザー吸収制御によるシリコンの微細加工に関する基礎研究

草場光博 大阪産業大学

本研究では、2波長のパルスレーザー光を組み合わせ、レーザーと固体との相互作用を精密に制御した高効率・超微細レーザー加工技術の基盤を構築することを目指している。特にシリコンの微細加工をする上で重要パラメーターとなるアブレーション閾値の測定および表面形状変化について調べた。発振波長 800nm、パルス幅 150fs、繰り返し周波数 1kHz のフェムト秒レーザーパルスを BBO 結晶を用いて 2 倍波 (400 nm) に変換したものをアブレーション光源として用いた。ビーム形状はガウシアン形状でビーム径は約 25 μm (FW σ)であった。レーザーエネルギー安定度は約 10%(RMS)であった。シリコン基板は鏡面研磨されたシリコン (大きさ約 1.5 cm \times 1.5 cm、厚さ約 620 μm 、抵抗率 1-100 Ωcm 、算術平均面粗さ 10 nm) を用いた。レーザー照射により形成された加工痕はレーザー顕微鏡 (OLS4500, OLYMPUS) で観察し、加工痕の深さを測定することでアブレーション率を求めた。レーザーフルエンスに対するアブレーション率の関係からアブレーション領域は 2 つ存在し、シリコンの閾値フルエンスはそれぞれ 0.10 および 0.30 J/cm^2 であった。低フルエンス側のアブレーション閾値 (0.10 J/cm^2) は、ナノ秒レーザーによる値 (1.4 J/cm^2) に比べて 1/14 倍であった。図 1 にレーザーフルエンス 0.10 および 0.70 J/cm^2 で照射したときのシリコンの算術平均面粗さのパルス数

依存性を示す。0.10 J/cm^2 で照射した場合、200 パルスを境に算術平均面粗さに変化が見られた。電子顕微鏡観察結果より、これは表面に 200~300 nm の周期間隔の微細構造が形成されることによるものと考えている。また、0.70 J/cm^2 で照射した場合は、算術平均面粗さがパルス数の増加とともに増加する傾向にあり、マイクロメートルオーダーの構造が形成されることが分かった。

【成果報告】

- [1]”エキシマレーザー非熱的加工によるシリコン太陽電池表面ナノ微細構造形成”, レーザー研究, 47, (2019)pp. 160-163.
- [2]”フェムト秒レーザー照射によるシリコンおよびシリコン太陽電池の表面形状変化と結晶構造”, 電気学会光応用・視覚研究会, LAV-19-024(2019).
- [3]”Reflectance and Crystallinity of Silicon Solar Cells with LIPSS Produced by XeCl Excimer Laser”, The 15th Int. Conf. Laser Ablation, Mon PS-118(2019).
- [4]”800 nm と 400 nm のフェムト秒レーザー加工されたシリコン太陽電池表面の黒色化と結晶構造の比較”, レーザー学会学術講演会第 40 回年次大会, D02-20p-V-01(2019).

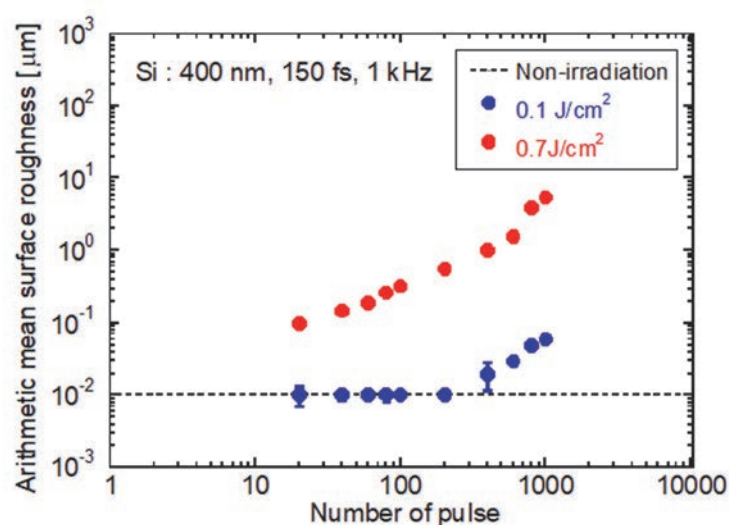


図 1 シリコン表面の算術平均面粗さのパルス数依存性

カーボンナノチューブを用いた ISOL 用標的の開発

大西哲哉 理化学研究所

[目的] 不安定核生成法の一つである ISOL 法では、生成した不安定核を取り出すために、標的を高温(2000℃近傍)で使用する。そのため標的材料には高温でも蒸気圧の低い炭化物が用いられるが、高温環境下では炭化物の焼結が進み、標的寿命は一週間程度である。先行研究において、カーボンナノチューブを用いた標的では標的寿命がかなり延長する結果が得られている。本研究では、カーボンナノチューブや他の炭素材料を用い、新規の ISOL 標的開発を目指す。

[実験手法] 対象とする元素の化合物(酸化物など)を炭素材料と混合し、高圧をかけ、厚さ 1mm、直径 20 mm 程度の円板標的を作成する。作成した標的は真空チェンバー内で高温に加熱し、炭化物へと変換する。作成した炭化物標的は、電子顕微鏡を用いて、そのナノ構造を調べる。その後、加速器を用いて電子ビームもしくは陽子ビームを照射し、生成量の変化から標的寿命や生成効率などを調べる。本年度はグラフェンを用いた標的作成を試みた(カーボンナノチューブを用いた炭化標的は非常に酸化(燃焼)されやすいため、安全性を考慮した)。作業場所は核燃物質取り扱いの必要から、理化学研究所仁科加速器研究センターホットラボ室の Hood で、仁科センター市川進一氏と共に作業を行った。手順としては、まず酸化ウランを硝酸に溶解し硝酸ウラニル溶液を作成する。次に硝酸ウラニル溶液をグラフェンに含浸後、脱硝・酸化する。その後、円板標的を作成し、真空チェンバー内にて炭化物へと変換する。

[結果] 酸化ウラン(U_3O_8 :3.95g)を硝酸ウラニル溶液に転換後、グラフェン(1.45g)に含浸、引き続き脱硝・酸化作業を行った。結果を写真 1 に示した。従来の炭素粉(粒径 $\sim 20\ \mu\text{m}$)を用いた場合と

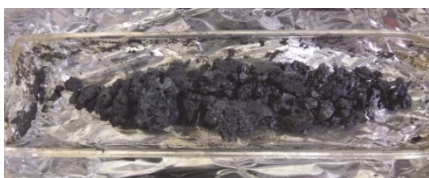


写真 1: 脱硝後のウラン+炭素

い、小粒の固めの塊が沢山できた。従来はもう少しサラサラとしていた。さらに、従来と大きく違うのはグラフェンの消費量である。炭素粉を用いた標的作成ではモル比で $\text{U}:\text{C}=1:8$ 程度になるように炭素を混合し、脱硝・酸化後のモル比は $\text{U}:\text{C}=1:6.3$

程度であった。しかしながら、同程度のグラフェン添加量 $\text{U}:\text{C}=1:8$

程度を用いた今回の実験では、脱硝・酸化後のモル比が $\text{U}:\text{C}=1:1.7$ となり、予想以上に炭素を消費してしまった。このまま標的を作成・炭化した場合、炭素が足りなくなり全体を炭化できないため、炭素粉やグラフェンなどの追添加を検討する必要が分かった。

[考察] グラフェンの結晶構造は比較的隙間が多く、脱硝・酸化作業時の流入空気中の酸素とグラフェンが反応し、二酸化炭素の形で消費されてしまったのではないかと推測する。この隙間構造が寿命を延ばすためのポイントでもあるので、今後はグラフェン使用量、並びに炭素の追添加などを検討しモル比の最適化を図る。さらに円板標的の作成と炭化及び照射実験を進める予定である。

[成果報告]特になし。

Development of a fast and efficient neutron trigger device for electron-RI scattering experiments

Akitomo Enokizono RIKEN

The main goal of this study is to research and develop a fast and efficient neutron trigger device for the SCRIT (Self-Confining RI Ion Target) experiment which is aiming at the world first facility for electron-RI scattering experiment at RIKEN. One of the future plans of the SCRIT project is to measure inelastic scattering processes and the neutron trigger device will be utilized for the future experiments. Since the SCRIT has the RI trapping device inside the electron storage ring, the neutron trigger device has to be installed in a high gamma background environment and a limited space. Therefore, a pulse-shape discrimination (PSD) type plastic scintillator, Eljen Technologies EJ-276 which is commercially available, is employed for the gamma/neutron detector. In addition, a compact ADC digitizer card with FPGA chip on-board (Tokuden Cosmo-Z 100MHz) will be used for the readout.

As the first step, the PSD capability was measured using EJ-276 and a conventional VME 100MHz digitizer board (V1724). Figure 1 (a) shows a sample of signal with ^{252}Cf source. Since the scintillator make PSD possible using a different amount of delayed scintillation emissions between gamma and neutron interactions, one can characterize the PSD as the ratio of the tail/total charges as shown in the figure (b). The integration times for total and tail regions have been optimized to maximize the PDS in the result, and the gamma and neutron peaks can be observed at ~ 0.22 and ~ 0.23 respectively. Here the capability of the PSD can be quantified as the figure of merit (FoM) = (The distance of the center of peaks)/(The sum of FWHMs). In this study the FoM was estimated as ~ 1.7 .

The detector has more room be improved with respect to FoM . The most effective improvement will be achieved by reducing the noise level on the detector since the tail region is very sensitive to it. A low noise power supply for the PMT is used for the study, but it was found that there were many other noise contributions which have to be suppressed.

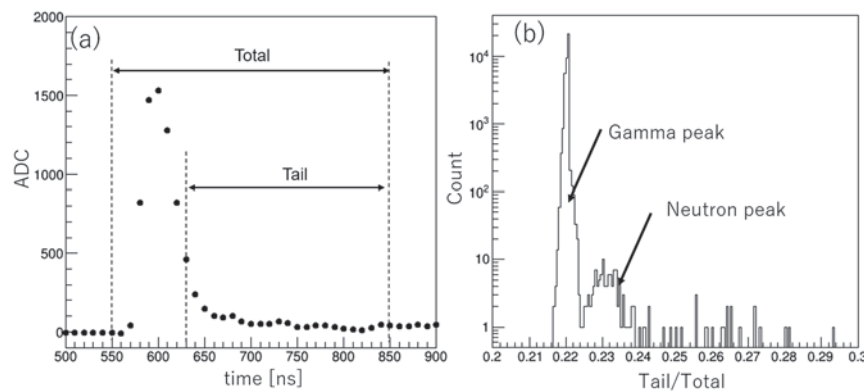


Figure 1 (a) A sample of ^{252}Cf signal taken with EJ-276 and 100MHz ADC digitizer. (b) The ratio of Tail/Total using the optimized integration parameters.

化学反応の量子制御を目指した CEP 安定化自由電子レーザーのための 省電力型超伝導加速空洞の製作方法の高度化

羽島良一 量子科学技術研究開発機構

位相制御された自由電子レーザーを実現するために必要な省電力型超伝導加速空洞の製造技術の高度化に向けて、4 K で動作可能な超伝導スポーク加速空洞の製造技術の確立を目指した研究を進めた。

電子ビーム溶接（EBW）条件出し試験を行い、その結果、焦点位置ずれとして、 $\pm 5\text{mm}$ 、入射角度 20 度以内であれば、溶接部分に大きな違いは見られないことを確認した。1 回で溶接する範囲を細かく分割すると焦点位置ずれや入射角度を小さくすることができるが、作業工程が増え、重なり部分も多くなるので、好ましくない。そのため、それぞれの溶接区画は出来るだけ大きくなるように溶接を行う方針とした。EBW 装置の回転軸からスポークのビーム軸とのオフセット、回転角度をパラメータとして、焦点位置ずれや入射角度を小さくする条件を探した結果を図 1 に示す。側面部分はスポーク側面形状で直線や円弧などある程度の大きさの区画に分割することにより、焦点位置ずれは 3.8mm 以下に、入射角度は 17.3 度以下にすることができる。また根元部分は 2 分割することにより、焦点位置ずれは 2.6mm 以下に、入射角度は 19.1 度以下にすることができる。

これらの結果をもとにフルスポーク溶接のための治具を製作し、フルスポーク形状にするための EBW の準備を進めた。

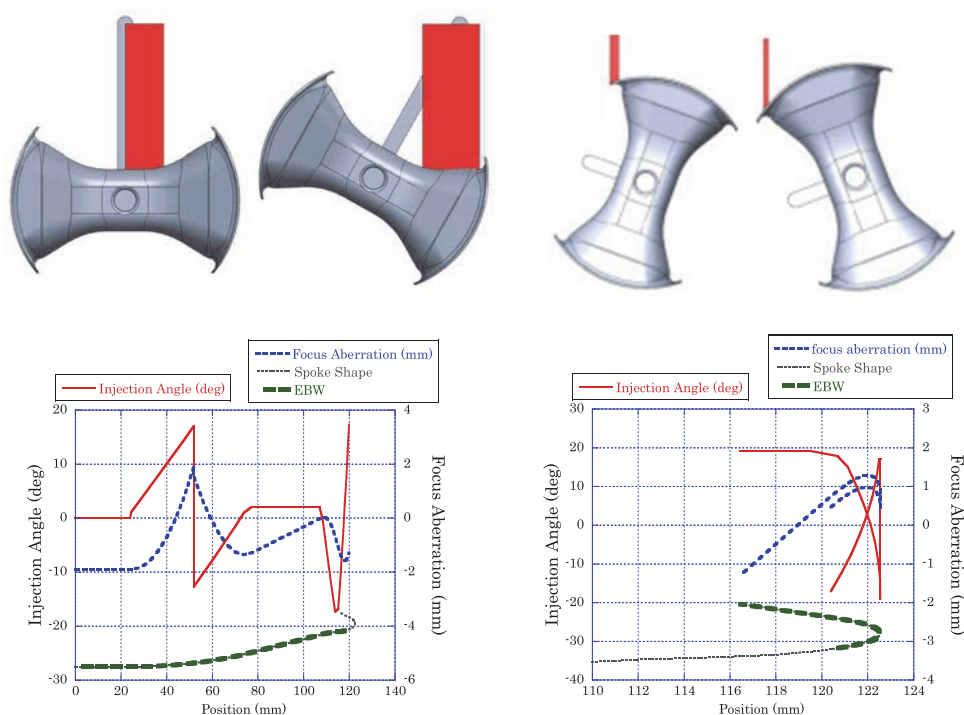


図 1：スポーク空洞の側面部分（左）と根元部分（右）の EBW 照射範囲と焦点位置ずれ、入射角度の変化

発表論文

[1] 沢村 勝 他、第 16 回日本加速器学会年会論文集、pp.709-711 (2019).

グラファイト化薄膜テープ標的を用いたレーザー駆動イオン加速実験

近藤康太郎 量子科学技術研究開発機構

集光強度が 10^{19} W/cm² を超える高強度レーザーと物質との相互作用は高い強度の電磁場の発生を引き起こすとともに、MeV 級のイオンや相対論的電子さらには X 線等の電磁波が発生し、物理現象自体もさることながら応用的面においても興味深い。レーザーと薄膜物質との相互作用によるイオン加速の中で、比較的その加速メカニズムの理解が進んでいる TNSA (Target Normal Sheath Acceleration) は、再現性が高く、加速されたイオンの空間パターンも比較的良好であるため、炭素イオンビームを用いた医療応用を含めた研究に適した手法である。しかし、TNSA において、薄膜の表層に存在する炭化水素を代表とする吸着汚染層からのイオン、特に電荷質量比の高い水素イオンが高強度レーザーにより標的主成分の重イオンより先立って加速されるため、炭素イオンをはじめとした重イオンの発生および加速効率の低下が引き起こされている。

そこで、我々は先行研究で進められている加熱による熱脱離反応に伴う汚染層の洗浄処理を施した手法ではなく、外部レーザー照射により、積極的に物質改質した薄膜を用いることで、重イオン加速の格段な高度化を狙う。具体的には、XeCl エキシマレーザーを照射させ、炭化が期待されるポリイミドテープ薄膜を標的として用いる。一方、京都大学化学研究所先端ビームナノ科学センター・レーザー物質科学研究領域が有する高強度フェムト秒レーザーは集光強度が 10^{19} W/cm² を超えるため、MeV/u 級のイオンを発生させることができる。数 MeV/u の炭素イオン発生を高効率に発生させることができれば、医療用シンクロトン加速器の入射器としての利用が視野に入るため、このパラメーター領域で炭素イオン発生純度、発生量、エネルギーの高度化を図ることの意義は非常に大きい。本研究では、XeCl エキシマレーザーにより物質改質させた薄膜の炭化を実験的に明らかにするとともに、その薄膜標的を用いて高強度レーザー駆動の炭素イオン加速の実証を目指す。

大阪産業大学工学部、京都大学化学研究所との共同・協力研究により、XeCl エキシマレーザーが照射されたポリイミドの炭素化が顕微ラマン分光結果より実験的に確認されるとともに、炭素膜厚制御に関する知見を得た[1]。また、加速されるイオンの角度分布および計測されるイオンエネルギー可変型の小型トムソンパラボラ分光器を開発[2]した。標的試料の評価および診断装置の開発により、エキシマレーザーによって炭化された薄膜標的を用いたレーザー駆動イオン加速実験の準備が整った。今年度末に京都大学化学研究所先端ビームナノ科学センター・レーザー物質科学研究領域が有する高強度フェムト秒レーザーを用いて炭素イオン加速の実験を行う予定である。

[1] 草場博光, 児子 史崇, 近藤 康太郎, 西内 満美子, 榊泰直, 桐山博光, 橋田昌樹, 阪部周二, 電気学会論文誌 A (2020) 掲載予定

[2] Sadaoki Kojima, Shunsuke Inoue, Thanh Hung Dinh, Noboru Hasegawa, Michiaki Mori, Hironao Sakaki, Yoichi Yamamoto, Teru Sasaki, Keiichiro Shiokawa, Kotaro Kondo, Takashi Yamanaka, Masaki Hashida, Shuji Sakabe, Masaharu Nishikino, and Kiminori Kondo, submitted.

High pressure approach to the synthesis of novel ferroelectric photovoltaic transition metal oxides

Wei-tin Chen National Taiwan University

Introduction

Although the photovoltaic effect in ferroelectric oxides has been known for decades, the low power conversion efficiency (PCE) due to large band gap (typically ~ 3 eV) make these transition metal oxides (TMO) undesirable for photovoltaics. The renewed interests were stimulated owing to recent discovery of photovoltaic effect in ferroelectric BiFeO₃ single crystal and thin film samples, where their efficient ferroelectric polarization-driven carrier separation and the large above-bandgap generated photo-voltages may enable PCE beyond the maximum in a conventional *p-n* junction solar cell. Therefore, searching for ferroelectric TMOs with large electric polarization, small band gap and final high output power is of great interest and can lead this scientific curiosity toward the future solar energy applications. Among recent studied polar transition metal oxides, ScFeO₃ shows multiferroic properties and is one of the promising ferroelectric photovoltaics materials. With high pressure high temperature techniques, it is promising to explorer and modify ScFeO₃ related materials with potential ferroelectric photovoltaics properties.¹ With this purpose, Shimakawa Lab at ICR is one of the most experienced facility to conduct such researches.

Results and discussion

The target ScFe_{1-x}Cr_xO₃ solid solution (SFCO) with $x = 0.1, 0.15, 0.2$ and 0.5 were prepared with 8 and 10 GPa and 1300 C HPHT synthesis conditions. The preliminary result indicated that the substitution limit for LiNbO₃-type SFCO is below $x = 0.2$ with conducted synthesis conditions. Further extreme condition synthesis were carried out with 17 GPa and 1000 C HPHT synthesis condition, and it was shown that the solid solution with $x = 0.1, 0.15, 0.2$ and 0.5 were all crystalize in GdFeO₃-type structure (Fig.1). The resultant lattice constants and volumes followed Vegard's law and confirmed that substitution were successful. The GdFeO₃-type instead of LiNbO₃-type structure, however, indicated that the obtained SFCO compounds would be lack of desired spontaneous polarization. In order to obtain the target compounds exhibiting ferroelectric and photovoltaic behaviors, it is essential to explore SFCO compositions with various synthesis conditions. Further systematic experiments are in schedule to construct detailed compositional-pressure-temperature phase diagrams.

References

1. T.-Y. Cai *et. al.*, *Phys. Rev. Applied.*, **8**, 034034 (2017)

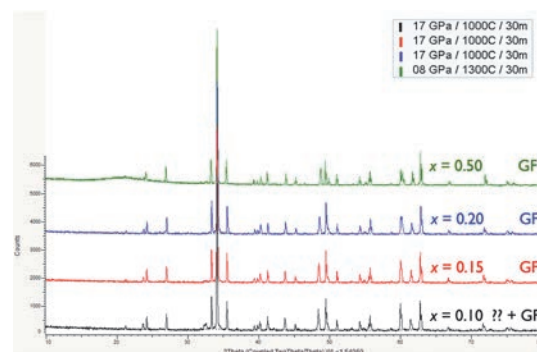


Figure 1 In house XRD patterns of solid solution synthesized with ultra HPHT conditions.

Catalysis research of transition metal oxides

Haichuan Guo Ningbo Institute of Industrial Technology

Introduction

The catalysis properties of transition metal oxides are strongly related with the crystal structure and band gap of bulk materials. Transition metal oxides synthesized under extreme conditions (high temperature and high pressure) always exhibit unusual structure and band gap. In this research, we synthesized A-site ordered perovskite-structured oxides $\text{CaCu}_3\text{Sn}_4\text{O}_{12}$ (CCSO) and $\text{SrCu}_3\text{Sn}_4\text{O}_{12}$ (SCSO) using high-pressure equipment in ICR and investigated the properties of catalysis reaction.

Experiments and results

Raw materials of $\text{CaCO}_3/\text{SrCO}_3$, CuO and SnO_2 were mixed and calcined at 1000°C . Obtained powder was packed in Pt capsule and treated at 6 GPa and 1000°C for 30 minutes using cubic-anvil high-pressure equipment in ICR. Because the redox reaction is always accompanied by electron transfer, catalysis properties were investigated by measuring the resistance change of sample in different organic gas specimens. Powder sample was coated on Al_2O_3 substrate, where Au electrodes were precoated. The ratio of resistance of sample measured in 100 ppm organic gas (R_g) to that measured in air (R_a) was used to appraise the catalysis activity. As shown in Fig. 1, SCSO exhibits higher resistance change than CCSO, which indicates the higher catalysis activity of SCSO than CCSO. The substitution of Ca^{2+} using larger Sr^{2+} changes the lattice parameter from 7.6424 \AA to 7.6761 \AA , and also affect the bond length, bond angle as well as band gap in the oxide, thereby increases the catalysis activity.

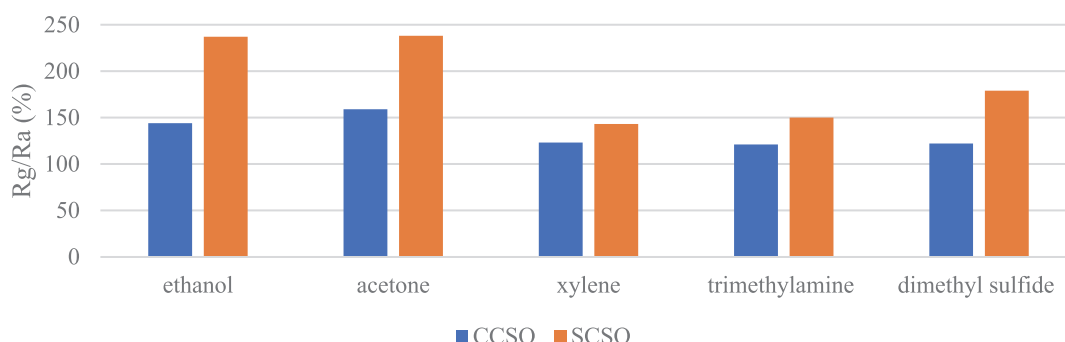


Fig. 1 resistance changes of CCSO and SCSO in organic gases

In addition, a new iron carbide catalyst used in oxygen-reduction reaction was also investigated using Mössbauer spectrum equipment in ICR. The research paper has been submitted.

“Small molecule activation using anionic crypto-FLPs”

Rainer Streubel University of Bonn

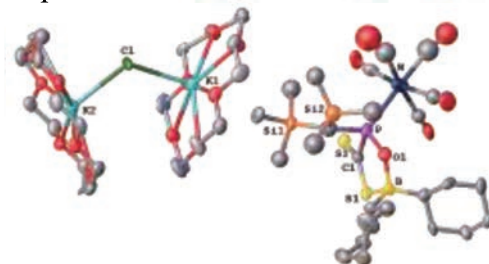
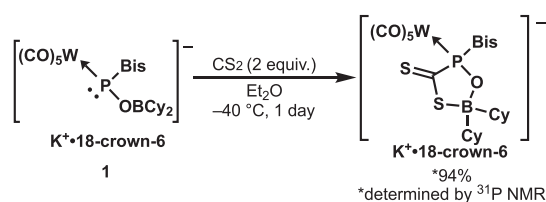
This collaborative research project was carried out with Prof. Norihiro Tokitoh (ICR, University of Kyoto) including 3 PhD exchange students (Florian Gleim and David Becker from Bonn and Kento Iwai from Kyoto).

Objectives: The purpose of the project is to develop novel chemistry using anionic FLPs, featuring group 14/15 elements with an anionic phosphorus as Lewis base and a group 14 element (E = C-Pb) in tetravalent coordination with E-halogeno functionality, in small molecule activation.

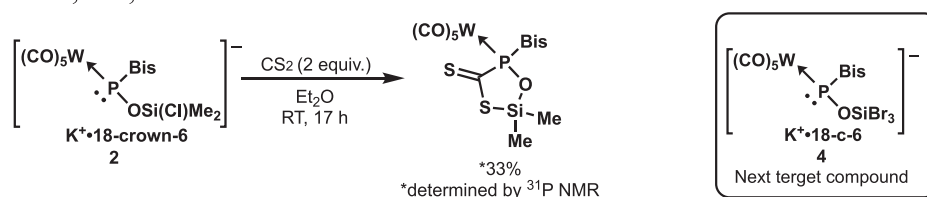
Experimental methods: Inert-gas synthesis techniques, analytical methods (NMR, IR, UV/vis, CV, X-ray)

Experimental results: The studies focused on i) reactions of crypto-FLPs containing B (**1**) and Si(Cl) (**2**) LA centers with carbon disulfide and ii) synthesis of new derivatives (**3**) bearing Si(Br) LA centers.

Discussion: Reactions of **1** with CS₂ led to the targeted product which was confirmed as co-crystal with KCl.



In case of **2**, the reaction with CS₂ may have yielded the targeted product according to ³¹P NMR spectroscopy, but could not be isolated. The newly targeted SiBr-substituted derivative **4** might have been formed, too, but couldn't be isolated due to time constraints.



Publications: R. Kunzmann, Y. Omatsu, G. Schnakenburg, A. Espinosa Ferao, T. Yanagisawa, N. Tokitoh, R. Streubel, *A synthon for unknown 1,3-zwitterions? – A K/OR phosphinidenoid complex with an additional Si-Cl function*, *Chem. Commun.* **2020**, submitted; *Synthesis and Reactivity of Siloxy(organyl)phosphane Metal(0) Complexes*, presentation at the 99th Chemical Society Japan Meeting, 16th -19th March, **2019**, Kobe/Japan by Y. Omatsu, R. Kunzmann, A. Schmer, Y. Mizuhata, R. Streubel, N. Tokitoh; workshop “*In Pursuit of Unprecedented Heavier Main Group Element Compounds*” by Prof. N. Tokitoh, Bonn, October 23-25, **2019**; scientific lecture & discussion “*Chemistry of tricyclic 1,4-diphosphinines and bis(N-heterocyclic carbenes)*” of Prof. R. Streubel, Kyoto, November 25-30, **2019**).

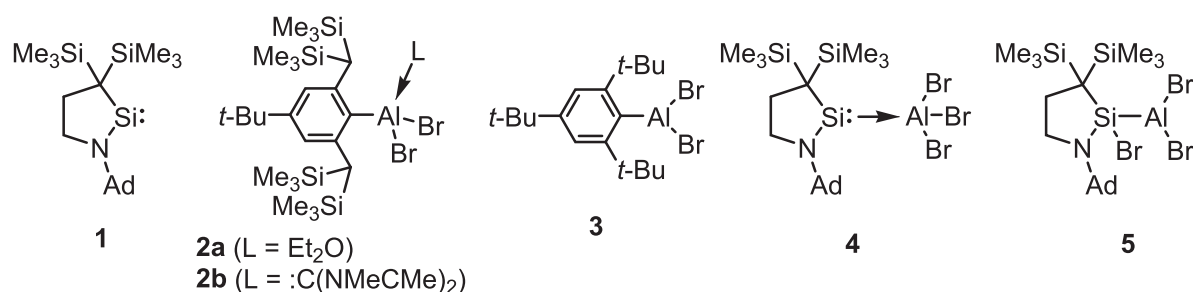
Development of unsymmetrical π -electron systems of heavier main group elements and elucidation of their property

Takeaki Iwamoto Tohoku University

Objectives: We aimed at the development of novel π -electron systems of heavier main group elements that have multiple bonds between two different elements, especially group-14 and -13 elements, which are still scarce compared to other π -electron systems.

Experimental methods: To synthesize the unsymmetrical π -electron systems $R_2Si=AlR'$, we investigated the preparation of the corresponding dihalogenated precursor $R_2SiX-AlR'_X$ by the insertion reaction of isolable silylene **1**, which was developed by our group (group-14 element part), into the Al-X bond of halogenated aluminum compounds (group-13 element part).

Experimental Results and Discussion: We examined the reactions of **1** with several haloalmanes such as **2a**, **2b**, and **3** that contain a bulky aryl protecting group under various reaction conditions. However, the reactions did not proceed even upon heating. Interestingly, the reaction of **1** with less bulky $AlBr_3$ proceeded cleanly to provide the silylene-coordinated $AlBr_3$ (**4**), which was identified by NMR spectroscopy and X-ray diffraction analysis, in a moderate yield in contrast to the expected Al-Br insertion product **5**.



The present results, especially the formation of **4**, imply that the insertion reactions of silylene **1** into the aluminum-halogen bond to provide the desired precursor $R_2SiX-(AlR'_X)$ are difficult reflecting the stronger aluminum-halogen bond compared with the corresponding silicon-halogen bond. However, **4** can provide a promising precursor for $R_2Si=AlR'$. As a preliminary result, we found that one bromine group in **4** can be replaced by an amido group (NR''_2) to provide $R_2Si \rightarrow AlBr_2(NR''_2)$ which may provide the desired species $R_2Si=AlR'$ after the reductive debromination.

This project was done in collaboration with Professor Norihiro Tokitoh (ICR Partner Researcher) and Professor Shigeyoshi Inoue (International Collaborating Researcher, Technical University of München, Germany).

Mechanistic studies of C–H bond functionalization reactions catalyzed by 3d transition metals

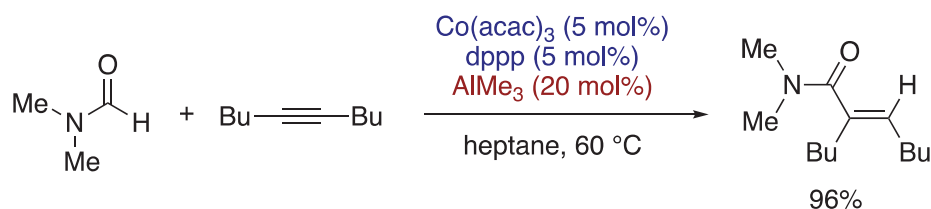
Naohiko Yoshikai Nanyang Technological University

Objective

This research project aims at the development of highly efficient C–H bond functionalization reactions catalyzed by 3d transition metals, especially cobalt, through collaboration with the group of Prof. Masaharu Nakamura (Kyoto University, ICR). Combining the expertise of both the research groups, the project intends to gain deeper mechanistic insight into cobalt catalysis and translate the knowledge into more efficient and selective cobalt catalysis.

Results and Discussion

Our earlier study on the cobalt-catalyzed, chelation-assisted hydroarylation of alkynes provided insight into the nature of low-valent cobalt species generated from cobalt salts, monodentate phosphines, and Grignard reagents. This insight, along with literature precedents on the mechanism of C–H activation by 3d transition metals such as nickel and cobalt, inspired us to explore the potential of low-valent cobalt catalysts for C–H activation without chelation assistance. Upon extensive screening study, we have found that a catalytic system comprised of a cobalt salt, a diphosphine ligand, and trimethylaluminum (AlMe_3) promotes the addition of formamides to alkynes with high *syn*-selectivity (see below scheme). A series of control experiments suggest that AlMe_3 not only acts as a reductant to generate a low-valent cobalt species but also as a Lewis acid to activate the formamide. The C–H activation is assumed to proceed via a so-called ligand-to-ligand hydrogen transfer mechanism. The scope of this cobalt/aluminum catalytic system has been extended to the addition of other Lewis basic substrates such as pyridones, pyridines, thiazoles, and oxazoles to alkynes via site-selective C–H activation. The nature of the catalytically active low-valent cobalt–diphosphine species is currently under investigation.



Reference

Wang, C.-S.; Di Monaco, S.; Thai, A. N.; Wang, C.; Yoshikai, N. *ChemRxiv* **2020**, DOI: 10.26434/chemrxiv.11760519.v1.

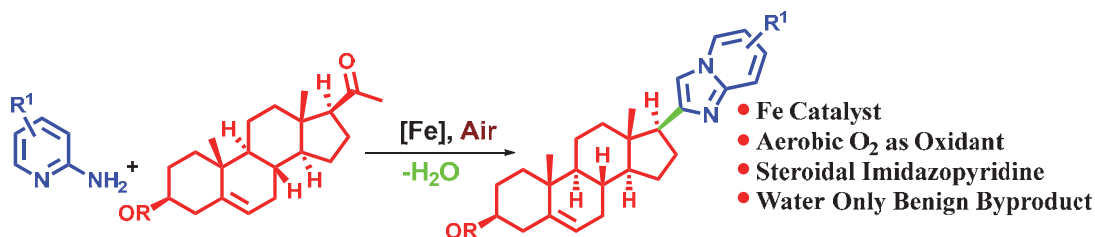
Development of iron-catalyzed strategies for diversity oriented synthesis of heterocycles and carbocycles

Alakananda Hajra Visva-Bharati University

Objective: Fe-catalyzed synthesis of Steroidal Imidazo[1,2-*a*]pyridines

Imidazopyridine, an important class of nitrogen containing heterocycles, shows a wide range of biological activities such as antitumor, antiparasitic, antiviral, antimicrobial, fungicidal, anti-inflammatory, hypnotic etc. In addition, this motif is the core structure of some marketed drugs such as necopidem, zolpidem, olprinone, saripidem, zolimidine, alpidem, etc. Furthermore, few of them exhibit excited-state intramolecular proton transfer.

An efficient and practical method has been developed for the synthesis of steroidal imidazo[1,2-*a*]pyridines *via* cost-effective and environmentally benign FeCl₃-catalyzed tandem C-H functionalization/oxidative amination. A library of imidazo[1,2-*a*]pyridines were directly synthesized from readily available 2-aminopyridines and steroidal ketones in aerobic conditions.



Presently we are focusing on the precise role of FeCl₃ and late stage modification of the compound. To the best of our knowledge this is the first report for the synthesis of steroidal imidazo[1,2-*a*]pyridines *via* iron-catalyzed tandem C-H functionalization/oxidative amination. Easily available basic chemicals as starting materials, less expensive metal catalyst, aerobic reaction conditions, tolerance of a wide range of functional groups, operational simplicity and practical applicability on a gram-scale are the notable advantages of this present protocol.

Iron-catalyzed carbometalation of heterobicyclic alkenes: development of asymmetric reactions and application to synthesis of polycyclic aromatic hydrocarbons

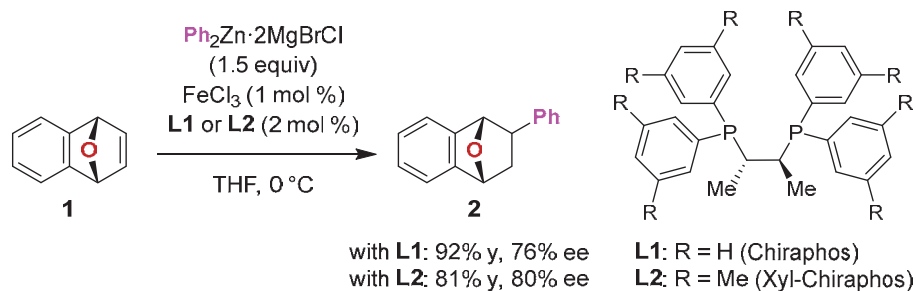
Shingo Ito Nanyang Technological University

Objective

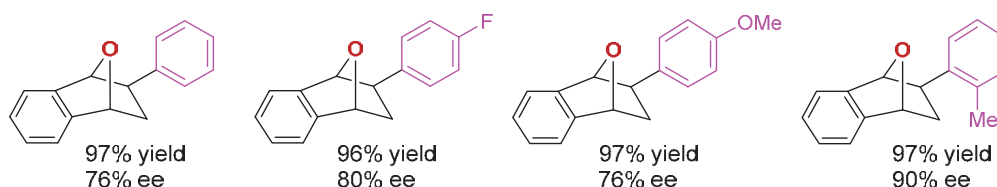
We previously developed the iron-catalyzed diastereoselective carbometalation of heterobicyclic alkenes that proceeds without undesired β -heteroatom elimination.¹ In this collaborative research, we developed an asymmetric version of this carbometalation reaction, which could provide important building blocks in organic synthesis.

Results and Discussion

In order to develop enantioselective carbometalation of oxabicyclic alkene **1** with phenylzinc reagent **2**, the reaction conditions were screened. As a result it was found that (*S,S*)-chiraphos (**L1**) and its 3,5-xylyl analogue (**L2**) afforded the carbometalation products in good yields with high enantiomeric excess values of 76 and 80%, respectively.



With the established method in our hand, the scope of the carbometalation reaction of oxabicyclic alkenes **1** was investigated, as shown partially in the figure below. A variety of alkene substrates and arylzinc reagents could be used. The highest enantiomeric excess value of 90% was achieved when the *o*-tolylzinc reagent was used.



Reference

- 1) S. Ito, T. Itoh, M. Nakamura, Diastereoselective carbometalation of oxa- and azabicyclic alkenes under iron catalysis, *Angew. Chem. Int. Ed.* **2011**, 49, 454–457.

Open-cage fullerenes incorporating hydrogen as n-type composite materials for polymer solar cell applications

Shih-Ching Chuang National Chiao Tung University

Solar cell have been attracting considerable attention for several years. Organic photovoltaics (OPVs) is a potential photovoltaic devices for the development of solar technology. Thin-film organic photovoltaics (OPVs), which embed poly(3-hexyl thiophene-2,5-diyl) (P3HT) and fullerene derivative,¹ [6,6]-phenyl-C₆₁ butyric acid methyl ester (PC₆₁BM) in the active layer,² have been recognized for generating power efficiently under illumination.³ For higher power conversion efficiency (PCE) of OPVs, we are focused on active layer which requires n,p-materials with balanced carrier mobility for reduction of the space charge which causes carriers recombination. Therefore, we have explored derivatives that is a series of open-cage fullerenes as n-type materials⁴ and intended to incorporaing hydrogen in a n-type open-cage fullerene material in order to improve photovoltaic properties by examining the aggregation behavior of n-type materials in a thin film.

First, we prepared open-cage fullerenes **6** according to a reported method.⁴ For H₂-insertion into the cage, the derivative **6a-b** was exposed to 445 atm of hydrogen at 200 °C for 8 h to provid H₂@**6a-b**, which were determined to be 70/66 (Figure 1).

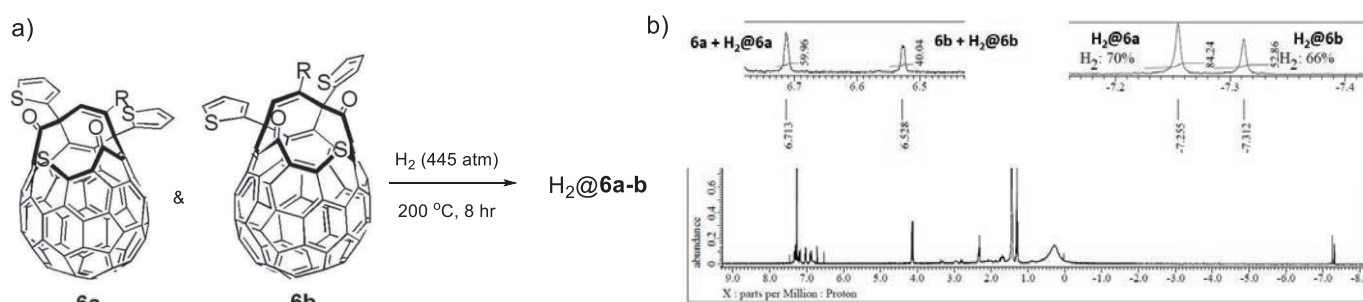


Figure 1. ¹H NMR spectroscopy of the encapsulation ratio of H₂@**6a-b**

In summary, the open-cage fullerene derivatives **6a-b** have been synthesized and the encapsulation ratio of H₂ inside **6a-b** is 70% and 66%, respectively. Future encapsulation of H₂ inside **6a-b** at higher ratio and application study in OPVs are in progress.

[1] Thilgen, C.; F. Diederich, *Chem. Rev.* **2006**, *106*(12), 5049-5135.

[2] Hummelen, J. C.; B. W. Knight; F. LePeq; F. Wudl; J. Yao; C. L. Wilkins, *J. Org. Chem.* **1995**, *60*(3), 532-538.

[3] Kim, J. Y.; K. Lee; N. E. Coates; D. Moses; T.-Q. Nguyen; M. Dante; A. J. Heeger, *Science* **2007**, *317*(5835), 222-225.

[4] Chen, C.-P.; Y.-W. Lin; J.-C. Horng; S.-C. Chuang, *Adv. Energy Mater.* **2011**, *1*(5), 776-780.

中赤外レーザー光源の開発とナノ物質科学への応用

板谷治郎 東京大学

目的

ペロブスカイト半導体は、高いキャリア移動度、高い光電変換効率など優れた光学および電気的特性有することから太陽電池だけでなく LED やレーザーなど様々な光デバイスへの応用研究が精力的に行われている。一方で、近年、高強度な光パルスと固体材料との非線形光学相互作用を介して、高次高調波発生 (HHG) が精力的に研究されている。強い光電場によって結晶内部の電子や正孔 (キャリア) が強く駆動される結果、入射光の整数倍の高いフォトンエネルギーをもつ光を発生する現象と考えられている。本研究では、簡便に大面積な薄膜試料の作製が可能なペロブスカイト半導体に対し、新たな高調波発生光源への応用と発生メカニズムの理解を目指し研究を行った。

実験方法・実験結果

溶液処理によって作製した 3 種類のペロブスカイト半導体[MAPbX₃; MA: methylammonium), X: I, Br, Cl]の多結晶薄膜試料に、強い中赤外レーザーパルス (ピーク電場: 10MV/cm、波長: 3.5μm) を照射し、可視光から紫外領域にわたる高次高調波発生を測定した。バンドギャップエネルギーの大きな MAPbCl₃ 試料 (E_g=3.2eV) では、高調波成分の試料を伝搬中の再吸収が抑制され、13 次に至る高次高調波成分 (フォトンエネルギー4.6eV) の観測に成功した。発生効率は、高調波発生実験のモデル物質の一つである半導体 GaSe に比べて発生効率が 10 倍以上に達することがわかった。

考察

理論的な数値計算手法を用いて高調波発生メカニズムについての考察をした結果、レーザー電場によって伝導帯と価電子帯の間でキャリア分布が非線形に変化することが高調波発生主な原因であることが初めてわかった。従来、高次高調波の発生メカニズムとして光電場で励起された電子が、非調和な伝導帯内を電子が加速運動することが主要な原因であると考えられてきたが、その理解の深化に成功したと言える。今回の研究で得られた、ペロブスカイト半導体からの高効率な高調波発生観測と、新たな発生メカニズムの提唱は今後の強電場非線形光学の更なる発展に寄与するものと考えられる。以上に述べた共同研究による成果は、学術論文として公表した[1]。

成果報告

[1] Hideki Hirori, Peiyu Xia, Yasushi Shinohara, Tomohito Otake, Yasuyuki Sanari, Hirokazu Tahara, Nobuhisa Ishi, Jiro Itatani, Kenichi L. Ishikawa, Tomoko Aharen, Masashi Ozaki, Atsushi Wakamiya, and Yoshihiko Kanemitsu, "High-order harmonic generation from hybrid organic-inorganic perovskite thin films", APL Materials, 7, 041107 (2019). [doi: 10.1063/1.5090935, Editors' Pick]

Study on the mechanism for the stability of an In-doped novel Fe–Pd phase

Yasutomi Tatetsu Meio University

Transforming crystal structures of materials by adding pressure, heat, or other elements is one of the key methods to discover novel physical properties. Many scientists have been investigating the possibility of creating novel materials by introducing third elements into stable binary nanoparticles with advanced chemical synthesis techniques. Recently, a new $Z3$ -type $\text{Fe}(\text{Pd},\text{In})_3$ crystal structure, which is shown in the figure below, was discovered by Teranishi's group in Kyoto University. The new structure was synthesized by introducing a third element of In into $L1_2$ - FePd_3 , which is the thermodynamically stable phase of binary Fe–Pd systems. Although the addition of In might be the key behind this new finding, the physical aspects of In in stabilizing the new structure is unclear and cannot be understood deeply only through experiments.

In this study, we performed theoretical analyses for the stability of an In-doped novel Fe–Pd phase. We calculated formation energies of In-doped Fe–Pd systems using first-principles calculation code, OpenMX, to check the systems' stability. The model structures for the calculations were based on the chemical composition ratio of $Z3$ - FePd_3 obtained from experiments. The In sites were chosen by replacing Fe or Pd sites with a special-quasirandom-structure method implemented in the Alloy Theoretic Automate Toolkit. We investigated stable sites for In in the $Z3$ - FePd_3 structure by comparing formation energies and we found that an In stably occupies the Pd site rather than the Fe site. There are two different Wyckoff positions of Pd labelled by 2e and 2g in $Z3$ - FePd_3 . From detailed analyses, we concluded that the new $Z3$ -type $\text{Fe}(\text{Pd},\text{In})_3$ structure, in which a Pd atom at a 2e site is replaced with an In atom, is more stable than In-doped $L1_2$ - FePd_3 structures. We reached this conclusion by checking the formation energies. These results are consistent with the experimental results from XRD, EXAFS, and STEM-EDS analyses. This represents that the In atoms replace Pd atoms at the 2e sites in $Z3$ - FePd_3 . Further experimental and theoretical analyses are needed for deeper understanding of how an In effects the physical properties of $Z3$ -type $\text{Fe}(\text{Pd},\text{In})_3$.

We presented the results at the following three conferences below;

- May 17th ~ 19th, 2019: 20th Seminar on magnetism in Kyusyu-Yamaguchi-Okinawa 2019 (Kumamoto)
- Nov. 23rd, 2019: 19th Seminar on solid state physics at University of the Ryukyus (Okinawa)
- Mar. 2nd ~ 6th, 2020: APS March meeting (Denver, USA).

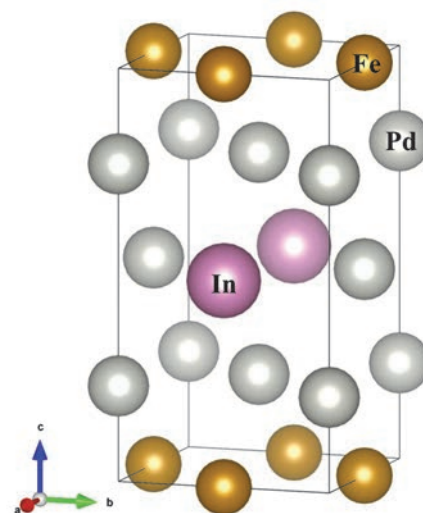


Figure : Novel structure of $Z3$ -type FePd_3

ウルシオール金属錯体を構成要素とする新規機能性塗料の開発

橘洋一 京都市産業技術研究所

【目的】

一般的に知られる黒色の漆は、顔料を使うことなく、漆に鉄粉を混合し攪拌することで得られる。これは、漆の主成分であるウルシオール（長鎖炭化水素を有するカテコール誘導体）と鉄イオンの錯体形成によるものとされている¹⁾。漆の硬化反応に寄与するカテコールは鉄イオンと反応するが、得られる黒漆塗膜は、漆本来の光沢・高級感を維持した状態となる。そこで、鉄イオンとカテコールとの錯体形成について、得られた黒漆塗膜の電気・光特性を評価し、新規機能性塗料へ向けた検討を行った。

【実験】

初めに、天然の漆に対し水酸化鉄(II)を所定の割合（0, 0.1, 0.25, 0.5, 0.75 wt%）で混合することで黒漆を得た。得られた黒漆を 20 °C/60% の条件下で乾燥させ、黒漆塗膜を形成させた。塗膜の膜厚は、濡れ膜厚で 55 μm , 110 μm とした。その後、黒漆塗膜を用い、200 nm～2500 nm における透過率測定（日立ハイテクサイエンス社製）及び絶縁破壊電圧（アジレント・テクノロジー社製）について検討を行った。

【結果】

得られた黒漆塗膜写真を図 1 に示す。混合する水酸化鉄(II)の割合が 1 wt% の場合、得られた黒漆の粘度が非常に高く、塗膜としての成形性が非常に悪かったため、本実験系での混合する水酸化鉄(II)の割合の最大は 0.75 wt% とした。また、水酸化鉄(II)の割合の減少に従って、塗膜の色は飴色

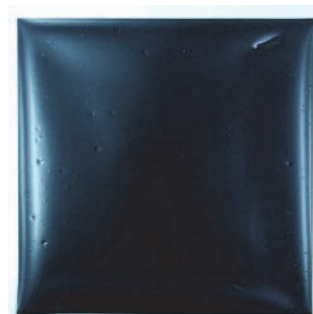


図 1. 得られた黒漆塗膜

次に、得られた塗膜の透過率測定を行った。水酸化鉄(II)を混合していない漆塗膜の場合、赤外領域において透過率は 90% を示し、波長の減少と共に透過率が減少し、500 nm において 0% となった。一方、水酸化鉄(II)を混合した場合、水酸化鉄(II)の割合の増加に従い減衰波長が高波長側へとシフトした。最終的に、水酸化鉄(II)を 0.75 wt% 混合した系では、赤外領域中で透過率の減少が見られ、可視光領域において透過率が 0% となった。

次に、黒漆塗膜の絶縁破壊電圧について検討を行った。その結果、膜厚による差は見られたものの、非常に高い絶縁破壊強さを有することがわかった。

【参考文献】

1) 漆—その科学と実技 寺田 晃, 小田 圭昭, 大藪 泰, 阿佐見 徹 1999, p87.

【謝辞】

塗膜物性測定に際し、三井化学株式会社 伊東氏にご協力頂きました。感謝申し上げます。

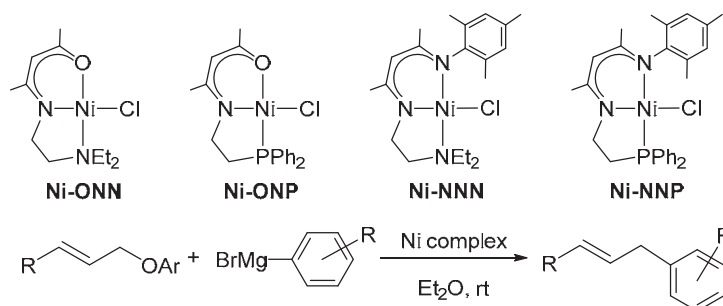
Study on nickelate complexes constructed by a monoanionic tridentate pincer-type ligand

Yoshitaka Yamaguchi Yokohama National University

Transition metal-catalyzed cross-coupling reactions are one of the most powerful tools for modern synthetic organic chemistry. The reactions of allylic electrophiles with aryl metal reagents provide reliable procedures for the construction of C(sp³)-C(sp²) bonds. Allylic electrophiles bearing efficient leaving groups such as allylic halides, acetates, and phosphates are commonly used in these reactions. In contrast, allylic ethers have been considered less-reactive electrophiles in the reaction, whereas these electrophiles are easily accessible, cheap, and easy to handle. Therefore, the development of an effective metal catalyst for the cross-coupling reaction utilizing allylic ethers as electrophiles has attracted considerable attention.

In recent years, tridentate pincer-type complexes have generated a lot of interest because the pincer-type ligand stabilizes the metal complexes and its properties can be tuned to achieve the best reactivity of the complex. We have recently reported the synthesis of a series of pincer-type nickel(II) complexes utilizing a combination of β-aminoketonato or β-diketiminato frameworks with a third donor such as an amino or phosphino group. Our systematic study on these nickel(II) complexes revealed that the modification of the ligand framework has a significant influence on the catalytic performance in the cross-coupling reaction of aryl halides with arylmagnesium reagents (*Dalton Trans.* **2018**, 47, 8003. *Eur. J. Inorg. Chem.* **2019**, 126.). In these reactions, we presumed that an anionic nickel(0) species, namely nickelate complex, derived from the reduction of nickel(II) complex with an excess amount of a Grignard reagent is an active intermediate in the reaction. Therefore, activation and smooth scission of the C-X bond in the electrophiles will be achieved. In order to elucidate the reactivity of the nickel(II) complex toward the relatively robust C-O bond in an allylic ether, we investigate the cross-coupling reaction of allylic ethers with arylmagnesium reagents using nickel(II) complexes.

To evaluate the catalytic activity of four types of nickel(II) complexes, we carried out the reaction of cinnamyl phenyl ether with 3 equivalents of *p*-tolylmagnesium bromide using 2.5 mol% of nickel complexes in THF at room temperature. Complex **Ni-ONP** showed high catalytic activity to give the coupled product in 86% yield. The choice of the solvent used is essential to produce the coupled product in satisfactory yield. After several examinations, Et₂O provided the best result, affording the product in 99% yield, from which the product was isolated in 94% yield. We also investigated the substrate scope of the reaction using various allylic ethers with arylmagnesium reagents (see reference [1]).



In this program, we have investigated the cross-coupling reaction of allylic aryl ethers with arylmagnesium reagents catalyzed by pincer-type nickel(II) complexes. Complex **Ni-ONP** bearing a β-aminoketonato framework tethering a PPh₂ group showed excellent catalyst performance. The reactions of a range of cinnamyl ether derivatives proceeded with high regioselectivity to afford the linear coupled products in high yield. Further investigations on mechanistic aspects are currently underway in our laboratory.

[1] Hashimoto, T.; Funatsu, K.; Ohtani, A.; Asano, E.; Yamaguchi Y. “Cross-coupling reaction of allylic ethers with aryl Grignard reagents catalyzed by a nickel pincer complex”, *Molecules* **2019**, 24, 2296.

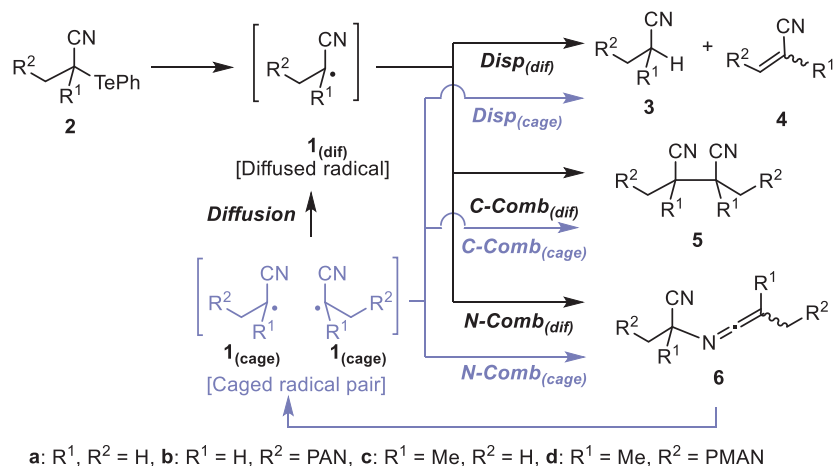
アクリロニトリル系ポリマー末端ラジカルの反応機構研究とその合成応用

中村泰之 物質・材料研究機構

研究の目的: ラジカル重合の基本反応の一つである停止反応の機構の理解は長年の課題であったが、近年の我々の研究により大きく進展している。本課題では化学研究所の山子茂教授と共同し、分野で高い重要性を持つポリマーであるアクリロニトリル系ポリマーについて、その重合停止反応の機構の詳細を明らかにした。

結果と考察: アクリロニトリルの重合成長ラジカル末端を模したモデルラジカル **1** の停止反応を有機テルル化合物 **2a** の光活性化反応を用いて行い、NMR により生成物を同定した。不均化 (**3a**、**4a**)、C-C 結合反応 (**5a**) に加えて、ポリアクリロニトリル末端モデルラジカル反応として初めて C-N 結合生成物 (**6a**) の生成を確認・単離し、それぞれの生成比（反応選択性）を決定した。不均化・C-C 結合へはこれまで我々が報告したように高粘度で不均化の選択性が増加するバルク粘度およびマイクロ粘度の効果が見られた。一方で C-N 結合の選択性に対する粘度の効果は明確ではなく、異なる溶媒パラメータの反応への関与が示唆された。同様にポリアクリロニトリル末端ラジカル停止反応においても不均化・CC 結合・CN 結合による生成物が生じることを確認し、モデル低分子ラジカル反応と同様に溶媒粘度と選択性に相関性を有することを示した。選択性はモデル低分子ラジカルで CC 結合と CN 結合は同程度の主機構であるのに対し、ポリマー末端ラジカルでは CC 結合が主であった。ケテンイミン **6** は熱的に不安定であり高温条件下では分解してラジカルペア (**1(cage)**) を与え、溶媒ケージ内でまたは拡散したラジカルとなることを経て停止反応を起こし、最終的に不均化・結合生成物を与えた。

本研究ではメタクリロニトリルの重合停止反応、および C-N 結合生成物の反応性についても詳細に検討した。



発表等：李、中村、山子、第 68 回高分子学会年次大会、2019、2K16

高性能ペロブスカイト太陽電池作成を指向した 高活性酸化スカベンジャーの開発

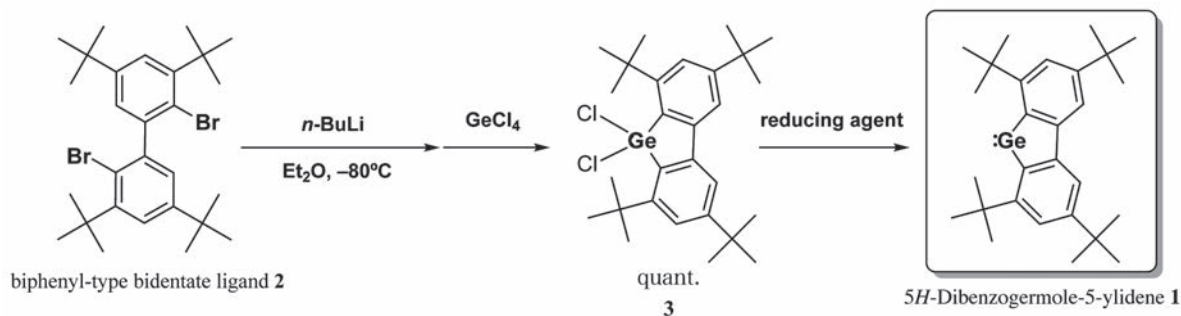
笹森貴裕 名古屋市立大学

1. 目的

本研究では、京都大学化学研究所・若宮淳志教授と連携して「高効率鉛フリーペロブスカイト太陽電池創出のための、有機物酸化スカベンジャーの開発」に取り組み、元素科学と機能物性化学の融合による先駆的な研究成果を格段に発展させることを目的とする。若宮教授が精力的に取り組んでいる高効率鉛フリーペロブスカイト太陽電池開発において、問題となるのは Pb^{2+} の代替として用いる金属イオンの酸化耐性が乏しい点である。 Pb^{2+} や Sn^{2+} など、用いる金属種のごく僅かな酸化も防ぐ高活性な有機酸化スカベンジャーの開発が必須となる。しかし、一般的な金属の酸化スカベンジャーは、作成したペロブスカイトへの混入が純度低下を招き、これもまた性能低下の一因となる。そこで、酸化スカベンジャー自身有機溶媒に可溶であることは勿論、酸化スカベンジャーとして作用した副生物もまた有機溶媒に可溶であるような、高性能有機物酸化スカベンジャーとして、新たなゲルマニウム二価化学種（ゲルミレン）の合成を目的とした。

2. 実験方法

目的とするゲルマニウム二価化学種（ゲルミレン）の自己多量化や不均化反応を防ぎ、また有機溶媒への溶解度を担保するために、かさ高い置換基を有するビフェニル型配位子を設計し、これをゲルマニウム上に導入した、新規な「ジベンゾゲルモール-5-イリデン誘導体 **1**」を合成目標とした。図のスキームに従い、合成研究を行った。



3. 実験結果と考察

二座配位子 **2** をリチオ化し、塩化ゲルマニウム(IV)を導入し、対応するジクロロゲルマン **3** を定量的に得た。化合物 **3** を $t\text{-BuLi}$ や KC_8 などの還元剤により還元し、目的とするゲルミレン **1** を発生させた。捕捉反応やスペクトル測定などにより **1** の発生を確認した。若宮教授に加え、共同研究者の吉田久美教授（名古屋大）、光藤耕一准教授（岡山大）、土屋敬広准教授（北里大）と研究討論を行い、研究を進めることができた。

4. 成果報告

論文作成準備中

ヘテロダイン干渉分光法を用いた鉛ペロブスカイト太陽電池の光電流の研究

小川佳宏 上越教育大学

鉛ペロブスカイト太陽電池は、その優れたエネルギー変換効率から新しい太陽電池材料として期待されている。鉛ペロブスカイト太陽電池の電氣的・光学的特性を理解する上で、媒質中の光キャリアダイナミクスを理解することが重要である。本研究では、鉛ペロブスカイト太陽電池の電子構造と電子-格子相互作用を、ヘテロダイン干渉分光法を用いて明らかにする。

ヘテロダイン干渉分光法では、相対位相を同期制御した光パルス対を用いており、実験系の振動の影響を受けないことから可視光領域でフーリエ分光を行うことができる。また、光電流をプローブとして用いることで電気感受率の実部と虚部を測定することができる。試料として、MAPbBr₃単結晶 (MA=CH₃NH₃) を用いた。薄膜試料ではなく数 mm 角の単結晶を用いることで、表面や界面の影響を小さくすることができる。また、バルク結晶ではバンド端の吸収スペクトルを測定することは困難であるが、光電流をプローブとすることでバンド端の測定を可能とした。

図 1(a)にヘテロダイン干渉分光法により測定した、バンド端における 160 K と 250 K での電気感受率の虚部のスペクトルを示す。バンドギャップエネルギー E_g の低エネルギー側にピークがあることがわかる。この低エネルギー側のピークのエネルギー E_A は温度低下に伴い高エネルギーシフトをするが、 E_g は低エネルギーシフトをする。このことから、この低エネルギー側のピークは励起子などが関係した遷移でないことがわかる。図 1(b)に E_g と E_A のエネルギー差 ΔE の温度依存性を示す。MAPbBr₃単結晶の LO フォノンのエネルギー(15.3 meV)を用いてボーズ分布関数でフィッティングしたものを実線で示す。実験値とよく一致したことから、低エネルギー側のピークはフォノンが関係した遷移であることがわかる。また、このピークの強度の温度依存性の解析から、この遷移が間接遷移であることが示された。以上のことから、このピークが MA⁺イオンの熱揺らぎに由来する Rashba スピン分裂バンドであることが示唆される。

[成果報告] 小川佳宏, 田原弘量, 金光義彦, ” 鉛ペロブスカイト太陽電池のヘテロダイン干渉分光 II “, 日本物理学会 2019 年秋季大会 2019 年 9 月 11 日

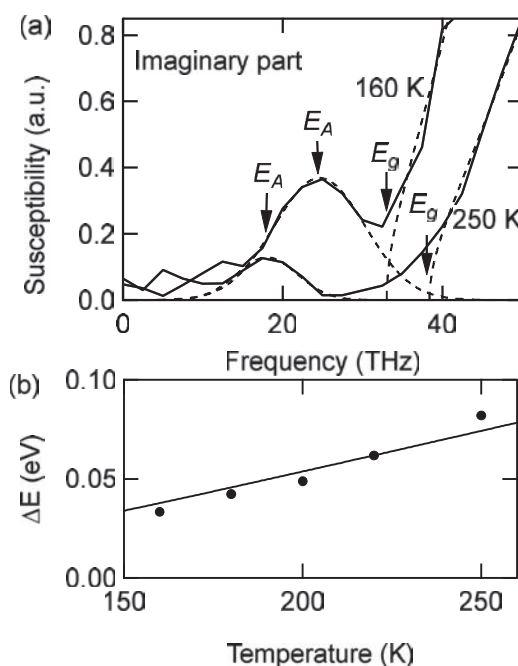


図 1(a) バンド端における電気感受率の虚部のスペクトル (b) E_g と E_A のエネルギー差 ΔE の温度依存性

Network analyses for data-driven exploration and hypothesis testing in microbial ecology

Samuel Chaffron CNRS UMR6004

Microbial communities fulfill important ecological and biogeochemical roles in our environment. Continuous technological developments in nucleic acids sequencing are revealing the under-explored diversity of microbes forming these communities. However, little is known about their functioning and how the various community members interact with each other, and how they affect and are affected by their surrounding environment. The purpose of this research project was to implement and use network analyses to elucidate the ecological roles of microbial communities and associated viruses in the global ocean, as well as within the human gut.

In collaboration with Romain Blanc-Mathieu and Prof. Hiro Ogata, we first analyzed *Tara* Oceans global omics data to infer associations between viruses of eukaryotes and carbon export efficiency (CEE) in the euphotic layer of the global ocean. This work revealed significant associations between 62 viruses (out of 1523 tested) and CEE. A partial least squares (PLS) regression model based on the relative abundance of viral sequences (large dsDNA and smaller RNA and ssDNA viruses) explained a substantial part of variation in the measured CEE. In this model, 58 and 25 viruses were positively and negatively associated with CEE, which support the view that two viral modes of activities likely operating simultaneously can increase or decrease carbon export, respectively. Most of the identified viral lineages were either new or previously not associated with carbon export in the ocean. To gain insight into the host of these viruses, we developed a phylogeny-guided co-occurrence based viral host prediction method (TIM, for Taxon Interaction Mapper; <https://github.com/RomainBlancMathieu/TIM>). Using this method, several viruses were predicted to infect ecologically important hosts such as green algae, haptophytes, diatoms, copepods, and fungoid protists. Our results, recently published as a pre-print article (<https://www.biorxiv.org/content/10.1101/710228v1>), demonstrate that network analyses applied to metagenomics data is a powerful approach to predict new virus-hosts interactions in the global ocean, and potentially across other ecosystems. Thus, we also started to explore and mine human microbiomes and viromes using network-based modeling in order to better understand the ecological functions of prophages in association with Inflammatory Bowel Disease (in collaboration with Hiroki Nishiyama, D3, ICR).

Scientific presentations

1. Ogata H., Blanc-Mathieu R., Kaneko H., Endo H. Global genetic data reveal lineages of giant viruses and other eukaryotic viruses associated with the carbon export efficiency. 4th Ringberg Symposium on Giant Virus Biology [November 17-29, 2019, Ringberg Castle, Tegernsee, Germany, Oral presentation on Nov 19 by Ogata H.]
2. Meng L., Endo H., Blanc-Mathieu R., Ogata H. NCLDV host prediction with marker gene co-occurrence analysis in marine metagenomes. Environmental virus seminar [November 2, 2019, Uji Campus, Kyoto University; Oral presentation by Meng L.]
3. Blanc-Mathieu R., Dahle H., Ogata H., Sandaa R.-H. A persistent algal virus with an unprecedented amount of metabolic genes. Annual meeting of the Japanese Society of Microbial Ecology [September 10-13, 2019, Yamanashi University, Oral presentation on September 11, by Blanc-Mathieu R.]

Distribution of prasinoviruses and their association with natural host in the global ocean

Nigel Grimsley CNRS UMR 7232

Prasinoviruses are members of the nucleocytoplasmic large DNA viruses (NCLDV) and typically infect unicellular green algae in the class Mamiellophyceae such as *Bathycoccus*, *Micromonas*, and *Ostreococcus*. Since the Mamiellophyceae is a major component of marine phytoplankton assemblages, it is important to elucidate the biogeography of prasinoviruses at the global scale. Previous studies revealed that the prasinoviruses are commonly present in the surface ocean with higher contribution levels to overall NCLDV community^{1,2}. However, the sampling sites in the previous report were restricted within narrow oceanic area and thus we do not have comprehensive information on the global distribution and diversity of prasinoviruses. In this study, we elucidate the global patterns of the distribution and diversity of prasinoviruses.

To assess the community structure of prasinoviruses, we used type B DNA polymerase (PolB) as marker gene. We have extracted prasinovirus PolBs from the non-redundant gene catalog (OM-RGC.v2) constructed from 370 metagenomic samples from *Tara* Oceans projects by using HMM search and subsequent phylogenetic mapping onto reference sequences. As a result, we detected 395 PolB sequences classified as prasinoviruses. We are now analyzing the detailed phylogenetic position of prasinoviruses, the global pattern of their distribution, as well as the association with their potential host organisms. Additionally, we made use of these environmental PolB sequences to design new PCR primer set specified to the oceanic prasinoviruses. I and my colleagues have been working on isolating prasinoviruses from the natural environments, and now we have 29 PolB sequences from the isolates. From the alignment combining PolB sequences from the isolate cultures and those from the global metagenomes, we detected a highly conserved domain across prasinoviruses in the ocean. We are planning to design a new prasinovirus-specific primer set based on the consensus sequences of this domain, by using the bioinformatic pipeline developed in a previous work³. It would cover prasinovirus species in the a wide range of oceanic habitats, and contribute to the targeted detection and evaluation of overall prasinovirus community in the ocean.

References

- 1 Hingamp, P. *et al.* Exploring nucleo-cytoplasmic large DNA viruses in Tara Oceans microbial metagenomes. *ISME J* **7**, 1678-1695, doi:10.1038/ismej.2013.59 (2013).
- 2 Derelle, E. *et al.* Diversity of viruses infecting the green microalga *Ostreococcus lucimarinus*. *J Virol* **89**, 5812-5821, doi:10.1128/jvi.00246-15 (2015).
- 3 Li, Y. *et al.* Degenerate PCR primers to reveal the diversity of giant viruses in coastal waters. *Viruses* **10**, 496, doi:10.3390/v10090496 (2018).

Integrating omics data and module-based network with deep learning to develop cancer type predictive models

Jinn-Moon Yang National Chiao Tung University

Research Purpose: Cancer classification has been a crucial topic of research in cancer treatment. To classify cancer types, various machine learning approaches have been developed to reduce the dimensionality of mRNA expression data and improve the classification accuracy. However, current studies focus on dealing with unbalanced data, but not emphasize on exploring mechanism across multiple cancer types. A crucial step toward understanding cellular systems properties is to analyze the topology of biological networks and biochemical progress in cells. To construct the protein-protein interaction (PPI) network as completely as possible, genome-scale interaction discovery approaches, such as high-throughput yeast two-hybrid screening and co-affinity purification, have been proposed. However, current network analysis approaches usually used the comprehensive but complicated PPI network to describe cellular behaviors. To address these issues, we will collaborate with Professor Tatsuya Akutsu, who has years of experience in mathematical analyses of biological networks. We will propose a deep learning model and study module-based mechanisms across multiple cancer types, and propose a modularity structure matrix, called MS-matrix, to identify functional modules for studying cancer mechanisms.

Results : We have developed novel deep learning-based methods, feature-based strategy (FES) and image-based strategy (IMS), for identifying cancer subtypes by integrating evolutionary profiles and gene expression data. Evolutionarily conserved genes/proteins were identified and utilized in FES whereas the distances were computed for all pairs of genes based on the coevolutionary correlation score and were transformed into image data using multidimensional scaling (MDS) analysis. We demonstrated the effectiveness of these methods by comparison with existing methods through breast cancer subtype classification and multiple cancer type classification [1], where integration of PPI data is left as future work. In addition to this study, three students in my laboratory in NCTU visited ICR and discussed the possibilities of collaborations on identification of binding atoms of ligands for protein kinases, deep learning-based approach for analysis of phosphopeptide binding domains, and identification of consensus contact regions in protein interacting interfaces.

Publication:

[1] C-Y. Lin, P. Ruan, R. Li, J-M. Yang, S. See, J. Song, and T. Akutsu: Deep learning with evolutionary and genomic profiles for identifying cancer subtypes, *Journal of Bioinformatics and Computational Biology*, 17(3), 1940005, 2019.

Next-generation bioinformatics approaches for the accurate identification of protease-specific substrate cleavage sites

Jiangning Song Monash University

In collaboration with Prof Tatsuya Akutsu and his research group at the Bioinformatics Center, Institute for Chemical Research, Kyoto University, we have carried out research activities and generated research outcomes, which are briefly summarized as follows:

Objectives:

Understanding of the mechanisms of regulation of proteolysis by proteases is very important for elucidation of cellular processes. The key to this understanding is to identify the complete repertoire of specific substrates that each protease targets.

Experimental methods:

Substrate cleavage site prediction can be formulated as a binary classification problem, i.e. being classified as either a cleavage site (positive) or non-cleavage site (negative). We employed a machine learning technique- support vector regression (SVR) to build the iProt-Sub models to predict the substrate cleavage probability of proteases.

Experimental results and discussions:

We have developed the iProt-Sub tool and constructed protease-specific prediction models for 38 proteases. Our experimental evaluations indicate that the proposed iProt-Sub method outperforms those previously developed methods. After its publication in *Briefings in Bioinformatics* in 2019, iProt-Sub has been utilized as a powerful tool for proteome-wide prediction of protease-specific substrates and their cleavage sites. The paper has been cited for 106 times in Google Scholar and the web server has been accessed by 10,000+ visits worldwide.

Publications:

- [1] J. Song, Y. Wang, F. Li, T. Akutsu, N. D. Rawlings, G. I. Webb, K-C. Chou: iProt-Sub: a comprehensive package for accurately mapping and predicting protease-specific substrates and cleavage sites. *Briefings in Bioinformatics* 20(2): 638-658 (2019)
- [2] F. Li, Y. Wang, ..., J. Revote, T. Akutsu, K.C. Chou, A.W. Purcell, R.N. Pike, G.I. Webb, A.I. Smith, T. Lithgow, R.J. Daly, J.C. Whisstock, J. Song. Twenty years of bioinformatics research for protease-specific substrate and cleavage site prediction: a comprehensive revisit and benchmarking of existing methods. *Briefings in Bioinformatics* 20(6):2150-2166 (2019)
- [3] J. Wang, B. Yang, ..., M. Hayashida, T. Akutsu, G. I. Webb, R. A. Strugnell, J. Song, T. Lithgow: Systematic analysis and prediction of type IV secreted effector proteins by machine learning approaches. *Briefings in Bioinformatics* 20(3): 931-951 (2019)
- [4] J. Wang, J. Li, B. Yang, ..., T. Akutsu, Y. Zhang, ..., J. Song, T. Lithgow: Bastion3: a two-layer ensemble predictor of type III secreted effectors. *Bioinformatics* 35(12): 2017-2028 (2019)

Viral impacts on microbial ecosystems in the highly-enclosed inlet, Uranouchi Bay, Kochi

Keizo Nagasaki Kochi University

Viruses are important regulators of the marine microbial communities such as bacteria, protists, and metazoans. Through the selective infection and cell lysis, viruses are thought to increase the recycling rate of materials for the microorganisms, and consequently contribute to the homeostasis of marine ecosystems. *Megaviridae* is a proposed virus family, which infect mainly autotrophic and heterotrophic protists in the ocean. Recent studies revealed the extremely high taxonomic diversity of *Megaviridae* in the marine environments (Li et al., 2018; 2019), suggesting the potential diversity of their host organisms in the sea. Analyzing the temporal variations in detailed community structures of *Megaviridae* and their potential hosts would be a feasible solution for evaluating the potential impacts of the viruses to the eukaryotic communities as well as predicting unknown virus-host associations in the sea.

In this study, we conducted a short-term, high-frequency sampling (1 sampling per day, 9 days) in the Uranouchi Bay (Kochi, Japan), a semi-enclosed inlet where massive algal blooms by several species occur every year, during a bloom event in May-June 2019. Additionally, we performed a long-term, low resolution sampling (1.5 samplings per month on average) from January 2017 through June 2019 at the same area. By using the DNA samples collected in these observations, detailed community compositions of *Megaviridae* and eukaryotes were analyzed with amplicon sequencing targeting the marker genes. We found that the community composition of *Megaviridae* changed dramatically over time, and was more pronounced with the developments of algal blooms. This suggests that *Megaviridae* might infect various eukaryotic microbes including bloom forming algae than previously elucidated, and have potential to control the dynamics of red-tide events in the study site. Further analyses are in progress to elucidate the causality of community dynamics between *Megaviridae* and their potential host organisms.

With these results, a presentations was made for research conference as below.

- Proding F., Endo H., Takano Y., Li Y., Tominaga K., Isozaki T., Blanc-Mathieu R., Gotoh Y., Nagasaki K., Yoshida T., Ogata H. Exploring community changes of bloom forming eukaryotic phytoplankton and *Megaviridae* in Uranouchi Inlet, Japan. Research meeting on environmental viruses [November 2, 2019, Uji Campus, Kyoto University; Oral presentation by Proding F.]

[References]

- Li, Y. et al. Degenerate PCR Primers to Reveal the Diversity of Giant Viruses in Coastal Waters. *Viruses* 10, 496, doi: 10.3390/v10090496 (2018).
- Li, Y. et al. The Earth Is Small for "Leviathans": Long Distance Dispersal of Giant Viruses across Aquatic Environments. *Microbes Environ* 34, 334-339, doi:10.1264/jsme2.ME19037 (2019).

新規巨大ウイルスの単離とゲノム・トランスクリプトーム解析

武村政春 東京理科大学

小さな細菌と同程度の粒子径、ゲノムサイズを有する大型 DNA ウイルス（いわゆる「巨大ウイルス」）の分離報告が近年世界で相次ぎ、巨大ウイルス研究が加速している。研究代表者は近年これまでの巨大ウイルスとは大きく異なる系統の新規巨大ウイルス（メドゥーサウイルス）を分離し、化学研究所・緒方らの協力を得て全ゲノム解析を行った。本研究では、京都府南部の水圏において新規ウイルスの探索を試み、分離された新規ウイルスのゲノム解析を行うことを目的とした。

近年の先行研究において青木らは同一のサンプルあるいは地理的に比較的近傍な陸水環境から採取されたサンプルからマルセイユウイルス科に属する巨大ウイルスを複数分離した。そして、同一地点において複数の異なるマルセイユウイルスが存在することをマーカー遺伝子の配列解析から明らかにした。しかし、マルセイユウイルス科の地理的に局所的な空間におけるゲノムレベルでの多様性に関しては依然明らかではない。

Acanthamoeba castellanii と共培養する手法を用いて、宇治川水系 2 か所と宇治市内の池から採取した試料から細胞変性効果(CPE)を示す事例を複数検出し新規ウイルス株を分離した。これらの新規ウイルス株と青木らの先行研究により分離されたウイルス株の合計 22 株のゲノムシーケンスを行い、冗長性（同一ゲノム型）を除いた後、14 種類のマルセイユウイルスと 1 種類のメドゥーサウイルスのほぼ完全なゲノム配列が得られた。こうして得られたゲノムデータに基づき比較ゲノム解析を行った結果、遺伝子配列比較による系統分類とオーソログ保有パターンによる系統分類の結果が類似しており、遺伝子レベルの進化とゲノムレベルの進化は同調傾向にあることが示唆された。同一地点に複数のゲノム型が存在することから、同一宿主への複数株の同時感染を経てゲノム組み換えが行われる可能性があるのではないかと仮説を立て、それを検証した。これにより、アメーバ感染性の巨大ウイルスにおいてゲノム組み換えが進化に寄与していることが初めて明らかになった。なお、ウイルスの分離、ゲノム解析は主に吉田亘騎（緒方研M2）が行った。

論文発表

1. Yoshikawa G., Blanc-Mathieu R., Song C., Kayama Y., Mochizuki T., Murata K., Ogata H., Takemura M. Medusavirus, a novel large DNA virus discovered from hot spring water. J. Virol., 93, e02130-18 (2019).
2. Aoki K., Hagiwara R., Akashi M., Murata K., Ogata H., Takemura M. Fifteen marseilleviruses newly isolated from three water samples in Japan reveal a local diversity of Marseilleviridae. Front. Microbiol. 10, 1152 (2019).

学会発表

1. 吉田亘騎, 武村政春, 遠藤 寿., Blanc-Mathieu R., 緒方博之. 京都府南部水系からの新規マルセイユウイルス株の分離と今後の比較ゲノム解析. 環境ウイルス研究集会 [November 2, 2019, Uji Campus, Kyoto University; Oral presentation by 吉田亘騎]

環境サンプルからの赤潮藻類の濃縮とその藻類に感染するウイルスの同定

吉田天士 京都大学

Background: Red tide is a phenomenon of discoloration in seawater, caused by the algal bloom of some phytoplankton species. Previous studies have demonstrated that nucleocytoplasmic large DNA viruses (NCLDV) are involved in red tide and infect unicellular microalgae. Co-culture with their host is the “Gold Standard” for the identification of virus-host relationship but limited by our ability to cultivate microorganisms (thus hosts). Therefore, consideration should be put into cultivation-independent approaches.

Methods: We used cell sorting and samples collected from red tide outbreaking seawater at Uranouchi Bay to identify the hosts of NCLDVs. Samples were collected from the surface (SRF) and deep chlorophyll maximum water (DCM) layers. Sorting of cells was done with a S3e cell sorter (Bio-Rad) and triggered on the gates based on FSC (cell sizes), SSC (internal complexity), FL4 (chlorophyll).

Results: Microalgal cells and smaller cells (or particles) were sorted out of the environmental community. Microscopy observation confirmed sorted microalgal cells are *Caratium* sp.. For virus detection, we used Megaprimers pair PP45 to investigate the presence of “Megaviridae”. It was shown that besides complete *Caratium* sp. cells, “Megaviridae” signals could be detected from other sorted groups and original sample. This on-going study has shown the ability and potential of cell sorting to identify the hosts of NCLDVs in the marine environment. This work was performed mainly by Lingjie Meng (PhD student) of Ogata laboratory (ICR) using the laboratory equipment of the PI (Takashi Yoshida).

Publication:

Li Y., Endo H., Gotoh Y., Watai H., Ogawa N., Blanc-Mathieu R., Yoshida T., Ogata H. The earth is small for “leviathans”: long distance dispersal of giant viruses across aquatic environments. *Microbes Environ.* 34, 334-339 (2019).

Presentations:

Meng L., Endo H., Blanc-Mathieu R., Ogata H. NCLDV host prediction with marker gene co-occurrence analysis in marine metagenomes. 環境ウイルス研究集会 [November 2, 2019, Uji Campus, Kyoto University; Oral presentation by Meng L.]

生物ネットワーク構造の局所構造変化の網羅的解析

志賀元紀 岐阜大学

分子生物学では、分子レベルでの膨大かつ網羅的な計測データの情報解析（バイオインフォマティクス）が益々重要となっている。また、論文などに発表された新規の知見がデータベース化されており、このような様々な知識を取り入れることによって、計測データ解析の高効率化かつ高精度化することが期待されている。本共同研究課題では、細胞状態（健康・疾病など）による生体分子ネットワーク構造の変異を網羅的に検出するアルゴリズムの開発に取り組み、これによって正確な分子間相互作用データ解析を目指した。

疾病メカニズムの理解には、疾病の有無によって、どのように生体内ネットワークの構造が変化するかを正確に理解する必要がある。しかしながら、生体内分子の種類数は非常に多く、その組み合わせからなる相互作用を網羅的に解析することは計算コストの観点から困難である。また、その組合せ数に対して観測データ数が非常に小さいため、偽陽性誤りを多数発生させる問題がある。この問題を解決するために、本研究ではスパースモデリングに基づく相互作用の網羅的な変異検出法[1]を開発してきた。開発手法は、セーフスクリーニングとよばれるアプローチであり、膨大にある状態が変異したノードペアの候補の中から有力な候補だけを初期スクリーニングによって取り出せるので計算量を大幅に減らせる利点がある。さらに、候補として残すべきノードペアを誤って削除されることがないことが理論的に保障されており、この点も本手法の優れた点である。人工的に生成したデータ、また、癌細胞と健常細胞を比較するための遺伝子発現量データセットを用いて、開発法の実行時間を評価したところ、通常の変異検出法よりも数十倍以上に計算時間を高速化できることが示された。今後は、分子生物学における様々なデータセットへの応用、また、ノード数がより多いデータセットを解析するためのスケーラビリティの改善が課題として挙げられる。

関連文献：

[1] 佐藤浩基, 志賀元紀, 山田誠, “マルコフネットワーク構造変化検出におけるスパース KLIEP モデルのセーフスクリーニング”, 信学技報 IBISML2018-52, vol. 118, no. 284, 61-68, 2018.

分子ネットワーク解析のための統計的機械学習法の開発と応用

茅野光範 帯広畜産大学

本研究では、統計的機械学習の観点から、遺伝子ネットワークの推定や実験条件（健常者と患者等）によるネットワーク構造が異なる遺伝子、つまり、遺伝子の相関ネットワークの case/control による差分解析に必要となる効率的な機械学習・統計学的解析方法を提案する。

まず、問題を明らかにする。図 1 は、5 つの遺伝子 A-E の発現量のうち 2 つの遺伝子の散布図（図 1 左）、全ての 5 遺伝子の発現量のヒートマップである。図 1 において、Sample1-50（例えば、健常者）では、遺伝子群 A-E の任意の対は互いに相関している（図 1 左の×印）が、Sample 51-100（例えば、がん患者）では、遺伝子群は互いに相関が無く、ランダムに発現している（図 1 左の◆印）。いくつかの遺伝子が互いに相関している（Sample 1-50）。Sample51-100 では、この相関構造が崩壊しており、すなわち、これらの遺伝子機能が、がんなどにより崩壊していることを意味する。本研究では、このような相関変化をもつ遺伝子群を効率的に検出するための機械学習・統計的な解析方法を提案する。

我々は、これまで、手法の提案、数値実験による提案手法の評価、公共の遺伝子発現データ（Gene Expression Omnibus ; GEO から入手した延べ約 100 万個の遺伝子群）に提案手法を適用し、生物学的に意義のある遺伝子群が検出出来ることを確認した。また、先行研究で報告されている、相関ネットワークが変化する遺伝子群の具体例を集め始め、これらの成果を元に研究代表者と共同研究者との共著論文を執筆し、修正を重ねている。今後、グラフネットワーク理論（馬見塚教授、Nguyen 助教、山田グループリーダー）、計算機統計学（Wicker 教授）、アルゴリズムやマイニング理論（瀧川准教授）を駆使した機械学習・統計学的な分子ネットワーク解析法の提案が考えられ、また、これらの解析法の具体的な生命科学現象への応用（例えば農学への応用、大西准教授）を検討している。

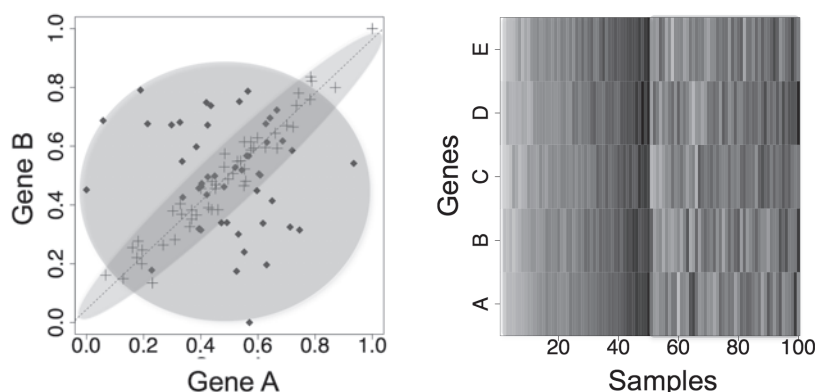


図 1 case/control により相関構造が変化する遺伝子対 A, B（左）と、同様な相関構造変化を持つ遺伝子群 A-E のヒートマップ（右。濃いほど発現量が高い）。遺伝子 A-E の中から任意の対をとると左図のような相関構造の変化が見られる。[Kayano M., Shiga M. and Mamitsuka H., IEEE/ACM Trans.

Comp. Biol. Bioinform., 11(1): 154-167, 2014 より転載]

Control and analysis of complex networks via minimum dominating sets

Jose C. Nacher Toho University

Research Purpose: Different from random networks, many biological information networks including metabolic networks, protein-protein interaction networks, and ncRNA-protein interaction networks have the scale-free property (i.e., power-law degree distribution). We have been developing theory and methods for analyzing these scale-free networks. In recent years, we have been focusing on controllability of scale-free networks and developing theory and methods based on the minimum dominating set (MDS), which is a well-known concept in graph theory. In particular, we developed a new concept, the probabilistic minimum dominating set (PMDS), by extending the MDS for handling weighted networks in which edges have some weights. However, PMDS is not enough to analyze such networks as metabolic networks because metabolic networks have another type of parameters: stoichiometric matrices. Therefore, it is needed to combine PMDS with stoichiometric matrices.

Results : We have developed a novel method for analyzing metabolic networks by combining PMDS with stoichiometric matrices [1]. The method consists of the following steps. (1) The stoichiometric matrix is constructed from a given metabolic network and used to compute the orthonormal kernel matrix. (2) The reaction correlation coefficient, which is the cosine of the angle between the reaction rows in the kernel, is computed for each pair of reactions and is used as the strength of control between both reactions. (3) PMDS is computed based on the strengths of edges. We applied the method for analysis of metabolic networks corresponding to four healthy and cancer tissues. The results suggest that cancer metabolism is easier to be controlled. In addition to this study, we developed a deep learning-based method for lung cancer classification integrating protein interaction network and gene expression profiles [2]. Furthermore, we studied how human protein-protein interaction networks are affected by virus infection from a viewpoint of controllability via MDS [3].

Publications:

- [1] J-M. Schwartz, H. Otokuni, T. Akutsu, and J. C. Nacher, Probabilistic controllability approach to metabolic fluxes in normal and cancer tissues, *Nature Communications*, 10, 2725, 2019.
- [2] T. Mastubara, T. Ochiai, M. Hayashida, T. Akutsu, and J. C. Nacher, Convolutional neural network approach to lung cancer classification integrating protein interaction network and gene expression profiles, *Journal of Bioinformatics and Computational Biology*, 17(3), 1940007, 2019.
- [3] V. Ravindran, J. C. Nacher, T. Akutsu, M. Ishitsuka, A. Osadcenco, V. Sunitha, G. Bagler, J-M. Schwartz, and D. L. Robertson, Network controllability analysis of intracellular signalling reveals viruses are actively controlling molecular systems, *Scientific Reports*, 9, 2066, 2019.

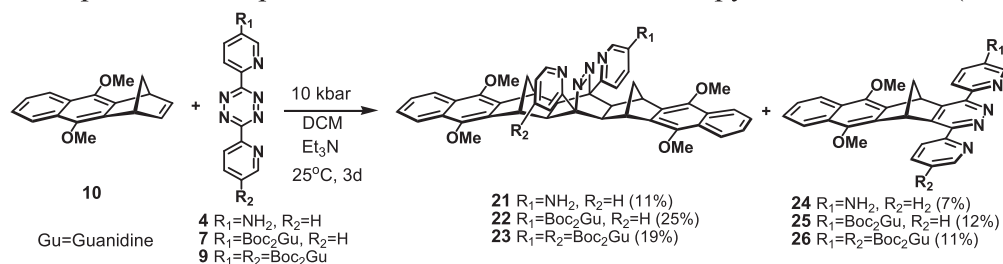
Application of s-tetrazines in guanidine functionalization of fullerenes

Davor Margetic Rudjer Boskovic Institute

Objectives

Synthesis of novel guanidinium tetrazine reagents and investigation of their reactivity for fullerene derivatization with partner ICR researcher Professor Murata Yasujiro.

Experimental results. Aminotetrazine **4** was prepared by condensation of 2-cyanopyridine and 5-amino-2-pyridinecarbonitrile with hydrazine hydrate and oxidation 1,4-dihydrotetrazine with diacetoxyiodobenzene. Diamino tetrazine was prepared in an analogous manner. Guanylation reactions of tetrazine showed that reactivity of aminotetrazine is smaller than of previously used aromatic amines. The screening of reaction conditions and reagents showed that *N,N'*-Di-Boc-*S*-methylisothiourea (BSTU) is reactive enough to provide guanidinyl tetrazine **7** in small yield. BSTU reagent was also employed in the synthesis of symmetrical, bis-guanidine tetrazine **9**. Several experiments were carried out to investigate cycloaddition reactivity of tetrazines **4**, **7** and **9**. High pressure promoted cycloadditions of tetrazines **4**, **7** and **9** with alkene **10**, irrespective of tetrazine used provided two products: 2:1 bisadducts **21-23** and pyridazines **24-26** (Scheme 1).



Scheme 1. Cycloaddition reactions of tetrazines **4**, **7** and **9** with alkene **10**.

Cycloadditions of bis(2-pyridyl)tetrazine **11** and **7** with fullerene were carried out in different reactions conditions and complex mixtures of products were formed. Invariably, guanidinyl tetrazine **7** showed lower cycloaddition reactivity in comparison with **11** and fullerene reactivity was lower than alkene **10**.

Theoretical results. B3LYP/6-31G* calculations were carried out to predict reactivity of *s*-tetrazines. Relative Diels-Alder reactivity of tetrazines was estimated by the examination of frontier molecular orbitals (FMO). All tetrazines react in DA reaction with norbornadiene in an inverse electron-demand fashion. The presence of amino or guanidine substituents at *s*-tetrazine does have a small effect on the FMOs. The transition state calculations of reactions with two dienophiles (norbornadiene and fullerene) afforded TS structures corresponding to concerted, synchronous mechanism. Overall, activation energies for cycloadditions with C₆₀ are higher than reactions with norbornadiene, which is in good accordance with experimental observations. Electron donating amino and guanidine substituents on tetrazine raise the *E*_{act}, whereas protonation provided the similar effect as predicted from FMO analysis: increase of reactivity.

Four lectures were delivered from 3-6 February at Universities in Japan.

Coupling of planar and curved π -systems for the development of novel functional materials

Akimitsu Narita Max Planck Institute for Polymer Research

Objective: For the project purpose of coupling the planar π -conjugated molecules developed at the Max Planck Institute for Polymer Research (MPIP) with unique curved π -systems synthesized by the ICR partner researchers, Prof. Takashi Hirose and Prof. Yasujiro Murata, the project goal in FY2019 was to achieve proper functionalization of the π -systems for enabling the coupling reactions. To this end, we have studied direct borylation of dibenzo[*hi,st*]ovalene (DBOV), which is a planar polycyclic aromatic hydrocarbon (PAH) with promising optical properties, such as strong red emission and capability of stimulated emission and single-photon emission.

Results and discussion: Iridium-catalyzed direct borylation of DBOV with two mesityl groups (**DBOV-Mes**) was carried out. After optimizing the reaction conditions, the borylation reaction proceeded by heating **DBOV-Mes** and pinacolborane in a mixture of tetrahydrofuran and mesitylene (1:1) at 90 °C, under the presence of 10 mol% Ir(cod)(OMe)₂ and 20 mol% di-*tert*-butylbipyridine (dtbpy) (Figure). MALDI-TOF MS analysis indicated formation of a mixture of four products, namely mono- to tetra-adducts. Selective formation of a product with a certain number of functionalization could not be achieved, suggesting limited difference in the reactivity of C–H bonds at different positions. Nevertheless, this achievement of the direct borylation of DBOV will be a basis for the coupling of this promising planar π -system with the curved counterpart being developed by ICR partner researchers. Scale up of the synthesis and separation by the products by HPLC is currently ongoing.

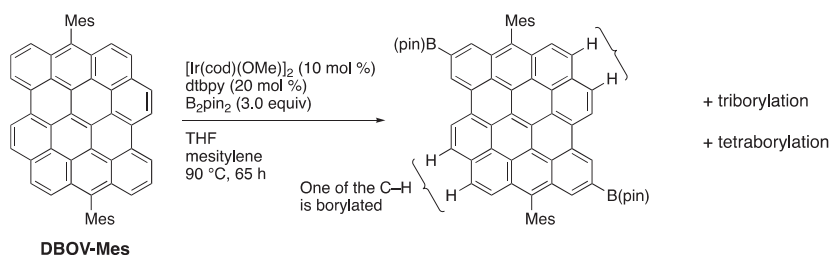


Figure: Attempted Ir-catalyzed direct borylation of **DBOV-Mes**.

Workshop and meeting:

Prof. Takashi Hirose, Prof. Yasujiro Murata, and I have organized “*The 1st Germany–Japan–China Joint Workshop on Extremely Large π -Systems*” on July 18th, 2019 at the Joint Research Laboratory, where 5 researchers and PhD students from MPIP, 6 researchers from ICR, and 2 researchers from China (formerly at MPIP) have given oral presentations (program attached). On July 19th, 2019, we had a joint group meeting, where the five from MPIP and the two from Chinese universities discussed the collaborative projects and further opportunities for the cooperation together with the group of Prof. Hirose and Prof. Murata.

Design, synthesis, and characterization of charge transport materials for non-lead perovskite

Akinori Saeki Osaka University

The use of toxic lead in a high efficient perovskite solar cell is one of most serious issues, which is disadvantageous over the environmental and economical aspect. Therefore, researchers have made great efforts to explore less-toxic lead-free perovskites with high environmental stability. Bismuth-based halide materials such as dimer structure of $A_3Bi_2I_9$ ($A = Cs, CH_3NH_3^+$ (MA), $(CH_3)_2NH^+$ (FA)) and double perovskite of $Cs_2AgBiBr_6$ have been previously investigated. However, direct observation of charge carrier generation, transport, and transfer process including non-radiative recombination is mostly unexplored. In this work, the dynamics of photogenerated charge carrier was investigated by using time-resolved microwave conductivity (TRMC)¹. Photoconductivity and charge carrier transport /transfer from perovskite to electron transfer layer (ETL) and hole transfer layer (HTL) were comparatively evaluated for the dimer and double perovskites, which showed a good correlation with the solar cell performance.

TRMC measurements of dimer $A_3Bi_2I_9$ were carried out for the single layer films (single), bilayer films (n/i) composed of mp-TiO₂ as n-type ETL and perovskite as the intrinsic (i) layer, and triple layer films (n/i/p) composed of mp-TiO₂, perovskite, and PTAA as p-type HTL (Fig. 1a). The single layer films showed very similar TRMC transients among the samples ($Cs_3Bi_2I_9$, $MA_3Bi_2I_9$, and $FA_3Bi_2I_9$) in both intensity ($1-2 \times 10^{-4} \text{ cm}^2 \text{ V}^{-1} \text{ s}^{-1}$) and decay speed (Fig. 1b). The n/i films showed distinct increase of $\phi\Sigma\mu$ maxima ($\phi\Sigma\mu_{\text{max}}$) and effective lifetime (τ) compared with the single layers. This is explained by electron transfer from $A_3Bi_2I_9$ to mp-TiO₂ and retarded charge recombination, where the electron mobility in $A_3Bi_2I_9$ is assumed much smaller than that in TiO₂ ($\sim 10^{-1} \text{ cm}^2 \text{ V}^{-1} \text{ s}^{-1}$). Although electron transfer to mp-TiO₂ was observed, the increase of $\phi\Sigma\mu_{\text{max}}$ from single layer to n/i layer was moderate (1.3–3.0 times), which suggests that electron transfer is not so efficient. Despite the low hole/electron transfer, the charge recombination is suppressed to some extent, which would merit the solar cell performance. Consequently, photovoltaic devices with a normal structure (FTO/compact TiO₂/mp-TiO₂/perovskite/PTAA (doped)/Au) were prepared. $Cs_2AgBiBr_6$ -based device gave the J_{sc} of 1.2 mA cm^{-2} and PCE of 0.72%, which is consistent with the high $\phi\Sigma\mu_{\text{max}}$ and charge transfer efficiency observed in TRMC evaluation. Our work paves the way to the development of efficient HTL and ETL² for non-lead perovskite materials.

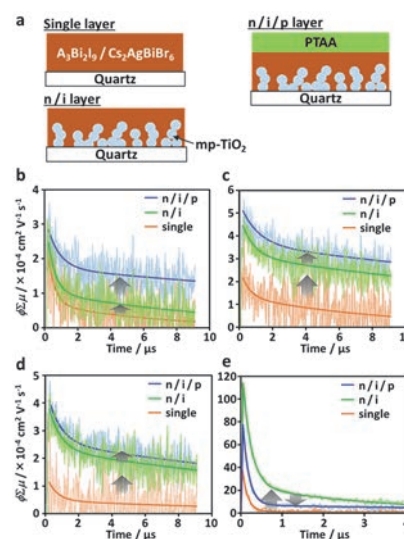


Fig. 1. (a) Schematics of film sample for TRMC measurement. TRMC transients of (b) $Cs_3Bi_2I_9$, (c) $MA_3Bi_2I_9$, (d) $FA_3Bi_2I_9$, and (e) $Cs_2AgBiBr_6$ thin films.

[1] R. Nishikubo, A. Saeki, *J. Photopolym. Sci. Tech.* **2019**, 32, 735.

[2] T. Nakamura, N. Shioya, T. Shimoaka, R. Nishikubo, T. Hasegawa, A. Saeki, Y. Murata, R. Murdey, A. Wakamiya, *Chem. Mater.* **2019**, 31, 1729.

新規 π 共役系ポリマーの開発と有機薄膜太陽電池への応用

尾坂 格 広島大学

【研究背景と目的】 π 共役系ポリマーは、有機エレクトロニクスにおいて重要な材料群である。イミドを有する π 電子系骨格は、強い電子欠損性を持つため、特にドナーアクセプター型ポリマーの有用なビルディングユニットである。最近我々は、チアゾールを導入した新規イミド系骨格であるジチアゾリルチエノチオフェンビスイミド (TzBI) を開発し、これを有するポリマー (PTzBITT: Figure 1) が、良好な n 型特性を示すことを報告した。

本研究では、TzBI とクアテルチオフェンから成る TzBI 系ポリマー PTzBI4T を合成した (Figure 1)。PTzBI4T は、ポリマー主鎖のドナー性が強く、 n 型の挙動は示さず p 型として半導体特性を示すことを見出した。

【実験結果と考察】 PTzBI4T は、両端にチオフェンが置換した TzBI (TzBI2T) の臭素体とビチオフェンのスズ体との Stille 反応により合成した。TzBI2T とビチオフェンの臭素体を用いた DArP 法による重合を試みたが、十分な分子量を有するポリマーは得られなかった。また、PTzBI4T の電子物性を評価したところ、PTzBITT よりも HOMO が 0.71 eV、LUMO が 0.19 eV 上昇したことが分かった。これは、電子豊富なチオフェン環の数が増加し、ポリマー主鎖の電子ドナー性が向上したためと考えられる。PTzBI4T と n 型材料として PC₆₁BM を用いた OPV を作製し光電変換特性を評価すると、変換効率 2.2%を示した。今後、DArP 法による重合の検討を行う予定である。

【成果報告】

<論文> (1) Y. Teshima, et al. *ACS Appl. Mater. Interfaces*, **2019**, *11*, 23410–23416. (2) Y. Teshima, et al. *Bull. Chem. Soc. Jpn.*, **2020**, *93*, 561–567.

<学会発表> (1) 手島 慶和, 他「チアゾールを有する電子欠損性イミド系骨格の有機デバイスへの応用」, 第 80 回 応用物理学会秋季学術講演会, 東京, 9・2019 (2) Y. Teshima, et al. “Dithiazolylthienothiophene Bisimide: A Novel Electron-Deficient Building Unit for N-type Semiconducting Polymers” NCU-HU Joint Symposium on Materials Chemistry and Physics 2019, Taipei (Taiwan), Nov., 2019.

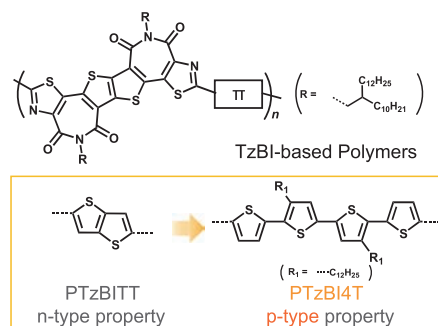


Figure 1. Chemical structure of TzBI-based polymers; PTzBITT and PTzBI4T.

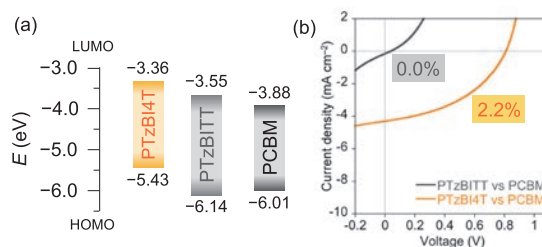


Figure 2. (a) Energy diagrams of the TzBI-based polymers and PC₆₁BM. (b) J - V curves of TzBI-based polymer solar cells.

Preparation of novel branched block copolymer with well-controlled stereoregularity and evaluation of its molecular aggregation state

Tomoyasu Hirai Osaka Institute of Technology

It is well accepted that natural polymers such as RNA and DNA form one-handed helical conformation. On the other hand, controlling of one-handed helical conformation in synthetic polymer has still limitation. So far, formation of one-handed helical conformation polyacetylene derivatives could be achieved by mixing with polymer and small amount of chiral dopants. This approach, however, limited to be used for polymer with rigid main chain such as polyacetylene derivatives.

Polymethyl methacrylate (PMMA) with well-controlled stereoregularity forms helical conformation. If the helical conformation can be controlled to be one-handed and can be kept, it will give a major impact for development of separation membrane field. To achieve one-handed helical conformation in methacrylate derivatives, we design and prepared novel polyhedral oligomeric silsesquioxane (POSS)-containing polymethacrylate designated (PMAPOSS) with well-controlled stereoregularity. Figure 1 shows the chemical structure of PMAPOSS and block copolymer consisting of PMAPOSS and PMMA designated PMAPOSS-*b*-PMMA. The PMAPOSS and PMMA-*b*-PMAPOSS was prepared using a living anionic polymerization using Grignard reagent as an initiator. The stereoregularity of the obtained polymer was evaluated using signals at 45 ppm in ^{13}C NMR spectrum, which can be assigned to the quaternary carbon next to the α -methyl groups in the main chain. We concluded that PMAPOSS and PMAPOSS-*b*-PMMA was in isotactic. To evaluate the helical conformation in PMAPOSS, PMAPOSS and chiral alcohol are mixed and casted on silicon wafer, subsequently, the film was evaluated using vibrational circular dichroism (VCD) spectroscopy measurements (Figure 2). Clearly split-type Cotton effect could be seen between PMAPOSS with *R* or *S* chiral dopants. This results indicate that PMAPOSS formed one-handed helical conformation. Helical conformation in PMAPOSS-*b*-PMMA was also evaluated using VCD spectroscopy. They also showed split-type Cotton effect. Moreover, the signals were much more pronounced than that of PMAPOSS. PMMA segment regulates molecular motion of PMAPOSS, resulting in formation of stable dynamic one-handed helical conformation.

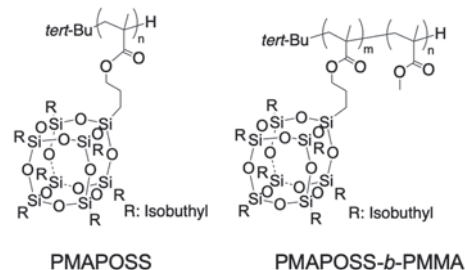


Figure 1. Chemical structure of PMAPOSS and PMAPOSS-*b*-PMMA.

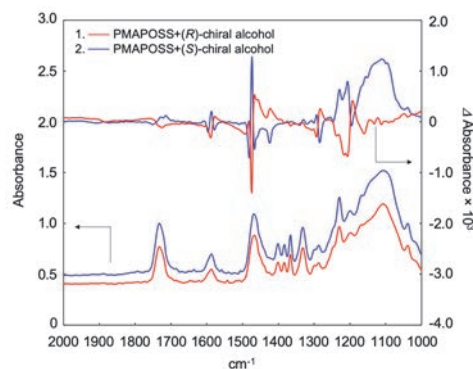


Figure 2. VCD spectrum of PMAPOSS with *R* or *S* chiral alcohol.

キラルネマチック液晶のアンカリング挙動に関する研究

赤木和夫 立命館大学

緒言：液晶は外場に応じてその配向を変化させるが、固体表面に存在する液晶は、表面との強い相互作用（アンカリング力）により配向変化の規制を受け、運動が制限される。この界面アンカリング現象は、液晶のディスプレイのような応用の観点からも注目される。一方、界面からの規制を受けない表面は、液晶の材料応用を拡張すると期待される。京都大学化学研究所の辻井敬亘教授らは、ポリヘキシルメタクリレート（PHMA）系濃厚ポリマーブラシ界面、および PHMA を主成分とする側鎖を高密度に有するグラフトポリマー（ボトルブラシ）（PHMA 系 BB）架橋膜上のネマチック液晶が、面内方向のアンカリングがほぼゼロであるゼロ面アンカリング状態となることを見出した。本研究は、この特異的な表面をキラルネマチック液晶系に拡張することを企図した。その足がかりとして、ブラシ状構造がネマチック液晶に対してゼロ面アンカリングとなるメカニズムの解明に取り組んだ。

実験：図 1 に架橋性モノマー含有 PHMA 系 BB の化学構造を示す。このボトルブラシの薄膜上（膜厚 10~100 nm）にネマチック液晶（mixtures; $T_{NI}=112^{\circ}\text{C}$ ）を塗布し、膨潤させた。膨潤前後の膜厚変化を分光エリプソメータにより評価した。また、種々の混合比の架橋性モノマー非含有 PHMA 系 BB と液晶を混合し、偏光顕微鏡（POM）観察に供した。

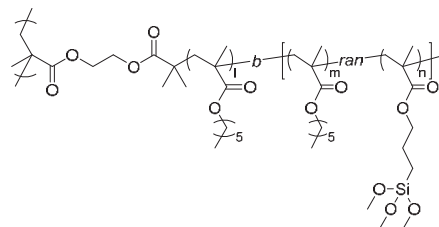


Figure 1. Chemical structure of PHMA bottlebrushes.

結果・考察：PHMA 系 BB の乾燥膜厚に対する膨潤膜厚の関係を図 2 に示す。プロットの傾きより PHMA の膨潤度を 1.6 と求めた。液晶/BB 混合物の POM 観察において、先に求めた各 BB 膜の膨潤度以下に対応する液晶濃度では、マクロ相分離及び複屈折は観察されなかった。すなわち、液晶と BB は当該濃度では相溶し、かつ、膨潤 BB 膜内部は液晶相を形成しないと示唆された。この結果から、低アンカリング特性の発現には、ブラシが液晶に膨潤し、かつ、液晶分子はランダム（等方的）であることが肝要と考察した。

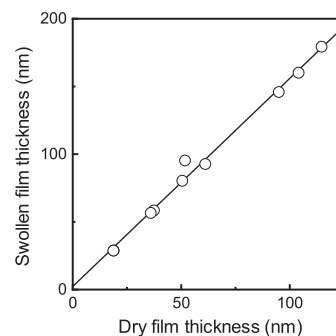


Figure 2. Relationship between LC-swollen and dry film thicknesses of bottlebrushes.

また、キラルネマチック液晶の母液晶である PCH302 と PCH304 の混合物 (ref. Akagi et al., *Angew. Chem. Int. Ed.*, **2014**, 53, 10641) に対しても、本 BB 膜は弱アンカリング性を示した。本研究の推進により、新規なキラル液晶デバイスの開発に期待がもたれる。

Molecular engineering of organic semiconductors toward the control of molecular packing in thin films via a thermal precursor approach

Mitsuharu Suzuki Osaka University

Objective. This project intends to achieve high-quality organic semiconducting thin films by taking advantage of a unique solution deposition method called “thermal precursor approach”. In this method, thin films of small-molecule semiconductors are prepared in two steps: (1) solution casting of well-soluble precursor compounds, and then (2) heating to remove tentative solubilizing groups to generate intended semiconducting compounds. For example, tetrabenzoporphyrin (BP) can be deposited from a solution of CP, a thermal precursor which undergoes the *retro*-Diels–Alder reaction upon heating (Fig. 1). This approach provides unique opportunities in the preparation of organic thin films; for example, one can employ solution-based processes for depositing insoluble compounds, such as BP, without relying on solubilizing permanent substituents that are often large, flexible, and insulating.

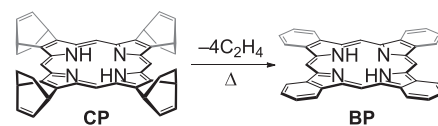


Fig. 1 Thermal conversion of CP to BP.

During this grant period, we concentrated on the evaluation of BP–DPP conjugates to study the relationship between the molecular structure and molecular orientation in thin films prepared via the thermal precursor approach.

Methods. Six different BP–DPP conjugates, *Cn*-DBD, *Cn*-BDB, and *Cn*-BD ($n = 4$ or 10 ; Fig. 2), were deposited on silicon wafer via the thermal precursor approach from solutions of the corresponding CP derivatives in chloroform. Molecular orientation in the thin films before and after heating was analyzed with p-polarized multiple-angle incidence resolution spectrometry (pMAIRS).

Results and Discussion: The CP moieties showed a weak tendency, on average, to orient toward the face-on geometry

in all the precursor films. On the other hand, molecular orientation after the thermal conversion largely differed among the compounds; namely, C10-DBD and C10-BD preferentially adopted the edge-on orientation, while the other derivatives preferred the face-on orientation (Fig. 2, inset). Comparative analysis of these and BP's data indicated that the difference in molecular orientation would be correlating to the mobility of molecules during the thermal conversion.

Publication/Presentation: N. Okamoto et al. Relation between Molecular Structure and Orientation in Organic Thin Films Prepared via a Thermal Precursor Approach: A Case Study of Tetrabenzoporphyrin Derivatives. The 67th JSAP Spring Meeting (12a-PB3-9, Scheduled for March 12, 2020).

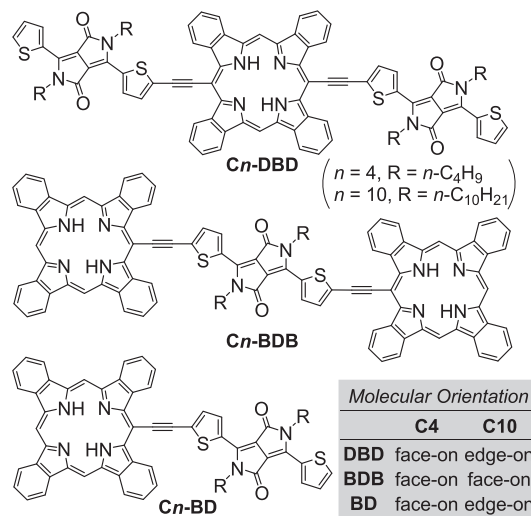


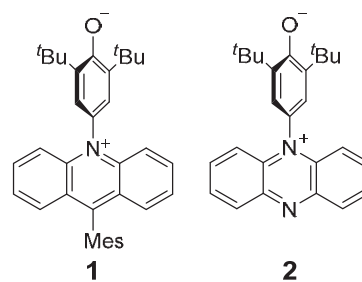
Fig. 2 BP–DPP conjugates studied in this work, and their dominant orientation in thin films (inset).

電子ドナー性アニオンと電子アクセプター性カチオンを連結した π 共役双性イオンの合成と物性

清水章弘 大阪大学

【目的】HOMO と LUMO のエネルギー差 (ΔE_{H-L}) の小さな分子は興味深い光学的・電気化学的特性を示す。 π 共役系の拡張により、 ΔE_{H-L} を減少させることができるが、大きな π 共役分子は合成が困難であったり、溶解性に問題があったりすることが多い。一方、電子ドナーと電子アクセプターを弱く相互作用させることにより、小さな π 共役系でありながら ΔE_{H-L} を小さくすることができる。本研究では、高い HOMO 準位をもつ電子ドナー性のアニオン (フェノキシド) と低い LUMO 準位をもつ電子アクセプター性のカチオン (アクリジニウムまたはフェナジニウム) を、大きな二面角を介して弱く相互作用させた π 共役双性イオン **1**, **2** を設計・合成し、分子設計の有効性の確認および電子構造と物性の解明を目的とした。

【結果と考察】**1**, **2** を合成し、X 線結晶構造解析等により同定した。**1** と **2** の電子ドナー部位と電子アクセプター部位の二面角は $60\sim 70^\circ$ であり、弱い相互作用の発現が示唆された。**1**, **2** はラジカルカチオンへの酸化とラジカルアニオンへの還元に対応する両性の酸化還元特性を示し、酸化電位と還元電位の差から、 ΔE_{H-L} が約 1 eV と非常に小さいことがわかった。また、ジクロロメタン



中において、1000 nm を超える近赤外吸収を示した。したがって、本研究の分子設計の有効性が示された。興味深いことに、**1** の近赤外吸収は、溶媒の極性が高くなると短波長側にシフトする負のソルバトクロミズムを示したのに対し、**2** の近赤外吸収は溶媒の極性に依存せず、波長はほとんど変化しなかった。一般に、双性イオンは基底状態の分極が励起状態の分極よりも大きいため、負のソルバトクロミズムを示すことが知られている。したがって、**2** の吸収特性は双性イオンとしては非常に珍しい現象である。今後、類似の構造の双性イオンの研究を通じて、その原因を明らかにする予定である。また、**1** と **2** の蛍光スペクトルを測定したが、蛍光は観測されなかった。双性イオンの骨格が柔軟であり、かつエネルギーが小さいために、無輻射失活が優先したと考えられる。

【成果報告】(1) ナフトキシドーフェナジニウム連結型双性イオンの合成と物性、越智 勇太・清水章弘・新谷 亮、第 30 回基礎有機化学討論会、2019 年 9 月 25 日－27 日、大阪 (2) フェナジニウムを基盤とする双性イオンの合成と物性、越智 勇太・清水 章弘・新谷 亮、日本化学会 第 100 春季年会 (2020)、2020 年 3 月 22 日－25 日、千葉

The elemental and isotopic composition of particulate trace metals in the subarctic Pacific Ocean: sources and internal cycling

Tung-Yuan Ho Academia Sinica

Objectives:

The major objective of this joint study is to investigate the sources and internal cycling of trace metals in the water column of the Northwestern and subarctic Pacific Ocean spatially and also to evaluate the impact of anthropogenic aerosols originating from East Asia on the processes. My host at ICR, Kyoto University, is Prof. Yoshiki Sohrin.

Methods:

Seawater samples were taken on Taiwan and Japan GEOTRACES cruises carried out previously. Both dissolved and suspended particulate samples were collected for trace metal elemental and isotopic composition analysis. Elemental and isotopic composition of trace metals were determined by HR-ICPMS and MC-ICPMS, respectively. The detailed information of the sampling and pretreatment are described in the following publications.

Result and Discussions:

The details of the results and discussions may be found in the following two publications.

Publications:

Liao, W.-H., S. Takano, S.-C. Yang, K.-F. Huang, Y. Sohrin, and T.-Y. Ho* (2020) Zn isotopic composition in the water column of the Northwestern Pacific Ocean: the importance of external sources. *Global Biogeochemical Cycles* doi: 10.1029/2019GB006379.

Takano*, S., W.-H. Liao, H.-A. Tian, K.-F. Huang, T.-Y. Ho, and Y. Sohrin (2020) Sources of particulate Ni and Cu in the water column of the northern South China Sea: evidence from elemental and isotope ratios in aerosols and sinking particles. *Marine Chemistry* doi: 10.1016/j.marchem.2020.103751

During the visit at ICR, Kyoto University, in December 2019, I have also discussed with Dr. Zheng and Prof. Sohrin on the following study and provided my comments and suggestions.

Zheng, L.*, T. Minami, S. Takano, T.-Y. Ho, and Y. Sohrin. (ready for submission) Sectional distribution patterns of Cd, Ni, Zn, and Cu in the North Pacific Ocean: systematic importance of scavenging.

Application of $\delta^{98/95}\text{Mo}$ and $\delta^{186/184}\text{W}$ isotopes ratios for the reconstruction of late miocene oxygenation in the Arabian sea

Gurumurthy GP. Birbal Sahni Institute of Palaeosciences

The monsoon system in the Indian subcontinent is the most dramatic climatic phenomena on earth. The monsoon intensification following the Himalayan formation has altered the hydrological regimes in the Indian subcontinent, resulting in enhanced weathering and chemical fluxes to ocean. This has led to amplification of primary productivity and biogeochemical changes of the northern Indian Ocean. The elevated burial of organic matter increases the oxygen demand in water column, thus favoring the organic accumulation in sediments under reduced conditions. The question of ocean oxygenation changes is extremely important because majority of modern tropical oceans are experiencing perennial oxygen minimum zones (OMZs) in the intermediate water depths which are expanding rapidly due to anthropogenic stress. Despite the significance of OMZ in the Arabian Sea, there is no long-term data to discern the causative factors, seasonality, and timescale of its evolution. The International Ocean Discovery Program (IODP) has carried out drilling in the recent years with an objective to understand the exact timing of Himalayan formation and monsoon evolution. To complete our understanding of climate-tectonic interaction, one of the most interesting and pertinent aspect of research is the connection between monsoon evolution and associated ocean biogeochemical changes. The study takes advantage of recent IODP-355 expedition to Arabian Sea where the fellow was a Science Party member, and the sediment core samples from Site U1457 were used for the study (Fig. 1). The project intends to investigate the monsoon intensification effects on the ocean oxygenation on a tectonic timescale. The samples collected from the eastern Arabian Sea have been subjected to $\delta^{98/95}\text{Mo}$ and $\delta^{186/184}\text{W}$ were performed at Institute of Chemical Research (ICR) under the supervision of Prof. Yoshiki Sohrin, ICR, Kyoto University, and Mr. Tsujisaka for constraining the ocean redox evolution and its correlation with summer monsoon variability since late Miocene (9Ma).

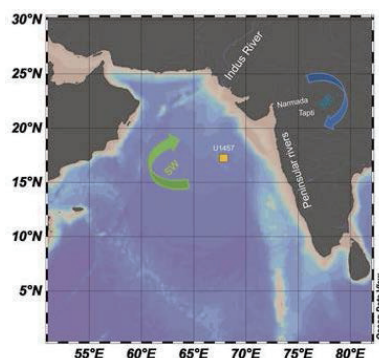


Figure 1: Location of IODP 355 Arabian Sea Monsoon Expedition drill site U1457.

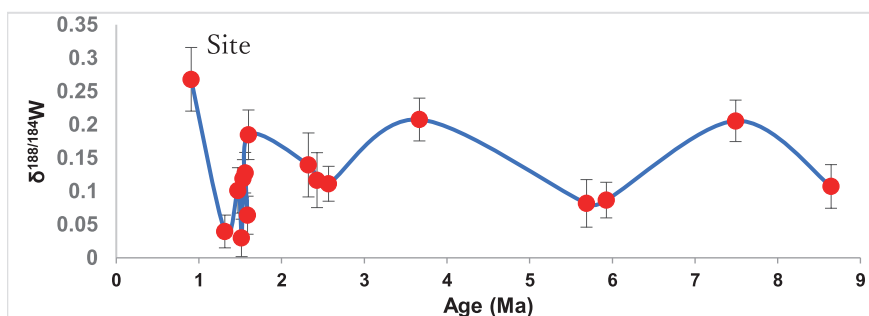


Figure 2: Downcore isotopic composition of $\delta^{188/184}\text{W}$ in the eastern Arabian Sea drill site U1457.

Investigation on the decay process of hot carriers in heavily doped semiconductor nanocrystals

Abderrazzak Douhal A. University of Castilla-La Mancha

The Localized surface plasmon resonance (LSPR) band can be tuned over a wide spectral range enabling solar energy utilization from ultraviolet (UV) to infrared (IR) regions. This excellent light-harvesting ability provide the technologies which convert wide range of light including IR region to chemical or electronic energies. However, the low conversion efficiency has been major drawbacks of LSPR-induced energy conversion.

LSPR materials of compound semiconductors, copper chalcogenide nanocrystals have shown unique carrier trapping mediated carrier transfer which demonstrate the efficient IR-responsive photocatalysts. This trap-mediated cascadic carrier transfer induced by LSPR excitation, so called plasmon induced transit hole transfer (PITCT), overcomes the limitation of low efficiency of plasmonic energy conversion realizing the efficient IR light to chemical energy conversion.^[1] However, the report has been limited and whole mechanism has yet to be elucidated.

In this international collaboration work, Prof. A. Douhal (UCLM, Spain) and Dr. M. Sakamoto (partner ICR researcher) elucidated the LSPR-induced behavior of hot holes in CuS NCs using time-resolved Vis to infrared spectroscopy. CuS NCs were prepared according to the previous research.^[1] Ultrafast transient absorption spectroscopy enables us the direct observation of carrier dynamics in LSPR-excited CuS. From the detailed investigation of ultrafast dynamics of LSPR-excite CuS NCs, we discovered that the unique relaxation process involving multiple trap sites occurred in CuS NCs. The direct observation of formation and decay processes of trap states provide us the important insight to controlling the LSPR-induced relaxation of heavily doped semiconductors. Because ultrafast relaxation of hot carrier is a major drawback of all plasmonic energy conversion systems, the calcified mechanism here should change the conventional consensus regarding LSPR-induced energy conversion due to the overwhelming advantage of high energy conversion efficiency.

Prof. A. Douhal has visited the lab of Dr. S. Sakamoto during few days of November 2019 for discussion and planification of further work. Dr. S. Sakamoto has visited the UCLM group during few days of January 2020, for further discussion and writing a draft of the expected publication.

Reference

- [1] Z. Lian, M. Sakamoto*, H. Matsunaga, J. J. M. Vequizo, A. Yamakata, M. Haruta, H. Kurata, and T. Teranishi, *Nat. Commun.* **2018**, 9, 2314.

Development of photocatalytic materials by quantitative charge carrier dynamics and structural analysis

Yasuhiro Tachibana RMIT University

Introduction

Photocatalytic water splitting is an ultimate technology to produce sustainable hydrogen gas from water using solar energy. Commercialization of photocatalytic devices requires low cost, high efficiency and durability, however materials meeting these requirements have not yet been identified. To develop such photocatalytic materials, it is vital to elucidate reaction mechanisms by monitoring photo-generated electrons and holes quantitatively, facilitating novel material design with optimization of material composition and structural modification. This proposed project aims at assessing water oxidation and reduction reactions with transient laser spectroscopies, and establishing a standard method to design high efficiency solar water splitting devices. We have conducted this project with Professor Teranishi at the ICR, developing novel photocatalytic nanomaterials.

Experimental

Reaction dynamics of water oxidation and reduction will be quantitatively assessed by state of the art transient absorption spectroscopies covering femtoseconds to 10 seconds and 350~6,600 nm under modified experiment conditions.[1] The quantitative charge carrier separation properties will be correlated with interfacial nanostructures.

Results and Discussion

We found that electron-hole recombination reactions are excitation intensity dependent, and mainly occur from nanoseconds to microseconds. The charge recombination reactions compete with hole reactions. Water oxidation quantum yield is evaluated to be 68 %. This is the upper limit of the overall water oxidation reaction yield, since subsequent interfacial charge recombination reaction, e.g. electrons in TiO₂ with oxidised water or hydrogen and oxygen gas reaction, cannot be observed. Slower water oxidation reaction component appears if photo-generated electrons are removed from TiO₂ prior to the charge recombination.[2]

Outcomes

[1] Tachibana et al. *J. Photopolym. Sci. Technol.*, **32**(5) 727-733 (2019).

[2] Manuscript in preparation.

Invited lectures at international conferences

[3] Y. Tachibana, Ultrafast Spectroscopy Symposium at Swinburne, *Melbourne, Australia*, 10-11 February 2020.

[4] Y. Tachibana, The 2019 Spring Meeting of the European Materials Research Society (E-MRS), *Nice, France*, 27 - 31 May 2019.

[5] Y. Tachibana, the ENHANCE international symposium, *Cologne, Germany*, 21 - 25 May 2019.

High frequency rheological and dielectric response of polymeric liquids

Sathish K. Sukumaran Yamagata University

Experimental techniques that probe the response of polymers to external fields typically use constant temperature conditions. Therefore, theoretical analysis of polymer dynamics and response uses isothermal response functions. However, high frequency processes might occur under closer to adiabatic conditions due to insufficient time for thermal equilibration. Therefore, combining the experimental/theoretical expertise of ICR (Hiroshi Watanabe, Yumi Matsumiya), and the computational and modelling expertise of international (Jorge Ramierz, Madrid; Manlio Tassieri, Glasgow) and domestic (Yuichi Masubuchi, Nagoya) researchers, we have initiated a collaboration between ICR and domestic and international partners.

As a first step, we investigated the effect of imposing adiabatic conditions on the linear rheology of an unentangled polymer melt using molecular simulations. We used a simple bead-spring model for the polymer and simulated it at high densities using molecular dynamics (Kremer-Grest model). The adiabatic simulations were performed at constant energy. For comparison, isothermal conditions were imposed using a Langevin thermostat. We applied oscillatory shear at several frequencies. Under adiabatic conditions, as expected, the temperature progressively increased with time. Also as expected, the increase at higher frequencies was significantly larger than that at lower frequencies. However, storage modulus, G' , and the loss modulus, G'' , under both the isothermal and the adiabatic conditions were rather close to each other. Therefore, for linear rheology, preliminary results appear to suggest that the imposed conditions do not matter. We are further exploring this regime both to confirm our preliminary results and also to check if this holds true for other external fields.

Related to this proposal, we have organised an international workshop entitled “Soft Matter Dynamics: Slow and Fast”, at the Institute for Chemical Research, Kyoto University, between March 25-26, 2020. About 30 leading experts in soft matter dynamics, about one-third from abroad, are scheduled to attend the workshop. Within the scope of the workshop, we also plan to discuss the relationship between slow and fast dynamics in soft matter. Further details can be found at the webpage: “<http://rheology.jp/nagoya/wsmd-2020-mar/>”. However, given the current coronavirus situation, it is unclear if the workshop can go ahead as planned.

As a side project, Masubuchi and I investigated planar elongational flow using the Primitive Chain Network Model, a coarsegrained model for simulations of entangled polymers. The findings have been published in *Nihon Reoroji Gakkaishi*, (Journal of the Society of Rheology, Japan), Vol. 48, No. 1 (2020).

Elongational rheology of telechelic-type ionomers

Quan Chen Changchun Institute of Applied Chemistry

Objectives: Associative polymers are physically cross-linked polymers that have a great potential to be applied as novel functional materials, like the self-healing, memory, stimuli-response materials. To understand the non-linear rheology of associative polymers is essential for optimizing their processing conditions, particularly in fiber spinning and membrane blowing where elongational flow is dominant. Although structure and dynamics of associative polymers have been extensively studied in the past half-century, studies of their nonlinear rheological behavior, particularly the elongational behavior under fast flow, are still quite limited. This study attempts to resolve the relationship between the stress growth, dissociation/re-association kinetics, and fracture behavior of telechelic ionomers.

Experimental methods: Linear viscoelasticity (LVE) and nonlinear elongational rheological properties were examined for telechelic chains having poly(isobutyl acrylate) as the backbone and -COONa as the end groups. These telechelic samples were synthesized *via* the RAFT polymerization.

Experimental results and Discussion: Linear viscoelastic (pseudo-) master curves was constructed for the -COOH based precursors and the -COONa based ionomers. The time temperature superposition (tTs) holds for the acid samples so the master curves were easily constructed. In contrast, tTs fails for the ionomer samples. For this case, we constructed a pseudo-master curves according to a protocol developed in our previous study (*JOR*, 2017, 61, 1199-1207).

For the acid precursor samples, increasing M_n led to a reduction of the terminal relaxation modulus and an increase of the terminal relaxation time, in accordance with a prediction of the Rouse model. The plateau modulus G_N was smaller than νkT expected from the nominal number density ν of the chains each sustaining the thermal modulus kT . ($\nu = \rho N_A / M_n$, with ρ and N_A being the mass density of the chains and the Avogadro constant, respectively.) The difference between G_N and νkT increased with increasing M_n . This result suggests that not every telechelic chain behaves as a network strand and an effective number density ν_{eff} of the chains sustaining the network decreases with increasing M_n . In other words, the decrease of this effective ν_{eff} on an increase of M_n is much stronger than a decrease of the nominal ν .

This difference between ν_{eff} and ν led to significant changes of the non-linear elongational behavior. The strain hardening and stretchability were commonly enhanced on an increase of M_n . This enhancement can be related to a higher freedom of conformational adjustment of the chain having larger M_n , possibly owing to a significant reduction of effective ν_{eff} explained above.

Publications:

1. Shuang Liu, Shilong Wu, Zhijie Zhang, Quan Chen and Hiroshi Watanabe, *Elongational Rheology of Telechelic Ionomers*, in preparation.
2. Shuang Liu and Quan Chen, *Elongational Rheology of Telechelic Ionomers*, IWEAYR-15 in Changchun, China, Jan 8-11, 2020.

都市大気エアロゾルの起源および発生メカニズム解明に関する研究

中口 譲 近畿大学

目的) 中国及び韓国では冬季において $PM_{2.5}$ が環境基準を超える日が多く、大きな社会問題となっている。また、中国大陸では春季には砂漠地帯で舞い上がった砂が偏西風に乗って日本にまでもたらされるが、この黄砂粒子には工業地帯で生じた汚染物質が吸着し、日本に到達する所謂越境汚染の可能性も指摘されている。本研究では日本国内で大気エアロゾルを捕集し、エアロゾル中のイオン成分分析ならびに微量重金属分析を行うことにより、中国大陸を起源とする物質が大気を経由して日本に到達する過程で、どの程度除去されるのか、また、通過点である東シナ海洋上で変質する可能性が有るならば、どのようなメカニズムで変成するか解明することを目的に研究を行った。

方法) 大気エアロゾル試料は、2019 年 3 月 25 日～5 月 23 日にかけて、大阪府東大阪市近畿大学 22 号館屋上に設置したハイボリュームエアーサンプラー（紀本電子工業製 AS-9）に PTFE フィルター（ADVANTEC 社製 90φ）を装着して、24 時間毎に交換して採取した。試料採取後のフィルターは Fine 部（粒子径 $2.5\mu m$ 以下）、Coarse 部（粒子径 $2.5\sim 10.0\mu m$ ）にカットし、水溶性イオン成分は HDPE ボトルに移し、純水を加え超音波照射を 15 分行い溶出し、これを $0.45\mu m$ フィルターでろ過した後、イオンクロマトグラフシステム（Dionex 社製、ICS-1500）にて分析を行った。微量重金属はカットしたフィルターを電子レンジ用反応分解容器（三愛科学製、P-25）に移し、高純度硝酸、高純度過塩素酸、高純度フッ化水素酸を加え、電子レンジ内で分解を行った後、誘導結合プラズマ質量分析装置（PerkinElmer 社製 NexION350）にて分析を行った。 $PM_{2.5}$ 、 PM_{10} の分析は微小粒子状物質自動計測器 SPM-613D にて行った。

結果) 2019 年は 4 月 6, 7, 16 日に黄砂が飛来した。NOAA の後方流跡線により解析した結果、この黄砂はゴビ砂漠上空を通過してきていることが分かった。黄砂時 4 月 6 日の $PM_{2.5}$ 、 PM_c (PM_{10} 濃度から $PM_{2.5}$ 濃度を差し引いた) はそれぞれ $50\mu g\cdot m^{-3}$ と、中国における黄砂の基準値 $1500\mu g\cdot m^{-3}$ に比べると低く、黄砂の規模としてはそれほど大きくはなかった。黄砂時は土壌起源の Al や Fe 濃度の増加は認められたが、人為起源で汚染物質と考えられているイオン成分である NH_4^+ と非海塩性硫酸については黄砂時に濃度上昇する傾向は認められなかった。また、重金属である Pb についても、特に濃度は増加しなかった。2016 年から 2019 年にかけて東大阪市に飛来する黄砂の規模を Al の乾性沈着量を基準として見れば、その規模は年々減少する傾向が認められ、土壌粒子に付着してもたらされる Pb についても同様の結果が得られた。以上の結果より黄砂による越境汚染の影響は年々減少していることが分かった。

成果報告（論文、学会発表等）

- 1) 西川 遼、辻阪 誠、佐野 到、中口 譲、宗林 由樹（2019）黄砂による中国大陸からの越境汚染に関する研究、2019 年度日本地球化学会第 66 回年会 講演要旨集 1P01
- 2) 西川 遼 修士論文（近畿大学） 東大阪市における黄砂による越境汚染に関する研究

Study on transportation and separation of metal ions through a liquid membrane using ionic liquid

Hiroshi Mukai Kyoto University of Education

Introduction Liquid membrane (LM) transportation is one of the membrane separation methods and can be applied to the separation and concentration of useful or harmful metals and compounds. This study aims to establish a new LM transportation system using ionic liquid (IL) taking account of the unique characteristics of IL. A supported membrane using membrane filter is often applied to IL. However, it often have trouble by the leak of the IL from the membrane pores and fail to be a separator of two aqueous phases. In order to obtain a stable membrane, a polymer membrane of polyvinyl chloride (PVC) containing IL was considered. The possibility of this PVC membrane as a LM for transportation of metal ions was investigated.

Experimental (1) Preparation of PVC membrane: 0.002 g of 1-Phenyl-3-methyl-4-benzoylpyrazol-5-one (PMBP) was dissolved in 1.38 g of 1-hexyl-3-methylimidazolium bis(trifluoromethanesulfonyl)imide ($[\text{C}_6\text{mim}][\text{Tf}_2\text{N}]$, $d = 1.38 \text{ g cm}^{-3}$) at the concentration of $0.005 \text{ mol kg}^{-1}$. This IL solution and 0.1 g of PVC were dissolved in 5 g of tetrahydrofuran in the glass petri dish of 49 mm inner diameter and were dried.

(2) LM transportation: The membrane was fixed at the center of the U-shaped reaction cell. The 25 cm^3 of aqueous supplying phase ($[\text{Cu}(\text{NO}_3)_2] = 2.0 \times 10^{-5} \text{ mol dm}^{-3}$, $[\text{CH}_3\text{COONa}] = 0.01 \text{ mol dm}^{-3}$, pH 3.0) and the 25 cm^3 of aqueous receiving phase ($[\text{CH}_3\text{COONa}] = 0.01 \text{ M}$, pH 0.1) were poured into each part of the reaction cell separated by the membrane. After a certain period of reaction time, the pH values, the volumes and the Cu concentrations of the supplying and receiving aqueous phases were measured.

Results and discussion The pH values of the supplying and receiving phases were kept constant through the experiments. The membrane was confirmed to work stably as a separator of the two phases. Table shows the results of LM transportation of Cu^{2+} ions under the different experimental conditions. Compared between Nos. 3 and 4, it was found that the dissolution of a carrier (PMBP) in IL is essential for the transportation of metal ions. This suggests that IL works as a dispersion media of complexes of metal ions with carriers in the LM. The active transportation (transportation rate 0.88) of Cu^{2+} ions was achieved for 48 h (No. 5). However, 10% of Cu^{2+} ions still remained in the LM. This suggests that the diffusion of metal complexes passing through the LM of 0.5 mm thickness is relatively slow. For the improvement of the transportation rate, it is necessary to fasten the diffusion of metal complexes in LM. It will be worth considering to apply the alternative voltage between the both interfaces of LM taking account of the electric conductivity of IL.

Table Results of liquid membrane transportation of Cu^{2+} under the different experimental conditions.

No.	PVC [g]	IL [g]	PMBP [g]	Time [h]	Transportation Rate [–]	Fraction in LM [–]
1	0.1	–	–	6	0.01	0.01
2	0.1	1.38	–	6	0.01	0.01
3	0.1	–	0.002	24	0.02	0.00
4	0.1	1.38	0.002	24	0.82	0.15
5	0.1	1.38	0.002	48	0.88	0.10

Study on gelation behaviors of polymer oleogels

OSAKA Noboru Okayama University of Science

Food-grade polymer oleogel is a physical gel formed by fibrillation of polymer chains by cooling using fatty acids or fats and oils as solvents. Since it can be made in any combination, it is expected as excellent food material for reducing and replacing trans fatty acids and saturated fatty acids, and assisting chewing. However, many of the existing researches have been studied from the viewpoint of applications using commercially available edible oils composed of various fats and oils. To reveal the gelation mechanism, we therefore prepared the oleogel from polymer and purified fatty acids or triglycerides as the ideal two-component systems, and investigated the *in-situ* structural changes during the gelation by the time-resolved wide- and small-angle X-ray scattering (WAXS/SAXS). The results also provide a systematic understanding of the influence of the structure of organic solvents from linear to three-arm to the gelation behaviors, which has been rarely studied in polymer science.

Ethylcellulose (EC, 45 cP) was supplied from NISSHIN & CO., LTD. Oleic acid (OA, 99%), methyl oleate (MO, 99%), glyceryl trioleate (GT, 99%) were purchased from Sigma-Aldrich. WAXS/SAXS measurements were carried out at BL40B2 of SPring-8. The exposure time was 12 s with the delay time of 8 s. The temperature interval corresponded to 1 °C during cooling at 3 °C/min.

Gelation temperatures of EC oleogels (20 wt%) were determined at the cross-over points between G' and G'' by the temperature sweep of dynamic mechanical experiments. They increased from 26 °C (EC/OA) and 40 °C (EC/MO) to 120 °C (EC/GT) due to the fewer interaction sites. Especially, a steric hindrance toward ester groups by the alkyl chain of the three arms highly increased the gelation temperature of EC/GT.

WAXS/SAXS measurements revealed that the structures of EC with some aggregates in OA remained almost unchanged (Figure 1). This result was also supported by the success in the application of time-temperature superposition of modulus vs angular frequency (data not shown). Therefore, it is considered that the gelation of EC/OA might be mainly caused by the decrease in the viscosity. On the other hand, EC in GT was revealed to form the worm-like chains at a high temperature from the fitting result (Figure 2). As the temperature decreased, they formed the higher-order structures with the sharp boundary. This structural development would be responsible for the gelation.

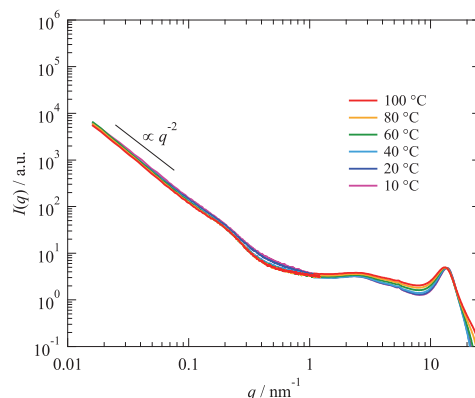


Figure 1: WAXS/SAXS profiles of EC/OA (20 wt%) during cooling.

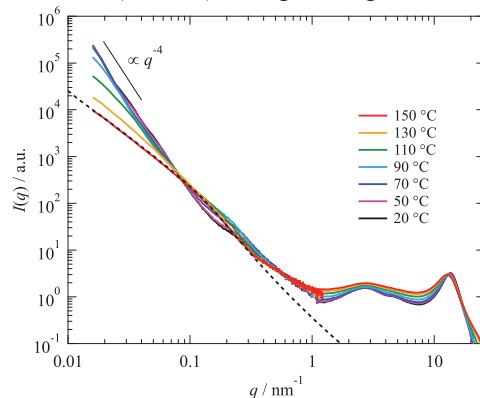


Figure 2: WAXS/SAXS profiles of EC/GT (5 wt%) during cooling. The dotted curve is the fitting curve.

機能性配位子保護量子ドットの緩和過程の解明

玉井尚登 関西学院大学

半導体ナノ結晶は、バルク材料と異なる光学的・化学的性質を持ち、発光材料、触媒、太陽電池、電子材料など多種多様な用途への応用が期待される材料である。特に、二種類の半導体ナノ結晶を接合した系では、コアとなる半導体ナノ結晶の表面欠陥を除去し発光効率を増大させたり、光励起によって生成した電子・正孔を分離する等の様々な効果が期待できる。本研究では、吸収係数の大きな CdSe ナノプレート (NPLs) に PbS 量子ドット (QDs) を接合し、CdSe NPLs を光捕集剤として作用させたときの CdSe NPLs から PbS QDs へのキャリア移動ダイナミクスをフェムト秒時間分解分光、ピコ秒発光分光により解析した。一方、半導体ナノ結晶の配位子がキャリアアクセプターとして作用することもあるが、その効果は十分に検討されていない。我々は、機能性配位子としてナノ結晶に単座および二座配位するポルフィリン誘導体を合成すると共に、サイズの異なった Cs 系ペロブスカイト CsPbBr₃ QDs に配位させてキャリア移動に及ぼす分子配向の効果を解析した。

4 層 CdSe NPLs および PbS QDs 接合 CdSe NPLs は京大化研・坂本, Lian らが合成した。単座および二座配位のポルフィリン誘導体はピロールとベンズアルデヒドを出発物質に 3 段階で合成を進め、NMR, MASS を用いて構造解析を行った。CdSe NPLs, PbS QDs 接合 CdSe NPLs, CsPbBr₃ QDs は高分解能 TEM 測定により構造解析を行った。フェムト秒過渡吸収測定は、増幅した Ti:Sapphire レーザーと OPA を励起光に用い、フェムト秒白色光をプローブ光として行った。また、近赤外領域のピコ秒発光ダイナミクスは、近赤外 MCP 光電子増倍管を検出器として時間相関単一光子計数法により解析した。

発光スペクトルは、CdSe NPLs に比べ PbS QDs 接合により NPLs の発光が消光すると共に近赤外領域に PbS 由来の発光が観測された。これは、NPLs から PbS への電子および正孔の両方が移動していることを示唆している。CdSe NPLs の可視領域発光寿命は、PbS 接合によって約 1 ns から 3 ps 以下と著しく短くなった。また PbS 近赤外発光は 5 ps 以内に立ち上がっており、電子・正孔が超高速で CdSe NPLs から PbS に移動している事がわかった。フェムト秒過渡吸収スペクトルから NPLs の heavy hole ブリーチを解析したところ、NPLs から PbS QDs への電子移動が 630 fs (64%) で起こっている事が明らかになった。更にこの時定数は励起光強度依存性があり、NPLs のマルチエキシトン生成によってキャリア移動が遅くなる事を見出した。

一方、CsPbBr₃ QDs の励起子発光は配位するポルフィリン誘導体の種類によって大きく異なり、単座よりも二座配位ポルフィリンの方が顕著な消光が確認された。またその効果は、QDs のサイズが小さい程強い消光を受けた。分子配向効果を明確に示したのは本研究が初めてである。フェムト秒過渡吸収および発光ダイナミクスの解析から、サイズの小さな QDs では波動関数の染み出しが大きく、ポルフィリン誘導体と QDs の相互作用が配位の影響を強く受けると考えられる。

新規部分フッ素化リン脂質分子群の 膜物性・構造のキャラクタリゼーション

園山正史 群馬大学

【目的】

私たちは際だった表界面物性を示すパーフルオロアルキル基(Rf)に着目し、膜タンパク質研究に広く用いられるリン脂質 Dimyristoylphosphatidylcholine (DMPC)および Dipalmitoylphosphatidylcholine (DPPC)のアシル鎖末端を、種々の長さの Rf 基により置換した部分フッ素化リン脂質群 *Fn*-DMPC および *Fn*-DPPC を開発している。一方、これらの部分フッ素化リン脂質のアシル鎖を構成する一本鎖分子である部分フッ素化脂肪酸に関する長谷川健教授との界面化学に関する共同研究から、「多層双極子アレーモデル」が Rf 化合物特有の性質を合理的に説明できること等を明らかにした。本研究では、Rf 基を有する二本鎖分子である *Fn*-DMPC および *Fn*-DPPC の脂質二分子膜の物性・構造を系統的に解析し、その特異的な性質の起源を明らかにすることを目的とした。

【実験方法】

高木らの方法により部分フッ素化リン脂質分子群をグラムスケールで合成した。脂質二分子膜の熱物性の解析には日立ハイテクサイエンス社製示差走査熱量計 DSC6100-Exstar6000 を用い、放射光 X 線回折測定は高エネルギー物理学研究機構 Photon Factory において行った。

【結果・考察】

広角 X 線回折測定結果を考慮すると、アシル鎖長および Rf 鎖長の違いに関係なくいずれの部分フッ素化リン脂質も DSC 曲線においてゲル-液晶相転移に由来する吸熱ピークを示した。一方相転移温度 T_m は、*Fn*-DMPC および *Fn*-DPPC で類似した顕著な Rf 鎖長依存性を示した。すなわち短い Rf 基 ($n=2, 4$) を有する場合、それぞれの部分フッ素化リン脂質の T_m はそれに対応する非フッ素化リン脂質に比べて約 20 °C 低下するのに対し、 $n=6$ に伸長すると非フッ素化リン脂質と同程度の温度まで上昇した。さらに $n=8$ では 80 °C に近い相転移温度を示し、Rf 基導入による脂質二分子膜の著しい安定化が明らかになった。これらのことは、一本鎖分子である部分フッ素化ミリスチン酸単分子膜単分子膜で見られた特徴に概ね一致した。 $n=8$ の脂質二分子膜で見られる際だった安定性は、ゲル相における広角回折測定からアシル鎖の hexagonal packing に由来することが示唆された。部分フッ素化リン脂質単分子膜の表面圧-分子断面積等温曲線の予備的測定も類似した傾向を示しており、今後、赤外反射吸収の測定から二本鎖分子における構造・物性の Rf 鎖長依存性を明らかにする。

【成果報告】

1. Morita K. et al., Thermotropic Transition Behaviors of Novel Partially Fluorinated Dimyristoylphosphatidylcholines with Different Perfluoroalkyl Chain Lengths (2019) *Chem. Lett.* **48**, 1105-1108.
2. Sonoyama, M., Membrane Properties of Partially Fluorinated Phosphatidylcholine Bilayer, 16th International Conference on Flow Dynamics (ICFD2019), Sendai, Nov. 8, 2019. 他 2 件口頭発表

スチレン系ブロック共重合体をベースとした 非共有結合性エラストマーの調製と力学特性

野呂篤史 名古屋大学

＜目的＞ 室温より T_g が高い高分子 A と室温より T_g が低い高分子 B とを連結させた ABA トリブロック共重合体は、A 成分が凝集して形成するハードドメイン間を柔らかい B 成分が橋架けして網目を形成しているために、伸縮性を示す熱可塑性エラストマー（TPE）として振る舞う。ポリスチレンーポリイソプレンーポリスチレントリブロック共重合体（SIS）はその典型例であり、最近では SIS の中央 I ブロックに酸無水物を付加し、これをアミンで処理することで、水素結合性官能基を導入した非共有結合性エラストマーが調製されている。引張試験も行われているが、特定の伸長速度での評価に留まっていた。そこで本研究では、SIS をベースポリマーとした非共有結合性エラストマーを調製し、異なる伸長速度での引張試験を行った。

＜実験方法＞ 数平均分子量 15 万（GPC 換算）、ポリスチレン含有率 19 wt% の SIS を無水マレイン酸と反応させ、無水コハク酸ユニットを 7.8 mol% 導入した。さらにそれと等モル量の *n*-ブチルアミンとを反応させて水素結合性官能基（アミド基とカルボキシル基）とした SIS（mSIS と記述）を合成した。溶液キャストにより膜試料とし、室温でつかみ具間距離約 10 mm、伸長速度を約 10、1.0、0.10 mm s⁻¹（初期歪み速度 $\dot{\epsilon}_0$: 1.0、0.10、0.010 s⁻¹）として引張試験を行うことで力学特性を評価した。

＜実験結果・考察＞ 引張試験により得られた応力-歪み曲線を Figure 1 に示す。官能基導入前の SIS の破断伸び ϵ_{\max} は、 $\dot{\epsilon}_0 = 1.0, 0.10, 0.010$ s⁻¹ ではそれぞれ 31.5、29.3、22.6 であり（Figure 1(a)）、伸長速度が低くなると ϵ_{\max} は小さくなった。一方、mSIS では、 $\dot{\epsilon}_0 = 1.0, 0.10, 0.010$ s⁻¹ でそれぞれ $\epsilon_{\max} = 31.7, 31.3, 32.1$ であり（Figure 1(b)）、 ϵ_{\max} は伸長速度に依存せず、ほぼ一定であった。mSIS では伸長中に水素結合が解離と会合を繰り返して応力を分散させるために、伸長時の時間が長くても、ハードドメインからのポリスチレン鎖の引き抜きは生じにくく、高伸長速度のときと同程度のひずみまで伸長できたと考えられる。

＜成果報告（学会発表等）＞

「非共有結合性の架橋点を有したブロック共重合体エラストマーの合成と力学特性」梶田貴都・田中春佳・野呂篤史・松下裕秀・野澤淳・小田亮二・橋本貞治、日本レオロジー学会第 47 年会、2020 年 5 月 13 日、東京（東京大学生産技術研究所）

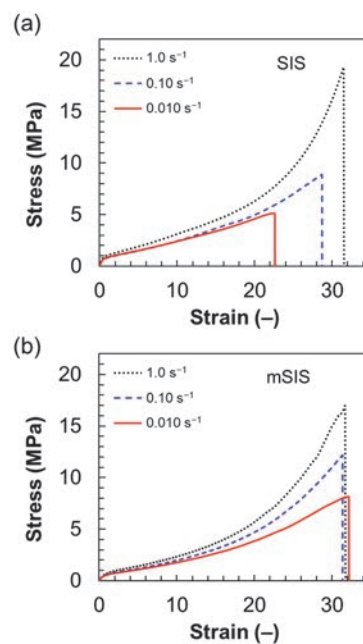


Figure 1. Stress-strain curves of (a) SIS and (b) mSIS.

Regulatory network of gene expression for plant cell morphogenesis

Li-Jia Qu Peking University

Objectives: The root epidermis of *Arabidopsis thaliana* has been intensively studied as an excellent model system of cell differentiation in plant science fields. In root epidermal cells, numerous transcription factor genes constitute a regulatory network, in which *GLABRA2* (*GL2*) serves as a genetic switch that suppresses root hair development in non-root-hair cells. We have studied on the regulatory network, and identified various transcription factor genes, including *Lj-RHL1-LIKE1* (*LRL1*), that is directly suppressed by *GL2* in non-root-hair cells. In this study, to understand the total regulatory system for root hair cell morphogenesis, we attempt to identify genes functioning downstream of *LRL1*.

Experimental Methods: A modified *LRL1* gene expressing LRL1-fusion protein with the glucocorticoid receptor domain at (LRL1-GR) by the *LRL1* promoter was introduced it into the *lr1* mutant line. For a control experiment, a similar modified *ROOT HAIR DEFECTIVE6* (*RHD6*) gene expressing RHD6-GR by the *RHD6* promoter was introduced into the *rh6* mutant line.

Results and Discussion: The RHD6-GR fusion gene complemented the short-root-hair phenotype of *rh6* depending on the presence of dexamethasone (DEX), a glucocorticoid derivative, indicating that the glucocorticoid-dependent transcriptional activation system works well. Similarly, the LRL1-GR fusion gene complemented the short-root-hair phenotype of the *lr1lr2/+* homo/hetero double mutant depending on the presence of DEX. Using the LRL1-GR transgenic line with the *lr1lr2/+* background, an induction experiment for the identification of LRL1 downstream target genes was performed. As a result, genes encoding regulatory proteins of plant Rho-type GTPases were detected as those transcriptionally activated by the treatment of root with DEX. This indicates that LRL1 transcriptionally activates these genes directly or indirectly in roots.

Conference Presentation: K. Yamada, M. Kato, T. Tsuge, T. Wada, R. Tominaga, L.-J. Qu, T. Aoyama, Functional Analysis of the *Arabidopsis* Transcription Factor Gene *LRL1*. The 61st Annual Meeting of JSPS, March 19-21 2020, Osaka.

Role of PX-PH-type phospholipase Ds in plant intracellular membrane traffic

Yohei Ohashi University of Cambridge

Objectives: Phospholipase D (PLD), an enzyme hydrolyzing glycerophospholipids to produce phosphatidic acid, is implicated in promoting a wide variety of cellular processes, including membrane trafficking, signaling for gene expression, and phospholipid metabolism, in eukaryotes. PLD is requisite also for plants in their development according to the genetic program and responses to environmental stimuli. However, particular processes promoted by PLD in plant cells largely remain elusive because plural species of PLD proteins function in various intracellular compartments differentially from or redundantly to each other. We analyzed intracellular localization of PLD ζ 1 and ζ 2, eukaryote-general PX-PH-type PLDs of *Arabidopsis thaliana*, in root tissues for a clue as to their functions in cell biological processes.

Experimental Methods: Transgenic *Arabidopsis* lines, which expressed fluorescence protein fusions of PLD ζ 1, PLD ζ 2, and their N-terminal partial proteins, were constructed, and crossed with lines expressing various fluorescence markers for intracellular localization.

Results and Discussion: PLD ζ 1-mCherry co-localized with a *trans*-Golgi network or Early Endosome (TGN/EE) marker when directed by the *PLD ζ 1* promoter. *PLD ζ 2* promoter-driven PLD ζ 2-GFP localized mainly to the tonoplast, and partly localized to punctate structures including the pre-vacuolar compartments or multivesicular bodies (PVCs/MVBs). These localization patterns were reproduced by fluorescent protein fusions of their N-terminal moieties containing the PX-PH domains. These results suggest that PLD ζ 1 and ζ 2 target different but consecutive compartments along the membrane traffic pathway to the tonoplast *via* their N-terminal domains.

Conference Presentation: R. Shimamura, Y.Y. Taniguchi, Y. Ohashi, M. Kato, T. Tsuge, T. Aoyama, *Arabidopsis* Phospholipase D ζ 1 and ζ 2 Target Different Intracellular *via* Their N-terminal Domains. The 18th International Workshop on Plant Membrane Biology, July 7-12 2019, Glasgow.

Site-selective protein acetylation by a small molecule

Lu Zhou Fudan University

Post-translational modifications (PTMs) play essential roles in regulating a myriad of cellular processes in mammalian cells, including signal transduction, metabolism, and gene transcription. Dysregulation of protein modifications causes metabolic diseases, neurodegenerative diseases and cancers. Among protein modifications, lysine acetylation is precisely controlled by acetyltransferases and deacetylases, and represents a PTM critical for signal transduction and cellular metabolism.

Our previous work reported that phosphoglycerate mutase 1 (PGAM1), an enzyme that converts 3-phosphoglycerate (3-PG) into 2-phosphoglycerate (2-PG), plays a pivotal role in coordinating glycolysis and biosynthesis to promote tumor growth. The activity of PGAM is suppressed by acetylation of an active site residue Lys-100 (K100) under oxidative stress and upregulated by protein deacetylase sirtuin 1/2. Lys-100 of PGAM is conserved from bacteria to mammals, increasing substrate recognition through electrostatic interaction with the carboxyl group of 3-PG. It has been shown that point mutation or acetylation of Lys-100 abolished substrate binding and enzymatic activity.

In this project, we collaborated with the Uesugi research group in ICR, Kyoto to design a small-molecule acetylase mimic that specifically acetylates Lys-100 of PGAM1 in vitro and in cultured cells. We also initiated a project to discover more small-molecule acetylases selective for a number of different proteins from a chemical library of acetyl ester compounds. The results are summarized below.

- Our collaboration has already led to the discovery of a small-molecule acetylase mimic that specifically acetylates Lys-100 of PGAM1. The molecule, referred to as KHA_c, has an acetyl ester group as an acetyl donor. Time-resolved crystallography experiments demonstrated that the acyl-transfer to Lys-100 is driven by “proximity effects”. Together with the Uesugi group, we examined the selectivity of the molecule and found that KHA_c is selective to PGAM1 at the proteome level. We have summarized the data and submitted for publication (under review).
- To discover more small-molecule acetylases selective for a number of different proteins, we screened a chemical library of 280 acetyl ester compounds. Each of these molecules was incubated with cell lysates or even live cells, and acetylated proteins were analysed by western blots with a pan-antibody against acetylated lysine. This screen identified 4 promising molecules that appear to acetylate particular proteins.

Proteomic approach to discovering specific inhibitors for bile-acid interacting enzymes

Xiaoguang Lei Peking University

Bile acids (BAs) are important amphipathic molecules produced in the liver that improve lipids digestion by emulsification. Bile acid metabolism and signalling have been gaining significance due to the relationship between bile acids and diseases such as cancer, type 2 diabetes, cardiovascular, cholestatic and fatty liver disorders (Thomas et al., 2008). While endogenous receptors for bile acids, in particular the nuclear farnesoid X receptor (FXR) and the plasma membrane bound G protein-coupled receptor (TGR5) have been widely investigated (Thomas et al., 2008), the biological significance of other bile acid-binding proteins remains unexplored.

Our group in Peking University recently discovered more than 600 novel bile acid-interacting proteins (Zhuang et al., 2017). In this project, we collaborated with the Uesugi group in ICR for analyzing those bile acid-interacting proteins and for discovering small molecules that selectively block the interactions. The Uesugi group of ICR has recently developed a chemical library of bile acid analogues. Bile acid analogues have shown to activate or antagonize known bile-acid interacting proteins (Thomas et al. 2008).

In 2019, our collaboration selected 5 proteins involved in important lipid metabolic pathways from the 600 bile acid-interacting proteins, and experimentally tested their ability to interact with bile acids. Consequently, we found Protein X as a bile acid-binding protein.

The enzymatic activity of protein X was evaluated in vitro with a simple fluorogenic assay. When the enzymatic reaction was measured in the presence of bile acids, most of them displayed limited effects on the enzymatic activity of protein X. In contrast, chenodeoxycholic acid (CDA) decreased the enzymatic activity. The results indicated that CDA reduced the enzymatic activity in a concentration dependent manner. Therefore we decided to focus on protein X for further study in ICR and Peking University. To identify specific inhibitors, the library of bile acids analogues will be screened in ICR.

Study of magnonic properties of ferrimagnets

Kab-Jin Kim KAIST

Objective:

The aim of the research is to understand the magnonic properties of rare earth (RE) – transition metal (TM) ferromagnetic alloys.

Experimental methods:

For this study, we patterned the RE-TM ferromagnetic films at prof. Teruo Ono's group in ICR and measured the electrical and optical properties at KAIST. The sample resistance as well as the Hall resistance was measured by sweeping the magnetic field. For optical measurement, we employed MOKE.

Experimental results:

We investigated device resistance as a function of magnetic field, because the magnon contribution is generally reflected by the device resistance through the electron-magnon scattering. In the existing theory, the resistance should be decreased as we increase the magnetic field, since the magnetic field suppresses the magnon excitation. We found that the resistance decreases with increasing magnetic field at high temperature, as expected. However, we found that the trend is reversed at temperatures below the magnetization compensation point, T_M (Fig. 1). We also found that the absolute value of slope increases with decreasing low temperature (Fig. 2).

Discussion:

The sign change at T_M indicates that the device resistance is closely related to the unique ferromagnetic properties. However, the increase of slope at low temperature suggests that the resistance variation is not originated from magnons but from other exotic properties. We currently speculate that the sperimagnetism of RE-TM ferrimagnet may play a role in the unexpected observations. Additional experiments are now ongoing.

Publication:

As mentioned above, the work is still ongoing.

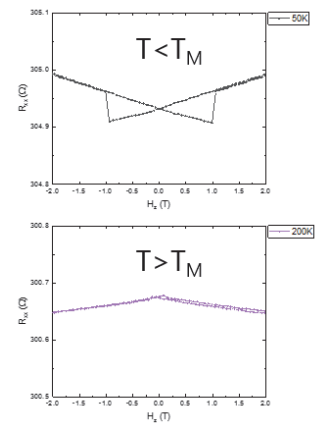


Figure 1. Device resistance (R_{xx}) as a function of magnetic field in GdFeCo wires. For higher (down) or lower (up) than the magnetization compensation point.

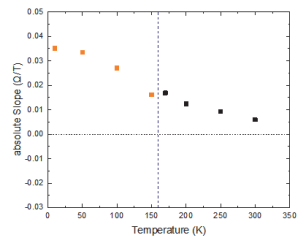


Figure 2. The absolute magnitude of slope in R_{xx} – H curve for several temperatures.

Development of highly efficient and stable blue organic light emitting diodes using thermally activated delayed fluorescent materials as sensitizer

Dongdong Zhang Tsinghua University

The prospect of using organic semiconductors for organic light-emitting diodes (OLEDs) has flourished since the pioneering work by Tang et al in the 1980s. OLEDs have enormous potential for application in smart phones, flat-panel displays, and solid-light illuminations. Highly efficient and stable blue materials remain the “Holy Grail” for OLEDs even though they are highly sought for practical applications. Thermally activated delayed fluorescence (TADF) emitters, as intrinsically pure organic materials, may provide an alternative solution for stable and efficient blue emitters. The lifetimes of the blue TADF devices are still far from satisfaction, and to my knowledge, only quite few guidelines have been proposed for highly efficient and stable blue TADF devices, which, however, are highly desired in both practical application and literatures. Building upon this scope, our research purpose is to develop well performed TADF emitters and fabricate highly-efficiency stable blue TADF devices. Generally, when TADF materials are used as dopants in OLEDs, two critical requirements should be fulfilled simultaneously: a small energy gap (ΔE_{ST}) between the singlet and triplet excited states, which enhances RISC from triplet excited states (T_1) to singlet excited ones (S_1), and a reasonable radiative decay rate (k_r), so as to overcome competitive non-radiative decay pathways and attain a high photoluminescence (PL) efficiency (Φ_{PL}). Also it is important to improve the reverse intersystem crossing speed to suppress the efficiency roll-off of OLEDs at high brightness.

In this work, we newly developed blue TADF emitter, 23XCz and 33XCz, which have an electron accepting unit to promote the RISC process. 23XCz and 33XCz showed blue emission with peak top wavelength shorter than 485 nm. The Φ_{PLS} of the two compounds were higher than 85%. The photoluminescence lifetime measurements revealed that both compounds showed clear delayed fluorescence with the order of several μs , which indicate the fast RISC process from T_1 to S_1 and make these compounds attractive candidates as emitters in blue OLEDs. The OLEDs using 23XCz and 33XCz as emitting dopants showed blue EL spectra almost same as respective PL spectra, indicating that excitons are well confined in the emitting layer. The maximum EQEs of the devices exceed 5%. These devices also maintain high EQEs even at high brightness at around 15000 cd m^{-2} thanks to the fast RISC process.

Highly efficient blue thermally activated delayed fluorescence emitters using sterically hindered donor skeleton

Jang Hyuk Kwon Kyung Hee University

Organic light emitting diodes (OLEDs) has been a major concern for flat panel display and solid-state lighting applications. In recent years, metal-free thermally activated delayed fluorescence (TADF) has been extensively studied as an efficient and cost effective method to utilize triplet excitons by reverse intersystem crossing (RISC) from the lowest triplet excited state (T_1) to the lowest singlet excited state (S_1). Since the first report of highly efficient TADF emitters by Adachi's group, a number of blue TADF emitters showing EQE's over 20% are developed. However most of these emitters displayed high efficiency roll-off due to exciton quenching (triplet-triplet annihilation and singlet-triplet annihilation, triplet-polaron quenching), poor operational stability by long-lived exciton degradation, and low thermal stability. To address this issue, we need to design new TADF molecules with high rate constant for RISC (k_{RISC}).

Recently, we developed a new electron donor unit for efficient TADF emitters. The electron donor unit has wide aromatic plane and can deliver a large spatial highest occupied molecular orbital (HOMO) volume to emitters, leading to small energy gap between S_1 and T_1 (ΔE_{ST}), high oscillator strength as well as a high k_{RISC} originated from a rigid ring system. In addition, the rigid donor skeleton is expected to restrict the rotation around donor-and acceptor units, resulting in narrower spectral line width than conventional TADF emitters.

In this year, we designed new TADF candidates using the above mentioned donor. From the screening based on evaluation of ΔE_{ST} and oscillator strength using quantum chemical calculation, we could find a series of TADF candidates. Owing to the large dihedral angle around 65° between the donor and acceptor unit, HOMOs, and LUMOs are well delocalized on donor and acceptor segments respectively. The quantum chemical calculation dictate that these compounds have small ΔE_{ST} value lower than 50 meV and large oscillator strength over 0.1, which makes designed compound attractive candidate for TADF emitters.

We tried to synthesize acceptor segment. Starting from a precursor, fluorophenyl groups were attached by Stille reaction to yield trifluorophenyl derivative. The trifluorophenyl derivative was afforded to aromatic electrophilic substitution reaction with donor unit in DMF solution in the presence of K_2CO_3 . High resolution mass spectra show the formation of target compounds. However, the yield is too low for further purification and isolation. Now we are trying to optimize the synthetic route for further device application.

Structural analysis of organic amorphous thin films using solid effect dynamic nuclear polarization NMR

Takeshi Kobayashi U.S. Department of Energy

Elucidating the conformation of molecules and their orientation in the amorphous films is a key to understand the photophysical properties of organic light-emitting diodes (OLEDs). For such studies, solid-state NMR (ssNMR) spectroscopy is a suited tool; however, its inherently low sensitivity has limited the applications. In particular, thin-films supported on a substrate are often incompatible to ssNMR, because very little of the thin-film components to be observed is contained in the sample. Recent advances in dynamic nuclear polarization (DNP)-enhanced ssNMR have achieved significant sensitivity improvement, often exceeding 100-fold \times , and have opened up a new route to study thin-film samples.

I. Search for Polarizing Agents for DNP ssNMR under static conditions. While NMR spectrum recorded under a static condition contains rich information about the molecular conformations, most of DNP polarizing agents (PAs) have been developed for being used under a magic-angle spinning. Therefore, it is necessary to search for PAs that can efficiently enhance the signals from the organic amorphous films under static conditions. Following the previous screening of PAs using a model system, we have applied DNP-enhanced $^{31}\text{P}\{^1\text{H}\}$ cross-polarization (CP) experiments to a POPy₂ amorphous thin-film deposited on a sapphire substrate to compare various PAs in terms of DNP enhancement $\epsilon_{\text{on/off}}$ (defined as the ratio of the signal intensities obtained with and without microwave (MW) irradiation). Among the PAs examined, biradical molecules TEKPol showed the largest signal enhancement ($\epsilon_{\text{on/off}} \sim 40$), and also the highest sensitivity gain due to the fast DNP build-up. Indeed, ^{31}P NMR powder pattern was obtained from the thin-film within a reasonable experimental time (Figure 1), demonstrating the feasibility of the measurement of molecular orientations in the film at the thickness of realistic organic devices.

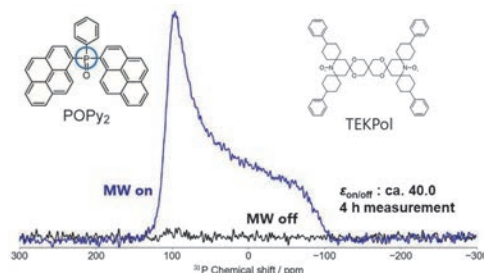


Figure 1. DNP-enhanced $^{31}\text{P}\{^1\text{H}\}$ CPMAS NMR spectra of POPy₂ film (300 nm thick) spin-coated on a sapphire substrate. The spectra were obtained with and without MW irradiation under static conditions. The POPy₂ and TEKPol (0.6 mol% with respect to the POPy₂) were mixed in chloroform before spin coating.

II. Measurement of torsion angle of TADF materials. We estimated the torsion angle of thermally activated delayed fluorescence (TADF) material, DACT-II depicted in Figure 2, by using DNP-enhanced ^{15}N NMR spectroscopy in combination with theoretical calculations. By comparing the chemical shift anisotropy δ_{CSA} (-48.0 ppm) and the asymmetry parameter η (0.15) derived from the ^{15}N NMR signal of the carbazole nitrogen with the DFT computed values, the torsion angle of the DACT-II in the amorphous film was estimated to be in the range between 40° and 45°. This angle differs from that obtained from the optimized structure by DFT calculation.

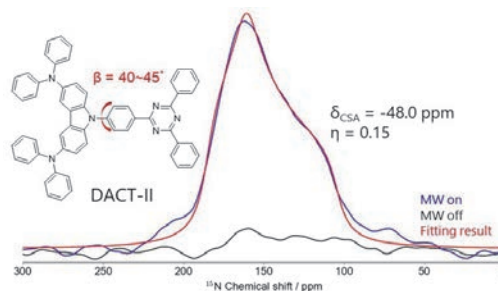


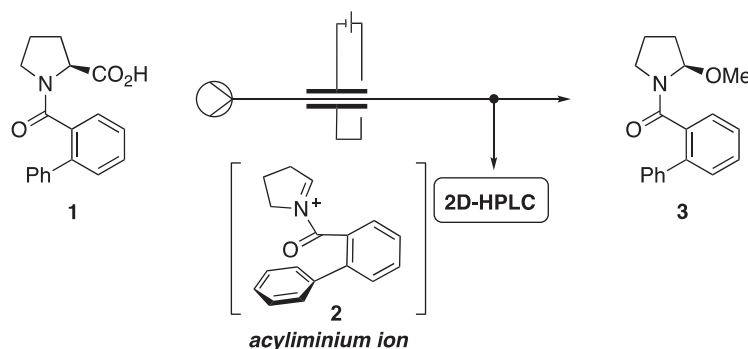
Figure 2. DNP-enhanced ^{15}N NMR of amorphous DACT-II film deposited on a sapphire substrate and the line fitting (red line). The spectra were obtained under static conditions.

Memory of chirality using flow electrochemistry

Thomas Wirth Cardiff University

Objectives: Amino acid derivatives undergo non-Kolbe electrolysis to afford enantiomerically enriched α -alkoxyamino derivatives through intermediate chiral carbenium ions. We explored this concept with the flow electrochemical setup we have developed earlier. The products of these reactions contain *N,O*-acetals which are important structural motifs found in bioactive natural products. The reaction is performed in a continuous flow electrochemical reactor coupled to a 2D-HPLC for immediate online analysis. This allowed a fast screening of temperature, electrode material, current, flow-rate and concentration in a DoE approach. Through the combination with online HPLC analysis we could also demonstrate that stereoselective reactions can benefit from a hugely accelerated optimisation by combining flow electrochemistry with multidimensional analysis.

Results and discussion: The enantioselective electrochemical oxidation of *N*-arylcarbonylated L-proline **1** to the chiral methoxylated amide **2** (Scheme 1) was optimised using a DoE-approach in a flow electro-microreactor coupled to an online 2D-HPLC. The short reaction times combined with fast analysis time made a rapid screening of charge, electrodes, flow rate, concentrations, temperature and thickness of the PTFE membrane possible. We established an efficient method to intensively screen several parameters to quickly optimised asymmetric transformations and obtain high yields (up to 100%) and enantioselectivities (up to 70% *ee*) within a short period of time as well as reducing waste. Once optimised, the reaction was scaled-up and the products were isolated without loss in enantioselectivity. The optimal conditions were successfully tested on different alcohols and protecting groups. The methodology presented here might find useful application in the rapid optimisation of other stereoselective transformations. We are very grateful to Prof. T. Kawabata (ICR) and his group for interesting discussions and advice.



Scheme 1. Electrochemical oxidation of *N*-arylcarbonylated prolin derivative **1** to chiral alkoxyated amide **3** in a flow electro-microreactor.

Publication: [Memory of Chirality in Flow Electrochemistry: Fast Optimisation with DoE and Online 2D-HPLC](#): M. Santi, J. Seitz, R. Cicala, T. Hardwick, N. Ahmed, T. Wirth, *Chem. Eur. J.* **2019**, 25, 16230 – 16235. (<http://dx.doi.org/10.1002/chem.201904711>)

Creation of functional molecules based on hydrogen bond networks

Jonathan Clayden University of Bristol

Objectives: The aim of the joint project is to create advanced functional molecules based on hydrogen bond networks. This year, we focused on the creation of axially chiral molecules whose chirality is retained by hydrogen bond(s). Chiral binaphthyls have been extensively used in asymmetric synthesis. Aiming at developing a new type of chiral binaphthyl skeletons, Kawabata's group at ICR has prepared chiral binaphthyl surrogate **1** (Scheme 1, Figure 1), in which the chirality was retained by an inner N-H-N hydrogen bond. The half-life of racemization of **1** was estimated to be 6 months at 20° C (*JACS*, **2009**, *131*, 54). Here, we report creation of chiral binaphthyl surrogates with further robust chirality and its organopalladium complexes.

Results and discussions: In order to create more advanced chiral binaphthyl surrogates with an inner hydrogen bond, molecule **2** with a quinoline substructure was designed and prepared (Figure 2). Molecule **2** was found to be further resistant to racemization than **1**, probably due to the additional hydrogen-bond donor property of the quinoline moiety. The X-ray structure of **2** showed a binaphthyl skeleton consisting of the N-H-N,N hydrogen bond (Figure 3a). The CD spectra of **2** obviously indicate the enantiomeric relationship (Figure 4a). The absolute configuration was assigned based on TD-DFT calculations. The corresponding Pd derivative **3** was successfully prepared and revealed to be a

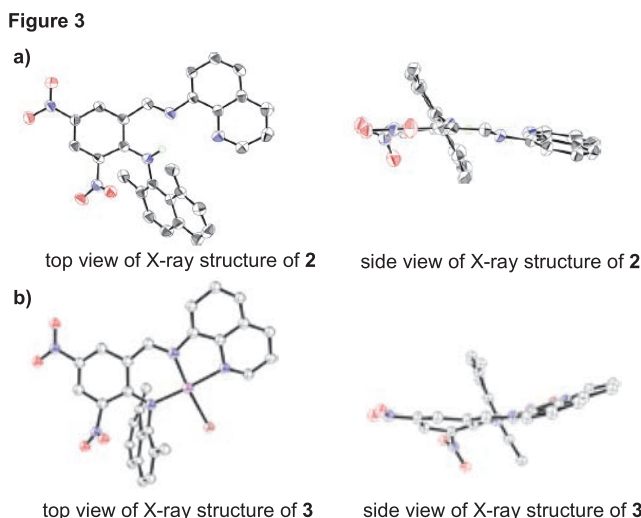
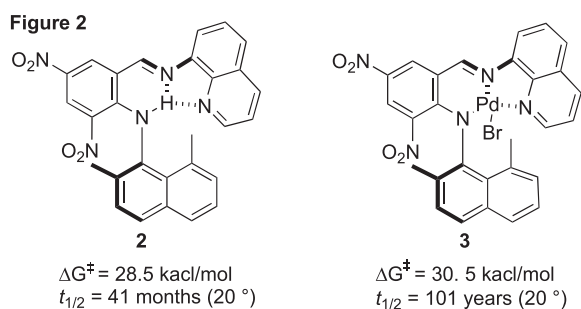
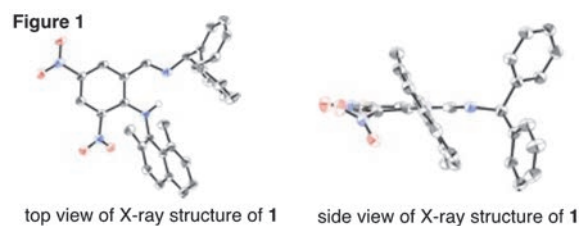
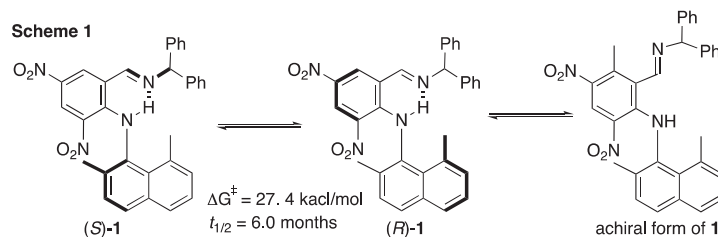
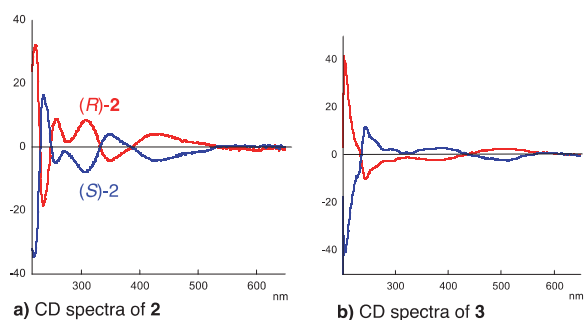


Figure 4



further robust chiral material (Figures 2, 3b, and 4b). A novel organopalladium complex **3** is expected to be a potentially useful novel type of organopalladium catalysts. We are grateful to Prof. T. Kawabata (ICR) and his group for discussions and collaborations.

Micro- and nano-structural characterization by advanced transmission electron microscopy of novel functional materials for battery development

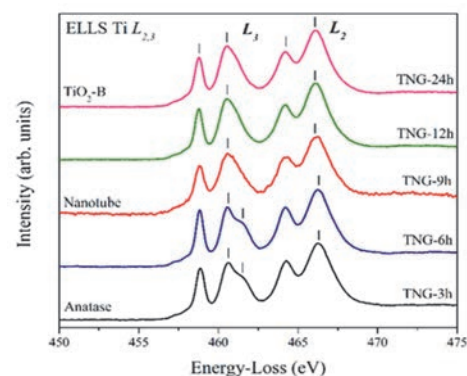
Torranin Chairuangstri Chiang Mai University

Our research group in Thailand has been collaborating with researchers at the ICR including Hiroki KURATA, Mitsutaka HARUTA and Tsutomu KIYOMURA in micro- and nano-structural characterization by advanced transmission electron microscopy of novel functional materials for battery development. Three manuscripts are being prepared for publication in refereed journals. The results can be summarized as follows:

I. Novel $\text{TiO}_2(\text{B})/\text{Nitrogen-doped Graphene Hybrid-composites (TNG)}$ as Anode in Advanced Power Batteries

Novel $\text{TiO}_2(\text{B})/\text{Nitrogen-doped graphene hybrid-composites (TNG)}$ were investigated by TEM at the ICR. Different morphologies of TiO_2 dispersed on nitrogen-doped graphene sheet were confirmed as anatase and bronze (B) phases (Fig.1). The best battery performance was obtained from the nanorods $\text{TiO}_2(\text{B})/\text{nitrogen-doped graphene (TNG-24h)}$ electrode with high specific capacity of 500 mAh g^{-1} at 1C (539.5 mA g^{-1}).

Fig. 1 TEM-EELS results showing Ti L_{2,3}-edges taken from TiO_2 in the TNG samples



II. Novel Zn-Mg Alloys as Anode in Metal-Air Batteries

Zn-(0-5wt.%)Mg and Zn-3Mg-(0-3wt.%)Bi alloys were investigated. ZnO and ZnO₂ were found as surface oxides on the pure zinc, whereas MgO₄ has been found in addition as a surface oxide on Mg-rich phases ($\text{Mg}_2\text{Zn}_{11}$ and MgZn_2) on the Zn-Mg alloys (Fig.2). The O K-edge structure taken from surface oxides on Zn-rich and Mg-rich phases by STEM-EELS also showed different characteristics and hence has a potential to be used as oxide fingerprint. The findings are useful for enhanced understanding on passivation behavior of these novel Zn-Mg alloys as compared to that of the pure zinc.

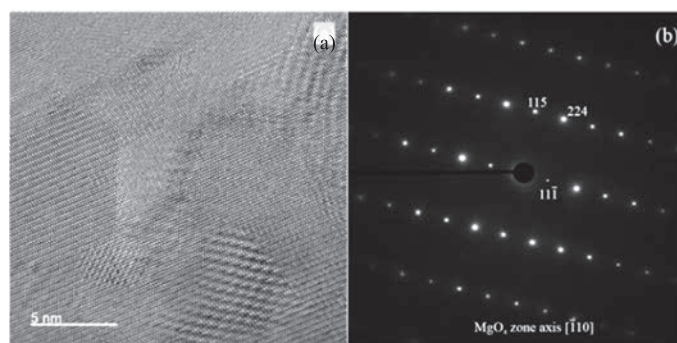


Fig. 2 (a) HRTEM image of an oxide product in Zn-3wt.%Mg on a Mg-rich phase, and (b) corresponding SADP

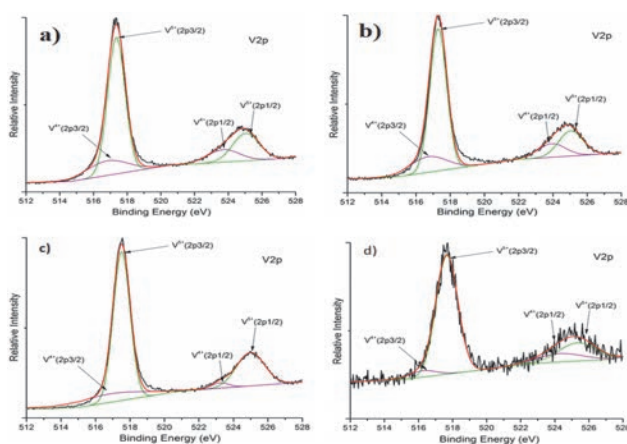


Fig. 3 XPS spectra of vanadium (V2p) of samples with a) 35, b) 40, c) 45 and d) 50 mol.%

III. Novel Nano Crystalline/Amorphous Vanadium Lithium Borate Glasses as Cathode in LIBs

Structural and local chemical analyses of vanadium-lithium-borate glasses containing V_2O_5 35-60 mol.% and prepared by a melt-quenched method were studied. Nanocrystalline phase of LiV_3O_8 was found by HRTEM. The oxidation state of vanadium was confirmed by XANES showing the majority of V^{5+} . This information is helpful for local environment interpretation in compliment to the results obtained from XPS, which classified vanadium sites into different environments. These evident can support the presence of vanadium in two environments as in amorphous matrix and nano-crystalline LiV_3O_8 (Fig.3).

Structural and functional analysis of the surface components of bacterial outer membrane vesicles

Maria Michela Corsaro University of Naples Federico II

Objectives:

The main objectives of this project were the isolation and structural characterization of the lipooligosaccharide (LOS) from *Shewanella vesiculosa* HM13 outer membrane vesicles (OMVs), to detect, if present, any differences with the LOS characterized from the cells (Casillo, 2019). To do this, the cells of a rifampin-resistant mutant were grown, and both the cells and OMVs were analysed.

Experimental:

Dried cells (3.8 g) and vesicles (202 mg) were extracted with phenol/chloroform/light petroleum (PCP) method to recover LOS with a yield 3% w/w from dried cells and 19% w/w from dried vesicles. Polyacrylamide gel electrophoresis (PAGE) was performed with sodium deoxycholate (DOC) as detergent, as reported (Casillo, 2019). All the chemical analyses, NMR and MALDI-TOF spectra were obtained as already reported (Casillo, 2019).

Results:

Both PCP extracts were analysed by DOC-PAGE and the gel showed, for both samples, the presence of the bands at low molecular masses, thus revealing a rough LPS (LOS). The same fast migrating species was observed for the cells of the bacterium *S. vesiculosa* HM13 grown at 4°C (Casillo, 2019). In addition, the GC-MS analysis revealed the presence of Glc, GlcN and both L,D- and D,D-heptoses, in agreement with the previous results (Casillo, 2019).

The LOSs from the cells and OMVs at 18°C were de-*O*-acylated with anhydrous hydrazine and the products obtained (LOSs-OH) were analysed by negative ions MALDI-TOF mass spectrometry, revealing that the signals attributable to the core fragments are the same of that obtained at 4°C (Figure 1) (Casillo, 2019).

Finally, full 2D-NMR analysis of the oligosaccharides obtained after a strong alkaline hydrolysis of the LOSs-OH revealed again the same backbone structure in both samples.

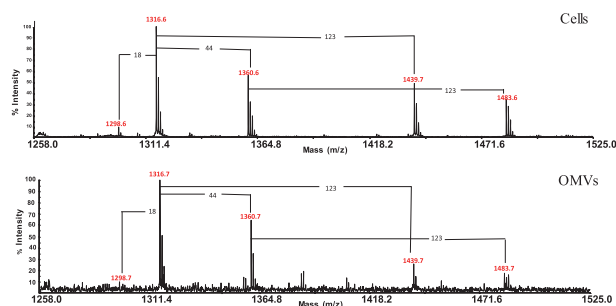


Figure 1. Negative ions MALDI-TOF mass spectra recorded in reflectron mode of the LOSs-OH.

Casillo, A. et al. Marine Drugs (2019), 17, 34.

Construction of low-temperature protein expression system by using cold-adapted microorganisms

Xianzhu Dai Southwest University

Objectives:

The objective of this research was to construct a new recombinant protein expression system that operates at low temperatures close to 0°C by using cold-adapted bacteria as the host. Low-temperature expression alleviates heat-denaturation of proteins and suppresses enzyme activities. Thus, the system is expected to be useful for the production of thermolabile proteins and for the production of enzymes that exhibit toxicity to the host due to their catalytic activity.

Results:

We isolated a cold-adapted bacterium, *Pseudoalteromonas nigrifaciens* Sq02, from *Seriola quinqueradiata* (yellowtail) as a prospective host for heterologous protein production system operating at low temperatures. This strain secreted a single major protein of about 70 kDa, named P320, to the culture supernatant. Deletion of the P320 gene demonstrated that P320 functions as an adhesion factor and facilitates biofilm formation. The amount of P320 in the culture supernatant was estimated to be 30 mg/L-culture and 75 mg/L-culture at 4 °C and 18 °C, respectively, when the cells were grown in the LB medium containing 3% NaCl. It was expected that this strain is useful as the host for heterologous protein secretion at low temperatures. P320 was also found in the cellular fraction as one of the major proteins. Thus, the promoter of the P320 gene was supposed to be suitable for overproduction of foreign proteins in *P. nigrifaciens* Sq02 as the host. We evaluated the promoter activity of the upstream non-coding region of the P320 gene and found that the 375 bp region has a strong promoter activity. Four enzymes (PepF, LAP, PepQ, and BglA) from a psychrophilic bacterium, *Desulfotalea psychrophila* DSM12343, were successfully overproduced in the cells of *P. nigrifaciens* Sq02 by using this promoter. The yields of these proteins at 4 °C and 18 °C were higher than or comparable to those obtained with the previously constructed low-temperature protein production system by using an Antarctic bacterium, *Shewanella livingstonensis* Ac10, as the host. We next examined whether P320 can be used as a carrier to deliver foreign proteins to the extracellular milieu. As the result, we found that PepF, LAP, PepQ, and BglA can be secreted as a fusion protein with P320 at 4 °C and 18 °C by using *P. nigrifaciens* Sq02 as the host. Thus, this system is supposed to be useful as a secretory protein production system operating at low temperatures.

Search for four-wave-mixing in the vacuum – Unveiling dark components in the Universe –

Kensuke Homma Hiroshima University

Purpose and Method

The purpose of this study is to search for Four-Wave-Mixing (FWM) phenomena in the vacuum in order to understand dark components in the Universe. So far, we have constructed and improved an ultra-high vacuum chamber in ICR toward the search. In this vacuum chamber, two-color laser pulses are collinearly combined and focused into the vacuum along the same optical axis. If photon-photon interactions occur in the vacuum environment, generation of intrinsic FMW photons via the stimulated interaction $\omega + \omega \rightarrow (2-u)\omega + u\omega$ is enhanced, where ω is the energy of the creation laser pulse and $u\omega$ is the energy of the inducing laser pulse with $0 < u < 1$. The signal photon energy in this scattering process corresponds to $(2-u)\omega$.

Progress and Achievements

The quantification of background signal photon yields from the known atomic processes is quite important, because we need to subtract them from the signal yield in order to discuss the dark components in the vacuum. We have succeeded to quantify background yields from the surface origin as well as the residual gas origin. As the present status, we have submitted a search result to a journal and we are now preparing for the next submission on the proceeding search result. We summarize a published proceedings and relevant invited talks during FY2019 as follows.

Published proceedings:

- [1] Searches for pseudo Nambu-Goldstone Bosons by stimulated resonant photon-photon scatterings with high-intensity lasers,
Kensuke Homma, Soryuushiron Kenkyuu Vol.28, No.3, 30-34, 2019. (with acknowledgement to the ICR support)

Invited talks in international conferences:

- [1] Perspective to search for dark components in the Universe with coherent photon collisions,
Kensuke Homma, 3rd Johns Hopkins Workshop, Kavli IPMU, Kashiwa, Tokyo, Japan (2019.6.5)
- [2] Stimulated Radar Collider Toward a Laboratory Search for a Dark Energy Candidate,
Kensuke Homma, 28th ANNUAL INTERNATIONAL LASER PHYSICS WORKSHOP, Gyeongju, Korea (2019.7.11)
- [3] Probing Quantum Vacuum at E4: Search for dark components in the sub-eV – 10 eV mass range,
Kensuke Homma, 1st ELI-NP User Workshop, Măgurele-Bucharest, Romania (2019.10.08)
- [4] Perspective of searching for axion-like particles in the mass range 10^{-7} - 10^3 eV with stimulated photon-photon collider,
Kensuke Homma, Zimanyi School 2019, Wigner Research Center for Physics, Budapest, Hungary (2019.12.02)

Development of biosensors by combining stimuli-responsive polymer brushes with electrochemical analysis

Ying Ma South China University of Technology

Quantitative measurement of metabolites in human body fluids is important for diagnosis, management of metabolic disorders and associated diseases. The related analytes such as glucose, cholesterol, L-lactate, or xanthine can generate hydrogen peroxide (H_2O_2) in the presence of their respective oxidases, and their detection can be indirectly performed through the measurement of H_2O_2 . Therefore, an ultrasensitive H_2O_2 sensor is critical to screen these species.

In this project conducted in collaboration with Prof. Kohji OHNO, we developed a new H_2O_2 -responsive polymer brush on a gold electrode surface, which demonstrated an H_2O_2 -dependent electrochemical behavior and enabled an ultrasensitive H_2O_2 sensor. The experiment includes three key parts: (1) Polymer synthesis via atomic transfer radical polymerization (ATRP), which contains the synthesis of a disulfide-carrying radical initiator and a H_2O_2 -responsive monomer aminophenylboronic acid pinacol ester acrylamide (APBPEAA), and the subsequent preparation of a block copolymer. (2) Electrochemical study of polymer brush-modified electrode. The polymer brush was prepared via the “graft to” method, and their electrochemical behavior was studied using 1 mM $\text{Fe}(\text{CN})_6^{3-/4-}$ as a redox probe. (3) Electrochemical luminescence (ECL) detection of H_2O_2 using $\text{Ru}(\text{Bpy})_3^{2+}$ as an ECL reagent.

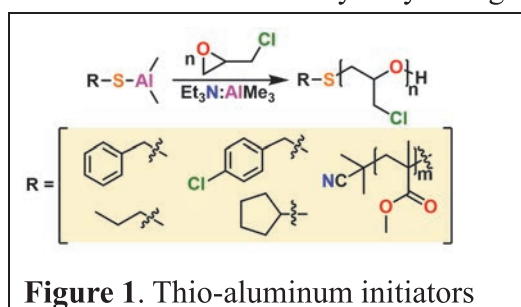
The results show that the polymerization was well controlled via ATRP, and the resulting polymer has a low polydispersity index (PDI) with their molecular weight tunable in the range of 6-15 K Da. The polymer brush can be prepared on a gold electrode surface via the formation of Au-S bond. The presence of polymer brush on the electrode surface significantly hinders the electron transfer of $\text{Fe}(\text{CN})_6^{3-/4-}$ owing to the high hydrophobicity of pinacol ester, accompanying an obvious current decline in the CV curve. Incubation of polymer brush-modified electrode in H_2O_2 solution incurred the removal of pinacol ester group into a hydrophilic phenol group, leading to the more hydrophilic surface and increased current intensity. This current change is very dependent on the concentrations of H_2O_2 used. The corresponding electrochemical impedance spectra (EIS) confirmed the change of electron transfer resistance in the absence and presence of H_2O_2 . Inspired by this observation, we combined this H_2O_2 -responsive polymer brush with an ultrasensitive ECL method, which reveals the H_2O_2 -dependent change of ECL intensity. The resulting sensor demonstrated good performance for the determination of H_2O_2 in terms of limit of detection (LOD) of 0.02 μM and linear range of 0.1-20 μM . This result is advantageous over most of reported H_2O_2 using electrochemical or optical methods.

We are working on the profiling of metabolites using this method and a manuscript is in preparation.

Exploring new polyether nanocomposite electrolytes to enhance energy storage of lithium ion batteries

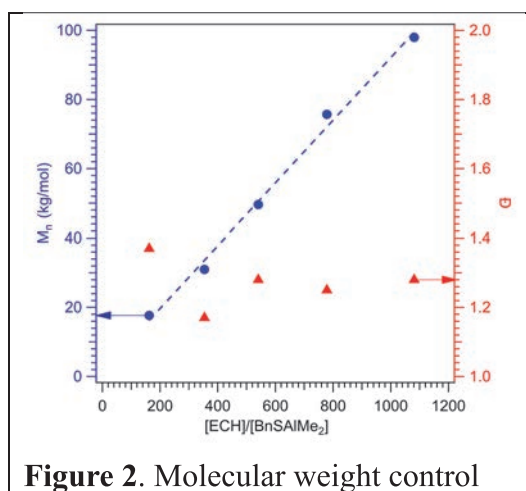
Robert C. Ferrier, Jr. Michigan State University

Objective. The overall objective was to develop polyether-based nanocomposite electrolytes for lithium ion batteries by combining the polyether polymerization techniques pioneered by the PI and the surface initiated polymerization techniques developed by the ICR partner researcher, Prof. Ohno from Kyoto University. **Experimental Methods.** Aluminum-based initiators were characterized via X-Ray crystallography and ^1H NMR spectroscopy. Polymers were



characterized by size-exclusion chromatography (SEC), ^1H and ^{13}C NMR spectroscopy, differential scanning calorimetry (DSC), and electrospray ionization with mass spectrometry (ESI-MS). Polymerization kinetics were monitored via ^1H NMR spectroscopy. **Experimental Results.** Five

aluminum-based initiators were produced from the reaction of trimethyl aluminum and a thiol containing compound (**Figure 1**). All five initiators resulted in living polymerizations of epoxide monomers with controlled molecular weight and low dispersity (**Figure 2**). Polyether compositional control was achieved through copolymerization. Polymerization kinetics were found to depend on the thiol-ligand used to produce the initiator. **Discussion.** Thio-aluminum initiators provide extensive polymer end group control through thiol ligand choice. They also allow for facile synthesis of vinyl-block-epoxide polymers through macroinitiators formed from thiol end terminated polymers, extending polymer compositional control. For the funded project, initiation from thio-aluminum compounds is imperative to polymerize from the surface of silica nanoparticles to create the polyether nanocomposite electrolytes. The surface initiated polymerizations are proceeding now in Prof. Ohno's lab. Therefore, this work significantly advances our research to reaching the overall goal. **Publications.** A journal article entitled "Aluminum-based Initiators from Thiols for Epoxide Polymerizations" co-authored by the PI and his ICR partner researcher, Prof. Ohno of Kyoto University, was submitted to *Macromolecules* and is under review. A talk to be given by the PI at the American Chemical Society Spring Meeting in Philadelphia, PA entitled "Versatile, Thio-aluminum Initiators for Epoxide Polymerizations."



Fluorinated polymer-brush-grafted nanoparticles: Precise synthesis and applications to membrane technology

Vincent Ladmiral University of Montpellier

Objectives: The objective of this project, conducted in collaboration with **Professor OHNO Kohji**, is to prepare, and study original core-shell nanoparticles composed of a silica core and a fluorinated (co)polymer (VDF-based copolymers) functional shell, and to examine their potential application as building blocks for filtration membranes. These nanoparticles (SiPs) were prepared by surface-initiated RAFT polymerization of fluoromonomers.

Experimental methods: SiP-XA were prepared using a previously published method (*Chemistry - A European Journal* **2019**, 25, 8, 2059). The RAFT polymerization of trifluoroethylene from SiP-XA was performed as follows: A carius tube containing *tert*-amyl peroxy-2-ethylhexanoate (1.7mg), free xanthate (FXA) (5.1 mg) and a solution of SiP-XA (1% wt, 50 mg) in DMC (3mL) was degassed using three freeze-pump-thaw cycles. Gaseous TrFE (2g) was then introduced into the tube at the liquid N₂ temperature using a custom-made manifold. The tube was sealed under dynamic vacuum at the temperature of liquid N₂, and placed horizontally in a shaking water bath thermostated at 73 °C. After a number of hours, the tube was opened to air, the DMC suspension was diluted with THF and centrifugated to collect the PTrFE-grafted SiP. The suspension/centrifugation cycle was performed 8 times to perfectly purify the SiPs. The soluble PTrFE was recovered. Similar procedure were used to polymerize VAc or to copolymerize VDF and TrFE.

Discussion: As shown in Table 1, the SI RAFT polymerization of TrFE and copolymerization of VDF and TrFE seemed to have proceeded as expected. The high dispersities are likely due to the unavoidable chain inversions known to gradually lead to loss of control especially when high molar masses are targeted. These encouraging results need to be confirmed.

Table 1: Results of the surface-initiated RAFT polymerization from SiP-XA

	Ratio M:CTA:I	Time (h)	Mn Free polymer (g/mol)	Đ Free Polymer	Mn grafted (g/mol)	Đ grafted polymer	Graft density (Chains/nm ²)
SiP-P(VDF-TrFE)	1000:1:0.5	24h	13,200	1.7	/	/	/
SiP-PTrFE	1000:1:0.5	24h	17,400	1.75	17,300	2.37	0.08
SiP-PVAc	1000:1:0.3	15h	28,500	1.6	/	/	0.56
SiP-PVAc	100:1:0.03	15h	5,000	1.8	/	/	0.40

Publications: A publication is planned. More work is required to reproduce and confirm the results obtained so far. We anticipate to publish a scientific article before December 2020.

Determine the three-dimensional structure of ^{13}C labeled α -synuclein(61-95) in the Langmuir-Blodgett film and supported phospholipids bilayers by p-MAIRS FT-IR

Chengshan Wang Middle Tennessee State University

A. Objectives:

1. Synthesize and purify ^{13}C labeled α -syn(61-95) containing residues 61-95 of α -syn(61-95).
2. Screen the conformation and orientation of specific residue of α -syn(61-95) in LB film.
3. Screen the conformation and orientation of specific residue of α -syn(61-95) in supported phospholipids bilayers.

B. Experimental methods:

The experimental details about peptide synthesis & purification, LB film preparation, circular dichroism (CD), and p-Polarized Multiple-Angle Incidence Resolution Spectroscopy (pMAIRS) measurements are described in the publication below in section D.

C. Experimental results and Discussion:

X-ray crystallography and NMR are two major methods to determine protein's structure. However, both of them have challenges to elucidate the structure of membrane proteins, which weighs $\sim 30\text{-}35\%$ of the total proteins. Dr. Wang and Dr. Hasegawa are developing a method for membrane proteins structure with residue resolution by pMAIRS, which will be a supplement to X-ray crystallography and NMR. CD results showed that α -Syn(61–95) is unstructured in pure water. At the air-water interface, α -syn(61–95) was found to change its conformation to helix and form stable Langmuir monolayer at the air-water interface. Then, the Langmuir monolayer was transferred to silicon slide as LB film and the tilted angle of the axis of α -syn(61–95) in LB film was determined by pMAIRS to be 30.1° . All the details are described in the publication in section D. In addition, ^{13}C label was introduced to 93G in α -syn(61–95) and the axis of the helix at 93G was found to be very parallel (i.e., the tilted angle is almost 0°) to the interface. Another publication are in preparation now for this results. This paper will fully exhibit the power of pMAIRS to quantitatively determine the tilted angle of an α -helical model peptide in residue level. As a consequence, pMAIRS was an important technique to address three dimensional structure of membrane protein with high resolution. On the whole, Objective 1 and 2 in section A were completely accomplished and Objective 3 is on the way.

D. Publication.

One paper has been published about Figure 1A to 1C as shown below. Another paper is in preparation about Figure 1D.

Wang C., Sharma S. K., Olaluwoye O. S., Alrashdi S. A., Hasegawa T., Leblanc R. M. *Colloids & Surfaces B: Biointerfaces*, 2019, 183, 110401.

<https://www.sciencedirect.com/science/article/pii/S0927776519305454>

Real-time imaging of single-molecule mRNA with different methylation states

Timothy J. Stasevich Colorado State University

RNA methylation is important for mRNA stability, transportation, and translation. Monitoring the dynamics of RNA molecules depending on their RNA methylation status should provide important information on the relationship of RNA methylation and RNA metabolism. This joint research project aims to develop a method to visualize mRNA with different methylation states. As the first step, we tried to observe the intracellular movement of RNA bound with an engineered sequence-specific RNA binding proteins at single-RNA level; this would help us observe specifically methylated RNAs. So far, we have developed single-molecule mRNA imaging techniques¹⁻³ and Dr. Imanishi from Kyoto University has established the method to target specific mRNA using artificial RNA binding proteins based on Pumilio-fem-3 mRNA binding factor (PUF) proteins^{4,5} (Fig. 1). Based on these studies, reporter DNAs and PUF-GFP proteins were designed. Reporter vectors contain an epitope-tag coding region, a protein coding region, sequences of PUF binding site (PBS), and MS2 stem loop coding regions. The PUF-GFP expression vector encodes a superfolder GFP (sfGFP) fused with PUF RNA binding domains. PUF-sfGFP proteins were expressed in *E. coli* and purified. For visualization, U2OS cells were bead-loaded with reporter DNA, purified PUF-sfGFP, Halo-tagged MCP¹ labeled with JF646 fluorophore, and Cy3-labeled anti-FLAG Fab¹. After 6 hr, dotted signal of PUF and reporter RNA were detected within living cells, however these signals were not colocalized. Further optimization of the sequences of reporter mRNA should improve the colocalization efficiency.

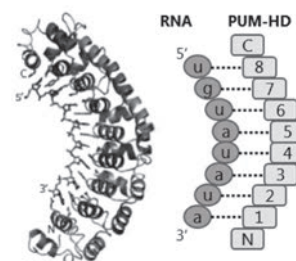


Fig. 1. Structure of RNA/PUM-HD complex (PDB ID; 1M8Y). Each PUF repeat recognizes single RNA base.

1. Morisaki T *et al.*, *Science*, 352, 1425-1429 (2016). 2. Lyon K *et al.*, *Mol. Cell*, 75, 172-183 (2019). 3. Moon SL *et al.*, *Nat. Cell Biol.* 21, 162-168 (2019). 4. Shinoda K *et al.*, *ChemBioChem*, 19, 171-176 (2018). 5. Shinoda K *et al.*, *Chem. Commun.* 56, 1365-1368 (2020).

Structural and functional analysis of curvature-inducing peptides

Anne S. Ulrich Karlsruhe Institute of Technology

Membrane remodeling, which includes fission, fusion, protrusion and vesiculation, acts as an important factor in many cellular mechanism, such as membrane trafficking, movement growth and division. It has been known that an emerging research field of membrane remodeling, curvature and lipid packing, shows a great effect on the formation and structural dynamics of cell membranes. Thus, a means of modulating membrane curvature and lipid packing become focused and expected to have therapeutic potential.

Epsin-1, an essential protein involved in clathrin-coated pit formation at the initial stage of clathrin-mediated endocytosis, possesses curvature-inducing ability in membranes. In our collaboration studies with Professor Shiroh Futaki, Institute for Chemical Research, Kyoto University, an amphipathic helical peptide derived from the N-terminal (position of 1–18) of epsin-1, named EpN18 [XSTSSLRRQXKNIVHNYS-amide, X = norleucine], has been shown to yield positive curvature and lipid packing loosening by inserting the hydrophobic face in the membranes. However, while promising as an appliance to modify membrane structures, EpN18 shows relatively mild membrane-remodeling activity, and high concentration (20–40 μM) is needed to induce curvature. Since aggregation of peptides is often accompanied by peptide-mediated membrane remodeling, oligomerization may increase the curvature inducing ability of EpN18, thereby yielding an enhanced effect than the monomeric peptide. In this study, we demonstrated the enhanced effect of EpN18 by constructing branched EpN18 trimer. EpN18 trimer indicated efficient internalization level of octaarginine (R8), a cell-penetrating peptide (CPP). The cellular uptake of R8 is notably promoted by EpN18 trimer in a lower concentration than monomer. The generalized polarization analysis using the polarity-sensitive dye (di-4-ANEPPDHQ) also indicates the efficacy of branched trimeric EpN18 in loosening the lipid packing. Circular dichroism (CD) spectrometric analysis in the presence of liposomes showed that EpN18 trimer has a higher α -helical content compared with the monomer. The higher positive curvature inducing ability of EpN18 trimer has also confirmed by solid-state ^{31}P NMR. Overall, trimerizing peptides is thus considered as a promising approach for the enhancement of membrane-remodeling activity. We are now preparing the manuscript to report these results.

Research of multi-qubit diamond quantum processors

Marcus W. Doherty Australian National University

Quantum communication and quantum computation are expected to establish a new paradigm and advance our understanding of quantum mechanics. It is considered that they will provide cryptography that can not be decoded and super parallel computation that is much faster than that of ordinary computers. Besides these, technical issues intriguing questions concerning quantum mechanical phenomena can be addressed.

Recently, NV centers (Figure 1) in diamond are significantly interested as a candidate of a resource for demonstration and the realization of them [1]. It is because that single spins can be coherently controlled [2] and electrically driven single photon source are realized at room temperature (RT) in the NV center. In other solid materials such as quantum dot or superconducting devices, those are realized only in extremely low temperature.

In this project, we would like to develop further this system with multi-nuclear spin qubits. We propose to realize the multi-qubits systems and generation of entanglement in this project.

We theoretically discuss new architectures for enhancement of speed and fidelity of quantum processor by using multi-qubits NV centers in diamond. We discuss the usage and production of isotopically engineered diamonds. By using isotopically engineered diamonds, the enhancement of speed and fidelity of quantum processor is expected. It is considered that quantum communication and quantum computation will e.g. provide secure data encryption and super parallel computation that in certain cases outperforms classical computers. The realization of them has strong impact not only to science but also to industry and society.

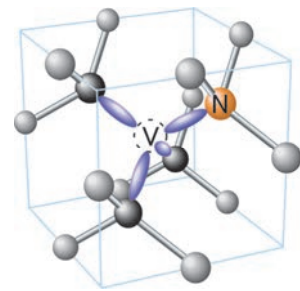


Fig. 1, The NV center
(Nitrogen-Vacancy complex)
in diamond.

- [1] M. W. Doherty, N. B. Manson, P. Delaney, F. Jelezko, J. Wrachtrup, L. C. L. Hollenberg, Physics Reports 528 (1), 1-45 (2013).
- [2] P. Neumann, N. Mizuochi, F. Rempp, P. Hemmer, H. Watanabe, S. Yamasaki, V. Jacques, T. Gaebel, F. Jelezko, J. Wrachtrup. Science, 320, 1326 (2008).

Research on shallow NV center in diamond

Gopalakrishnan Balasubramanian Max-Planck Institute for Biophysical Chemistry

Recently, NV centers in diamond are significantly interested as a candidate of a resource for quantum sensing with nano-scale spatial resolution and ultra-high sensitivity. It is because that single spins can be coherently controlled and the spin coherence time is significantly long even at room temperature (RT) in the NV center.

For the higher spatial resolution, a shallow NV center with nano-scale distance from the surface is expected to be utilized, however one of the biggest issue is that the shallow NV center is unstable. Toward the stabilization of the shallow NV center, establishment of a reliable technique to characterize the nano-scale depth from the surface is required.

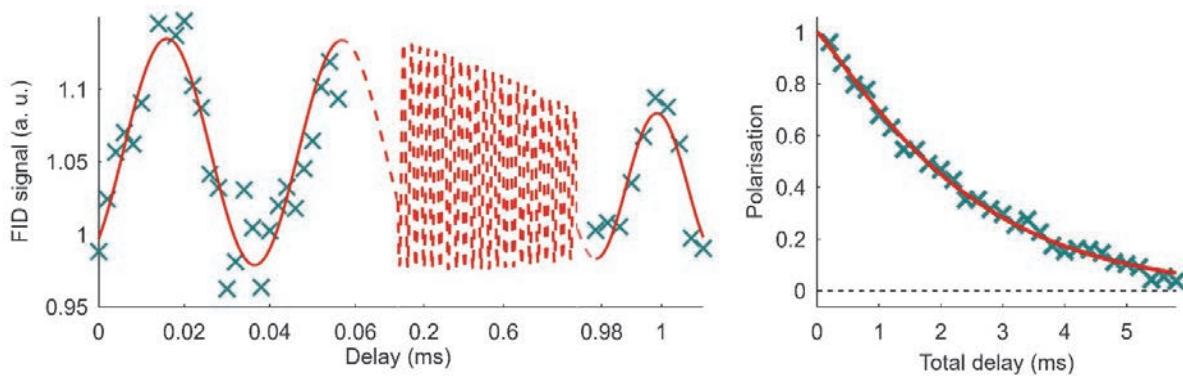


Fig. 1. Coherence times (data: blue crosses, fits: red lines). (Left) $T_2^* \approx 1.5$ ms. (Right) $T_2 \approx 2.4$ ms.

Previously, we investigated the NV centers in Phosphorus doped n-type diamond [1]. We demonstrated the stabilization of the charge state of the NV center in Phosphorus doped n-type diamond [1]. Furthermore, ultra-long coherence times have been measured and the highest sensitivity of the single NV center was measured by using it [2]. Our samples are epitaxially grown by chemical-vapour deposition onto Ib-type (111)-oriented diamond substrates with enriched ^{12}C (99.998%) and phosphorus concentrations of $\sim 5 \times 10^{16} \text{ cm}^{-3}$. We found single electron spins in NV centres with the longest inhomogeneous spin-dephasing time ($T_2^* \approx 1.5$ ms) and Hahn-echo spin-coherence time ($T_2 \approx 2.4$ ms) ever observed in room-temperature solid-state systems (see Fig. 1). By using the ion-implantation technique, we generated shallow NV centers with nano-scale distance from the surface in n-type diamond. We demonstrated the stability of the NV centers and longer coherence times.

- [1] Y. Doi, T. Fukui, H. Kato, T. Makino, S. Yamasaki, T. Tashima, H. Morishita, S. Miwa, F. Jelezko, Y. Suzuki, N. Mizuochi, Physical Review B, 93, 081203(R) (2016)
- [2] E. D. Herbschleb, H. Kato, Y. Maruyama, T. Danjo, T. Makino, S. Yamasaki, I. Ohki, K. Hayashi, H. Morishita, M. Fujiwara, N. Mizuochi, Nature Communications, 10, 3766 (2019)

Effect of dipole alignment along chain backbone on dielectric relaxation of type-A polymers at association/dissociation equilibrium

Youngdon Kwon Sungkyunkwan University

Introduction: Dielectric relaxation of type-A chains reflects global motion of the chains but is also affected by the relative alignment of the dipoles along the chain backbone, namely, by the dipole inversion. Head-to-head association of type-A unimers gives symmetrically dipole-inverted dimer, and the association/dissociation equilibrium of these unimer and dimer results in motional coupling of those chains thereby affecting the dielectric behavior. In fact, for this head-to-head case, eigenmode analysis has been conducted to reveal that the motional coupling results in moderate retardation and acceleration of the dielectric relaxation of the unimer and dimer obeying the reptation dynamics.¹ In contrast, the coupling has no effect on the dielectric relaxation of Rouse unimer and dimer.² Namely, the effect of motional coupling on the dielectric relaxation changes with the type of chain dynamics. Nevertheless, this effect was not clarified for head-to-tail associating unimers and their dimer having no dipole inversion (illustrated in Figure 1). Thus, for completeness, this study makes the eigenmode analysis of the dielectric relaxation for this case of head-to-tail reaction.

Results and Discussion: For the unimer and dimer obeying either Rouse or reptation dynamics, the time evolution equation for the averaged bond vector $\langle \mathbf{u}_j(n_j, t) \rangle$ (cf. Figure 1) is commonly described by³

$$\frac{\partial \langle \mathbf{u}_j \rangle}{\partial t} = D_j \frac{\partial^2 \langle \mathbf{u}_j \rangle}{\partial n_j^2} - \frac{1}{\tau_j^*} \left\{ \langle \mathbf{u}_j \rangle - \langle \mathbf{u}_j \rangle^{\text{created}} \right\} \quad (1)$$

where the index j specifies the chain ($j = 1$ and 2 for the unimer and dimer), D_j is the diffusivity of respective chains, and τ_1^* and τ_2^* , respectively, coincide the association and dissociation times τ_{as} and τ_{ds} shown in Figure 1. The bond vector $\langle \mathbf{u}_j \rangle^{\text{created}}$ of a chain j created by the association/dissociation reaction is described by $\langle \mathbf{u}_i \rangle$ of a chain i ($i \neq j$) before the reaction according to the conformational mapping noted in Figure 1. Equation 1 can be solved with the aid of the eigenmode expansion of $\langle \mathbf{u}_j \rangle$ and kernel calculation for the resulting expansion coefficients, and the dielectric relaxation function is calculated accordingly.³

Figure 2 shows the dielectric relaxation times of the unimer and dimer obtained from this calculation.³ Clearly, the dielectric relaxation of the unimer and dimer are retarded and accelerated, respectively. This reaction effect was found to be much more significant for the head-to-tail case than for the head-to-head case irrespective of the chain dynamics. In addition, the dielectric relaxation function exactly coincides with the viscoelastic relaxation function if the unimer and dimer obey the reptation dynamics. This result in turn suggests an interesting method of resolving some detail of the chain dynamics under the reaction through comparison of dielectric and viscoelastic responses of the associative type-A chains.

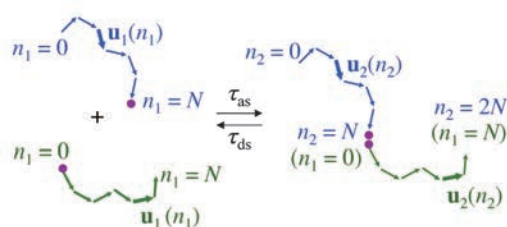


Fig. 1 Head-to-tail associating unimer and resulting dimer.

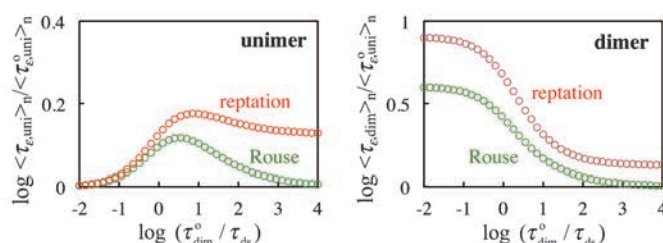


Fig. 2 Normalized dielectric relaxation time of unimer (left panel) and dimer (right panel) obeying reptation and Rouse dynamics.

References:

1. Watanabe, Matsumiya, Kwon *Macromolecules* **2018**, 51, 6476–6496.
2. Watanabe, Matsumiya, Kwon, *J. Rheol.* **2017**, 61, 1151–1170.
3. Kwon, Matsumiya, Watanabe *Macromolecules* **2019**, 52, 8484–8502.

植物表皮細胞の分化における制御ネットワークの研究

富永るみ 広島大学

〔目的〕 トライコームや根毛細胞など多様な形態や機能を持つ表皮細胞は、植物細胞分化の制御機構を研究する上で格好の材料であり、これまでに多くの遺伝学および分子生物学的研究がなされてきた。その結果、細胞分化制御に関与する様々な転写因子が同定され、それら転写因子を中心とした転写制御ネットワークも明らかになりつつある。我々はこれまで、シロイヌナズナのトライコームや根毛細胞分化を制御する *CPC* ファミリー遺伝子の機能を中心に解析を進めてきた。*CPC* ファミリーは R3 タイプの MYB 転写因子をコードしており、そのうち TRY と ETC2 のタンパク質分解速度が、他のメンバーと比較して極めて早いことがわかった。このタンパク質分解機構の詳細をさらに明らかにするために以下の解析を進めた。

〔実験〕 リン酸化は、タンパク質の機能を制御する基本的なメカニズムである。TRY および ETC2 タンパク質のリン酸化候補部位を検索し、該当するセリンおよびスレオニン残基をアラニン置換したコンストラクトを導入した形質転換体を作成した。

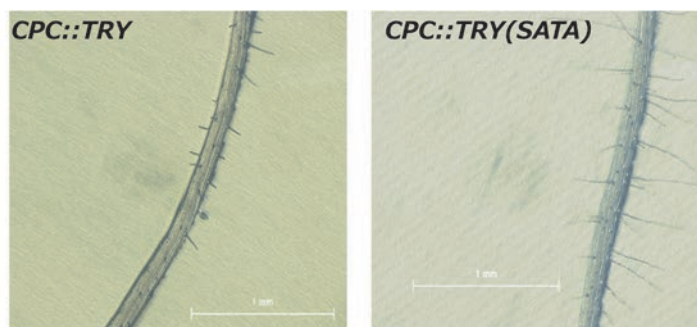


図1 CPC::TRYおよびCPC::TRY(SATA)形質転換体

〔結果と考察〕 本研究で作出したアミノ酸置換型の形質転換体 [CPC::TRY(SATA)] は、コントロール (CPC::TRY) に比べて有意な根毛数の増加を示した (図1)。この結果は、アミノ酸置換により TRY タンパク質の分解が抑えられ、根毛形成を誘導する R3-MYB 転写因子の機能が回復したことを示唆する。アミノ酸置換によるタンパク質分解の抑制は、TRY(SATA)-GFP 融合タンパク質の蛍光局在観察やウェスタンブロッティングによっても確認した。ETC2 についても同様の解析結果が得られた。これらの成果により、TRY および ETC2 のリン酸化がタンパク質の安定性に作用し、根毛・非根毛細胞形成の運命決定に影響を及ぼすことが明らかになった。現在、これらのリン酸化のメカニズムについてさらに解析を進めている。CPC ファミリータンパク質の分解活性の違いが、実際にどのような役割を果たしているのかを明らかにすることは、表皮細胞分化制御ネットワークの全体像の解明へ手がかりを与えるものである。

〔成果報告〕 K. Yamada, M. Sasabe, Y. Fujikawa, T. Wada, R. Tominaga,
PLOS ONE, 10.1371/journal.pone.0205522 (2018)

アシルドーパミンの新機能

伊藤昭博 東京薬科大学

転写因子Zはがん細胞の生存に関与する。今回、我々は転写因子Zを活性化する内因性分子を発見した。化学研究所から提供された約 300 個の脂質関連内因性分子ライブラリーから、転写因子Zを安定化させる因子としてアシルドーパミン類を見出した。本研究では、どのような癌種でアシルドーパミンの生合成が活発であるかを見いだした。その上で、がん細胞でアシルドーパミンの生合成する酵素群を同定を試みた。

生理的条件下でアシルドーパミンが転写因子Zを活性化するかどうか明らかにするために、内因性のアシルドーパミンが恒常的に産生されているがん細胞の探索を行った。転写因子Zの発現レベルが高い細胞の中にアシルドーパミンを産生している細胞があるのではないかと考え、約 40 種類のがん細胞における転写因子Zの発現レベルを検討した。その結果、膵臓由来の複数のがん細胞で転写因子Zの発現レベルが高いことを見出した。アシルドーパミンの生合成酵素経路として、チロシンを出発材料とし、チロシン水酸化酵素 (TH)、芳香族 L - アミノ酸脱炭素酵素 (AADC)、脂肪酸アミド加水分解酵素 (FAAH) の三種類の酵素の関与が示唆されている。これら膵臓がん細胞や前立腺がん細胞の培養液中からチロシンを除去すると、転写因子Zの発現レベルが低下したことから、チロシンを出発材料としたアシルドーパミン生合成経路が、転写因子Zの安定化に重要であることを示唆する結果を得た。一方、高濃度のドーパミンを添加したところ、転写因子Zが安定化することを見出した。安定同位体含有体アシルドーパミンを内部標準として用いて、質量分析法により細胞内のアシルドーパミンの量を測定したところ、ドーパミン添加により細胞内の内因性のアシルドーパミン量が増加していることを示唆する結果を得た。以上の結果から、これら細胞においてチロシンを出発材料とするアシルドーパミン生合成経路を介してアシルドーパミンが合成され、転写因子Zの安定化に寄与していることが示唆された。

がん細胞の代謝全体に与えるアシルドーパミンの影響を検討するために、メタボローム解析を実施した。その結果、アシルドーパミン処理により解糖系に関わる代謝物量が顕著に上昇することを見出した。以上の結果から、アシルドーパミンは転写因子Zを活性化することにより、がん代謝の特徴であるワールブルク効果を制御する内因性脂質代謝物であることが示唆された。

ビタミンDの新機能の調節

長澤和夫 東京農工大学

本研究の目的は、人工ビタミンDの創製である。この人工ビタミンDは、古典的なビタミンDの作用に影響を与えず、ビタミンDによる脂質代謝制御を選択的に阻害する。この共同研究の成果は 2019 年に *ACS Chemical Biology* 誌に発表した。

転写因子 SREBP (Sterol Regulatory Element-binding Protein) は、脂質恒常性維持の司令塔である。我々と上杉研究室との共同研究では、SREBP を強く阻害する内因性分子を発見した (*Cell Chem. Biol.*, 2017)。上杉研究室にて、約 300 個の脂質関連内因性分子ライブラリーを細胞でスクリーニングし、SREBP を制御する分子として水酸化ビタミンDを再発見した。水酸化ビタミンDは、SREBP タンパク質とその運び屋である SCAP を選択的に分解することが分かった。通常、ひとつの脂質関連内因性化合物は、細胞内で複数の役割を果たしている。例えば、水酸化ビタミンDには、ビタミンD受容体を介したカルシウム代謝（骨形成）という役割がある。本共同研究では、SREBP 分解活性はあるが、ビタミンD受容体を活性化しない化合物を創製した。SREBP の過剰な活性は前立腺がんなどの増殖や転移に重要であり、これらの人工ビタミンDは創薬シーズとなる可能性がある。

- **選択性の高い誘導体の探索** 東京農工大学の私たちの研究室では、これまで約 200 種類のビタミンD誘導体を化学合成してきた実績がある。これらのビタミンD誘導体ライブラリーおよび、A 環部に着目した構造展開から得られる新規誘導体（前年度までに得た知見）を利用し、ビタミンD受容体には作用せず、SREBP を阻害する新規化合物の創成に成功した。副作用につながる可能性のある VDR 活性の回避と、代謝安定性の向上を目標に、更なる誘導体展開及び活性評価を行った。その結果、25OHD よりも高い安定性を示し、また細胞レベルでは長時間処理でもほとんど VDR 活性を持たない化合物を見出した。
- **化学ツールとしての利用** 人工ビタミンDの研究によって、細胞レベルでは、SREBP 抑制活性のみをもつ化合物と、VDR 活性のみをもつ化合物を作り分けることができた。つまり、ビタミンDの持つ SREBP 抑制活性と VDR 活性という二つの独立した機能を化合物で分離できる。これらの第一世代人工ビタミンDをツールとして用い、細胞に添加した後に網羅的遺伝子発現解析を行った。その結果、天然のビタミンDによって発現が誘導される遺伝子の中に、VDR によって誘導されず SREBP によって抑制されている遺伝子を発見した。天然のビタミンDのみでは、これらの遺伝子は同定できない。解析をすすめ、ビタミンDによって誘導される SOAT1 が SREBP によって抑制されていることを発見した。

高スピン偏極電流源の開発のためのコバルトフェライト薄膜の 磁気・電氣的性質の評価

田中雅章 名古屋工業大学

電子の電荷とスピン自由度の両方を電子デバイスに利用するスピントロニクス分野では、効率的にスピン自由度が偏った(スピン偏極)電子を注入(スピン注入)することで、デバイスの性能を向上できる。我々は電子が持つスピン自由度によりバリア高さが異なるために、電子の透過確率がスピン自由度により異なる強磁性絶縁体薄膜を用いてスピン注入を実現するトンネル型スピンフィルター効果の研究を行っている。

これまでの研究で、コバルトフェライト $\text{Co}_x\text{Fe}_{3-x}\text{O}_{4+\delta}$ ($0.4 < x < 0.6$) が非磁性導電体 TiN(001) 層上に [001] 方向にエピタキシャル成長した場合、面内の引張り歪みにより垂直磁気異方性が誘起されることを明らかにした。本研究では $\text{Co}_x\text{Fe}_{3-x}\text{O}_{4+\delta}$ を用いた応用上有利な垂直磁化型のトンネル型スピンフィルター効果の観測を目的に研究を行った。

MgO(001) 基板上に TiN(20 nm)/ $\text{Co}_{0.6}\text{Fe}_{2.4}\text{O}_{4+\delta}$ (5 nm)/MgO(1 nm)/ $\text{Co}_{0.25}\text{Fe}_{0.75}$ (1.5 nm)/ $\{\text{Tb}/\text{Co}\}_n$ (13 nm) 構造の多層膜をパルスレーザー堆積法とスパッタ法で作製した。反射高速電子線回折像から $\text{Co}_{0.6}\text{Fe}_{2.4}\text{O}_{4+\delta}$ 層, MgO 層, $\text{Co}_{0.25}\text{Fe}_{0.75}$ 層はエピタキシャル成長していることを確認した。化学研究所小野研究室のフォトリソグラフィ装置などを用いて直径数 μm の磁気トンネル接合(MTJ)素子への加工を行い、トンネル磁気抵抗(TMR)効果の測定を実施してスピン注入の観測を行った。

図 1 に測定温度 50 K, バイアス電圧 200 mV で MTJ 素子に膜面垂直方向に磁場を印加した際の磁気抵抗測定の結果を示す。磁場の掃引により抵抗値にシャープな変化が見られる。これは磁場の掃引により $\text{Co}_{0.6}\text{Fe}_{2.4}\text{O}_{4+\delta}$ 層と $\text{Co}_{0.25}\text{Fe}_{0.75}$ 層の磁化が互いに平行, 反平行状態になり, それに伴って抵抗値が変化する TMR 効果によるものと考えられる。今回得られた TMR 効果では互いの磁化が平行のときは反平行のときより抵抗値が大きい。これは $\text{Co}_{0.6}\text{Fe}_{2.4}\text{O}_{4+\delta}$ 層のバリア高さが多数スピンの電子より少数スピンの電子のほうが低いという第一原理計算の結果を反映したものである。以上のように, $\text{Co}_{0.6}\text{Fe}_{2.4}\text{O}_{4+\delta}$ を用いた垂直磁化型のトンネル型スピンフィルター効果の観測に成功した。

(国内会議発表)

- M. Tanaka, K. Naruse, K. Nomura, K. Kutsukake, T. Okuno, S. Honda, T. Ono, and K. Mibu, “Electron tunneling through perpendicularly magnetized cobalt ferrite films grown on metallic TiN layers”, 第 79 回応用物理学会秋季学術講演会, 2019 年 9 月 19 日 (他 1 件).

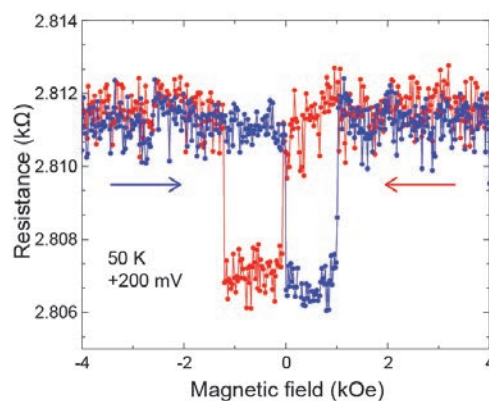


Fig. 1 Magnetoresistance for the MTJ at 50 K.

Develop of the epitaxial thin film of Wyle semimetal Mn_3Sn

Taro Nagahama Hokkaido University

Introduction: In the spintronics, developments of alloy material are one of the most important issues. In particular, the alloys with Kagome structure consisted of 3d transition metal and Sn has attracted much attentions. Mn_3Sn is an antiferromagnetic material with non-collinear magnetic structure. Since it is considered to be a Wyle magnetic material, large Hall effect, anomalous Nernst effect, and magneto-optical effect are reported. So far, these researches often have been conducted with bulk materials. It is expected that the thin films allow us to fabricate the junctions or multilayer structures which are necessary to realize novel functional devices. In this study, we grew the $\text{D0}_{19}\text{-Mn}_3\text{Sn}$ thin films epitaxially.

Experiments: The films were grown on $\text{Al}_2\text{O}_3(0001)$ substrates by the molecular beam epitaxy (MBE) method with the base pressure of 8×10^{-8} Pa. The film structures were $\text{Al}_2\text{O}_3(0001)/\text{Pt}(111)/\text{Mn}_3\text{Sn}(30 \text{ nm})/\text{Al}_2\text{O}_3$. The Mn and Sn were deposited simultaneously at 573 K on the Pt(111) buffer layer. The epitaxial growth and the surface morphology were confirmed by reflection high energy electron diffraction (RHEED) and the crystal structures were investigated by X-ray diffraction (XRD). The magnetoresistance measurements were carried out in the cryostat.

Results and discussions: Fig.1 is the in-plane X-ray diffractions of the Mn_3Sn thin films on $\text{Al}_2\text{O}_3(0001)$. One can find some diffraction peaks that could be assigned to Mn_3Sn crystal, so that we concluded that epitaxial Mn_3Sn films were grown on Al_2O_3 . The epitaxial relationship was estimated as $\text{Al}_2\text{O}_3(0001)\text{substrate} [1-100] \parallel \text{Pt}(111)[1-10] \parallel \text{Mn}_3\text{Sn}(0001) [11-20]$. The films exhibited no anomalous Hall effect due to anisotropy of the AHE. We also fabricated the bilayer of $\text{Fe}_3\text{Sn}(0001)/\text{Mn}_3\text{Sn}(0001)$. As shown in Fig.2, the magnetoresistance curve at 7K showed shift of the hysteresis because of the exchange coupling between ferromagnetic Fe_3Sn and antiferromagnetic Mn_3Sn .

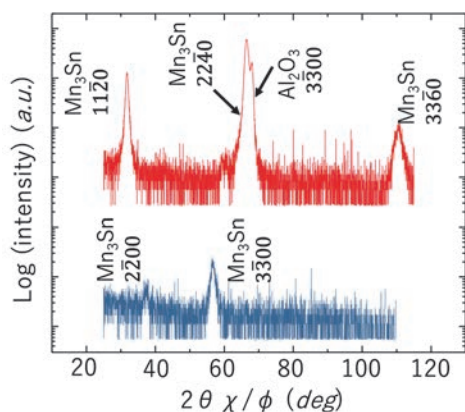


Fig.1 in-plane XRD profile of epitaxial Mn_3Sn thin film.

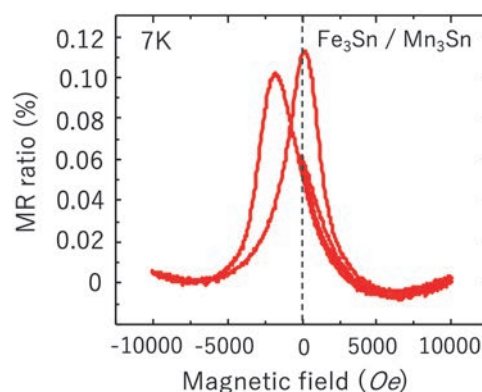


Fig.2 Magnetoresistance curve of $\text{Fe}_3\text{Sn}/\text{Mn}_3\text{Sn}$ bilayer at 7K.

Publication and Conference: 1. Y. Goto et al., " Tunnel magnetoresistance effect in a magnetic tunnel junction with a B2- Fe_3Sn electrode", AIP Advances 9, 085322 (2019). 2. A. Maeno et al., " Fabrication of D0_{19} - and B2-type Fe_3Sn epitaxial films and comparison of magneto-transport properties", MMM2019,USA.

Effect of microstructure on damping constant in polycrystalline Bi-YIG thin films prepared by sol-gel method

Keisuke Yamada Gifu University

【Introduction】 $\text{Bi}_x\text{Y}_{3-x}\text{Fe}_5\text{O}_{12}$ (Bi-YIG) has attracted more attention because of its potential application in spintronics devices utilizing the spin pumping and spin Seebeck effects [1]. This paper reports our latest experimental findings on the variation of the Gilbert damping constant α with respect to microstructural change in nanocrystalline Bi-YIG ($0 \leq x \leq 1.4$) thin films fabricated on a Si substrate by a combination of co-precipitation, spin-coating, and annealing processes.

【Experimental Method】 Bi-YIG thin-film samples were chemically synthesized by co-precipitation and spin-coated onto Si substrates. The samples were subsequently annealed at temperatures T_a ranging from 973 K to 1273 K for 30 min in an ambient atmosphere. Their structure and magnetic properties were characterized by X-ray diffractometry, scanning electron microscopy (SEM), and ferromagnetic resonance (FMR) measurements. FMR measurements were performed at ICR of Kyoto Univ.

【Results and Discussion】 The diffraction peaks associated with the garnet phase are observed dependence on both Bi composition x and T_a in the Bi-YIG samples. With increasing Bi composition x , the average particle size estimated by SEM imaging increases from 41 (51) nm to 55 (64) nm at $T_a = 973$ (1023) K, while the average particle size decreases as Bi composition x increases at $T_a = 1073$ K (see Fig. 1). As shown in Fig. 2, the value of α increases in the range from 2.1×10^{-2} to 5.0×10^{-2} at all samples for T_a as Bi composition x increases. This result indicates that the value of α is more affected by Bi composition x than the microstructure in the surface on the samples. It is considered that the substitution of Bi^{3+} for Y^{3+} changes the lattice constant and the crystal structure, leading to the increased α .

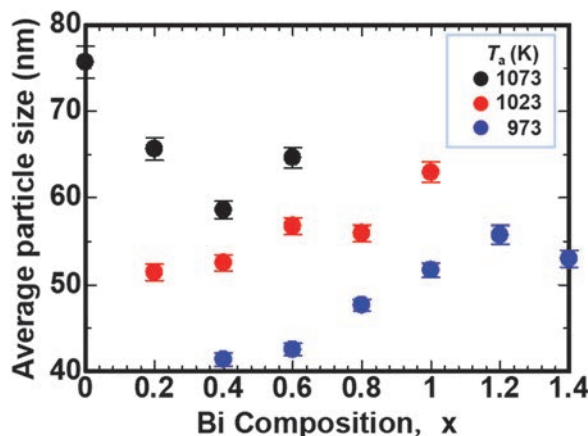


Fig. 1 Average particle size of the samples plotted as a function of x .

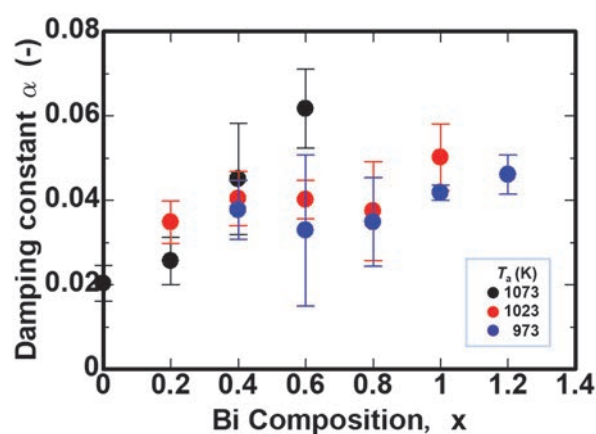


Fig. 2 Variation of the Gilbert damping constant with Bi composition x for each T_a .

[1] G. Siegel, et al., *Sci. Rep.* **4**, 4429 (2015).

【Achievement report】 This research presented as bachelor thesis at AY 2019, Gifu University, title of "共沈法により作製した Bi-YIG 薄膜の微細構造とスピン物性の相関解", by Mikiya Yamamoto at Gifu University.

Giant isotope effects of deuterium atoms terminating on nanocrystalline silicon and their use

Takahiro Matsumoto Nagoya City University

The hydrogen isotope deuterium is attracting special interest for the manufacturing of silicon (Si) semiconductors, Si-microchips and optical fibers as well as the synthesis of isotopically-labeled compounds. However, the facile production of deuterium and hydrogen deuteride in a controlled manner is a challenging task. In this collaborative research program (grant # 2019-88), we demonstrate a giant exchange reaction from hydrogen- to deuterium-termination by using the surface of nanocrystalline Si (n-Si). We have successfully obtained four times enrichment of deuterium termination from a dilute deuterium solution.

Figure 1 shows the D termination ratio as a function of dipping duration for 5%- (blue circles), 10%- (green circles), and 20%- (red circles) D₂O solution determined by the FTIR absorbance. For the comparison, SIMS data points obtained in 10%-D₂O solution are also given by the orange circles. The rates both of Si-D and Si-H productions can be expressed as

$$\frac{d[\text{SiD}]}{dt} = k_H[\text{SiH}][\text{HDO}] - k_D[\text{SiD}][\text{H}_2\text{O}], \quad (1)$$

$$\frac{d[\text{SiH}]}{dt} = -k_H[\text{SiH}][\text{HDO}] + k_D[\text{SiD}][\text{H}_2\text{O}], \quad (2)$$

where [SiD] and [SiH] is the density of Si-D or Si-H terminations (cm⁻²), [HDO] and [H₂O] is the concentration of HDO and H₂O in volume (cm⁻³), and k_H and k_D are the reaction rates. Theoretical lines which describe the D termination ratio, [SiD]/([SiD]+[SiH]), as a function of dipping duration for 5%- (blue line), 10%- (green line), and 20%-D₂O solution (red line) agree with the experimental results, where these curves are fitted by the same reaction rates as k_H=2 × 10⁻³ (Hz · cm³) and k_D=5 × 10⁻⁴ (Hz · cm³).

In summary we have obtained four times enrichment of deuterium termination by using n-Si. We believe that this enrichment protocol without using a precious rare metal catalyst opens a way toward metal-free, energy-free, and non-toxic economical H/D exchange reaction.

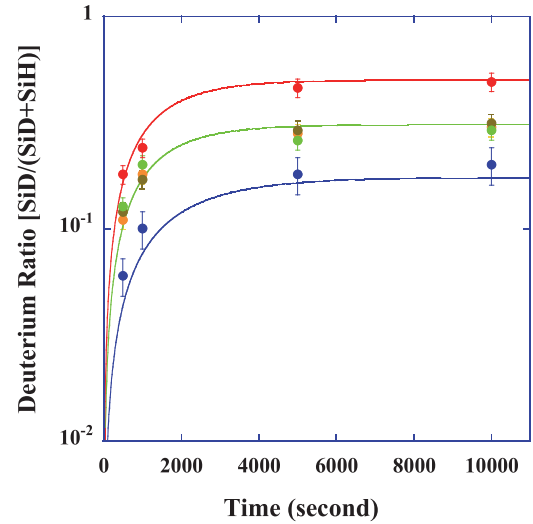


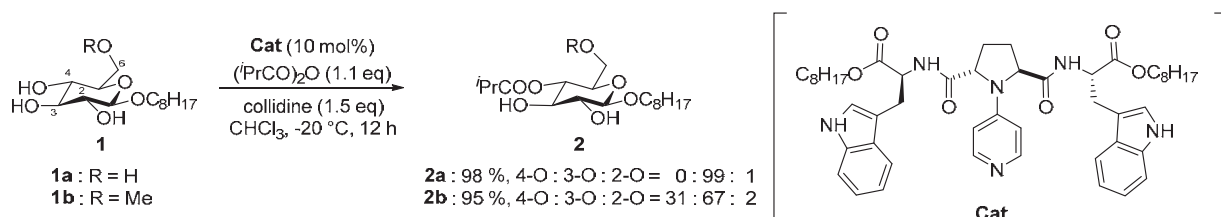
Figure 1. D termination ratio as a function of dipping duration for 5%- (blue circles), 10%- (green circles), and 20%-D₂O solution (red circles) obtained by FTIR. SIMS data are also given by the orange circles.

4-ピロリジン-ピリジン型分子触媒による 化学選択的アシル化反応の理論的解析

山中正浩 立教大学

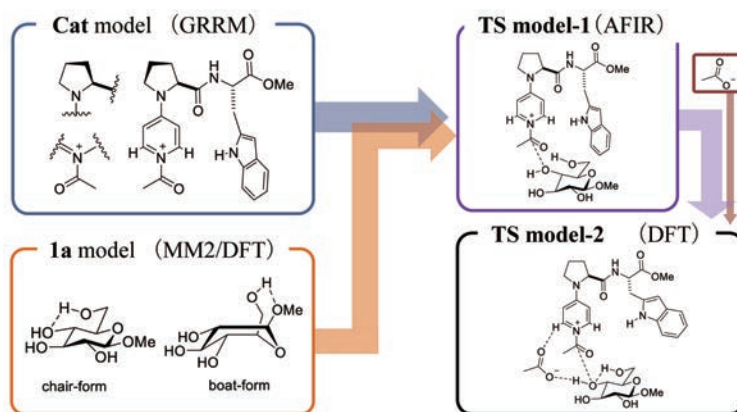
【目的】

川端らによって開発されたピロリジノピリジン触媒 (**Cat**) は、 β -L-グルコース誘導体に対する 4 位選択的モノアシル化反応を達成している。その位置選択性については、6 位水酸基の関与が示唆されているが、その詳細は明らかになっていない。昨年度に引き続き、GRRM/AFIR 法による遷移状態の網羅探索に続く DFT 計算によって、4 位選択性の要因について理論的検討を行った。

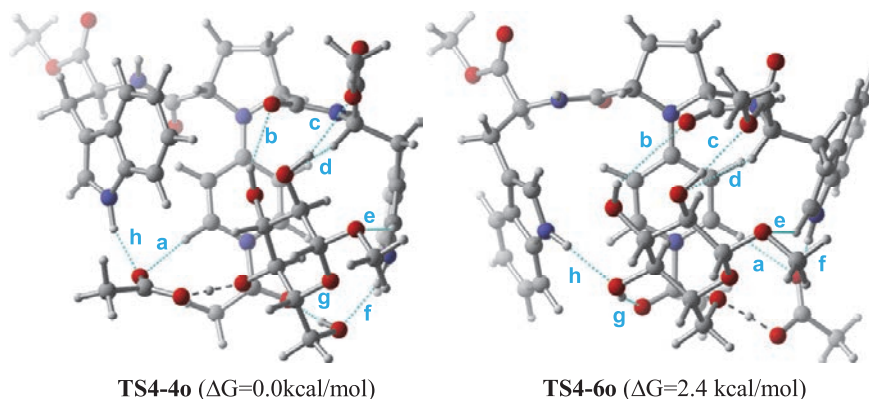


【結果・考察】

GRRM (Global Reaction Route Mapping) 計算・DFT 計算により探索した **Cat** モデルの安定な 4 種類の平衡構造(EQ)と、MM2 計算・DFT 計算により探索した **1a** モデルのイス形・舟形それぞれの安定構造を組み合わせ、AFIR (Artificial Force Induced Reaction) 計算を行い、モノアシル化



反応における遷移状態 (TS) モデルを探索した。さらに得られた TS モデルに対して、より現実に近い TS モデルとしてカルボキシレートアニオンを導入して構造最適化を行った後 (B3LYP/6-31G*, B3LYP-D3/6-31+G**), エネルギー的に安定な TS モデルについて実在系に近い C_2 対称な **Cat** モデルへと拡張して TS 構造探索を行った (B3LYP/6-31+G**). 4 位選択的モノアシル化の TS (**TS4-4o**) は 6 位選択的モノアシル化の TS (**TS4-6o**) に比べて安定となり、実験事実



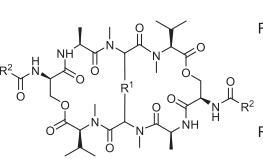
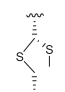
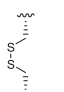
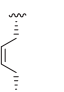
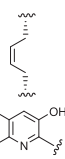
に良い一致を示した。**TS4-4o** では、6 位の水酸基がアシル基 (g) とインドール環 NH 部位 (f)、3 位の水酸基とアミド CO 部位 (b) の間に効果的な水素結合を構築していることが分かった。このような効果的な水素結合ネットワークによって **TS4-4o** が安定化し、4 位選択的アシル化が達成されていることを見出した。

α-フッ素化アミノ酸を含む抗腫瘍性環状オクタデプシペプチドの 合成と生物学的評価

永澤秀子 岐阜薬科大学

【目的・方法】我々はがん細胞の特異的な微小環境ストレス適応系を解除する作用を有する新規がん治療薬の創製を目指し、低酸素誘導因子(HIF)-1 阻害剤・抗腫瘍剤のエキノマイシ(Ec)の 2 環性オクタデプシペプチド骨格に着目した構造活性相関研究を行った。Ec は、架橋部に特徴的なチオアセタール結合を持ち、ジスルフィド結合をもつトリオスチン A (TA) に比べて二桁低い IC₅₀ を示す。そこで架橋部の構造展開により、より強く拘束された環状ペプチド類を合成し、評価した。

【結果と考察】結晶構造を比較したところ、Ec は TA と比較して、よりコンパクトな球形配座をとり、2 つの発色団部分がかなり接近していることが明らかとなった。そこで、架橋部の拘束による配座制御が活性を向上させると考え、チオエーテル、セレノエーテル、アルケン、アルキン、アルキレンなど種々の架橋結合を持つ誘導体と、架橋部を開裂して自由度を高めた誘導体を合成し、抗腫瘍活性や HIF-1 転写活性化阻害作用を調べた。予想通り、架橋部開裂体では活性が大幅に低下し、架橋部を拘束したチオエーテルやセレノエーテル、シスアルケンで置換した誘導体は Ec に匹敵する細胞毒性ならびに HIF-1 阻害作用を示した。更に架橋部をシスアルケン、芳香環を 3-ヒドロキシキノリンとしたアルケン型誘導体 **2** は天然物 Ec を上回る強力な細胞毒性ならびに HIF-1 転写活性化阻害作用、HIF-1α 蛋白質発現抑制効果を示した（細胞毒性；IC₅₀ = 0.22 nM, HIF-1 阻害；IC₅₀ = 0.090 nM）。以上より、Ec の二環性オクタデプシペプチド構造は、がん微小環境標的創薬の scaffold として有用であることが示唆された。

compound	Ec	TA	alkene 1	alkene 2
				
IC ₅₀	2.0	212	2.9	0.22
MTT [nM] (72 h, MCF-7)	0.35	26.9	1.0	0.09
HIF-1 [nM] (Luc. assay)				

【成果報告】学 Kota Koike, Masanobu Nagano, Masahiro Ebihara, Tasuku Hirayama, Mieko Tsuji, Hiroaki Suga and Hideko Nagasawa “Design, Synthesis, and Conformation–Activity Study of Unnatural Bridged Bicyclic Depsipeptides as Highly Potent HIF-1 Inhibitors and Antitumor Agents” J. Med. Chem., in press.

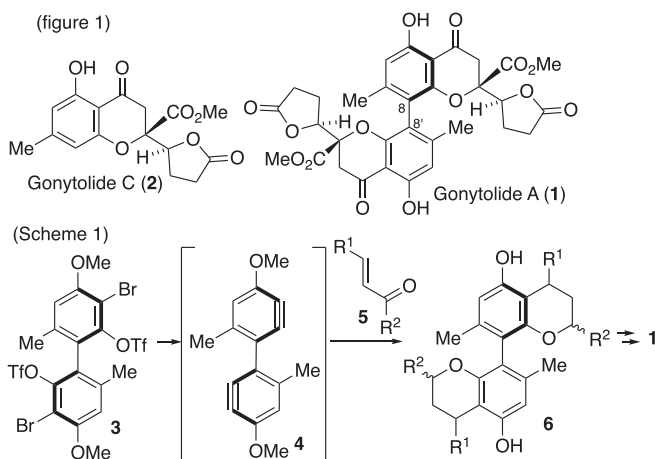
学会発表：1. Kota Koike, Masanobu Nagano, Masahiro Ebihara, Tasuku Hirayama, Mieko Tsuji, Hiroaki Suga, Hideko Nagasawa, “Structural Modification and Biological Evaluation of Quinomycin Antibiotics Focusing on Cross-bridge Structures of Bicyclic Depsipeptide” 27th International Society of Heterocyclic Chemistry Congress, Kyoto, Sep. 2019.

2. 永澤秀子、小池晃太、辻美恵子、平山祐、海老原昌弘、長野正展、菅裕明「強力な抗腫瘍活性と HIF-1 阻害活性を有する高度に拘束された二環式デプシペプチド化合物の開発」、第 78 回日本癌学会学術総会、京都、Oct. 2019.

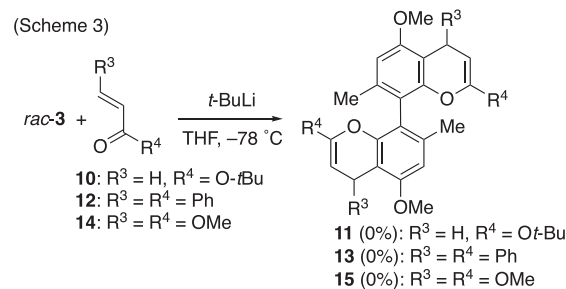
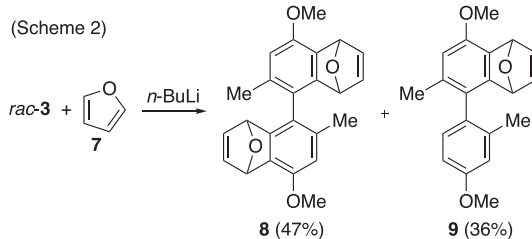
Studies on total synthesis of gonytolides

Tomoyuki Yoshimura Kanazawa University

Gonytolides A (**1**) and C (**2**) were isolated from *Gonytrichum* species (figure 1).¹⁾ Gonytolide A consists of a dimer of **2** connected at C(8)-C(8') position where has axial chirality and shows a promoting-activity of an innate immune response. We planned an enantioselective total synthesis of gonytolide A (**1**) using [4+2]cycloaddition between chiral bibenzynes **4** and α,β -unsaturated carbonyl compound **5** as a key reaction (Scheme 1). A bibenzynes **4** generated from chiral biphenyl **3** would have a very short half-life of racemization. The keys to achieving high asymmetric induction via **4** are 1) effective generation of bibenzynes **4** at low temperature to reduce racemization, and 2) accelerating cyclization between



4 and **5** compared to racemization of **4**. To confirm a generation of bibenzynes **4**, cycloaddition of *rac*-**3** and furan was investigated. Treatment of *rac*-**3** with *n*-BuLi in the presence of furan (**7**) at -78°C gave a diastereomeric mixture of binaphthyl **8** and phenylnaphthalene **9** in 47% yield and 36% yield, respectively (Scheme 2). This result indicated generation of bibenzynes **4** from *rac*-**3** took place via lithium-bromine exchange followed by elimination of triflate. Then cycloaddition between *rac*-**3** and α,β -unsaturated carbonyl compound **5** was investigated (Scheme 3). Reaction between *rac*-**3** and *tert*-butyl acrylate (**10**) with 4.5 equiv of *t*-BuLi did not give the desired product **11** but recovered *rac*-**3** in 52% yield probably due to nucleophilic addition of *t*-BuLi to **10**. Similar results were observed by reaction with chalcone (**12**) or methyl 3-methoxycacrylate (**14**). It was assumed that generation of **4** in high concentration and low reactivity of **5** would lead to these results. Investigation of proper carbonyl compounds and reaction conditions are in progress.



Presentation: This research had been disclosed in 2019 年度有機合成化学北陸セミナー on September 27th, 2019 in Kanazawa as a poster presentation.

Reference: Kikuchi, H.; Isobe, M.; Sekiya, M.; Abe, Y.; Hoshikawa, T.; Ueda, K.; Kurata, S.; Katou, Y.; Oshima, Y. *Org. Lett.* **2011**, *13*, 4624-4627.

Analysis of the physiological functions of membrane vesicles produced by intestinal bacteria and fermented food-derived bacteria and their application

Atsushi Kurata Kindai University

Introduction:

The gastrointestinal tract is inhabited by a complex community of bacteria, the gut microbiota. The bacteria perform various functions involved in host energy metabolism and stimulations of host immune system. Most bacteria release membrane vesicles (MVs) with the size ranging from 50 to 400 nm. The MVs contain specific proteins, DNA, or RNA from the bacteria. It has been assumed that the MVs released by intestinal bacteria play critical roles in the host-bacteria interactions. Thus, the first objective of this study is to explore MVs-producing bacteria using intestines and fermented foods as isolation sources. The second objective is to analyze production mechanisms of MVs from bacteria and physiological functions of MVs toward host organisms. The third objective is to develop novel expression systems for heterologous proteins using MVs-producing bacteria.

Results:

1. Properties of MVs produced by intestinal bacteria

We found that *Lactobacillus plantrum* and *Bifidobacterium infantis* isolated from human intestines produce MVs with the size of 50-100 nm. MVs were prepared from culture supernatants from each strain by filtration and ultracentrifugation. Proteins of MVs of each strain were analyzed by LC-MS/MS. As the results, GroES, GroEL, and five kinds of lipoproteins were detected in MVs from *L. plantrum*. MVs from *L. plantrum* were recognized by human Toll-like receptor 2 of HEK293 cells and the MVs stimulated Peyer's patch cells to produce IgA. It has been reported that Toll-like receptor 2 mediates recognition of microbial products, such as lipoproteins. Therefore, we plan to analyze and characterize the lipoproteins associated with MVs from *L. plantrum*.

2. Mechanistic analysis of cargo transport to MVs

Shewanella vesiculosa HM13 isolated from intestinal contents of a horse mackerel (*Trachurus japonicus*) produces MVs that contain a single major cargo protein of about 49 kDa named P49. The P49 gene is located in a gene cluster containing genes that code for homologs of proteins involved in surface glycolipid biosynthesis. The genes coding for these proteins were disrupted, and localization of P49 in these mutants was analyzed. We found that P49 was found in the extracellular space without being associated with MVs. The results suggest that surface glycolipids of MVs play an essential role in tethering of P49 to MVs.

Studies on the physiological significance of two alanine dehydrogenases in *Geobacillus kaustophilus*

Taketo Ohmori Osaka Institute of Technology

Introduction: Alanine dehydrogenase (AlaDH, EC 1.4.1.1) catalyzes the NAD-dependent reversible oxidative deamination of L-alanine to pyruvate. This enzyme is broadly distributed among various microorganisms and plays an important role in both alanine utilization and synthesis. In *Bacillus subtilis*, AlaDH is related to the energy supply during spore formation and is necessary for normal sporulation. We found that *Geobacillus kaustophilus* has two putative AlaDH genes (*GK2752* and *GK3448*, amino acid sequence identity: 75%) within its genome by using GenomeNet Database Resources. We constructed the expression vectors of *GK2752* and *GK3448*, respectively, and overexpressed these recombinant proteins using *Escherichia coli*. Both recombinant proteins showed the AlaDH activity. In this research, to understand the physiological function of the two AlaDHs in *G. kaustophilus*, we attempted to identify the AlaDH expressed in the vegetative cells and the spores.

Methods: *G. kaustophilus* was grown in LB medium to prepare the vegetative cells. To prepare the spores, *G. kaustophilus* was grown in the Difco sporulation medium. AlaDHs were purified by ammonium sulfate precipitation, Dye-ligand chromatography and preparative Native-PAGE. The mobility of these purified AlaDHs were compared to that of the recombinant *GK2752* and *GK3448* by SDS-PAGE or Native-PAGE. The N-terminal sequence of the purified AlaDH from the vegetative cells was determined by protein sequencer PPSQ31A.

Results and Discussion: AlaDHs expressed in vegetative cells and spores were homogeneously purified by ammonium sulfate precipitation, Dye-ligand chromatography and preparative Native-PAGE. In this study, we demonstrated the simple and efficient purification process of AlaDH from *G. kaustophilus*. The mobility of the purified AlaDH from the vegetative cells precisely corresponded to that of the recombinant *GK3448* enzyme, not that of the recombinant *GK2752*, by SDS-PAGE. Furthermore, N-terminal sequence analysis revealed that N-terminal sequence (12 amino acid residues, MIIGVPKEIKNN) of the purified AlaDH exhibited 100% sequence identity with that of *GK3448* enzyme. These results suggest that *G. kaustophilus* expresses only AlaDH from *GK3448* gene in vegetative growth state. On the other hand, the active-staining by Native-PAGE revealed that the mobility of the purified AlaDH from the spores precisely corresponded to that of the recombinant *GK2752* enzyme. This result demonstrated that AlaDH from *GK2752* gene is expressed in only spore state of *G. kaustophilus*. These results suggest that, in *G. kaustophilus*, two AlaDHs (*GK2752* and *GK3448*) play physiologically distinct roles at different growth stages.

学会発表: [1] 大森勇門、亀井咲也香、安達泰志、大島敏久 第66回日本生化学会近畿支部例会 京都大学宇治キャンパス 2019.5.25、[2] 大森勇門、亀井咲也香、安達泰志、大島敏久 日本農芸化学会 2020年度大会 九州大学伊都キャンパス 2020.3.25~28 発表予定

異常高原子価イオンを含む機能性酸化物合成とその構造物性研究

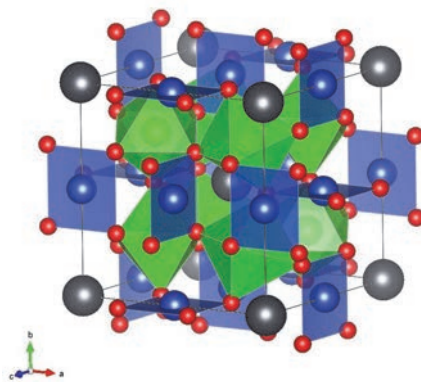
齊藤高志 高エネルギー加速器研究機構

【目的】 Cr^{4+} 、 Fe^{4+} 、 Co^{4+} 、 Ni^{3+} 、 Cu^{3+} 等は異常高原子価イオンと呼ばれ、特徴的な電子状態を持つために、金属-絶縁体転移や巨大磁気抵抗、負性熱膨張など、非常に興味深い性質を引き起こすことが知られている。これらのイオンを安定化するためには高い酸化雰囲気が必要とするためその合成は容易ではなく、これらを含む酸化物の合成や物性に関する理解はまだ十分とはいえない。そのため異常高原子価イオンを含む新物質を合成し、その結晶構造と物性の相関を明らかにすることは固体化学・物性物理の観点から非常に重要である。これまでに我々は A サイト秩序型ペロブスカイト構造を持つ $\text{LaCu}_3\text{Cr}_4\text{O}_{12}$ を合成した[1]。またこの物質が室温において $\text{Cu}^{(2+\delta)+}$ および異常高原子価 $\text{Cr}^{(4-\delta)+}$ を含むが、220K 以下では Cu-Cr 間電荷移動を起こして $\text{Cu}^{(3-\gamma)+}$ および異常高原子価 $\text{Cr}^{(3+\gamma)+}$ を含む低温相へと変化し、珍しい反強磁性金属状態を取ることを見出した。そこで本研究では $\text{LaCu}_3\text{Cr}_4\text{O}_{12}$ における La^{3+} を Pb^{2+} に置換した $\text{PbCu}_3\text{Cr}_4\text{O}_{12}$ の合成を試み、異常高原子価イオンを含むと期待されるこの物質の結晶構造と物性を明らかにすることを目的とした。

【実験方法】A サイト秩序型ペロブスカイトの合成には一般的に高圧力を必要とし、また異常高原子価イオンを含む化合物の合成には高い酸化雰囲気が必要である。一方 Cr は高圧力・高酸化雰囲気では容易に Cr^{6+} へと変化することから、温度、圧力、酸素量の制御が重要である。そこで化学研究所附属元素科学国際研究センター先端無機固体化学研究領域所有の高圧合成装置を用いて、 $\text{PbCu}_3\text{Cr}_4\text{O}_{12}$ の合成を試みた。得られた試料について粉末 X 線回折、粉末中性子線回折、および磁化測定を行った。

【実験結果】 PbO 、 CuO 、 CrO_2 の混合粉末を 9GPa の圧力下、1000℃で 30 分間加熱後、減圧することによって $\text{PbCu}_3\text{Cr}_4\text{O}_{12}$ の合成に成功した。粉末 X 線回折による結晶構造の結果、この化合物は Pb と Cu が単純ペロブスカイト構造における A サイトにおいて 1:3 の割合で秩序配列している A サイト秩序型ペロブスカイト構造を持つことが見いだされた(Fig.1)。磁化測定から、 $T_C \sim 100\text{K}$ の強磁性的な振る舞いが見られた。

【考察】X 線結晶構造解析の結果、Pb、Cu、Cr のいずれもが混合原子価を取っている可能性が示唆されており、Pb-6s、Cu-3d、Cr-3d、O-2p の電子準位が混成した複雑な電子状態を持つと予想される。さらなる精密な結晶構造及び磁気構造の評価のため、粉末中性子回折データの解析を現在進めている。

Fig.1 $\text{PbCu}_3\text{Cr}_4\text{O}_{12}$ の結晶構造

[1] T Saito, Y. Shimakawa, et al., Phys. Rev. B (Rapid), 95, 041109 (2017).

溶媒含浸樹脂を用いた白金族元素抽出における界面活性剤の利用

倉橋健介 大阪府立大学工業高等専門学校

1. 目的

白金族元素は自動車用排ガス触媒や窯業の坩堝、電子部品など様々な工業分野で用いられているが、年間産出量は少なく、供給源が偏在していることから、リサイクルに注目が集まっている。白金族元素分離法の一つである溶媒抽出法は、簡便な抽出操作で比較的高い選択性が得られることに加え、安価であるという利点がある。しかし、溶媒抽出は大量の有機溶媒を用いることから、人体や環境への暴露の問題がある。そこで、有機溶媒の暴露の少ない分離法として、多孔性樹脂に抽出剤を固定化する溶媒含浸樹脂に着目した。先行研究では、白金族元素の溶媒抽出による分離において抽出相へ界面活性剤を添加することで、抽出率が飛躍的に増大することを見出している。この界面活性剤が示す協同効果を溶媒含浸樹脂においても適用するため、本年度は溶媒抽出において界面活性剤を添加した場合の抽出機構について、抽出速度の観点から解析を行った。

2. 実験方法

有機相は、溶媒として 2-ethyl-1-hexanol と isooctane を 4 : 6 で混合した混合溶媒を使用した。0.01 M Di-n-hexyl Sulfide を含む有機相に、界面活性剤として任意の濃度の Cetyltrimethylammonium Bromide (C16TAB) を添加した。水相は Pd 濃度が 100 ppm (0.94 M) となるよう、1000 ppm Pd 標準液を用いて調製した。調製した有機相と水相を 0.6 ml ずつ試料チューブに入れ、任意の時間、振とうした。振とう後のサンプルを 3000 rpm で 5 分間遠心分離し、水相のみを分取して、水相に含まれる Pd 濃度を測定した。測定は ICP-OES により行い、Ni を内標準とした内標準法で定量した。

3. 結果と考察

C16TAB を有機相に添加した場合、添加量が臨界ミセル濃度である 0.9 mM を超える場合では、添加していない場合に比べ抽出速度の大幅に向上したが、臨界ミセル濃度を大きく下回る 0.3 mM では界面活性剤を添加しない場合とほとんど変わらない結果となった。また、添加量が臨界ミセル濃度以上では抽出速度に大きな違いが見られなかった。また、1.5 mM の C16TAB を水相に添加して抽出を行ったところ、有機相に添加した場合と同様の抽出速度の向上を観察できた。これは、逆ミセルのような界面活性剤による会合体の形成が抽出速度に影響したためと考えられる。

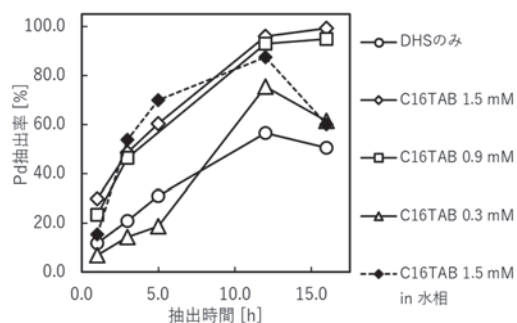


Fig. 界面活性剤の添加濃度に対するPd抽出速度の変化

4. 成果報告

- 1) 中谷亮ら, 日本分析学会第 68 年会, 千葉大学 西千葉キャンパス, 2019.9.
- 2) 川崎裕太ら, 第 22 回化学工学会学生発表会, 岡山大学 津島キャンパス, 2020.3.

ポリマーブラシ付与強磁性プレート粒子の精密合成による 強磁性フォトニック液晶の実現

内田幸明 大阪大学

近年、工場内の自動化システムや、車載ネットワーク、IoT の急激な広がりに対応するため、安価なポリマーを材料とする光ファイバーによる、可視光を用いた短距離通信システムが注目されている。しかし、通信速度やシステムに組み込まれたノードの数が増加するにしたがって、ケーブル同士の干渉や配線の複雑化や、小径に曲げるための可撓性が限界に達する等の問題が発生する。その解決には、光ファイバーフリーの短距離光伝送システムが有望である。

研究代表者(内田)は磁場による光の遠隔操作を可能にする光伝送素子として、柔軟なフォトニック構造を持つコレステリック液晶 (CLC) に注目し、室温で動作する安定常磁性 CLC の合成を行い、全方位レーザー発振を示す CLC カプセル [1] を実現してきた。また、上記のように CLC のフォトニック特性や、磁気光学効果の研究だけでなく、液晶相を鋳型とするナノシート分散液の合成手法の開発 [2] や、強磁性ナノプレートを分散させたネマチック液晶 (NLC) のランダムレーザー発振を弱磁場でスイッチングすることに成功している [3]。しかし、既知の方法で作られた強磁性ナノプレートは CLC に分散させようとすると凝集してしまい、強磁性 CLC を得られない。

本研究では、固体磁石の微粒子にポリマーブラシを付与し、CLC への分散を可能にすることで、強磁性 CLC を実現し、非常に弱い磁場 (数 mT) による発光特性・反射特性・屈折特性のスイッチングを目指して研究を進めてきた。

まず、共同研究者(大野工司准教授)が、表面開始リビングラジカル重合により各種ポリマーをグラフトした強磁性ナノプレートの分散液を合成した。次に、研究代表者(内田)と研究協力者らがこの強磁性ナノプレートを NLC に安定分散することを試みた。リビングラジカル重合の特長を活かして、グラフトポリマーの分子量を制御することで、ナノプレート表面の液晶の配向性が垂直配向のナノプレートと水平配向のナノプレートを得ることができ、これらを NLC に分散することで強磁性液晶だけでなく超常磁性液晶が得られることを見出した。一方、いずれの分子量のグラフトポリマーを有する強磁性ナノプレートについても CLC には安定分散しなかった。

CLC はらせん構造を持つのに対して、ナノプレート上のグラフトポリマーは一軸配向性である NLC と同様の配向構造を持つため相分離を起こし、安定分散できなかったと考えている。グラフトポリマーにもキラリティーを導入することで安定分散が起こる可能性がある。

参考文献

1. Y. Uchida, Y. Takanishi, J. Yamamoto, *Adv. Mater.*, **25**, 3234-3237 (2013).
2. Y. Uchida, T. Nishizawa, T. Omiya, Y. Hirota, N. Nishiyama, *J. Am. Chem. Soc.*, **138**, 1103–1105 (2016).
3. T. Naruta, T. Akita, Y. Uchida, D. Lisjak, A. Mertelj, N. Nishiyama, *Opt. Express*, **27**, 24426-24433 (2019).

Additive Manufacturing による多孔性高分子複合材料の 3 次元構造制御

村瀬浩貴 共立女子大学

多孔材料は、各種の分離フィルタ、各種電池セパレータ、透湿防水布としての快適性衣料、海水淡水化膜や水浄化膜などの環境関連材料、血液透析膜や細胞培養基材などの医療材料など幅広い分野で利用されている。これまで、様々な多孔材料が実用化されてきたが、モノリス (Monolith) は 3 次元ネットワーク状の骨格構造を持ち、ネットワークの骨格サイズと、その空隙である連続空孔のサイズを独立に制御できる次世代多孔材料として注目されている。京都大学化学研究所の辻井敬亘教授と榊原圭太助教は、界面化学的手法を駆使して、重合誘起スピノーダル分解を経由するエポキシ系ポリマーモノリスで新規な多孔材料を創生してきた。一方、報告者はこれまで、Additive Manufacturing (3D Printing) の技術を応用して、新規な構造を有する複合繊維や繊維-樹脂複合型布帛の開発、セルロースナノファイバーの 3 次元造形に取り組んできた。本研究では Additive Manufacturing の技術と、辻井教授と榊原助教の界面制御技術・高性能モノリス合成技術を融合し、3 次元構造を制御した新規ポリマーモノリスを創生することを目的とする。辻井教授らの技術では、ポリビニルアルコール (PVA) の基材の上にエポキシ系モノリスを形成することで、孔の閉塞したスキン層の発生を防ぐことに特徴がある。PVA 製の鋳型を Additive Manufacturing によって作製することにより、任意の 3 次元形状のモノリス膜を作製することが可能となると考えた。

まず基礎検討として、調達した 2 種類の 3D プリンティング用の PVA 樹脂と本技術のポリマーモノリスとの相性を確認した。その結果、ケン化度の低い K 社製 PVA 樹脂ではスキン層が形成され、ケン化度の高い M 社製 PVA 樹脂ではスキン層が形成されることが明らかとなった。そこで、M 社製 PVA 樹脂を用いて 3D プリンティングによりモノリスの鋳型を作製した。もっとも単純なモデルとして中空状のモノリスチューブが作製できる鋳型 (Fig.1a) を、3D プリンタ (久宝製作所製 Qhoria) を用いて作製した。この鋳型にモノマーを流し込みモノリスを作製後、鋳型を溶脱して得た中空モノリスが Fig.1b である。Fig.1d のモノリス内層表面の断面 SEM 写真に示すように、表面がスキン層で閉塞されることなく、中空状のモノリスを得ることに成功した。

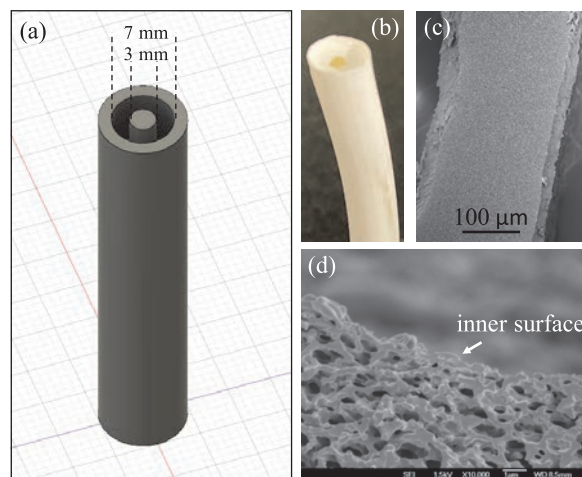


Figure 1. 3D printed template and hollow fiber of monolith
(a) Model of the template in 3D CAD
(b) Hollow fiber of monolith
(c) Cross section of the monolith
(d) Close-up micrograph of the monolith

Ferromagnetic single-electron transistor

Yutaka Majima Tokyo Institute of Technology

Ferromagnetic single-electron transistors (FM-SETs), which consist of ferromagnetic asymmetric source/drain nanogap electrodes and a Coulomb island, are promising candidates for the next-generation transistors due to their sub-10 nanoscale structures, ultralow power consumption and nonvolatility. Owing to shape anisotropy, parallel/antiparallel magnetizations of the electrodes can be realized by sweeping external magnetic field, which results in spin-dependent single-electron tunneling. For room temperature operation of FM-SETs, ferromagnetic asymmetric nanogap electrodes with a 10 nm scale gap separation is one of the critical building blocks. A ferromagnetic material with high uniaxial magnetocrystalline anisotropy (K_u) is also required to avoid thermal fluctuation of magnetizations of the nanoscale electrodes. Some of the strong candidates for high- K_u materials are ordered-phase Cobalt-Platinum alloys, such as $L1_0$ -Co₅₀Pt₅₀, which can be attained by annealing, leading to high thermal stability of magnetization and high coercivity. However, such electrodes which satisfy both a 10 nm scale gap separation and high thermal stability of magnetization have not been developed so far.

Here, we fabricate ferromagnetic Co₅₀Pt₅₀ asymmetric nanogap electrodes with a gap separation as small as 11.9 nm by electron-beam lithography (EBL), EB evaporation and annealing at 400 °C by a furnace, shown in Fig. 1, which can be a platform for ferromagnetic single-electron transistor. We have started to introduce magnetic nanoparticles between the nanogap, which was synthesized by Prof. Teranishi.

This study was partially supported by the Collaborative Research Program of Institute for Chemical Research, Kyoto University (grant 2019-98).

References

1. Ryo Toyama, Yutaka Majima, Ferromagnetic Co₅₀Pt₅₀ Asymmetric Nanogap Electrodes with a 10 nm Scale Gap Separation, 10th International Conference on Molecular Electronics & BioElectronics (M&BE10), Nara, June 26, 2019.

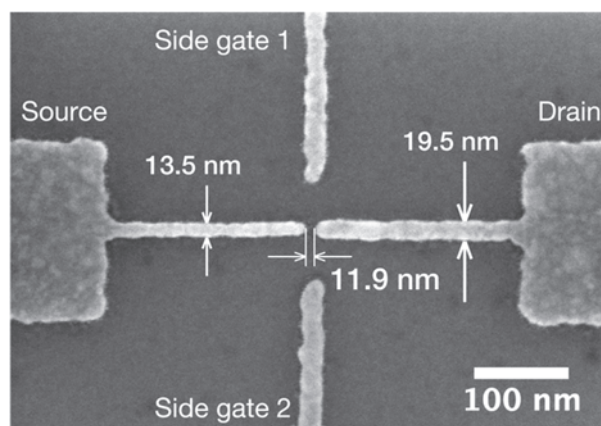


Fig. 1: SEM image of ferromagnetic Co₅₀Pt₅₀ asymmetric nanogap electrodes annealed at 400 °C by furnace.

パーフルオロアルキル鎖とアミノ酸頭部基を有する 新規な界面活性剤型防錆剤の探索

山田哲弘 千葉大学

【はじめに】 ステンレス・鉄などの表面にはタンパク質が吸着しやすく、食品・医薬品産業界において装置汚染という問題を引き起こしている。このことはタンパク質を構成するアミノ酸側鎖中に、鉄に対して優れた吸着性を有する官能基が存在することを示唆している。本研究は Rf 鎖を有する両親媒性分子を鉄材に吸着・配列させ、防錆作用を発現させることが目的であるが、まず鉄に対して吸着性に優れた頭部官能基の探索に力点を置いた（パーフルオロアルキル (Rf) 鎖の導入はまだ行っていないが導入の方法は確立できている）。ここでは、光照射によってチイルラジカルを生じやすいジスルフィド (-S-S-) 結合と水酸基に着目して、アミノ酸のシスチンと、複数個の水酸基を有するトリスヒドロキシメチルアミノメチル基（以後 THMAM 基）を親水部に持つ両親媒性分子を合成し（図 1）、鉄に対する吸着性を防錆効果から検討した結果について報告する。

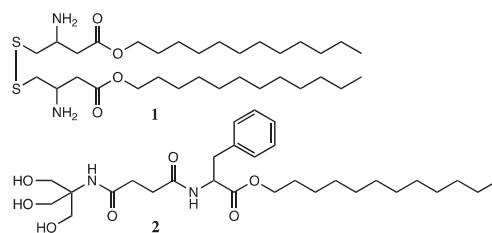


図 1 合成した分子の例

【実験】 シスチンをアミノ酸頭部とする **1** は L-シスチンを長鎖アルコールで酸触媒エステル化して得た。THMAM 基を持つ分子 **2** は DCC を用いてコハク酸イミドを長鎖カルボン酸に縮合し、この活性エステルとトリスヒドロキシメチルアミノメタンをジメチルホルムアミド/THF 混合溶媒中で反応させて得た。防錆効果は、研磨した軟鉄表面に被検分子の有機溶媒溶液をキャスト・風乾して酸性雰囲気下に置き、腐食の経時変化を観察して評価した。

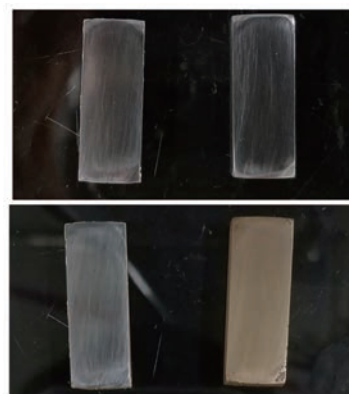


図 2 防錆効果の検証
左: **2** のエタノール溶液 (10 mM) 50 μ L をキャスト・風乾した鉄片, 右: 研磨後未処理の鉄片, 0.1 M 塩酸を含浸した濾紙とともにシャーレに入れ、経過を観察した。上図は酸性雰囲気下に暴露直後。両鉄片とも金属光沢あり。下図は暴露 3 日目。未処理の鉄片は全面に赤さびを生じたが、**2** をコーティングした鉄片は金属光沢を維持している。

【結果と考察】 図 2 は **2** のキャストフィルムで被覆した鉄材を酸性雰囲気下に暴露した直後と 3 日後の写真である。下の写真から、**2** をキャストした鉄片は酸性雰囲気下 3 日後でも完全な金属光沢を残している。金属光沢の維持は 7 日後まで持続した。同様の防錆検証を **1** で行ったが、金属光沢を残す部分は部分的であった。3 日間にわたる完全な機材保護を達成できたのは **2** を用いた今回が初めてである。今後は **2** のアルキル鎖を Rf 鎖とした分子やアミノ酸残機数を増やした分子を合成し、防錆効果の検証を行うとともに、鉄材への吸着方法をはじめとする詳細を検討する予定である。

【成果報告】

1. 藤本洸介, 下赤卓史, 長谷川健, 山田哲弘, 第 42 回フッ素化学討論会, 神戸大学百年記念館六甲ホール, P40 (予稿集 pp. 146-147), 2019. 11.
2. 富士亜美, 藤本洸介, 下赤卓史, 長谷川健, 山田哲弘 第 42 回フッ素化学討論会, 神戸大学百年記念館六甲ホール, P41 (予稿集 pp. 148-149), 2019. 11.

NanoBRET 型 CXCR4 結合解析によるペプチドリガンド評価系の構築

野村 渉 広島大学

ケモカインレセプターCXCR4 は HIV-1 感染時にウイルスが認識して侵入に利用する第二受容体として知られており、また、ケモタクシスによるがん細胞の転移や、関節リウマチにも関与しているため、重要な創薬標的分子である。研究代表者らの研究では主に CXCR4 に対して結合する低分子化合物の結合親和性を評価するためにスループット性に優れた手法として NanoBRET を活用してきた。NanoLuc という新規のルシフェラーゼをドナーとして利用し、CXCR4 に結合する既知物質にアクセプターとしての蛍光色素をコンジュゲートした化合物を競合物質とする。よって CXCR4 との相互作用時は BRET が起こるが、新規化合物に結合親和性があると BRET が解消され、その割合によって結合親和性を評価できる。また、洗浄操作と必要としないため、大規模の化合物評価も簡便に行える。生体機能設計化学・二木教授らは CXCR4 と相互作用するタンパク質ドメインから細胞膜透過性を示すペプチド配列を見出しており、細胞内物質デリバリー作用につながる細胞膜表面との相互作用機構の解明を目指している。CXCR4 との相互作用も示唆されているため、研究代表者らが開発を行う手法を利用して、それらペプチドの結合親和性を評価することとした。

研究代表者は、まずケモカインレセプターCXCR4 の N 末端に NanoLuc を融合したタンパク質 (NanoLuc-CXCR4) を安定発現する CHO 細胞株を構築した。N 末端融合 NanoLuc-CXCR4 からの生物発光エネルギーの蛍光アクセプターとして蛍光標識 CXCR4 アンタゴニストである TAMRA-Ac-TZ14011 を採用した。620 nm の蛍光と 460 nm の発光の比から、試験ペプチドと CXCR4 の相互作用が評価可能である (図)。まず、この系が CXCR4 リガンドの評価に適用可能であることを実証するために、この系を用いて求めた既知の CXCR4 リガンドの IC₅₀ 値は、SDF-1: 3.2 nM、Ac-TZ14011: 15.3 nM、FC131: 4.5 nM であり、これらの値は既存の他の高感度な方法で得られた値と同等であることが示され、この系の信頼性が確認できた。さらに、IL-6 分泌シグナル伝達ペプチドを NanoLuc-CXCR4 に融合することにより (secNluc-CXCR4)、CXCR4 の細胞表面への提示と NanoBRET アッセイシステムのダイナミックレンジが増加した。二木らの開発した CXCR4 と相互作用するタンパク質ドメインから由来の膜透過ペプチドとその誘導体計 6 種の CXCR4 との結合を上記のアッセイ法により検討したところ、ペプチド濃度 1 μ M で BRET が 30-50% 程度抑制されることが分かった。現在、これらのペプチドと CXCR4 との結合に関して更に詳細に検討しているところである。

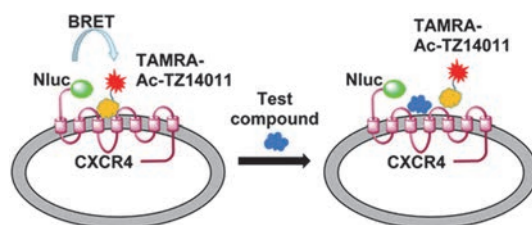


図. NanoLuc-CXCR4/TAMRA-Ac-TZ14011 系を用いた CXCR4 リガンド評価系

がん深部到達型修飾膜透過ペプチドの創出と大腸がん幹細胞効率的除去への展開

大橋若奈 富山大学

【目的】悪性腫瘍において化学療法により多くの腫瘍細胞が除去される一方で生き残る腫瘍細胞も存在する。生き残った腫瘍細胞はがん幹細胞とも呼ばれ腫瘍組織の再形成に寄与し、再発や転移の誘発、そして生命予後悪化の要因となっており、より一層効果的な腫瘍細胞の駆逐法は重要な課題となっている。一方腫瘍組織深部は血管形成の乏しさなどから化学療法剤が十分に行き渡っておらずこれががん幹細胞の生き残りを生み出しているとも考えられている。本課題では、がん幹細胞を除去するアプローチの一つとして効果的に細胞内へ透過する膜透過ペプチドを用いて化学療法剤が届きにくいとされる腫瘍深部への物質輸送法の検討を行った。腫瘍組織深部へ到達可能な物質輸送法が構築されれば、がん幹細胞標的化修飾を付与することでがん幹細胞の効果的な除去法の開発へとつながることが期待される。

【実験方法】ヒト大腸がん由来細胞 HT29 細胞を非接着条件下で培養し三次元細胞凝集塊（スフィア）を得た。蛍光標識した種々の膜透過ペプチド（CPP）配列をスフィアに投与し、スフィア内への移行を共焦点レーザー顕微鏡観察にて検証した。フローサイトメトリーにて取り込み量を測定した。細胞死誘導配列を付加した細胞死誘導 CPP をスフィアに投与し、ATP 測定による生存率の評価と光学顕微鏡観察による形態評価を行った。全ての CPP は共同研究者である二木教授（京都大学化学研究所）より提供され、京都大学化学研究所にて研究打ち合わせを行った。

【実験結果と考察】 FITC により緑色蛍光色素標識された CPP を投与したスフィアの共焦点レーザー顕微鏡画像を示す（図）。緑色蛍光を発する細胞はスフィアの表層、中央部などあらゆる部位から観察され、CPP は内部も含めたスフィア全体の細胞に及ぶことが示唆された。フローサイトメトリーを用いてスフィア細胞中に取り込まれた緑色蛍光値を測定し CPP のスフィアへの移行量を評価した結果、スフィアへの取り込み量は配列により異なることを認め、高効率でスフィア細胞内へ移行する配列を得た。細胞死誘導配列を付加した CPP をスフィアに投与し、生存率と形態の評価を

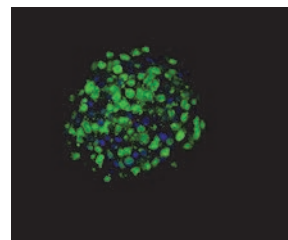


図. スフィアへのCPPの導入。
緑はCPPが移行したスフィア細胞を示す。スフィア中多くの細胞にCPPが移行しているのがわかる。青は核を示す。

行った結果、細胞死誘導 CPP 投与によりアポトーシス性の細胞死が誘導され、スフィアの生存率は有意な低下を示し、細胞死誘導 CPP が移行したスフィア細胞において細胞死が惹起されることが示唆された。腫瘍組織への効果的な薬物送達法は腫瘍の駆逐に加えて有害事象の軽減においても重要な課題であり、腫瘍組織と類似した内部環境を有するスフィアを用いた本検討により見出した腫瘍組織内部へ移行しうる候補 CPP を基盤として腫瘍抗原標的化修飾などの更なる腫瘍標的化の工夫を加えることにより、腫瘍組織への効果的な薬物送達法の開発へとつながることが期待される。

ダイヤモンド表面近傍の NV 中心作製

徳田規夫 金沢大学

【目的】ダイヤモンド中の NV 中心の単一スピンをプローブとした磁気センサ、電場センサ、温度センサが、高感度、高空間分解能などの観点から注目される。NV 中心のセンサ応用において、NV 中心は感度向上のため数ナノレベルの浅い領域に存在していることが望ましい。しかし、ナノレベルでの表面付近では、センサとして使える電荷状態が -1 価に荷電した NV^- の電荷状態が不安定になることや、スピンコヒーレンス時間の短時間化によりセンサ感度が著しく低下するなど、重要な克服すべき課題がある。この原因の有力な候補の一つとして表面付近の常磁性欠陥や不純物の存在が考えられる。本提案では、課題克服のため常磁性欠陥の極めて少ない原子レベルでの表面平坦化合成技術を用いることによる、表面から数ナノレベルの浅い NV 中心作製を目指した。

【実験と結果】ダイヤモンドにおいて、ある CVD 合成条件を満たすと、数十 μm 四方の面積において、原子レベルでフラットな表面を持つ試料を作成することができる[1]。成膜プロセスの提案や合成条件における窒素濃度の制御の条件出しを、共焦点レーザ顕微鏡によって行った。図に原子レベル平坦となっていると考えられる領域において、 $30\mu\text{W}$ という通常のパルス測定時よりも低いレーザ強度でスキャンした結果を示す。ここでスポットの形状から単一 NV 中心と思われる蛍光は複数観測されたが、いずれもレーザ照射により数秒で蛍光が消滅して

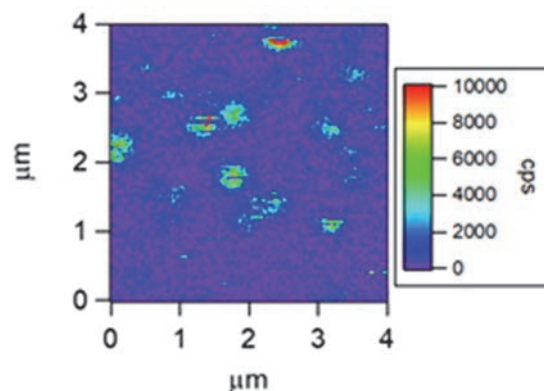


図 表面から数ナノレベルの領域における共焦点レーザスキャンイメージ

しまった。スキャンイメージでは左下から右、そして上の順番にスキャンしているが、沈むころの上弦の月のように下半分しか蛍光していないスポットは、スキャンによるわずかな時間のレーザ照射で消滅したことを示している。蛍光強度もバルク中の NV 中心よりも 1 桁ほど弱い。あまりに早く蛍光が消滅してしまうため、今回は ODMR やパルス波測定、PL スペクトル測定など NV であることを証明できる測定が実現しなかった。今後の課題として、新たな表面処理等を施して更なる安定化を行い、それらの測定を目指す予定である。また、共同研究成果として、ドレスト状態生成によるスピンコヒーレンス時間の桁違いの長時間化に成功した[1, 2]。今後の量子センサ感度向上につながる成果である。

【参考文献】 [1] N. Tokuda, et. al., Appl. Phys. Exp. 2 (2009) 055001. (b) N. Mizuochi, N. Tokuda, et. al., Jpn. J. Appl. Phys., 51, 090106 (2012).

【成果報告】 [1] 山下峻吾, 森下弘樹, Ernst David Herbschleb, 徳田規夫, 水落憲和、第 80 回 応用物理学会 秋季学術講演会、2020 年 3 月 14 日 (応用物理学会 講演奨励賞受賞)

[2] 山下峻吾, 森下弘樹, Ernst David Herbschleb, 徳田規夫, 水落憲和、第 67 回 応用物理学会 春季学術講演会、2020 年 3 月 14 日

ダイヤモンド中の NV 中心量子ビットの電氣的制御と電氣的検出

牧野俊晴 産業技術総合研究所

【緒言】優れた特性を持つダイヤモンド中の NV 中心は、量子情報や磁気センサなどへの応用が期待されている。NV 中心において電氣的なスピン検出法は、集積化等に向け、デバイス応用に重要な技術である。近年、NV 中心において電氣的なスピン検出が、電氣的磁気共鳴法（EDMR）によりなされている。本研究は、電極構造の工夫による高感度化や、核スピンの検出に向けて電氣的な電子・核二重共鳴検出に注目し研究を行った。また、電子デバイスとして必要とされる半導体特性を持つリンドープ n 型ダイヤモンドのスピンコヒーレンスの評価を行った。

【実験と結果】電氣的な電子・核二重共鳴検出では、 ^{14}N 核スピンエコーを図(上)に示した Davies ENDOR パルスシーケンスを応用して測定した。その結果、図(下)に示したように、室温下において核スピンコヒーレンスの電氣的検出に初めて成功した[1]。

また、リンドープ n 型ダイヤモンドを用い、NV 中心の室温での世界最長電子スピンコヒーレンス時間と、単一 NV 中心を用いた量子センサでの世界最高磁場感度実現に成功した[2]。この電子スピンコヒーレンス時間は、他の固体系電子スピンの中でも室温では一番長いものである。n 型ダイヤにより最長の電子スピンコヒーレンスを実現した点は意義深く、さらなる高感度化に加え、n 型半導体特性を活かした量子デバイスへの幅広い応用へ道を拓くものと期待される。

更に、マイクロ波が NV 中心の電子スピンに纏わりついたドレスト状態を生成することに成功し、電子スピンコヒーレンス時間の桁違いの長時間化に成功した。量子メモリへの応用や量子センサ感度向上に資する成果と期待される[3]。

【成果報告】

- [1] H. Morishita, S. Kobayashi, M. Fujiwara, H. Kato, T. Makino, S. Yamasaki, N. Mizuochi, *Scientific Reports*, 10, 792 (2020).
- [2] E. D. Herbschleb, H. Kato, Y. Maruyama, T. Danjo, T. Makino, S. Yamasaki, I. Ohki, K. Hayashi, H. Morishita, M. Fujiwara, N. Mizuochi, *Nature Communications*, 10, 3766 (2019).
- [3] H. Morishita, T. Tashima, D. Mima, H. Kato, T. Makino, S. Yamasaki, M. Fujiwara, N. Mizuochi, *Scientific Reports*, 9, 13318 (2019).

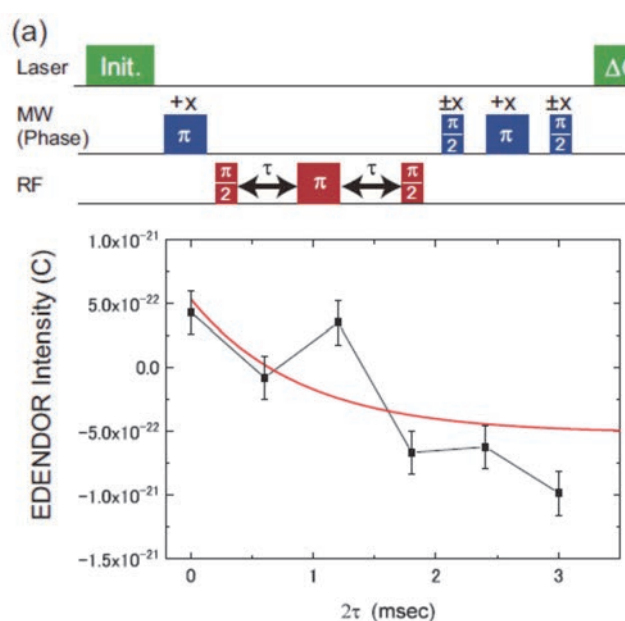


図 電氣的磁気共鳴法での核スピンエコーパルスシーケンス(上)と核スピンのエコー強度減衰(下)。

シクロパラフェニレンの励起ダイナミクスの環サイズ依存性

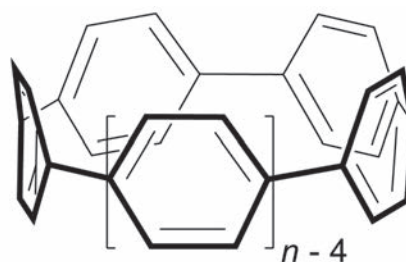
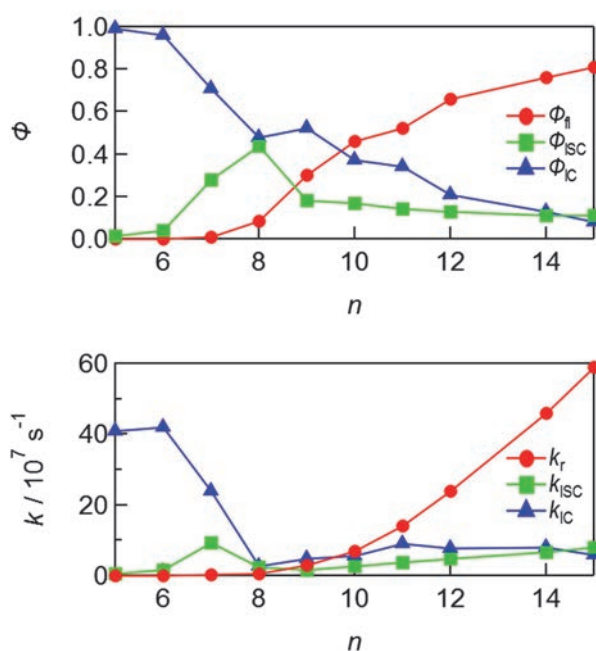
藤塚守 大阪大学

[n]シクロパラフェニレン([n]CPP, Fig. 1)はベンゼン環オリゴマーであるパラフェニレンが環状に結合した分子であり、アームチェア型カーボンナノチューブの最小単位であるとともに、高い歪みと環状に整列した p 軌道に由来する興味深い物性により関心を集めている。本申請者は、京都大学化学研究所の山子教授のグループと[n]CPP に関する共同研究を展開しており、時間分解分光を主に用いることにより、CPP 類の励起状態およびラジカルイオン状態に関する新たな知見を世界に先駆けて報告してきた。これまでの山子グループの研究により、5 から 24 個のベンゼン環から形成される CPP 類の合成が可能になっているが、励起状態物性が明らかになっているのはその一部であり¹⁾、[13]CPP より大きい CPP の励起緩和過程は解明されていない。本研究は、[14]-および[15]CPP の励起緩和過程を[n]CPP ($n = 5 - 13$)と比較することで、[n]CPP の励起緩和過程を支配する因子を解明することを目的とした。

[14]-および[15]CPP の蛍光量子収率は 0.76 および 0.81 と求められ、[13]CPP よりさらに増加した。また、蛍光寿命は 1.6 および 1.4 ns であったことより、環サイズの増加とともに蛍光放射速度定数が増加する傾向にあることが明らかになった。一方、[14]-および[15]CPP の三重項エネルギーは 2.15 および 2.16 eV であり、また、三重項生成収率は 0.14 および 0.13 であったことより、環サイズが大きくなると、三重項状態物性は大きく変化しないことが確認された。これらの測定より得られた、各緩和過程の量子収率および速度の環サイズ依存性を Fig. 2 に示す。環サイズが大きい場合には蛍光放射過程が主たる緩和過程であり、その速度は環サイズとともに増加することが確認された。

文献

1) Fujitsuka, M.; Lu, C.; Zhuang, B.; Kayahara, E.; Yamago, S.; Majima, T. *J. Phys. Chem. A* **2019**, *123*, 4737–4742.

Fig. 1. [n]CPP ($n = 5 - 15$)の分子構造Fig. 2. [n]CPP の蛍光、項間交差、内部転換の量子収率 (Φ)および速度(k)。

半屈曲性高分子溶液の非線形レオロジー

井上正志 大阪大学

近年、持続可能な社会の実現のために、天然高分子が材料として多く用いられるようになった。天然高分子の一つとして、セルロースナノファイバー(CNF)が注目されている。CNF は、棒状の硬い高分子であると考えられてきたが、最近、半屈曲性高分子としての挙動が観測されることが明らかになった¹⁾。半屈曲性高分子では、粘弾性緩和に、配向モード、曲げモード、伸長モードが観測される²⁾。CNF を材料として活用し、成形加工や実用物性を向上させるためには、半屈曲性高分子の非線形粘弾性を理解することが重要であるが、これまでの研究ではそうした認識もなく、またモード分割も行われておらず、十分解明されていない。本研究では、セルローストリフェニルカルバメート(CTC)を、半屈曲性高分子のモデル高分子として利用し、その非線形粘弾性について調べた。CTC は、不揮発性溶媒であるリン酸トリクレジル(TCP)に溶解し、粘弾性測定に適している²⁾。

CTC は大阪大学大学院理学研究科の佐藤研究室から提供を受けた。使用前に CTC を一晩室温で真空乾燥を行った。溶媒の TCP とともに共溶媒としてジクロロメタンを加え、室温で真空乾燥を行うことにより、ジクロロメタンを取り除き、測定試料とした。重量モル質量 M_w および M_n は、GPC 測定により求めた。経路長 L はモル質量を繰り返し単位当たりのモル質量 519 g mol^{-1} で割り、求めた重合度に投影長 0.51 nm を掛けて求めた。持続長 L_p は 5.75 nm とした。測定には、粘弾性測定装置を用いた。

粘弾性測定結果の一例として、種々のずり速度 $\dot{\gamma}$ における粘度成長関数 $\eta^+(t, \dot{\gamma})$ を、Fig. 1 に示す。図中、黒の波線は動的粘弾性測定から求めた線形域の粘度成長関数 $\eta^+(t, 0)$ を表す。 $\dot{\gamma}/\text{s}^{-1} < 0.1 \approx 1/\tau_w$ では、 $\eta^+(t, \dot{\gamma})$ は $\eta^+(t, 0)$ と一致し、線形挙動が観測された。一方、 $\dot{\gamma}/\text{s}^{-1} \geq 0.1$ では、定常値 $\eta^+(\infty, \dot{\gamma})$ が $\dot{\gamma}$ の増加とともに減少し、Shear Thinning の挙動を示すことがわかった。また、このずり速度域では、オーバーシュートが観測された。さらに、 $\dot{\gamma}/\text{s}^{-1} \geq 3$ では、短時間領域で $\eta^+(t, \dot{\gamma})$ が $\eta^+(t, 0)$ より大きくなる strain hardening が観測された。動的粘弾性と複屈折の測定結果を利用して、粘度成長関数を、配向緩和モード、曲げモード、伸長モードに分離し、それぞれの非線形度を求めた。その結果、何のモードも同程度の非線形性を示した。以上の結果は、曲げモード、伸長モードの非線形性が、セグメントの配向度に支配されていることを示唆する。

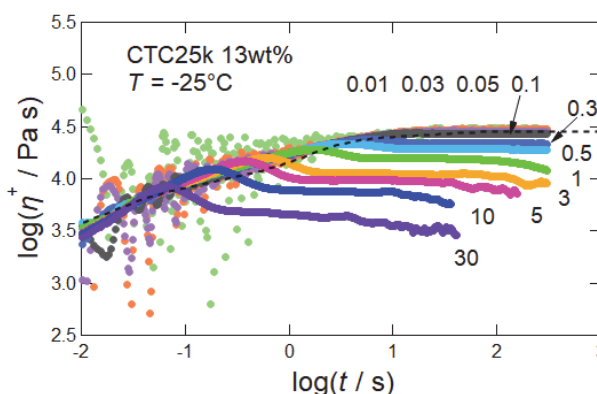


Fig. 1. CTC/TCP 溶液の緻密からみ合い領域における粘度成長関数.

1) Tanaka R, Kashiwagi Y, Okada Y, Inoue T *Biomacromolecules* **21**, 408 (2020)

2) Okada Y, Goto Y, Tanaka R, Katashima T, Jiang XY, Terao K, Sato T, Inoue T *Macromolecules* **51**, 9626 (2018)

Analysis of Soret effect for DNA in molecular-scale temperature gradient

Ryoko Shimada Japan Women's University

【Introduction】 In multi-component solutions subjected to a temperature gradient, different components tend to separate from each other along the gradient, which is known as the Soret effect. This study¹ focused on the Soret effect of DNA molecules in aqueous polyethylene glycol (PEG) solutions. Plasmonic heating from an array of metal domains was used to create a periodic temperature gradient with the periodicity comparable to the DNA molecule size to examine an *intra-molecular* Soret effect of DNA.

【Experiment】 The periodic array of silver (Ag) domains was fabricated by the nanosphere lithography. Polystyrene particles of a diameter 50 μm were used as a lithography mask to prepare a triangular lattice of Ag domains. Plasmonic heating from those Ag domains under emission of blue light (400 – 440 nm) created a spatially oscillating temperature (T) gradient with a large amplitude of $\sim 0.5 \text{ K}/\mu\text{m}$. Aqueous PEG solutions containing DNA molecules ($\sim 166 \text{ Kbp}$) were subjected to this T -gradient, and the conformation and displacement of DNA labeled with a fluorescent dye (SYBR Gold) were observed with a microscope.

【Results and Discussion】 Figure 1 shows time (t) evolution of optical microscope images of a dye-labeled DNA molecule (yellow object) in the PEG solution under the T -gradient. The plasmonic heating at the edges of Ag domains (marked with white circles) attracts DNA to the high- T edge, which confirms a positive Soret coefficient of DNA in the PEG

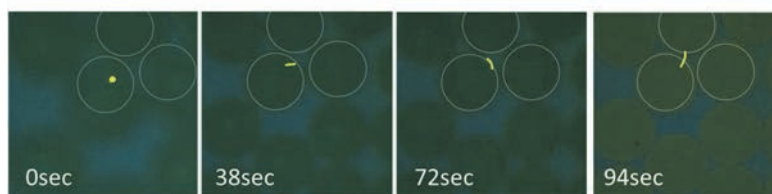


Fig.1 Motion of DNA molecule (yellow object) under T -gradient.

solution. The DNA molecule occasionally stretches along the high- T edge of a domain ($t = 72 \text{ sec}$) or between edges of two domains ($t = 94 \text{ sec}$), which suggests an *intra-molecular* Soret effect emerging in the T -gradient with the periodicity comparable to the stretched DNA size. Correspondingly, the DNA molecule appeared to be occasionally trapped near the high- T edge of the Ag domain(s) and exhibit no Fickian behavior. Brownian simulation of a Soret-active Hookean dumbbell mimics this non-Fickian behavior, as shown in Fig. 2.

1. R. Shimada and H. Watanabe, “Dynamics of DNA in periodic temperature gradient field created by plasmonic heating”, APS March Meeting (Denver, USA, 2020).

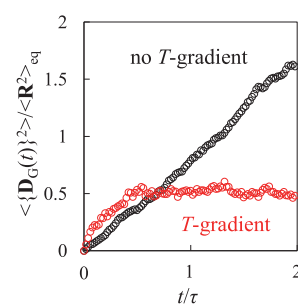


Fig. 2 Center of mass displacement \mathbf{D}_G of Soret-active dumbbell obtained from 2D-Brownian simulation. $\langle \mathbf{D}_G^2 \rangle$ is normalized by the equilibrium size of the dumbbell $\langle \mathbf{R}^2 \rangle_{\text{eq}}$ and plotted against time normalized by the relaxation time τ .

Fabrication of nanotopographical polymer surfaces for bactericidal properties

Maya Endoh Stony Brook University

Introduction. Fouling is the undesirable accumulation of a material on a wide variety of objects such as medical devices, ship hulls, membranes and has now become a global problem from land to ocean with both economic and environmental penalties. In this research, we aim to develop a new paradigm of designing a nanopatterned polymer surface to control a bacteria-polymer surface interaction. Our structural design is inspired by nature: highly dense nanopillars (with the heights and inter-spacing of about 100 nm) formed at the surface of cicada or dragonfly wings kill bacteria such as *Pseudomonas aeruginosa* [1]. In collaboration with Prof. Takenaka at ICR, we fabricated polymeric nanopillars on a solid using polystyrene-block-poly(methyl methacrylate) (PS-*b*-PMMA) diblock copolymers as a rational model and studied the bactericidal property against a model bacterium, *Escherichia coli* (E coli).

Experimental. A cylinder-forming PS-*b*-PMMA diblock copolymer was purchased from Polymer Source ($M_{w,PS} = 46\text{kDa}$, $M_{w,PMMA} = 138\text{kDa}$, $M_w/M_n = 1.16$, the volume fraction of PS is about 0.2). To achieve perpendicular oriented cylinder microdomains within entire thin films, we used our newly developed “neutral” substrate coatings for PS-*b*-PMMA that are composed of PS ($M_w = 17\text{kDa}$, $M_w/M_n = 1.06$, Pressure Chemical Co.) homopolymer chains adsorbed on a Si substrate (we hereafter assign as a “PS nanocoating”) [2]. The thickness of the PS nanocoating was about 2 nm and the coating completely covered the bare Si substrate. Spin-cast PS-*b*-PMMA thin films of 25 nm thick were then prepared on the PS nanocoating. Figure 1 shows a representative top view SEM image of the 25 nm-thick PS-*b*-PMMA thin film on the PS nanocoating after thermal annealing at 250 °C for 5 min and subsequent rapid quench to room temperature (within ~ 10 s). The rapid quench was to preserve the in-situ structure via the vitrification processes of the glassy blocks. The bright regions correspond to the PS component, while the PMMA domain was selectively removed by UV crosslinking of the PS domain and subsequent removal of the PMMA domain with acetic acid. Further experiments. Further image analysis along with grazing-incidence small-angle X-ray scattering experiment at NSLS-II (Brookhaven National Laboratory) revealed perpendicularly oriented cylindrical microdomains from the PS nanocoating surface.

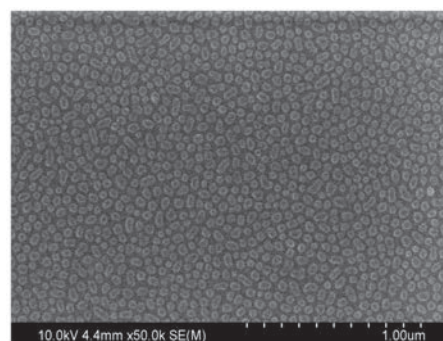


Figure 1, Top view SEM micrograph of the PS-*b*-PMMA thin film (25 nm in thickness) self-assembled on the PS17k nanocoating. The PMMA domain was selectively removed by UV crosslinking of PS domain (the bright regions), revealing perpendicularly oriented cylindrical microdomains.

Bactericidal properties of the nanopillars. The preparation of bacterial solutions and adsorption experiments on the PS nanopillars were as follows: *E. coli* cultures were thawed at room temperature and swabbed on nutrient agar medium in a petri dish. The petri dish was incubated at 37°C overnight and then multiple swabs of the resulting *E. coli* colonies were transferred into 25 mL of Lysogeny Broth (LB) medium in a centrifuge tube. 100 µl of the bacterial solution was pipetted out from the tube onto a clean petri dish. The PS nanopillars were placed on the bacterial droplet with the PS nanopillar side in contact with the solution and the uncoated side facing the air surface. The petri dish was thereafter covered and incubated at 37°C for 60 minutes. Post incubation, the incubated PS nanopillars were rinsed gently in distilled water twice and dried under air-flow with a very low pressure. Viability of *E. coli* on the samples was assessed using the BacLight Live/Dead staining kit (Molecular Probes, Life Technologies, Carlsbad, CA). The samples were incubated for 15 min in the staining solution and rinsed with phosphate buffered saline (PBS). The samples were then examined with an EVOS Microscope (ThermoFisher Scientific) using a standard green filter set to image live cells and a standard red filter to image dead cells. Both live and dead cells were counted with ImageJ software. The results are indicative that the PS nanopillars killed *E. coli* adsorbed after 12 h of immersion in a bacteria suspension, while *E. coli* adsorbed significant on a 25 nm-thick PS thin film (i.e., a “flat” surface) and were alive after the same immersion time. Figure 2 shows a representative SEM image of *E. coli* on the PS nanopillars. It is clear that the bacteria appears deflated on the PS nanopillars, while the bacteria were rod-shaped on the PS flat surface. As the bacterial cell adsorbs onto the nanopillars, the wetted surface area increases, and it is hypothesized that this stretches the cell wall until it is breached, leading directly to lysis. Further experiments using different PS nanopillar spacings and heights are currently in progress to understand the molecular mechanics behind the bactericidal property.

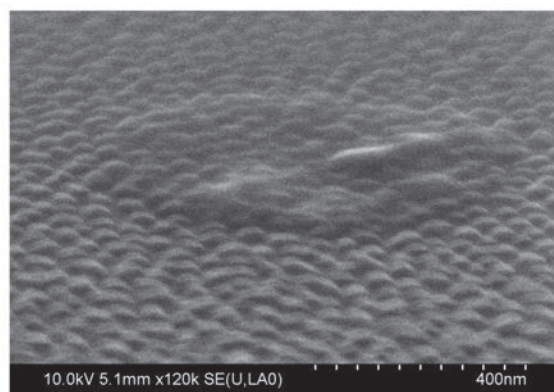


Figure 2. SEM micrograph of *E. coli* on the PS nanopillars.

References

- [1] Ivanova E. P. et al. *Small*, 8, 2489, 2012.
- [2] Morimitsu Y. et al. *Macromolecules*, 52, 5157, 2019.
- [3] Sivaniah, E. et al., *Macromolecules*, 36, 5894-5896, 2003.

Synthesis of structurally controlled polymers having green fluorescence protein chromophore and their photophysical properties in solution

Jye-Shane Yang National Taiwan University

Objectives

This collaborative and multidisciplinary research project was carried out together with Prof. Shigeru Yamago, who is an expert in polymer controlled synthesis at ICR, Kyoto University. Through this project, a master-degree student of NTU-chem, Mr. Hsuan Yu Lin, was able to work at ICR. The goal of this project is to prepare a chromophore-polymer conjugate with the green fluorescence protein chromophore (GFpC) analog *m*-DMABDI and the PNIPAM polymer. The target system is expected to perform temperature-responsive fluorescence turn on properties, as the PNIPAM structure is temperature dependent and the fluorescence property of *m*-DMABDI is highly dependent of the environmental polarity and proticity, as depicted in Figure 1.

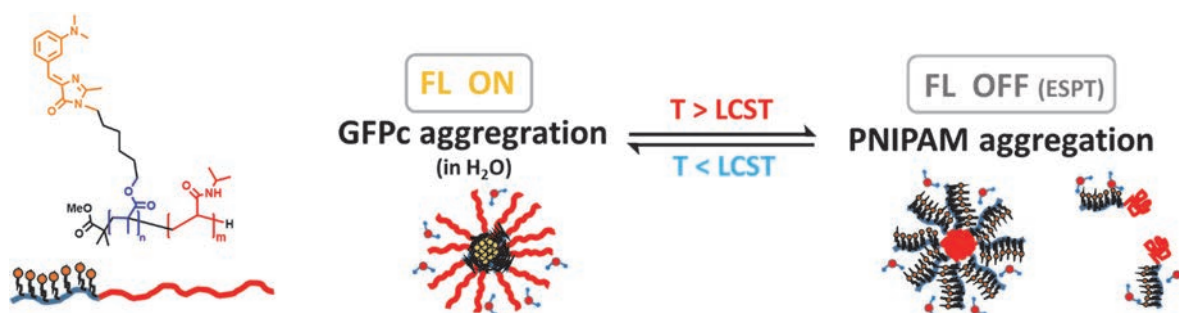
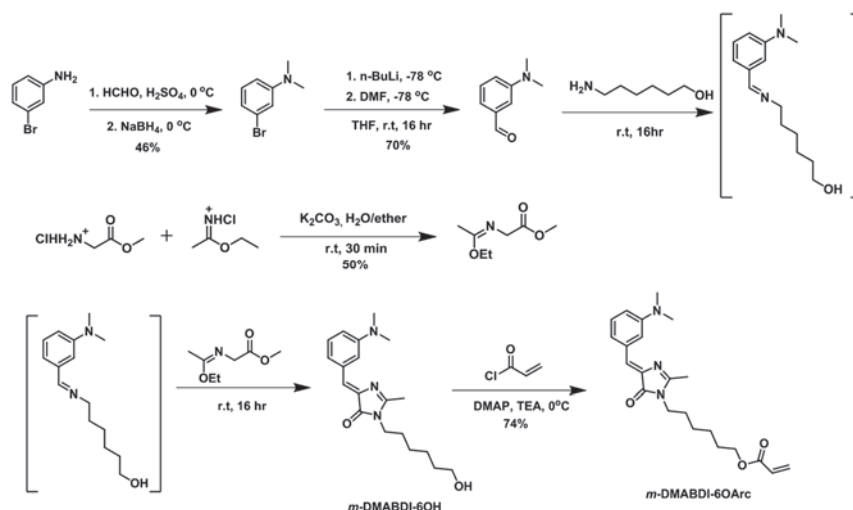


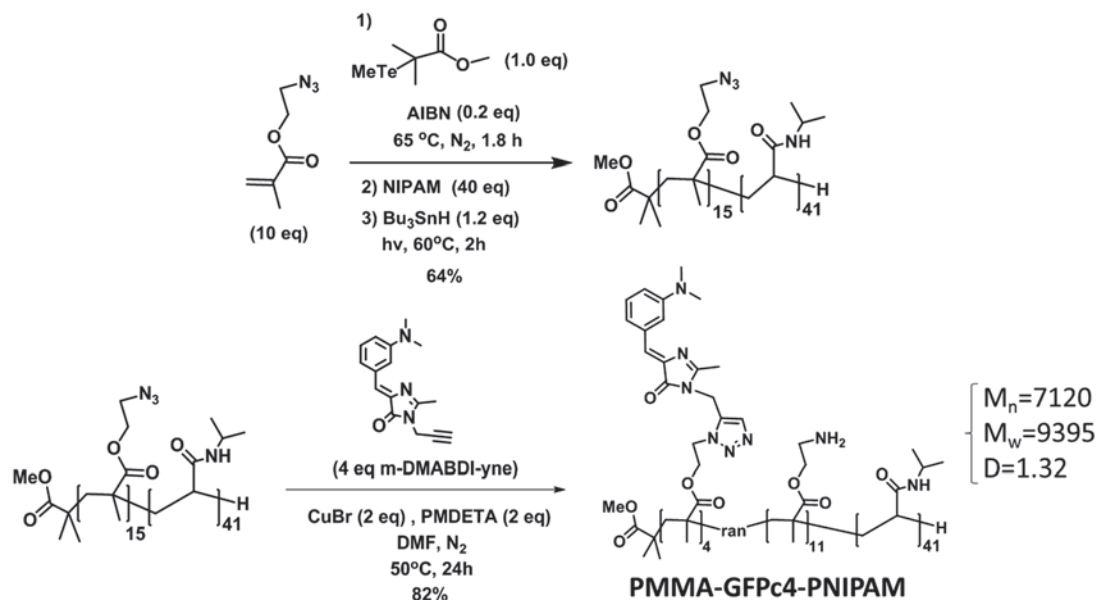
Figure 1. The structure of *m*-DMABDI-polymer conjugate and the temperature-dependent fluorescence on-off switching.

Experimental methods and results.

The key experimental work of this project is the molecular synthesis. Scheme 1 illustrates the synthetic routes for the *m*-DMABDI-monomer for subsequent polymerization.



Scheme 1. Synthesis of *m*-DMABDI-monomer



Unfortunately, the subsequent attempts for the polymerization by the TERP method and by the free-radical method have failed.

We then employed the click reactions to incorporate the GFPc via post-functionalization of the block copolymer as illustrated in Scheme 2.

Scheme 2. An alternative synthesis of *m*-DMABDI-polymer conjugate

The comparison of fluorescence images of PMMA-GFPc4-PNIPAM and *m*-DMABDI-yne at room temperature and at 75 °C is shown in Figure 2.

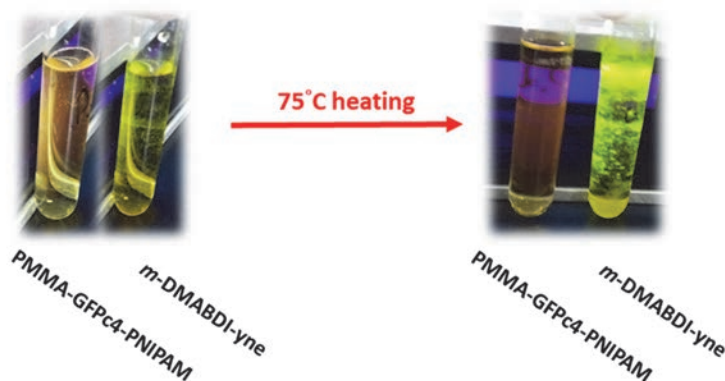


Figure 2. The on-off fluorescence switching of PMMA-GFPc4-PNIPAM and *m*-DMABDI-yne.

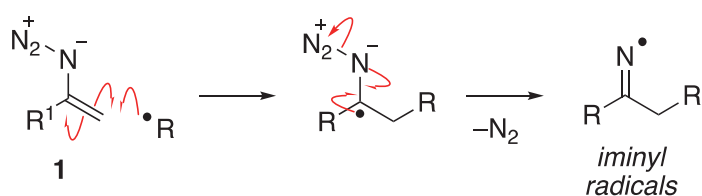
Discussion

Although the results need further optimization before a final publication could be generated, this project has initiated a research linkage between ICR, Kyoto University and NTU-Chemistry over the agreement between the two organizations. With such a seeding project, the collaboration between the two research groups will continue. We acknowledge the financial support of this project.

Vinyl azides as new monomers of radical polymerization for the fabrication of green polymers having chemically- and biodegradable properties

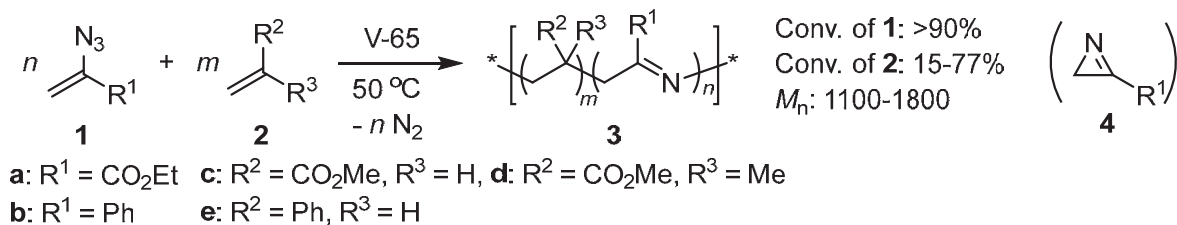
Shunsuke Chiba Nanyang Technological University

Radical polymerization is the most important polymerization method industrially for fabricating polymer materials. However, as the polymer backbone is constructed by stable carbon-carbon single bond, low degradability of the resulting polymer products has become significant issues in SDGs. Therefore, the development of degradable polymers by radical polymerization has been a significant challenge in synthetic polymer chemistry. We have been developing new radical chemistry using vinyl azides **1** as a radical acceptor (Scheme 1).¹⁻⁶ The key reactivity of vinyl azides **1** is the generation of an iminyl radical by the addition of carbon-centered radicals to the alkenyl moiety of vinyl azides **1** with the loss of dinitrogen gas.



Scheme 1. Reactivity of vinyl azides with radicals

We thus envisaged that, if vinyl azides **1** react with a polymer-end radical and the resulting iminyl radical further adds to other conventional vinyl monomers **2**, polymers **3** having an imine moiety, which is a highly reactive functional group to hydrolysis, would be synthesized (Scheme 2).



Scheme 2. Radical copolymerization of vinyl azide **1** and conventional monomer **2**

Copolymerization of vinyl azides **1** and conventional monomers **2** ($1/2 = 1/5$) was carried out in the presence of V-65 as a radical initiator at 50 °C. Nearly quantitative conversion of vinyl azides **1** was observed after prolonged heating for both **1a** ($R^1 = \text{CO}_2\text{Et}$) and **1b** ($R^2 = \text{Ph}$), and moderate to high conversion was observed for **2** (**2d**: 75-77%, **2e**: 15-22%, **2f**: 35-50%). Despite the conversion of **2**, the oligomers having the number average molecular weight (M_n) of 1000~1800 were observed in all case besides **1a/2c** combination. In addition, while vinyl azides **1** are known to decompose slowly to 2*H*-aziridines **4** under solvothermal treatments,⁷⁻¹⁰ no formation of **4** was observed under the current conditions. The structures of **3** were analyzed by mass spectra, which revealed the formation of copolymers having expected main-chain structures. The mass analysis also revealed the formation of dimeric oligomer **3**, which should be formed by the radical coupling of the generated iminyl radicals, suggesting that the cross propagation of the iminyl radical to monomer **2** is the rate determining step. This also means high molecular weight polymer **3** would be obtained by increasing the cross propagation reaction, and we are now working on this direction.

References

1. Hayashi, H.; Kaga, A.; Chiba, S. *J. Org. Chem.* **2017**, *82*, 11981.
2. Chiba, S. *Chimia* **2012**, *66*, 377.
3. Wang, Y.-F.; Toh, K. K.; Ng, E. P. J.; Chiba, S. *J. Am. Chem. Soc.* **2011**, *133*, 6411.
4. Wang, Y.-F.; Chiba, S. *J. Am. Chem. Soc.* **2009**, *131*, 12570.
5. Wang, Y.-F.; Lonca, G. H.; Chiba, S. *Angew. Chem. Int. Ed.* **2014**, *53*, 1067.
6. Wang, Y.-F.; Lonca, G. H.; Le Runigo, M.; Chiba, S. *Org. Lett.* **2014**, *16*, 4272.
7. Timén, Å. S.; Risberg, E.; Somfai, P. *Tetrahedron Lett.* **2003**, *44*, 5339.
8. Söderberg, B. C. G. *Curr. Org. Chem.* **2000**, *4*, 727.
9. Knittel, D. *Synthesis* **1985**, 186.
10. L'abbé, G. *Angew. Chem. Int. Ed.* **1975**, *14*, 775.

The 15th International workshop for East Asian Young Rheologists

Tadashi Inoue Osaka University

【Purpose of project】 The ICR budget was used to organize the 15 International Workshop on Young Rheologist in East Asia (IWEAYR-15). The purpose of this workshop is to promote international exchange among young faculty and graduate students in cooperation with researchers from various countries in East Asia, in several research fields such as polymer science and materials science. IWEAYR is an opportunity for participants to present their research results, discuss and exchange research ideas in a very friendly atmosphere. The workshop will deepen our research activity and form the basis for future cooperation. This year, IWEAYR-15 was held in Changchun, China. The participation of many undergraduate and graduate students fulfilled the mission of contributing to the strengthening of future cooperation. The budget was effectively utilized to support the participation of as many Japanese researchers as possible.

【Place and schedule of workshop】 IWEAYR - 15 was held from January 8 - January 1, 2020 at The CGIC Nanshan Hot Spring Hotel, Changchun, chaired by Prof. Quan Chen of Changchun Institute of Applied Chemistry, CAS.

【Purpose of the workshop】 From the beginning, the purpose of this workshop is to promote international exchange and collaboration among young faculties and graduate students who will be the main researchers in the field of rheology and material science in the near future, and therefore, to provide a place for research presentation and discussion, and to revitalize related fields. At the same time, in order to further develop joint research activities among several research groups, it is to provide a place for people exchange.

【Background of workshop】 This workshop has been held annually since the first IWEAYR in Seoul (February 2006). After that, it has been organized in Kyoto (January 2007), Shanghai (January 2008), Nakhon Ratchasima (January 2009), Busan (January 2010), Yamagata (January 2011), Beijing (February 2012), Phuket (January-February 2013), Seoul (February 2014), Fukuoka (February 2015), Shenzhen (January 2016), Pattaya (February 2017), Jeju Island (January 2018), Nagoya (January 2019) (in a circulating order of Korea, Japan, China, and Thailand). There have been some changes in the organization of the workshop due to various circumstances in the hosting countries, every IWEAYR has served as a place for faculties and graduate students to engage in international exchange and collaboration.

【Participants】 Firstly I should note that professor Chen, the organizer, was an alumni of IWEAYR. He understands the purpose of IWEAYR very well, and therefore the conference was conducted with meticulous attention to detail. The number of participants in this IWEAYR-15 was 31 professor and 91 students, which was the average level in recent years. Breakdown by country was Japan 45 (13+32), Korea 46(9+37), China 16(7+22), and Thailand (2+0). The main participants were:

Seung Jong Lee, Professor,	Seoul National University,	Korea,
Kyung Hyun Ahn, Professor,	Seoul National University,	Korea,
Youngdon Kwon, Professor,	Sungkyunkwan University,	Korea,
Wei Yu, Professor,	Shanghai Jiaotong University,	China,

Kang Sun, Professor	Shanghai Jiaotong University,	China
Chen-Yang Liu, Professor,	Chinese Academy of Science	China
Exkarach Deenang, Asso. Prof.	Udon Thani Rajabhat University	Thailand
Hiroshi Watanabe, Professor,	Kyoto University	Japan
Yuichi Masubuchi, Professor,	Nagoya University	Japan
Takashi Taniguchi, Asso. Prof.,	Kyoto University	Japan
Hiroshi Suzuki Professor,	Kobe University	Japan
Ruri Hidema, Associate Prof.,	Kobe University	Japan
Shigeru Okamoto, Asso. Prof.	Nagoya Institute of Technology	Japan



Prof. Chen, Organizer



Photo of Group E

【Overview of IWEAYR-15】 Total number of submitted papers was 91. On the first day, poster preview presentations were given by students (91) and poster presentations were held. On the second day, short long presentations (14) were given by doctoral students. Then, a group excursion was organized. The best presentation award was chosen by the participant's vote.

In the conference, there were many researches on new polymer materials such as nano composite materials and self-repairing materials as in the last year. In addition there were many basic researches on the analysis of various physical and rheological properties and hierarchical structure of reinforcing materials such as particle dispersion systems. Some issues such as theory, simulation, and flow control of soft matter were presented.

I have been participating in IWEAYRs in China three time. The present venue, the CGIC Nanshan Hot Spring Hotel was quite a nice hotel with hot swimming pool and it was the highest-grade hotel in the IWEAYR history. The workshop was supported by some Chinese companies and I felt the great development of the Chinese economy. Though Changchun is a very cold place, the interior of the hotel was extremely comfortable. At the time of departure from Japan, the first report of coronavirus, CO VID-19, had just arrived, and it was very lucky to participate in IWEAYR15 without any problem. It would have been necessary to postpone participation if the meeting had been held a week later.

【Summary】 My students all enjoyed the meeting and I believe that this experience will help maintain a network of young rheologists in East Asia. In conclusion, IWEAYR-15 successfully achieved its purpose. Finally, I should note that the next IWEAYR-16 will be held in Udon Thani, Thailand, in the winter time.

第8回日本-中国有機化学シンポジウム

濱島義隆 静岡県立大学

第8回日本-中国有機化学シンポジウム (The 8th Japanese-Sino Symposium on Organic Chemistry for Young Scientists) が2019年9月17日から20日の4日間にわたり開催された。本連携・融合促進型研究では、共同研究者の川端猛夫教授が組織委員長を務め、研究代表者は組織委員を務めた。なお、2023年に開催予定の第10回日本-中国有機化学シンポジウムでは研究代表者が組織委員長を務める予定である。本シンポジウムの詳細は以下のとおりである。

(1) 会議名称、期間、場所

会議名称：第8回日本-中国有機化学シンポジウム

The 8th Japanese-Sino Symposium on Organic Chemistry for Young Scientists

期間：2019年9月17日-20日

場所：京都ガーデンパレス、京都

(2) 会議の趣旨

近年のアジアにおける有機化学研究の隆盛は世界が認めるところである。我が国の化学・製薬産業界とアジア諸国とのつながりも年々強くなりつつある。このような状況をふまえ、本シンポジウムは元名古屋大学大学院農学研究科の磯部稔教授と上海有機化学研究所の林国強教授が日中間の有機化学の分野での協力が極めて重要であるとの認識に立って創始されたものである。本シンポジウムの講演は全て招待講演によって成り立っている。従って参加者はさほど多くはないものの、選りすぐられた気鋭の研究者達であるだけに、発表のレベルは高く、討論も非常に活発に行われる。過去7回のシンポジウムはこの主旨どおりに開催され、大きな成功を収めた。このシンポジウムによって参加者が大いに刺激を受けるとともに、これを契機に両国の研究者間の交流が一層活発となり、連携、共同研究も行われるようになった。

近年、中国の産業、経済の発展はめざましく、その基盤研究となる学術研究も質・量ともに飛躍的発展を遂げつつある。したがって、我が国の研究者が近隣の中国の研究者と切磋琢磨しながら共に卓越した研究を目指すことは、我が国の発展にとっても重要で、本シンポジウムを開催する意義は大きい。また、本シンポジウムでは参加者全員(参加費無料の学生をい除く)が同一の宿舎に宿泊し、密度の濃い議論と交流を深める点も特長である。なお、学生の積極的な参加を促すため、学生の参加は無料に設定し、さらに学生の優秀な発表者に対し、発表賞として、BCSJ Award for Poster Presentation を2名に、また Chemistry Letters Young Award を2名にそれぞれ授与した。

(3) 連携先研究機関

上海有機化学研究所、中国科学技術大学、静岡県立大学

(4) 講演者

中国側講演者

Qi-Lin Zhou (plenary lecture), Nankai University; Gong Chen, Nankai University; Xiao-Guang Lei, Peking University; San-Zhong Luo, Tsinghua University; Song Ye, Beijing National Laboratory for Molecular Science; Qian Zhang, Northeast Normal University; Xin-Jun Luan, Northwest University; Yang Li, Xi'an Jiaotong University; Xiang-Feng Shao, Lanzhou University; Ying-Chun Chen, Sichuan University; Zhuang-Zhi Shi, Nanjing University; Ran Hong, Shanghai Institute of Organic Chemistry; Jun-Li Hou, Fudan University; Xin-Yuan Liu, Southern University of Science and Technology; Liu-Zhu Gong, University of Science and Technology of China.

日本側講演者

丸岡啓二 (plenary lecture), 京都大学理学研究科; 西田篤司, 千葉大学薬学研究院; 磯部稔, 名古屋大学名誉教授; 赤井周司, 大阪大学薬学研究科; 濱島義隆, 静岡県立大学薬学研究科; 寺田眞浩, 東北大学理学研究科; 古田巧, 京都薬科大学; 上田善弘, 京都大学化学研究所; 大井貴史, 名古屋大学工学研究科; 有澤美枝子, 東北大学薬学研究科; 岩渕好治, 東北大学薬学研究科; 谷野圭持, 北海道大学理学研究院; 竹本佳司, 京都大学薬学研究科; 大野浩章, 京都大学薬学研究科; 笹井宏明, 大阪大

学産業科学研究所; 中村修一, 名古屋工業大学生命物質工学科; 佐々木茂貴, 九州大学薬学研究院;
高石和人、岡山大学工学部。

(5) 参加者77名

参加者名簿を添付書類として添付

(6) 要旨集、趣意書

添付書類として添付

(7) 会議の様子



ポスター賞受賞者



京都ガーデンパレスの講演会場



エキスカッション(金閣寺)

第 26 回酸化物エレクトロニクスに関する国際会議

松野丈夫 大阪大学

遷移金属酸化物は、通常の半導体には見られない多彩な機能特性を示すことから、次世代のエレクトロニクス材料として期待されている。近年、原子レベルでの酸化物作製技術が急速に発展したことで、急峻な界面を有する薄膜やヘテロ構造の作製が可能になり、新しい物性・機能が見出されている。このような酸化物薄膜やヘテロ構造が示す機能特性の探求・解明は、酸化物機能素子の開発に向けた研究開発「酸化物エレクトロニクス」の根幹となる重要な研究課題であり、酸化物エレクトロニクスの更なる発展には、材料設計や作製から機能特性探求やデバイス構築などに関わる広範な研究展開そして最新研究成果の共有が必須となっている。そこで本課題では、「26th International workshop on oxide electronics(第 26 回酸化物エレクトロニクスに関する国際会議)」を開催し、国内外の多彩な研究背景をもつ研究者が互いの最先端の研究成果を共有そして融合することで、今後の酸化物エレクトロニクスを下支えするパラダイムを構築し、更なる発展を目指した。

International Workshop on Oxide Electronics (iWOE: 酸化物エレクトロニクス国際ワークショップ) は、1995 年に始まり、今回で 26 回目の開催を迎える伝統ある国際会議である。銅酸化物高温超伝導の発見を契機として、酸化物の多様な物性と機能を俯瞰的に議論してその学術と技術の可能性を広げるフォーラムを提供してきた。当該研究分野における重要な最新研究成果が発表されることから、その誘致も競争率が高く熾烈であるが、2019 年度のアジア開催にあたり、日本の酸化物エレクトロニクス研究を先導する研究者が中心となり京都での開催が実現した。

会議は、2019 年 9 月 29 日～10 月 2 日までの 4 日間、京都大学・化学研究所のおうばくプラザ（きはだホールでの講演と併設セミナー室でのポスター発表）で行った。参加者は 18 か国から 170 名以上あり、12 件の招待講演、24 件の口頭発表に加えて、2 日間で 116 件のポスター発表が行われた。発表は「酸化物エレクトロニクス」の材料設計、作製から機能特性評価やデバイス構築などに関わる広範な分野をカバーし、最新情報の交換のみならず、本ワークショップの特色である並行セッションを排した同一会場での進行により、活発で深い議論を展開することができた。

プログラムの構成とトピックスは以下のとおりである。

- 9 月 29 日 : ウェルカム
- 9 月 30 日 : Transparent Conducting Oxides and Interfaces
Mechanical Control of Oxides
Nano-scale Ferroelectricity/Flexoelectricity
- 10 月 1 日 : Nano-scale Characterizations and Devices I
Interfaces and Electric Field Induced Effects
Nano-scale Characterizations and Devices II
バンケット

10 月 1 日 : Heterostructures and Superlattices
Spin-Orbit Interaction and Topological Properties

日本からの招待講演者として、材料研究を牽引している細野秀雄教授（東工大）と最先端テラヘルツ分光評価の田中耕一郎教授（京都大）に加え、独マックスプランク固体研究所のディレクターである高木英典教授（兼、東大）の 3 名を迎え、酸化物エレクトロニクス分野におけるフロントランナーとしての日本の現状を国際的な視点からアピールすることもできた。また、多くの若手研究者の参加があり、一般口頭講演では積極的に若手を登用して活発な議論を展開すると共に若手研究者の積極的な成果アピールの場とすることができた。発表の中で特に大きな注目を集めたのは、ごく最近に *Nature* 誌に掲載され、トピックスにも取り上げられた Ni 酸化物での超伝導の発見（米国、スタンフォード大学）の報告である。最新の研究成果について、実験の詳細を含め報告され、発表終了後も多くの質疑を受けるものであった。

9 月 30 日と 10 月 1 日の 2 日間にわたり実施されたポスターセッションでは、100 件以上の発表の中から 4 件の優秀ポスター賞を表彰した。また、酸化物エレクトロニクス分野の発展に貢献すると思われる優れた研究を行った若手研究者（40 歳未満）には、iWOE prize として毎年表彰を行っており、今回のワークショップでも会議に先立ち 7 月末に応募を受け付け、本ワークショップ期間で最終の選考を行い、2 名の受賞者を決定、表彰した。

本ワークショップが対象とする酸化物エレクトロニクス研究分野は、近年、原子レベルでの材料制御技術が急速に進歩したことで、界面特有の新しい物性・機能が相次いで見出されている。発表された酸化物薄膜やヘテロ構造の作成とそれらが示す新奇な物性に関する成果は、学術的に重要であるばかりでなく、新規な機能素子・デバイスの開発に向けて社会からも強く期待されるものである。



Atomic level analysis and fabrication of highly stable perovskite films and light emitting diodes

Juan Qiao Tsinghua University

Organometal halide perovskites (OHPs) with general formula AMX_3 (A : organic or inorganic cations, M : Pb or Sn, X : Cl, Br, I) have emerged as a strong candidate for solar cells and light emitting diodes. Most recently, the external quantum efficiency (EQE) of the perovskite light emitting diodes (PeLEDs) has boosted to over 20%, which bring renaissance of perovskites as emitters. However OHPs have a number of problems to be solved for bring these devices to the market. One of the main challenges is to overcome the poor stability of these OHPs for improving the device operation lifetime. The instability of OHPs mainly originates from the phase transition under relatively low temperature and ease of ion migration. To address the phase transition and ion migration problem of OHPs, we demonstrated that mixed phase with α/δ phase junction could be an efficient approach to improve phase stability and enhance the emission of perovskite films, and supramolecular cation- π interaction could be a very effective method to inhibit the cation migration in perovskite solar cells (Chem. Sci., 8, 800-805, 2016; J. Mater. Chem. C, 5, 11121-11127, 2017; Adv. Mater, e1707583, 4, 2018). However, in these works, we did not obtain atomic level information about the improved perovskite stability.

In this year, to obtain basic atomic level information about perovskite materials using solid-state NMR, we fabricated $MAPbI_3$ with different mixing ratio of MAI and PbI_2 precursors. The perovskite samples are prepared from a DMF solution of MAI and PbI_2 , by drying the solution at 100°C . for 10 hours in an Ar atmosphere. The solid state NMR spectrum measurement was performed using a 4 mm double resonance magic angle spinning (MAS) probe under a static magnetic field of 9.4 T. The MAS speed was set to 12 kHz.

The dipolar dephasing (DD) MAS NMR spectra are shown in Fig. 1. MAI produced a signal with a peak at 29.4 ppm, and $MAPbI_3$ fabricated from MAI: $PbI_2 = 0.5 : 1$ and $1 : 1$ showed a signal with a peak at 31.4 ppm. These results indicate that the all MAI reacted with PbI_2 to form $MAPbI_3$, and that no unreacted MAI remained. It was also found that impurity such as a reaction solvent or a decomposition product was not observed for these measurements. On the other hand, in $MAPbI_3$ from MAI: $PbI_2 = 3 : 1$, two peaks corresponding to MAI and $MAPbI_3$ were observed. Also the intensities of two signal was almost quantitative, indicating that that unreacted MAI remains in the sample without decomposition. In the ^{207}Pb DD MAS NMR spectra, PbI_2 showed a signal having a peak at -20 ppm, whereas for $MAPbI_3$ from MAI: $PbI_2 = 1 : 1$ and $3 : 1$, a signal with a peak at 1419 ppm was observed. On the other hand, $MAPbI_3$ from MAI: $PbI_2 = 0.5 : 1$, two signals corresponding to PbI_2 and $MAPbI_3$ were observed. Although the signal intensity of the signals of PbI_2 and $MAPbI_3$, were not completely quantitative, it was clearly shown that unreacted PbI_2 remained in the sample.

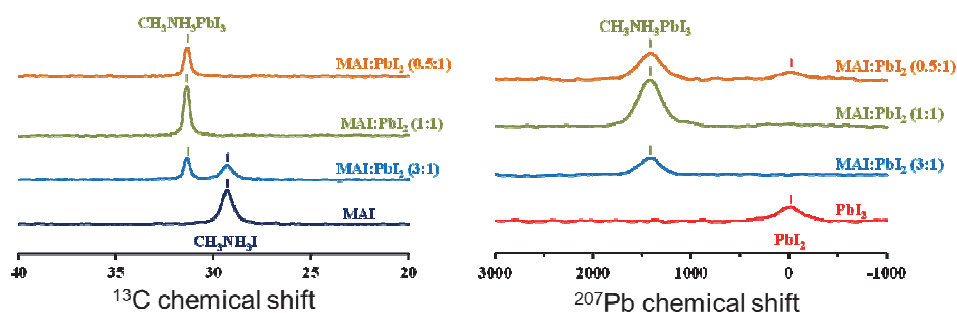


Figure 1. ^{13}C and ^{207}Pb NMR spectra for $MAPbI_3$ samples with different precursor ratio.

High-pressure synthesis of potential multiferroic oxides

J. Paul Attfield University of Edinburgh

Objectives: High pressure-high temperature (HPHT) synthesis is used to stabilize unusual oxidation states and coordination environments in transition metal oxides, resulting in interesting physical properties. In collaboration with Professor Shimakawa in ICR at Kyoto university, a unique high pressure multianvil apparatus which reaches up to 20 GPa and 2273 K is available to use. This equipment provides a good opportunity for synthesize the double corundum/perovskite with small tolerance factor and develop their potential multiferroics.

Experimental methods: The preparation of the precursor mixtures was performed via conventional solid-state route under ambient pressure. The precursor mixtures were then loaded into the pressure cell and synthesized under required temperature and pressure. Their structures were characterized using x-ray diffraction methods and their physical properties were explored using a Quantum Design PPMS and MPMS-SQUID.

Experimental results: A new double corundum $\text{Co}_2\text{InSbO}_6$ has been successfully synthesized at 8 GPa and 1373 K with polar $R3$ space group and lattice parameters $a = 5.28893(4)$ and $c = 14.0361(1)$ Å. Magnetic susceptibility and hysteresis loop indicated ferrimagnetic interactions with $T_C = 14$ K. Temperature dependent synchrotron x-ray diffraction show a potential NTO-type to OIL-type structural phase transition above 850 K.

A new double perovskite MnCoScSbO_6 has been successfully synthesized at 6 GPa and 1423 K with the non-polar monoclinic space group $P2_1/n$ and lattice parameter $a = 5.2692(1)$, $b = 5.42159(1)$, $c = 7.7104(1)$ Å and $\beta = 90.439^\circ$ (1). Magnetic properties measurements reveal two antiferromagnetic transition at $T_{N1} = 51$ K and $T_{N2} = 15$ K.

Discussion: In comparison with $\text{Co}_2\text{ScSbO}_6$ ($T_C = 61$ K), $\text{Co}_2\text{InSbO}_6$ reveals a very low transition temperature (14 K), and a high temperature phase transition. This may due to the large anti-site exchange between the A-site Co^{2+} and B-site In^{3+} . Further neutron diffraction is necessary to obtain precise cation sites and the potential magnetic structure.

$\text{Mn}_2\text{ScSbO}_6$ and $\text{Co}_2\text{ScSbO}_6$ are both NTO-type double corundum at 6 GPa, 1423 K. However, by mixing them with a ratio of 1:1 and synthesizing at exact same pressure and temperature, a monoclinic $P2_1/n$ double perovskite MnCoScSbO_6 formed. Introducing smaller Co^{2+} ion at A-site induce structural phase transition and change the magnetic structure. Further investigation of ratio 3:1 and 1:3 is necessary to fully understand the interesting $\text{Mn}_{2-x}\text{Co}_x\text{ScSbO}_6$ solid-solutions.

Publication: Publication process on $\text{Co}_2\text{InSbO}_6$ and $\text{Mn}_{2-x}\text{Co}_x\text{ScSbO}_6$ materials will be started once all characterization is finished.

Synthesis and characterization of novel organoselenium and -tellurium compounds

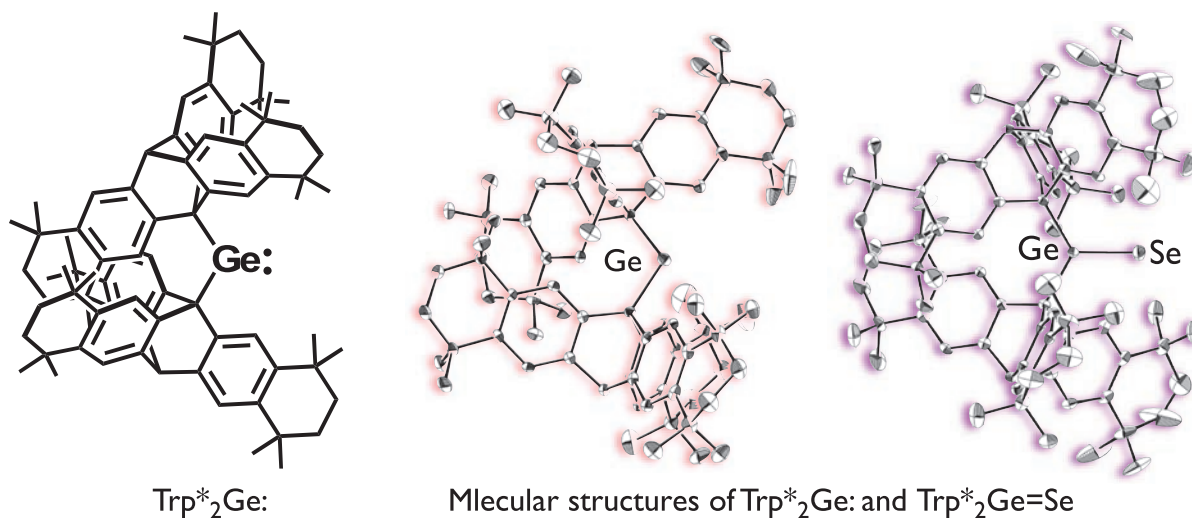
Mao Minoura Rikkyo University

It is generally known that germanium-chalcogen double bond compounds are highly reactive species and such double bond compounds can easily dimerize. By utilizing the bulky protecting group, it is possible to synthesize and isolate the germanium-chalcogen double bond compounds. Tokitoh *et al.* reported the synthesis of the germanium-chalcogen double bond compounds bearing large aromatic Tbt group. However, in the case of alkyl substituted species, the stable germanium-chalcogen double bond compound has never been reported due to the difficulty of the ligand design.

Recently, our group has designed and synthesized Trp*, *i.e.*, a novel triptycene (Trp)-based aliphatic bulky group that bears bulky fused ring-type substituents at the periphery of the Trp framework. In the present study, we took advantage of the steric protection of the Trp* group to synthesize the thermally stable germylene Trp*₂Ge: and the corresponding germanium-chalcogen double bond compounds.

The divalent germanium species, germylene with two Trp* groups, was synthesized and isolated by the reaction of Trp*Li and GeCl₂. The treatment of the Trp*₂Ge with elemental selenium afforded the germaneselone (Trp*₂Ge=Se). The isolated Trp*₂Ge and Trp*₂Ge=Se are thermally very stable and moisture sensitive, those molecular structures were determined by X-ray crystallographic analysis.

We thank Professors Norihiro Tokitoh, Yoshiyuki Mizuhata, and Mariko Yukimoto for their kind discussions.



Fumiaki Suzuki, Ryohei Nishino, Mariko Yukimoto, Koh Sugamata, Mao Minoura, *Bull. Chem. Soc. Jpn.* **2020**, 93, 249–251. doi:10.1246/bcsj.20190338

核融合プラズマ対向材中の水素・ヘリウム挙動に関する電子分光学的研究

宮本光貴 島根大学

核融合発電の実現には、高性能プラズマの安定維持に加え、それを取り囲む材料との相互作用を正確に把握しておく必要がある。現在建設の進む国際熱核融合実験炉（ITER）においては、プラズマ対向材料の大部分を占める第一壁にベリリウムの利用が予定されているが、取り扱い上の問題もあり、そこでの燃料水素同位体や反応生成物のヘリウム挙動に関する知見は極めて乏しい。そこで本研究では、ベリリウム試料中の水素同位体およびヘリウム挙動を微細組織変化と関連付けて評価することを目的とした。

直径 $\phi 20\text{mm}$ 、厚さ 1.5mm のベリリウムバルク試料を、機械研磨した後、カリフォルニア大学サンディエゴ校(UCSD)の高密度プラズマ発生装置(PISCES-B)を用いて、重水素とヘリウムから成る混合プラズマに、照射エネルギー $E_i \sim 40\text{--}100\text{ eV}$ 、試料温度 $T \sim 573\text{ K}$ 、照射量 $\Phi_D \sim 1 \times 10^{26}\text{ D/m}^2$ の条件で曝露した。曝露後の試料を FIB 装置により薄膜化加工し、京都大学化学研究所のモノクロメータ搭載低加速原子分解能分析電子顕微鏡により、微細組織観察、EDX 組成マッピング分析、および電子エネルギー損失分光測定を行った。

高密度プラズマに曝したベリリウム試料表面には、いずれも特異なコーン状組織の形成が観察された。特に $E_i \sim 100\text{ eV}$ 、 $\Phi_D \sim 1 \times 10^{26}\text{ D/m}^2$ 、 $T \sim 573\text{ K}$ で $\text{D+He}(\sim 10\%)$ 混合高密度プラズマに曝した試料では、 500nm を超える顕著なコーン状組織が観察された。

図 1 は、表面(SEM)および断面(TEM)の微細組織観察結果を示す。断面 TEM 観察像の解析から、個々のコーンは結晶性を有しており、多くは基板の結晶方位と一致することが確認された。さらに STEM-EDX による元素マッピング測定の結果、各コーンの頂点に Ta が局在していることが示された(図 2)。なお、Ta はプラズマ曝露時の試料ホルダーに使用されていたものである。Be 試料表面に堆積した不純物重元素の Ta がスパッタリングを抑制し、それ以外の部分が優先的にスパッタされることで、特異なコーン状組織の形成に至ったと考えられた。ITER においては、W が同時に使用されることから、同様に W を起点とした、スパッタリングによるコーン状組織の形成が予想される。

なお、本研究は小野興太郎名誉教授（島根大学）、倉田博基教授、治田充貴准教授（京都大学化研）らとの共同研究として実施されたものである。今年度は、これまでの成果を学術論文において報告している(K. Ono, M. Miyamoto et al., Journal of Applied Physics, 126(2019)135104)。本論文は、その重要性が高く評価され Editor's Pick に選出された。

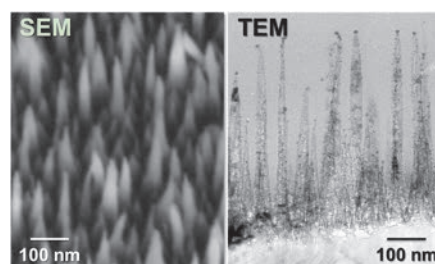


図 1 プラズマ曝露したベリリウム試料の表面(SEM)および断面(TEM)組織。

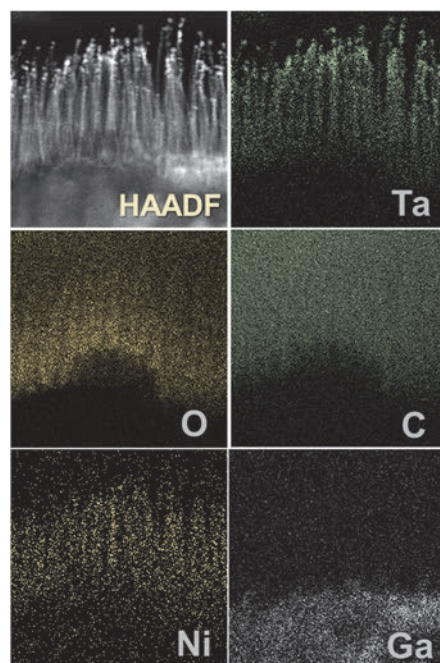


図 2 STEM-EDX による元素マッピング。

プラズモニック結晶上でのプラズモン-エキシトン結合

齊藤光 九州大学

近年、物質中の励起状態と表面プラズモンが強結合した状態に強い関心が寄せられ、電子線を用いたナノ顕微分光の分野においてもそのような強結合によるラビ分裂が観測された例も報告されるようになった。しかしながらこれまで電子線分光による観測例として報告されたものは酸化物[J. Wei et al., Nano Lett. 15, 5926 (2015)]のや遷移金属ダイカルコゲナイド[A. B. Yankovich et al., Nano Lett. 19, 8171 (2019)]のエキシトンが対象であり、有機分子の励起状態と表面プラズモンの強結合状態の観測は依然として電子線で達成されていない。そこで本研究ではプラズモニック結晶[D. Yoshimoto et al., ACS Photon. 5, 4476 (2018)]を利用したプラズモン共振器と塩素化銅フタロシアニンとを組み合わせた構造を作製し、走査透過電子顕微鏡

(STEM)-電子エネルギー損失分光(EELS)を用いて有機分子の励起状態と表面プラズモンが強結合した状態のイメージングを試みた。Fig. 1aのSTEM像に示すように電子線リソグラフィを用いて2種類の直径の金属ナノディスクを周期的に配列した構造を作製した。同構造は遷移金属ダイカルコゲナイドを模しており、大ディスクに分布する状態と小ディスクに分布する状態のエネルギー差から表面プラズモンのバンドギャップが形成されることがわかった。周期構造中の一部の大ディスクを小ディスクで置換すると、その欠陥に局在する状態がバンドギャップ中に形成されることがわかった(Fig. 1b-1e)。次に塩素化銅フタロシアニンの吸収ピーク(2 eV)に上述の欠陥状態のピークが重なるように周期を調整した構造の上に塩素化銅フタロシアニンを蒸着したところ、試料に電子線損傷を与えることなくデータを取得することができたが、欠陥位置で観測されたピークには明確なラビ分裂が観測されなかった。今後、有機分子とプラズモン共振器の結合がより強くなる構造を再検討する必要がある。

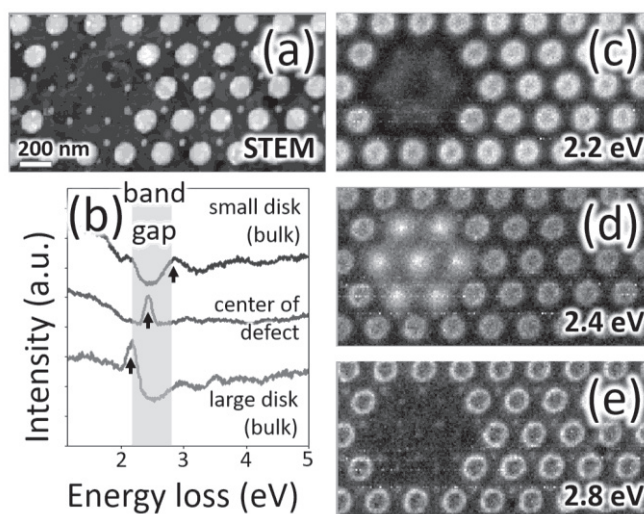


Fig. 1 周期 240 nm、ナノディスク直径 140 nm(大)・40 nm(小)の構造のEELS分析。(a)STEM像。(b)バルク中の大・小それぞれのディスク上、欠陥中央の小ディスク上から取得されたEELSスペクトル。(c-e) (b)に示された3つのピークに対応したエネルギーフィルターマップ。

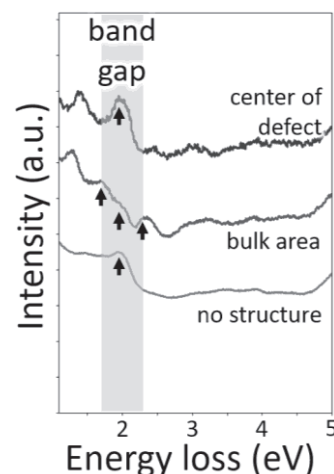


Fig. 2 周期 300 nm、ナノディスク直径 170 nm(大)・50 nm(小)の構造上に塩素化銅フタロシアニンを蒸着した試料のEELS分析。

完璧な π 共役二次元シートを持つフラットシリセンの設計

高橋まさえ 東北大学

【目的】「ケイ素版グラフェン」とも呼ばれる新材料「シリセン」は、炭素原子の代わりに同じ 14 族であるケイ素原子を使った二次元単原子層シートです。グラフェンは電子構造にエネルギーギャップがないため、論理回路への応用が望めなく、シリセンの実現が切望されています。しかし、シリセンは、平面構造のグラフェンとは異なり、一部の原子が浮き上がって座屈した凹凸構造をとるため、空気中できわめて不安定です。研究代表者は、極最近、平面構造のシリセン分子の理論設計に成功し、論文発表しました[M. Takahashi Sci. Rep. 2017, 7, 10855.]。

本研究は研究代表者が設計したフラットな構成単位をベースに二次元に拡張したフラットなシリセンを構築し、その物性を探索することを目的としています。第一原理計算による物質設計では、最適化構造を求めたのちに、その構造がポテンシャル曲面上で安定構造であることを振動解析により確認する必要があります。周期系の第一原理計算において、格子定数も含めた構造最適化とその振動解析の可能なアプリケーションは限られています。京都大学化学研究所のスーパーコンピュータにはこの目的にかなったアプリケーション (Materials Studio) が公開されています。

【結果と考察】2018 年度は、分子の第一原理計算ソフトにより設計発表したシリセン分子の結果と、Materials Studio のような周期系の第一原理計算ソフトを用いた結果について、いくつかの条件をクリアしすり合わせを行いました。2019 年度は、2018 年度に確立した条件で、平面ケイ素 2 次元シートの設計に着手しました。2019 年 6 月には国際会議 ICMAT 2019 で、11 月には ICMS 2019 で招待講演を行いました。ケイ素を 2 次元に敷き詰めたシリセンは凹凸構造をとり、空気中できわめて不安定です。平面構造に制限し、平面構造を有するシリセン分子の理論設計において研究代表者が示した指針に基づき、考えられる限りの二次元シートを設計し計算しました。しかし、単純な二次元への拡張では目的とする平面構造は得られず難航しました。現在、一つの系について、平面構造が安定となるシリセンシートの設計に成功しました。ディラックコーンは相対論的効果を入れなくても僅かにギャップが開き、バンド構造は半金属の性質を示唆していました。今後、相対論的効果、スピン密度および他の系の可能性について検討します。

【成果報告】

発表論文

- M. Takahashi, H. Matsui, Y. Ikemoto, M. Suzuki, N. Morimoto, *Sci. Rep.* **2019**, 9, 13104.

国際会議招待講演

- M. Takahashi, ICMAT2019, June 23-28, 2019, Marina Bay Sands, Singapore.
- M. Takahashi, ACCMS-10, July 22-26, 2019, City University of Hong Kong, Hong Kong.
- M. Takahashi, ICMS 2019, November 3-6, 2019, Jeju, Korea.

Synthesis and structures of acene molecules bearing chalcogenopyrylium units

Noriyoshi Nagahora Fukuoka University

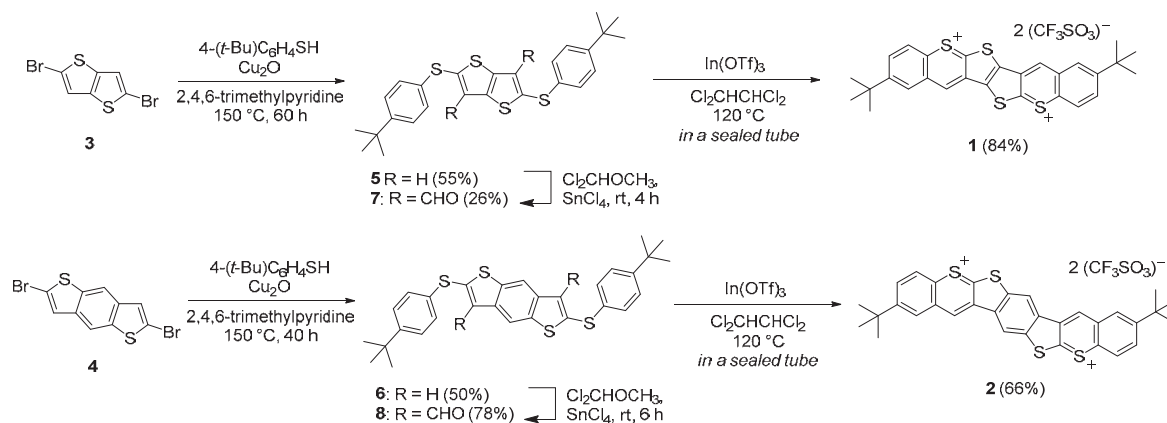
Introduction

A variety of organoelectronic devices are based on thiophene derivatives and therefore thiophene derivatives/analogues with improved properties are highly sought after. In this regard, thiophene-fused thiopyrylium salts can be expected to exhibit promising potential. However, examples on the synthesis of thiophene-fused thiopyrylium compounds have so far remained scarce. In this work, we present the synthesis of a new family of thiophene-fused thiopyrylium salts **1** and **2** together with the experimental and theoretical examination of their electronic structures.

Results and Discussion

Initially, the reactions of dibromothiophenes **3** and **4** with 4-*tert*-butylbenzenethiol provided thioethers **5** and **6** in moderate yield. Thus, we attempted the synthesis of thiopyrylium salts **1** and **2** via a Rieche formylation followed by a Friedel–Crafts cyclization. Thioethers **5** and **6** were treated with $\text{Cl}_2\text{CHOCH}_3$ in the presence of the Lewis acid SnCl_4 , which afforded diformylated compounds **7** and **8** in moderate yield. Subsequently, we attempted the Lewis-acid-promoted intramolecular Friedel–Crafts reactions of **7** and **8**. In a sealed vessel, we carried out a literature method for the $\text{In}(\text{OTf})_3$ -induced cyclization on **7** and **8** in $\text{Cl}_2\text{CHCHCl}_2$. Cold hexane was added dropwise to the resulting solution and the thus obtained reddish brown and orange powders of the stable bithiopyrylium salts **1** and **2** were isolated in 84% and 66% yield, respectively by centrifugation. None of the thermally stable bithiopyrylium salts showed any signs of decomposition and/or hygroscopicity under atmospheric conditions.

The ^1H NMR spectra of **1** and **2** show deshielded resonances for all aromatic protons, except for the *tert*-butyl groups, which are comparable to the ^1H NMR spectra of previously reported thiopyrylium salts. These results suggest the presence of a significant diatropic ring current in the π -framework. Moreover, based on theoretical calculations, it can be feasibly concluded that thiopyrylium salts **1** and **2** possess dicationic aromatic character with 26π (for **1**) or 30π electrons (for **2**), and thus satisfy the Hückel rule.

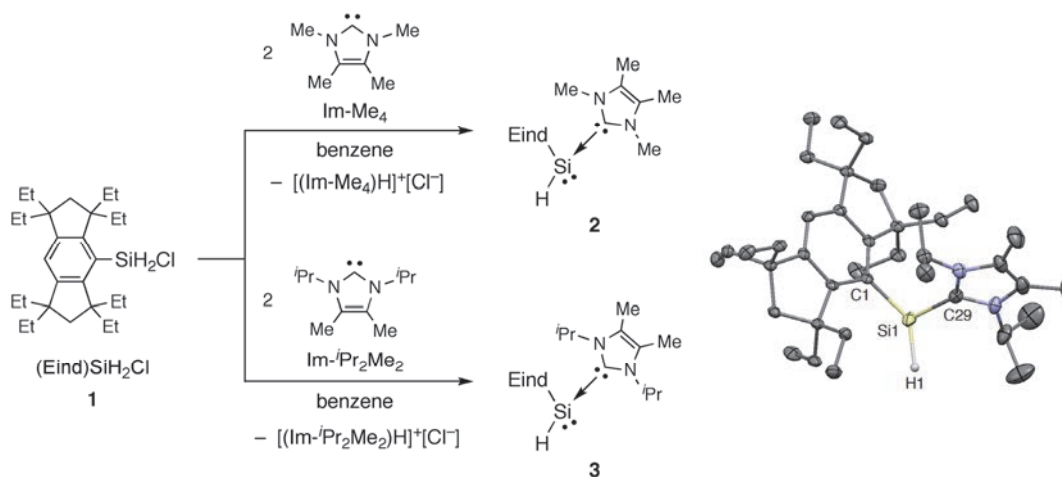


Synthesis and structural characterization of divalent species of heavier group 14 elements

Tsukasa Matsuo Kindai University

In this collaborative research, we have planned to examine the synthesis and structures of divalent species of the heavier group 14 elements by the combination of the steric protection with bulky Eind group (Eind = 1,1,3,3,5,5,7,7-octaethyl-*s*-hydrindacen-4-yl) and the coordination of *N*-heterocyclic carbenes (NHCs).

We have investigated the reaction of the Eind-substituted chlorodihydrosilane, (Eind)SiH₂Cl (**1**),¹⁾ with NHCs (Im-Me₄ = 1,3,4,5-tetramethylimidazol-2-ylidene and Im-*i*Pr₂Me₂ = 1,3-diisopropyl-4,5-dimethylimidazol-2-ylidene). As shown in Scheme 1, the dehydrochlorination reaction of **1** with 2 molar amounts of NHCs produced the mono-NHC adducts of the arylhydrosilylene, (Im-Me₄)→SiH(Eind) (**2**) and (Im-*i*Pr₂Me₂)→SiH(Eind) (**3**), together with the formation of imidazolium chlorides, [(Im-Me₄)H]⁺[Cl[−]] and [(Im-*i*Pr₂Me₂)H]⁺[Cl[−]]. The NHC adducts **2** and **3** have been characterized by NMR spectroscopy. In the ²⁹Si NMR spectra, one signal was observed at −77.8 (**2**) and −81.7 (**3**) ppm. The molecular structure of **3** has been determined by a single crystal X-ray diffraction analysis.



Scheme 1. Synthesis of **2** and **3** by the reaction of **1** with NHCs.

1) N. Hayakawa, T. Morimoto, A. Takagi, T. Tanikawa, D. Hashizume, T. Matsuo, *Chem. Lett.* **45**, 409–411 (2016).

Elucidation of the fluororous interactions in the crystal structures of fluorine-containing conjugated molecules by the single-crystal X-ray structural analysis

Tomohiro Agou Ibaraki University

Introduction

Helicenes have been paid increasing attention to because of their unique structures and optical properties leading to various applications. For examples, fluorine-substituted helicenes will exhibit improved electron-accepting ability, control of solid-state intermolecular interaction, and novel reactivity. Herein, we report the syntheses of helicenes fused with hexafluorocyclopentene (HFCP) moieties, and their molecular structures and optical properties were elucidated.

Results and Discussion

HFCP-fused helicenes **1-4** (Fig. 1) were synthesized starting from octafluorocyclopentene via oxidative photocyclization. Among these HFCP-fused helicenes, structures of **1a**, **1b**, **3**, and **4** were revealed by the X-ray crystallographic analysis (Fig. 2), showing that the HFCP-annulation did not affect the structures of the helicene skeletons. Chiral separation of helicenes **1a** and **1b** were achieved by chiral HPLC using the DAICEL ChiralPack® IA column, and their chiroptical properties, including circular dichroism (CD) and circularly polarized luminescence (CPL) characteristics, were investigated. For instance, the (*P*)- and (*M*)-isomers of Ph₂N-substituted helicene **1c** exhibited mirror-image CPL emissions (Fig. 3), and their luminescence dissymmetry factors were estimated to be 1.2×10^{-3} at 550 nm, suggesting their potential use for CPL-based chiroptical materials.

The author thanks ZEON cooperation for the generous gift of OFCP.

Outcome

Agou, T.; Kohara, M.; Tamura, Y.; Yamada, K.; Shiitsuka, K.; Hosoya, T.; Mizuhata, Y.; Tokitoh, N.; Hayashi, Y.; Moronuki, Y.; Ishii, A.; Tanaka, Y.; Muranaka, A.; Uchiyama, M.; Yamada, S.; Konno, T.; Fukumoto, H.; Kubota, T. *Eur. J. Org. Chem.* DOI: 10.1002/ejoc.202000152.

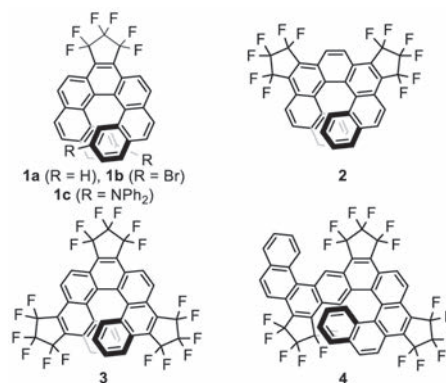


Fig. 1. HFCP-fused helicenes.

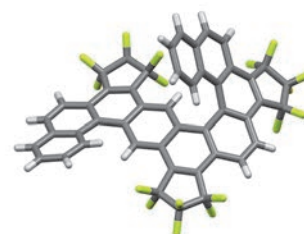


Fig. 2. Molecular structure of helicene **4**.

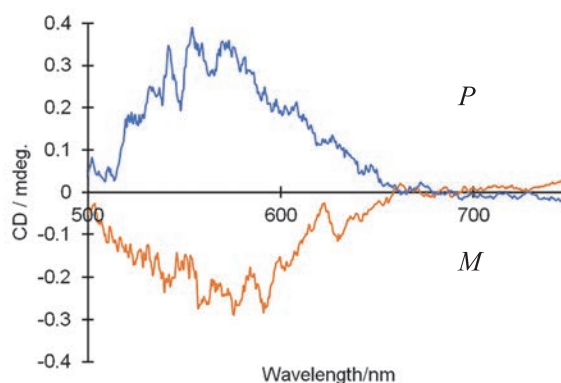


Fig. 3. CPL spectra of helicene **1** (R = NPh₂)
(in CH₂Cl₂, λ_{ex} 490 nm).

生体組織由来のカルボニル化合物を標的とする高感度質量分析 イメージング解析

秦野修 奈良県立医科大学

目的: 研究代表者は、カルボニル（ケトン）基をもつ化合物（ステロイドホルモン類）を誘導体化し、化学研究所の FT-ICR MS 装置を用いることにより、極めて高分解能（質量分解能 100 万）、かつ、高感度な質量分析検出、及び、イメージング解析を行なう系を構築している。又、光学顕微鏡切片の組織切片上で化学反応を行い、その反応行程の前後変化を、光学/蛍光顕微鏡、及び、電子顕微鏡（無蒸着 SEM 観察）レベルで追跡する実験系を構築している。本研究は、これらの手法を、これまでのステロイド解析に加えて、化学研究所・中村研究室が行っている再生可能バイオマス資源であるスギ等の人工森林木材から有用化合物生産を行う研究にも適用することを目的として行った。

実験方法、実験結果、考察:

共同研究者・研究協力者の磯崎・高谷・中村らは、鉄錯体触媒やイオン液体触媒を用いたスギ等の木質バイオマス分解過程において、ケトン基やアルデヒド基等のカルボニル化合物が生成されることを見出している。本研究では、これらのカルボニル化合物の高感度検出系の構築を目的として、リグニンモノマー（GHP, SHP）、及び、リグニンモデルダイマー（MPHPV）を、ターゲットとして研究を行った。代表者がステロイド類を用いて構築した GirT 試薬を用いた誘導体化手法と、化学研究所の超高質量分解能（R:100 万）の FT-ICR MS を用いることによって、これら化合物の高感度、且つ超高分解能（ m/z 値 0.001 程度）検出が可能となった。

又、スギ木幹部の光学顕微鏡切片（10-12 μm 厚の木口面、柀目面等）を作成し、鉄錯体触媒: $\text{Fe}(\text{tfsa})_2$ 、引き続き、 H_2O_2 水溶液による酸化処理を組織切片上で行った。この反応前後におけるリグニン分解過程をリグニン自家蛍光（DAPI フィルター）観察によって、又、組織立体構造の変化の解析を SEM 観察（無蒸着、低真空）を併用することにより行った（CLEM 法: Correlative Light & Electron Microscopy（光-電子相関顕微鏡法））。リグニン自家蛍光がほぼ消失（0.6 % 残存）した反応後の SEM 観察では、スギ仮道管の細胞壁の厚さが薄くなり、細胞壁間スペースが減少し、又、壁孔周辺が薄くなる結果を得た。同様の結果は、中村研究室において、X 線マイクロ CT による測定でも得られており、本研究結果はそれを支持するものであった。

今後は、更にリグニン以外の木質の主要成分であるセルロース、ヘミセルロース等の化学分解過程の解析を目指し、組織構造を保った光学顕微鏡切片上で化学反応を行い、SEM を含めた組織微細構造レベルでの変化の解析を行っていきたい。

成果報告: “CLEM imaging of rhododendrol-induced leukoderma in zebrafish and catalytic oxidation of Japanese cedar wood.” [Osamu Hatano](#), Masumi Hayazaki, Akie Hamamoto, Hiroshi Takemori, [Hikaru Takaya](#), Takafumi Shanoh, Ken Ohnishi, [Masaharu Nakamura](#)

ABiS Symposium: Forefront and Future of Electron Microscopic Imaging. Feb.14-15, 2020
Okazaki, Japan

2. 国際会議、シンポジウム・研究会報告

9th Pacific Symposium on Radical Chemistry [PSRC] (第9回環太平洋ラジカル化学会議) 実施報告書

会期：2019年6月16日（日）～21日（金）

会場：Asilomar Conference Center, Pacific Grove, California, USA

表記会議が米国モンレーの Asilomar Conference Grounds で開催された。この会議は、有機合成、高分子合成、有機材料科学、生命科学の鍵化学種である有機ラジカルに関し、環太平洋地域での研究の活性化と相互交流の促進を目的としている。2003年の第1回会議以降、2年毎に太平洋地区で開催されており、今回はその9回目である。今回の会議の主催した米国ミシガン大学の Corey Stephenson 教授と国際組織委員（10名）で運営を行い、山子は当該委員を務めた。京大化研の国際公共拠点は、ミシガン大学、アメリカ化学会・Thieme・Wiley・Cell Press 発行の関連雑誌、製薬・化学会社等と共に、スポンサーとして会議をサポートした。126名の参加者のうち、米国からの参加者が75名と最も多く、次いで日本（12名）、中国（7名）、カナダ（6名）、イギリス（6名）等、欧州を含め13か国からの参加があった。

会議は基調講演（Plenary Lecture、50分）6件、招待講演（Invited Lecture、30分）28件、若手招待講演（Young Investigator Lecture、25分）18件、若手ショートトーク（Short Talk、10分）9件、企業研究者講演（Industrial Lecture、4件）25分の他に、51件のポスター発表があった。これに加え、大学院での講義レベルの Short Course を設け、4名の講師がラジカルの基礎、電気化学、光酸化還元触媒、有機合成に関する講義を各1時間行ない、若手の育成を図った。実際には多くのシニア研究者も参加し、大変好評であった（写真参照）。会議は朝8時半から夜の9時過ぎまで、昼食、夕食の1時間を挟んでぶっ通しで続き、いずれも素晴らしい講演で充実しているものの、体力的にはなかなか大変な毎日であった。当然ながら（？）夜の講演の後にはアルコールを入れての交流が深夜まで続き、こちらも大盛況であった。

発表内容としては、近年の発展が目覚ましい光酸化還元触媒を用いた有機合成反応に関する研究が最も多く、産業界での利用に発展している状況も含め、最新の成果が紹介された。さらに、有機電解合成や制御ラジカル重合の新しい展開、ラジカル材料の開発、生体内ラジカル反応の解明やラジカルプローブを用いたイメージングなど、ラジカル化学に関する幅広い話題の提供があった。

バンケットでは優れたポスター発表6件に対して、ポスター賞が授与された。さらに、国際組織委員会で決定された次回の PSRC の開催予定について、2021年に京都で開催することを山子が紹介した。多くの参加者が高い研究の質と、密な交流に大いに満足して帰途に就いた。拠点の支援に深謝する。



山子 茂（高分子制御合成領域）

19th International Conference on Bioinformatics and Systems Biology (IBSB 2019)

開催報告

会期：令和元年 7 月 14 日（日）～ 7 月 18 日（木）

会場：京都大学宇治キャンパス 宇治おうばくプラザ（きはだホール、ハイブリッドスペース）および京都大学宇治キャンパス総合研究実験 1 号棟 CB207

参加者数：計約 70 名、内訳：招待講演者 4 名（スタンフォード大学 1 名、東京工業大学 1 名、国立シンガポール大学 1 名、ライフサイエンス統合データベースセンター (DBCLS) 1 名）、ボストン大学 14 名、ベルリンシステムズバイオロジーグループ 11 名、京都大学化学研究所附属バイオインフォマティクスセンター関係者約 40 名

内容：上記期間および場所において、19 回目となる国際会議 IBSB 2019 を開催した。本国際会議は、以下の 3 つのグループが構成するクローズドな国際会議である。

- 1) ボストン大学バイオインフォマティクスプログラム
- 2) ベルリンのフンボルト大学を含め複数の大学からなるシステムズバイオロジーのグループ
- 3) 京都大学バイオインフォマティクスセンターとその関係者からなるグループ

開催地を 3 つのグループの所在地である、ボストン、ベルリン、京都（日本）の 3 ヶ所の持ち回りで変えつつ毎年夏に開催しており、2001 年の開始から今年で 19 回目となる。例年、3 つのグループの主に大学院学生と博士研究員を中心とした 50－100 名程度の参加者がある。今回の参加人数は上記の通りであった。

今回、会議の最も重要な部分は、各日 1 件、計 4 件の招待講演であった。7 月 15 日はスタンフォード大学の James Zou 助教授が、機械学習の生命医科学応用、特に最近話題のゲノム編集技術への応用、さらに機械学習技術を応用する際に技術的課題について非常にわかりやすいレクチャーを行い、大変な好評を博した。16 日は東京工業大学の山田拓司准教授が、メタゲノミクスにおけるバイオインフォマティクス研究を披露すると同時に、がんを中心とした疾病での事例を幅広く紹介し、エネルギッシュな講演とともに強い印象を残した。17 日はシンガポール国立大学の See-Kiong Ng 教授が、時系列データでの外れ値や変化点検出を深層学習により行う手法についてわかりやすく説明を行い、最近の機械学習技術に対する聴衆の理解を深めた。さらに、17 日にいったん本会議が終了した後、18 日はチュートリアル／ハンズオンセミナーを行い、招待講演者として、DBCLS

(Database Center for Life Sciences)の山口敦子准教授がデータベース統合に関する幅広い解説を行い、受講者との質疑応答をも踏まえて、丁寧な説明が好評を得た。

上記招待講演以外に、参加者（大学院学生と博士研究員）による約20件の口頭発表及び約30件のポスター発表が15－17日の3日間に渡り行われ、連日盛況を博した。特に、口頭発表は各30分（20分程度の発表と10分程度の質疑応答）であったが、中には質疑応答時間が発表時間をはるかに超えてしまうような白熱した議論も見られた。また、ポスター発表においても、多くのポスターの前で、異なるグループからの参加者が白熱した議論を展開する光景を頻繁に見ることができた。17日には、ベストプレゼンテーション賞の表彰を行い、授与された発表は、ボストン大学の Kritika Karri and David J. Waxman で、タイトルは「Single-cell spatial reconstruction reveals zonation of xenobiotic-responsive lncRNAs (xeno-lncs) in mouse liver」であった。また、18日のチュートリアル／ハンズオンセミナーでは招待講演を含む3件の発表があり、参加者と一体となったセミナーが行われた。このような状況から、今回の国際会議でのセッションは、全体に、参加博士課程学生・博士研究員の勉学・研究を刺激し、また、異なるグループに属する学生・博士研究員同士の研究交流を促進する上で十分なものであった。

一方、会議は、招待講演と口頭・ポスター発表という通常のサイエンティフィック・プログラムのみならず、多くのソーシャル・イヴェントを含んでいた。14日にレセプション、16日午後にエクスカージョン、同日夜にバンケットを開催し、博士課程学生・博士研究員・教授等ほぼ全員の参加者の間で交流を深めた。

最後に、今回、IBSB を化学研究所の国際会議シリーズの一部とさせていただきました。サポートに感謝いたします。お陰で国際会議 IBSB を恙無く運営することができました。

馬見塚 拓（化学研究所附属バイオインフォマティクスセンター生命知識工学研究領域）



令和元年度 日本分光学会年次講演会・国際シンポジウム

主 催：(公社) 日本分光学会

共 催：京都大学化学研究所 国際共同利用・共同研究拠点，京都大学教育研究振興財団

協 賛：日本化学会，日本分析化学会，分子科学会

日 時：2019 年 5 月 15 日（水） 9 時～15 時

場 所：京都大学化学研究所・きはだホール

毎年 5 月に開催される日本分光学会の年次講演会を，令和元年度は京大化研で開催した．3 日間に渡る年次講演会は，そのうち 1 日を割いて国際シンポジウムも開催する習慣がある．今回は“Frontier of Surface Analysis by Advanced Vibrational Spectroscopy”をテーマに，表面・界面・薄膜の振動分光の最先端を特集して議論した．国際共共には本国際シンポジウムを共催していただき，非常に充実した環境でのシンポジウム開催が実現した．

このシンポジウムに先立ち，英国の Colin D. Bain と長谷川は，これまで北米でのシンポジウムをたびたび開催してきた．今回は，いまだ実現していなかった日本での開催をようやく実現したものである．

本シンポジウムのプログラムは，以下のとおりである．

1. K. Zhang (Hitachi Co.) “Tip-enhanced Raman spectroscopy using plasmon-resonance thin-film waveguide to analyse monolayer level organic thin film”
2. C. Marcott (Univ. Delaware) “Latest advances in nanoscale IR spectroscopy and imaging”
3. Shinji Ando (Tokyo Institute of Technology) “Evolution of chain orientation in aromatic polyimides thin films during thermal curing analyzed by variable temperature polarized multiple-angle incidence resolution spectroscopy (VT-pMAIRS)”
4. T. Hama (Hokkaido Univ.) “PM-IRRAS as a tool for in vivo surface analysis of living specimens: the plant leaf cuticle as a case

study”

5. Colin D. Bain (Durham University) “Total internal reflection Raman spectroscopy”
6. Y. Furukawa (Waseda Univ.) “Raman spectroscopy of thin polymer films used for electronic devices”
7. T. Shimada (Hirosaki Univ.) “Surface-Enhanced Infrared Absorption on periodic nanostructures”
8. S. Ye (Tohoku Univ.) “In situ vibrational SFG observation on the graphene/electrolyte interface”
9. Z. Chen (Univ. Michigan) “Molecular interactions between two-dimensional Materials and Biological molecules at solid/liquid interfaces”

常時，70 名程度の聴衆がいて活発に質疑が行われ，楽しいひと時があったという間に過ぎた．拠点の支援に，心よりの御礼を申し上げる．



長谷川健（分子環境解析化学研究領域）

The 1st Germany–Japan–China Joint Workshop on Extremely Large π -Systems

主 催：京都大学化学研究所 (ICR), Max Planck Institute for Polymer Research (MPI-P)

共 催：国際共同利用・共同研究拠点 (iJURO)

日 時：2019 年 7 月 18 日 (木) 9 時 30 分～18 時 00 分

場 所：京都大学化学研究所・共同研究棟 (CL-110)

平成 31 年度国際共同研究の研究代表者である成田明光博士 (マックスプランク高分子研究所, ドイツ) と協力して「ドイツ-日本-中国連携国際ワークショップ」を京大化研で開催した。

今回のワークショップでは“Extremely Large π -Systems”をテーマとしているが、有機合成化学や高分子化学、有機デバイス化学などの幅広い研究分野の最新成果を共有することで、それぞれの分野で新しい研究の方向性や観点が創発されることを目的とした。当日は、マックスプランク高分子研究所から成田博士を含む若手研究者 5 名、中国で活躍するナノグラフェン分野の研究者 2 名、京大化研の若手研究者 6 名の計 13 名が口頭発表を行った。

本国際連携ワークショップのプログラムは、以下のとおりである。

1. T. Iwamoto (ICR, Kyoto Univ.) “Stereoselective Iron-catalyzed Coupling and Addition Reactions”
2. A. Narita (MPI-P, Germany) “Synthesis, Characterizations, and Edge-Functionalization of Structurally Well-Defined Graphene Nanoribbons”
3. Y. Hashikawa (ICR, Kyoto Univ.) “Water Entrapped Inside Fullerene Cages”
4. Y. Hu (Central South Univ., China) “Nonplanar Aromatics: Design, Synthesis, and Properties”
5. Z. Qiu (MPI-P, Germany) “Synthesis of seven-membered-rings embedded negatively curved nanographene”
6. M. Wakioka (ICR, Kyoto Univ.) “Direct Arylation Polymerization: A Simple Yet Highly Precise Method for the Synthesis of π -Conjugated Polymers”
7. Q. Chen (MPI-P, Germany) “Bottom-up Synthesis of Nanographene: From Partial Zigzag to Full Zigzag Edges”
8. K. Suzuki (ICR, Kyoto Univ.) “Development of Highly Efficient TADF OLEDs and Analysis of Organic Amorphous Film Using Dynamic Nuclear Polarization Enhanced NMR”
9. X. Wang (Nankai Univ., China) “Heteroatom-Doped Nanographenes: Synthesis and Properties”
10. Y. Ueda (ICR, Kyoto Univ.) “Site- and Stereoselective Molecular Transformation”
11. X. Yao (MPI-P, Germany) “Synthesis and Characterizations of Nanographenes with Designed Edge Structures and Unique Properties”
12. T. Nakamura (ICR, Kyoto Univ.) “Weakly Interacting Hydrogen Bond Networks for Controlling Molecular Orientation of Organic Semiconductor Thin Films”
13. I. C.-Y. Hou (MPI-P, Germany) “Toward Lateral Extension and Photo-Responsiveness of Polycyclic Aromatic Hydrocarbons”

会場には常時 20 名程度が集まり、若手研究者が中心となって研究分野を超えた質疑応答・議論が活発に行われ、若手研究者にとって国際的な場で研究討論を行う良い研鑽の場となった。拠点の支援に、心よりの御礼

を申し上げる。



廣瀬崇至（構造有機化学研究領域）

**The 12th Taiwan-Japan Bilateral Symposium
on Architecture of Functional Organic Molecules**
(第 12 回台湾－日本機能性有機分子構築に関する二国間シンポジウム)
実施報告書

会期：2019 年 8 月 30 日（金）～9 月 2 日（月）

会場：コープイン京都（京都市中京区柳馬場蛸薬師上ル井筒屋町 411）

表記会議が市内のコープイン京都で開催された。この会議は機能性有機分子の設計・合成から物性の解明、さらには応用に向けた基礎化学を行っている台湾と日本の化学者が集まり、研究の活性化と相互交流の促進を目的としている。開始当初は隔年の開催であったが、最近ではほぼ毎年、台湾と日本とで交互に開催されており、今回はその 12 回目である。今回の会議は京大工学研究科の松田健児教授を中心に台日計 5 名の組織委員で運営を行い、山子はその一員を務めた。京大化研の国際共同拠点、京大の SPIRITS、王立化学会、化学関係の会社と共にスポンサーとして会議をサポートした。合計 32 名が参加し、その内訳は台湾 14 名、日本 17 名、ドイツ 1 名であった。

会議は初日のミキサーの後、研究発表が 2 日間にわたりコープインで行われた。さらに、最終日は exchange meeting との名目で、京大の研究室見学を兼ねたディスカッションの時間を作り、共同研究の可能性を探るなど、交流を深めた。

研究成果発表は 25 分の口頭発表のみであり、台湾 13 名、日本 14 名、ドイツ 1 名の研究者の発表に加え、スポンサーでもある王立化学会から、最近の学術論文の出版情報に関する紹介があった。本会議が構造有機化学、物理有機化学を中心とした研究者の集まりから始まったことを反映し、 π 共役分子を中心とした、新規有機分子の構築とその物性・機能に関する研究発表が最も多く、金属表面を利用する新しい合成法、新規 π 共役分子等の合成、センサーや光－エネルギー転換材料等の分子機能とその最適化、さらに、 π 共役分子のホスト－ゲスト化学や超分子高分子への展開等の発表があった。さらに、光－電子移動反応の機構解明、新規不安定活性種の創製、最先端放射光を用いた分子の集積状態構造の解析等、有機分子の構築、構造、機能に関する幅広い話題の提供があり、活発な質疑応答がなされた。

参加者全員が高い研究の質と密な交流に満足し、会議は成功裏に終了した。拠点の支援に感謝する。



山子 茂（高分子制御合成領域）

3. 成果発表論文

紙数の都合により、目次に記載した論文の一部についてのみ、別刷りを次頁以降に掲載する。

Reversible Isomerizations between 1,4-Digermabenzene and 1,4-Digerma-Dewar-benzenes: Air-Stable Activators for Small Molecules

Tomohiro Sugahara,[†] Jing-Dong Guo,^{†,‡} Daisuke Hashizume,[§] Takahiro Sasamori,^{*,||} and Norihiro Tokitoh^{†,‡}

[†]Institute for Chemical Research, Kyoto University, Gokasho, Uji, Kyoto 611-0011, Japan

[‡]Integrated Research Consortium on Chemical Sciences, Kyoto University, Gokasho, Uji, Kyoto 611-0011, Japan

[§]RIKEN Center for Emergent Matter Science (CEMS), 2-1 Hirosawa, Wako, Saitama 351-0198, Japan

^{||}Graduate School of Natural Sciences, Nagoya City University, Yamanohata 1, Mizuho-cho, Mizuho-ku, Nagoya, Aichi 467-8501, Japan

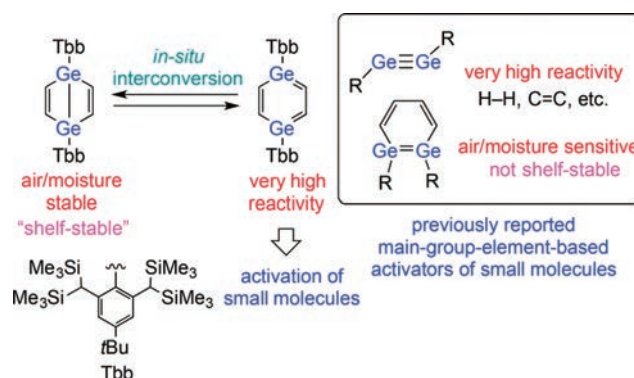
Supporting Information

ABSTRACT: The first examples of stable, crystalline, and air-sensitive 1,4-digermabenzene were isolated. These species photochemically isomerize into the corresponding air-stable digerma-Dewar-benzenes. More importantly, alkyl-substituted Dewar-type-1,4-digermabenzene can be considered as reversible “air-stable activators” for small molecules such as dihydrogen, carbon dioxide, and acetylene at room temperature. The regeneration of these activators can be accomplished via a thermal retro-isomerization that affords the corresponding 1,4-digermabenzene.

Classic aromatic compounds, i.e., $[4n + 2]\pi$ -electron cyclic conjugated systems such as benzene are widely known as intriguing chemical species with unusual electric, magnetic, and optical properties that have been applied to pharmaceuticals, organic electronic materials, and fluorescence probes.¹ In contrast to the wealth of physical functionality of benzene, its chemical functionality is relatively limited due to considerable aromatic stabilization energy.² However, replacing a C–H moiety of benzene with a main-group moiety (group 13/15 elements) significantly affects the physical and chemical properties of such cyclic- π -conjugated systems.³ Therefore, we are interested in the replacement of C–H or HC=CH moieties with moieties that contain heavier group-14 elements (E–R or RE = ER; E = Si, Ge, Sn, or Pb; R = organic substituent) in order to control the physical and chemical properties of the resulting metalla- and 1,2-dimetallabenzene.^{4–7} Although the isolation of the heavier-element analogues of benzene is difficult due to their extremely high propensity toward self-oligomerization and/or valence-isomerization,⁴ kinetic stabilization can effectively permit the isolation of stable metalla- and 1,2-dimetallabenzene (Chart 1).^{4–7}

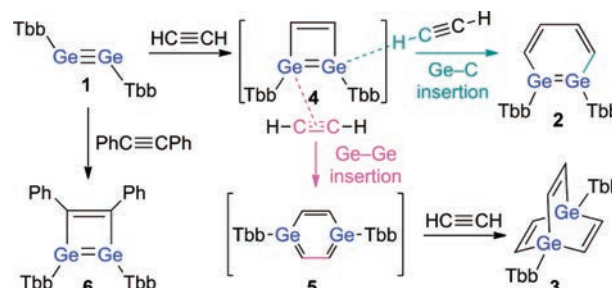
Although hitherto isolated 1,2-dimetallabenzene exhibit considerable aromaticity,^{6–8} they also show extremely high reactivity toward air, moisture, and alkynes. Accordingly, not only the physical but also the chemical properties of metalla- and 1,2-dimetallabenzene should be of great interest. While investigating the reactivity of the isolable digermene, TbbGe≡GeTbb (1; Tbb = 2,6-[CH(SiMe₃)₂]-4-*t*Bu-phenyl),⁷

Chart 1. Potential Small-Molecule Activators Containing Low-Coordinated Ge Atoms Such As Digermynes, 1,2-Digermabenzene, and 1,4-Digermabenzene



we observed that the reaction of 1 with acetylene resulted in the predominant formation of 1,2-digermabenzene 2 together with small amounts of 9,10-digermabarrelene 3 (Scheme 1).^{7b} The mechanism for the formation of 1,2-dimetallabenzene has been investigated on the basis of theoretical calculations,^{6c,7b} whereby 1,2-digermacyclobutadiene 4 was identified as a likely key intermediate for the final products (2 and 3). The Ge–C

Scheme 1. Synthesis and Potential Formation of Digermabenzene



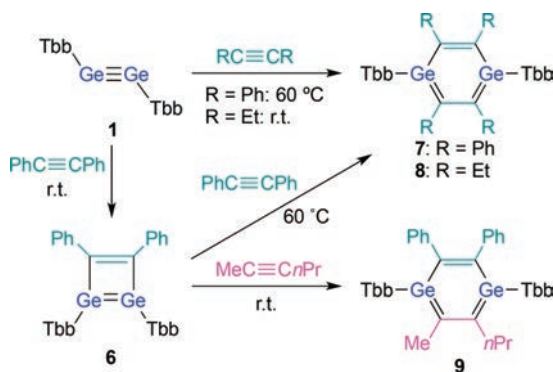
Received: January 5, 2019

Published: February 1, 2019

insertion of acetylene in **4**, initiated by a $\equiv\text{CH}\cdots\text{Ge}$ interaction, was calculated to afford **2** via a pathway with a slightly smaller barrier relative to that of a $\text{Ge}=\text{Ge}$ insertion of acetylene in **4** triggered by the $\text{C}\equiv\text{C}(\pi)\cdots\text{Ge}$ interaction that gives 1,4-digermabenzene **5**, followed by a facile further $[4 + 2]$ -cycloaddition with acetylene to furnish **3**. This proposed mechanism was experimentally corroborated by the isolation of 1,2-digermacyclobutadiene **6** from the reaction of **1** with tolan.^{7b,9} The aforementioned results of the theoretical calculations led us to speculate that the insertion of alkynes in the $\text{Ge}=\text{Ge}$ bond of **4** could be an appropriate synthetic route to unprecedented 1,4-digermabenzenes.¹⁰ While 1,2-dimetallabenzenes can be obtained from the reaction of stable dimetallynes¹¹ with alkynes,^{6,7} 1,3- and 1,4-dimetallabenzenes have not yet been isolated.^{12,13} The generation of a 1,4-silabenzene from the photochemical isomerization of a 1,4-disila-Dewar-benzene has been reported.¹⁴ The intriguing nature of the transiently generated 1,4-disilabenzene was demonstrated by, e.g., trapping with butadiene and benzene. However, further investigations on its chemical/physical properties, its aromaticity, and its behavior in the activation of small molecules have not been carried out, most likely due to the instability of the photogenerated species.¹⁵ Herein, we report the synthesis of stable 1,4-digermabenzenes, their photochemical isomerization reactions, and their behavior in the context of main-group-element-based activation of small molecules.

Stirring a mixture of tolan and 1,2-digermacyclobutadiene **6**, which was generated by the reaction of digermynes **1** with tolan, for 3 days in C_6D_6 at 60 °C quantitatively afforded the corresponding tetraphenyl-1,4-digermabenzene **7** (20% isolated yield)¹⁶ (Scheme 2). The alkyl-substituted 1,4-digermabenzene

Scheme 2. Synthesis of 1,4-Digermabenzenes 7–9



8 was obtained directly from digermynes **1**. Treatment of a C_6D_6 solution of digermynes **1** with an excess of 3-hexyne at room temperature quantitatively afforded 1,4-digermabenzene **8**. All attempts to isolate and/or observe the intermediate were unsuccessful, most likely due to the facile formation of **8**. Single crystals of **7** and **8** (*vide infra*) exhibit a crystallographic center of symmetry. However, we could not draw meaningful conclusions on whether the symmetry actually reflects the intrinsic electron density or if it is due to pseudocrystallographic symmetry caused by the severe disorder in the crystals. In order to circumvent this obstacle, unsymmetrically substituted 1,4-digermabenzene **9** was synthesized in 16% isolated yield from the reaction of the isolated 1,2-digermacyclobutadiene **6** with an excess of 2-hexyne in hexane at room temperature.

The structural parameters of isolated 1,4-digermabenzenes **7**–**9** were unambiguously determined by single-crystal X-ray diffraction analysis (Figure 1).¹⁷ 1,4-Digermabenzenes **7**–**9**

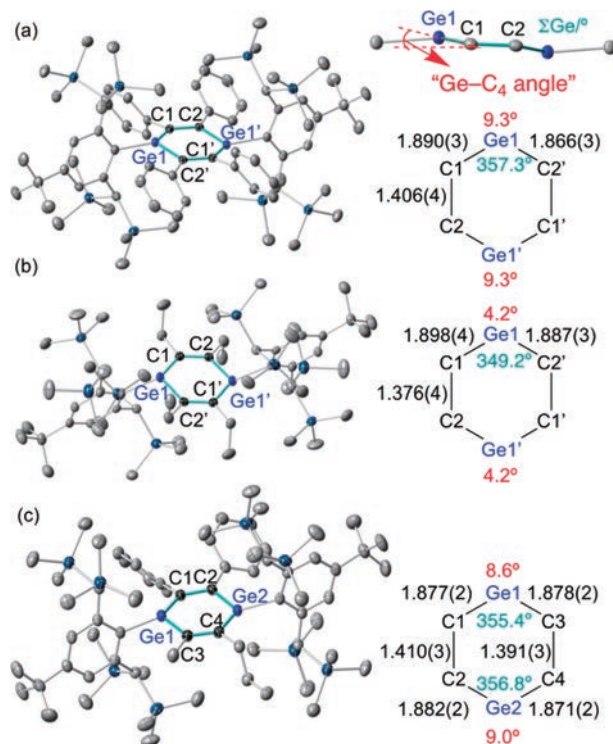


Figure 1. Molecular structures of 1,4-digermabenzenes (a) **7**, (b) **8**, and (c) **9** (ORTEP drawings with thermal ellipsoids set to 50% probability; hydrogen atoms are omitted for clarity) together with selected bond lengths (Å; black), Ge-C₄ bent angles (red), and angle sums around Ge (green).

exhibit virtually planar $[\text{Ge}_2\text{C}_4]$ rings, even though the Ge atoms slightly protrude the C_4 planes in a *trans*-pyramidalized fashion including Ge-C₄ angles of 4.0–9.0° (cf. Figure 1a). In addition, both Ge atoms are partially pyramidalized in a *trans*-pyramidalized fashion, which is reflected in the bond angle sums around the Ge atoms ($\Sigma\text{Ge} = 349\text{--}357^\circ$). 1,4-Digermabenzenes **7** and **8** contain crystallographic centers of symmetry at the center of the six-membered $[\text{Ge}_2\text{C}_4]$ ring, which would render a conclusion on the aromaticity based on the presence of bond alternation in the ring skeleton ambiguous. In the case of **9**, which does not contain a crystallographic center of symmetry, the four Ge-C bond lengths [1.877(2), 1.878(2), 1.882(2), 1.871(2) Å] in its $[\text{Ge}_2\text{C}_4]$ ring are similar to each other, suggesting a highly symmetric structure due to the cyclic conjugation of π -electrons as in aromatic rings. In addition, the Ge-C bond lengths fall in between typical values for Ge-C single and double bonds¹⁸ and are comparable to those of previously reported 1,2-digermabenzenes [1.883(2)–1.920(2) Å].⁷ The C-C bond lengths in the $[\text{Ge}_2\text{C}_4]$ ring [1.410(3) and 1.391(3) Å] fall within the typical range of C-C bonds in benzene rings. The structural features of 1,4-digermabenzenes **7** and **8** are very similar to those of **9**, suggesting that their highly symmetric structures should arise from the highly delocalized cyclic conjugation of π -electrons and not from crystallographic pseudodisorder. A combined consideration of the structural parameters suggests that the 1,4-digermabenzenes contain six

cyclic delocalized π -electrons on the $[\text{Ge}_2\text{C}_4]$ rings, which is indicative of considerable aromaticity.

The structural features of 7–9, including the experimentally observed bent geometries, could be reproduced by theoretical structure optimizations at the TPSSSTPSS-D3(BJ)/6-311G(2d,p) level of theory.¹⁹ The theoretically optimized structure of the parent 1,4-digermabenzene $\text{Ge}_2\text{C}_4\text{H}_6$ (**10**) at the MP2/6-311G(2d,p) or TPSSSTPSS-D3(BJ)/6-311G(2d,p) level of theory suggested completely planar geometries. Conversely, at the CASSCF(6,6)/6-311G(2d,p) level of theory, bent structures were obtained for **10** (Figure 2), suggesting that a partial open-

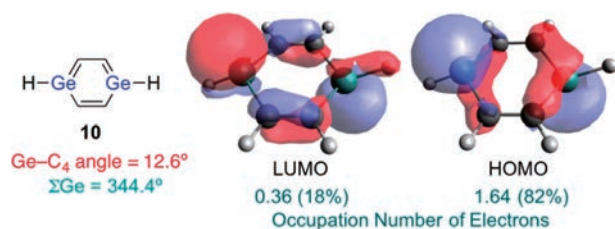
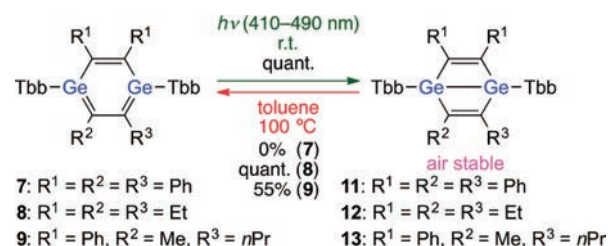


Figure 2. Frontier orbitals of parent 1,4-digermabenzene **10** calculated at the CASSCF(6,6)/6-311G(2d,p) level of theory.

shell character of the 1,4-digermabenzenes should be crucial to explain the bent structures. The corresponding diradical-character values ($y_0 = 0.36$) were calculated using the Yamaguchi scheme.²⁰ NICS(0) calculations^{21a} for 7–9 furnished negative NICS(0) values of -4.2 , -5.9 , and -5.0 , respectively, suggesting lower levels of aromaticity relative to benzene (-8.3 at the same level of theory). Similarly, NICS_{zz}(r) scan calculations^{21b} delivered NICS_{zz}(1.4) = -13.5 (**7**), NICS_{zz}(1.7) = -18.1 (**8**), and NICS_{zz}(1.5) = -15.6 (**9**), indicating that the alkyl-substitution might expand the frontier π -orbitals in the 1,4-digermabenzene ring relative to **10** (NICS(0) = -5.0 ; NICS_{zz}(1.4) = -17.3) based on the larger r values. The NICS(0) and NICS_{zz}(1.2) values for a planar geometry (D_{2h}) of **10** were much more negative (-6.6 and -19.6 , respectively) than those for a bent structure; in other words, a bent geometry of 7–9 would partially reduce their aromaticity.

1,4-Digermabenzenes 7–9 are NMR active and give sharp signals in their ^1H and ^{13}C NMR spectra, suggesting negligible radical character in C_6D_6 . The ^{13}C NMR signals for the $[\text{Ge}_2\text{C}_4]$ rings of 7–9 were shifted to low field [161.6–169.3 ppm], which is indicative of a ring current effect from the six π -electrons. The UV–vis spectra of 7–9 in hexane showed characteristic strong absorptions for their π – π^* electron transitions (**7**, $\lambda_{\text{max}}(\epsilon) = 442$ (10000) and 511 (8100); **8**, 468 (16000); **9**, 448 (2600)). Thus, it seems feasible to conclude that 7–9 retain their cyclic systems with six conjugated π -electrons in the crystalline state and in solution. Notably, 7–9 are photoresponsive when n -hexane solutions of 7–9 are exposed to LED light (410–490 nm).²² We observed facile photochemical isomerizations, resulting in the quantitative formation of the corresponding 1,4-digermabenzene Dewar-benzenes **11–13** (Scheme 3).^{17,23} While the photochemical isomerization of **7** into **11** was thermally irreversible, *i.e.*, a retro-conversion was not observed upon heating to 100 °C, **8** was regenerated quantitatively from heating **12** to 100 °C for 2 h in toluene. When a toluene solution of **13** was heated to 100 °C for 24 h, **9** was regenerated in 55% yield (^1H NMR yield). The thermal conversion of **11–13** can be reasonably interpreted in terms of the relative thermodynamic energies between the corresponding 1,4-digermabenzenes and the 1,4-digermabenzene Dewar-benzenes, *i.e.*, **11** is 6.9 kcal/mol more stable than **7**, and **12** is 2.2 kcal/mol less stable than **8**.¹⁹ Since the thermodynamic energies of **9** and **13** are comparable, the thermal reaction of **13** would result in a partial conversion giving **9**. It should be noted that **11–13** are inert toward air and moisture for at least 2 weeks, even though 7–9 are highly air- and moisture-sensitive.

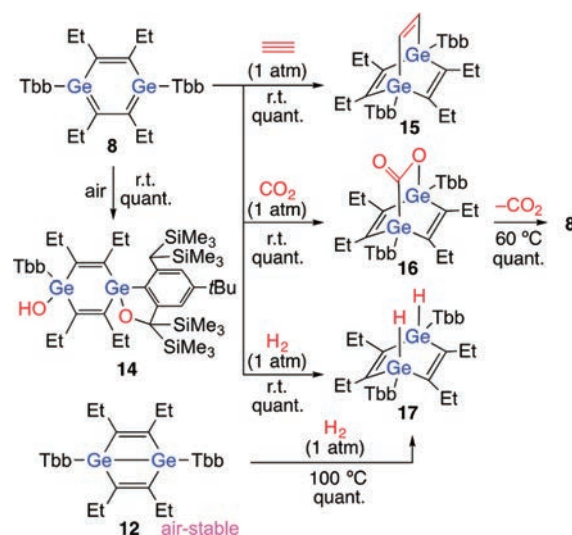
Scheme 3. Photoreactions of 1,4-Digermabenzenes 7–9



Dewar-benzenes, *i.e.*, **11** is 6.9 kcal/mol more stable than **7**, and **12** is 2.2 kcal/mol less stable than **8**.¹⁹ Since the thermodynamic energies of **9** and **13** are comparable, the thermal reaction of **13** would result in a partial conversion giving **9**. It should be noted that **11–13** are inert toward air and moisture for at least 2 weeks, even though 7–9 are highly air- and moisture-sensitive.

The extremely high reactivity of 7–9 toward air/moisture prompted us to examine their reactivity toward small inert molecules such as acetylene, CO_2 , and H_2 (Scheme 4).^{24,25}

Scheme 4. Reactions of 1,4-Digermabenzene **8** with Air, Acetylene, CO_2 , and H_2



Exposing **8** in C_6D_6 to air quantitatively afforded oxidized **14**. When an n -hexane solution of **8** was exposed to acetylene (1 atm), digermabarrelene **15** was quickly and quantitatively formed via a $[4 + 2]$ cycloaddition. Exposure of **8** in hexane to CO_2 (1 atm) quantitatively furnished $[4 + 2]$ cycloadduct **16**. Notably, the reaction of **8** with CO_2 is reversible, *i.e.*, heating a C_6D_6 solution of **16** to 60 °C afforded **8** via a retro- $[4 + 2]$ cycloaddition.²⁶ Moreover, **8** activates H_2 and cleaves the H–H bond, even under moderate conditions, *i.e.*, exposing an n -hexane solution of **8** to H_2 (1 atm, r.t., 30 min) afforded the reduced product **17**. Upon considering the photochemical and chemical reactivity of 1,4-digermabenzene **8** in its entirety, we developed the idea to activate H_2 with an air-stable compound. The reaction of air-stable 1,4-digermabenzene Dewar-benzene **12** with H_2 (1 atm, 100 °C, toluene, 2 h) resulted in the quantitative formation of hydrogen-adduct **17**, which should most likely be interpreted in terms of a thermal isomerization to give intermediate **8**, which can activate H_2 . Thus, 1,4-digermabenzene Dewar-benzene **12** can be considered as an air-stable main-

group-element-based activator for small molecules that can be thermally activated.

In summary, we have isolated the first stable 1,4-digermabenzenes (7–9), which exhibit central $[\text{Ge}_2\text{C}_4]$ rings with a cyclic conjugation of six π -electrons and indicate considerable levels of aromaticity despite their nonplanar structures. Compounds 7–9 are photoresponsive and easily isomerize into 1,4-digerma-Dewar-benzenes 11–13 upon exposure to visible light. In the case of alkyl-substituted 1,4-digermabenzenes 12 and 13, their thermal retro-reaction regenerates the 1,4-digermabenzenes. 1,4-Digermabenzene 8 is able to activate small molecules such as acetylene, CO_2 , and H_2 . 1,4-Digerma-Dewar-benzene 12 serves as a air-stable promoter for H_2 that can be thermally activated.

■ ASSOCIATED CONTENT

Supporting Information

The Supporting Information is available free of charge on the ACS Publications website at DOI: 10.1021/jacs.9b00129.

Experimental section and spectral data (PDF)

Theoretically optimized coordinates (XYZ)

Crystallographic data (CIF)

■ AUTHOR INFORMATION

Corresponding Author

*sasamori@nsc.nagoya-cu.ac.jp

ORCID

Tomohiro Sugahara: 0000-0002-7127-7571

Jing-Dong Guo: 0000-0002-3388-6181

Daisuke Hashizume: 0000-0001-7152-4408

Takahiro Sasamori: 0000-0001-5410-8488

Norihiro Tokitoh: 0000-0003-1083-7245

Notes

The authors declare no competing financial interest.

■ ACKNOWLEDGMENTS

This work was supported by JSPS KAKENHI grants JP15H03777 and JP15K13640 from MEXT (Japan), a Grant-in-Aid for Research at Nagoya City University, the Collaborative Research Program of the Institute for Chemical Research, Kyoto University, and the DAIKO FOUNDATION, as well as JURC, IRCCS, and KURCA (Kyoto University). The authors are grateful for the assistance of the Research Equipment Sharing Center at Nagoya City University. T.S. gratefully acknowledges support from a grant-in-aid for JSPS fellows (JP16J05501). The authors would also like to thank Mr. Toshiaki Noda and Ms. Hideko Natsume (Nagoya University) for the expert manufacturing of custom-tailored glassware.

■ REFERENCES

(1) (a) Taylor, R. D.; MacCoss, M.; Lawson, A. D. G. Rings in Drugs. *J. Med. Chem.* **2014**, *57*, 5845–5859. (b) Coropceanu, V.; Cornil, J.; Filho, D. A. d. S.; Olivier, Y.; Silbey, R.; Brédas, J.-L. Charge Transport in Organic Semiconductors. *Chem. Rev.* **2007**, *107*, 926–952. (c) Shimizu, M.; Hiyama, T. Organic Fluorophores Exhibiting Highly Efficient Photoluminescence in the Solid State. *Chem. - Asian J.* **2010**, *5*, 1516–1531. (d) Hong, Y.; Lam, J. W. Y.; Tang, B. Z. Aggregation-induced emission. *Chem. Soc. Rev.* **2011**, *40*, 5361–5388. (e) Zheng, Q.; Huang, J.; Sarjeant, A.; Katz, H. E. Pyromellitic Diimides: Minimal Cores for High Mobility n-Channel Transistor Semiconductors. *J. Am. Chem. Soc.* **2008**, *130*, 14410–14411. (f) Shimizu, M.; Takeda, Y.; Higashi, M.; Hiyama, T. 1,4-Bis(alkenyl)-2,5-dipiperidinobenzenes: Minimal Fluoro-

phores Exhibiting Highly Efficient Emission in the Solid State. *Angew. Chem., Int. Ed.* **2009**, *48*, 3653–3656.

(2) Minkin, V. J.; Glukhovtsev, M. N.; Simkin, B. Y. *Aromaticity and Antiaromaticity: Electronic and Structural Aspects*; Wiley: New York, 1994.

(3) (a) Märkl, G. 2,4,6-Triphenylphosphabenzene. *Angew. Chem., Int. Ed. Engl.* **1966**, *5*, 846–847. (b) Ashe, A. J., III The Group 5 heterobenzenes. *Acc. Chem. Res.* **1978**, *11*, 153–157. (c) Ashe, A. J., III *Topics in Current Chem.* **1982**, *105*, 125–155. (d) Herberich, G. E.; Ohst, H. Borabenzene Metal Complexes. *Adv. Organomet. Chem.* **1986**, *25*, 199–236. (e) Fu, G. C. The chemistry of borabenzenes (1986–2000). *Adv. Organomet. Chem.* **2001**, *47*, 101–119. (f) Berger, H.-O.; Nöth, H. Boron chemistry. 132. 1-phospha- and 1-arsa-4-boracyclohexadienes-2,5. *J. Organomet. Chem.* **1983**, *250*, 33–48. (g) Barnard, J. H.; Brown, P. A.; Shuford, K. L.; Martin, C. D. 1,2-Phosphaborines: Hybrid Inorganic/Organic P–B Analogues of Benzene. *Angew. Chem., Int. Ed.* **2015**, *54*, 12083–12086. (h) Noguchi, M.; Suzuki, K.; Kobayashi, J.; Yurino, T.; Tsurugi, H.; Mashima, K.; Yamashita, M. Planar and Bent BN-Embedded *p*-Quinodimethanes Synthesized by Transmetalation of Bis(trimethylsilyl)-1,4-dihydropyrazines with Chloroborane. *Organometallics* **2018**, *37*, 1833–1836. (i) Bosdet, M. J. D.; Piers, W. E. B–N as a C–C substitute in aromatic systems. *Can. J. Chem.* **2009**, *87*, 8–29. (j) Campbell, P. G.; Marwitz, A. J. V.; Liu, S.-Y. Recent Advances in Azaborine Chemistry. *Angew. Chem., Int. Ed.* **2012**, *51*, 6074–6092. (k) Bélanger-Chabot, G.; Braunschweig, H.; Roy, D. K. Recent Developments in Azaborine Chemistry. *Eur. J. Inorg. Chem.* **2017**, *2017*, 4353–4368.

(4) For selected reviews, see: (a) Tokitoh, N. New Progress in the Chemistry of Stable Metallaaromatic Compounds of Heavier Group 14 Elements. *Acc. Chem. Res.* **2004**, *37*, 86–94. (b) Nagase, S. Theory and Calculations of Molecules Containing Heavier Main Group Elements and Fullerenes Encaging Transition Metals: Interplay with Experiment. *Bull. Chem. Soc. Jpn.* **2014**, *87*, 167–195. (c) Tokitoh, N. Synthesis of Aromatic Species Containing a Heavier Group 14 Element by Taking Advantage of Kinetic Stabilization. *Bull. Chem. Soc. Jpn.* **2004**, *77*, 429–441.

(5) (a) Tokitoh, N.; Wakita, K.; Matsumoto, T.; Sasamori, T.; Okazaki, R.; Takagi, N.; Kimura, M.; Nagase, S. The Chemistry of Stable Silabenzenes. *J. Chin. Chem. Soc.* **2008**, *55*, 487–507. (b) Mizuhata, Y.; Fujimori, S.; Sasamori, T.; Tokitoh, N. Germabenzenylpotassium: A Germanium Analogue of a Phenyl Anion. *Angew. Chem., Int. Ed.* **2017**, *56*, 4588–4592. (c) Mizuhata, Y.; Fujimori, S.; Noda, N.; Kanesato, S.; Tokitoh, N. Generation of stannabenzenes and their monomer–dimer equilibration. *Dalton Trans.* **2018**, *47*, 14436–14444.

(6) (a) Kinjo, R.; Ichinohe, M.; Sekiguchi, A.; Takagi, N.; Sumimoto, M.; Nagase, S. Reactivity of a Disilyne $\text{RSi}\equiv\text{SiR}$ ($\text{R} = \text{Si}^i\text{Pr}[\text{CH}(\text{SiMe}_3)_2]_2$) toward π -Bonds: Stereospecific Addition and a New Route to an Isolable 1,2-Disilabenzene. *J. Am. Chem. Soc.* **2007**, *129*, 7766–7767. (b) Han, J. S.; Sasamori, T.; Mizuhata, Y.; Tokitoh, N. Reactivity of an aryl-substituted silicon–silicon triple bond: 1,2-disilabenzenes from the reactions of a 1,2-diaryldisilyne with alkynes. *Dalton Trans.* **2010**, *39*, 9238–9240. (c) Sugahara, T.; Guo, J.-D.; Hashizume, D.; Sasamori, T.; Nagase, S.; Tokitoh, N. The selective formation of a 1,2-disilabenzene from the reaction of a disilyne with phenylacetylene. *Dalton Trans.* **2018**, *47*, 13318–13322.

(7) (a) Sasamori, T.; Sugahara, T.; Agou, T.; Guo, J.-D.; Nagase, S.; Streubel, R.; Tokitoh, N. Synthesis and Characterization of a 1,2-Digermabenzene. *Organometallics* **2015**, *34*, 2106–2109. (b) Sugahara, T.; Guo, J.-D.; Sasamori, T.; Karatsu, Y.; Furukawa, Y.; Ferao, A. E.; Nagase, S.; Tokitoh, N. Reaction of a Stable Digermyne with Acetylenes: Synthesis of a 1,2-Digermabenzene and a 1,4-Digermabarrelene. *Bull. Chem. Soc. Jpn.* **2016**, *89*, 1375–1384. (c) Sugahara, T.; Guo, J.-D.; Sasamori, T.; Nagase, S.; Tokitoh, N. Regioselective Cyclotrimerization of Terminal Alkynes Using a Digermyne. *Angew. Chem., Int. Ed.* **2018**, *57*, 3499–3503.

(8) Baldrige, K. K.; Uzan, O.; Martin, J. M. L. The Silabenzenes: Structure, Properties, and Aromaticity. *Organometallics* **2000**, *19*, 1477–1487.

(9) Cui, C.; Olmstead, M. M.; Power, P. P. Reactivity of $\text{Ar}'\text{GeGeAr}'$ ($\text{Ar}' = \text{C}_6\text{H}_3\text{-2,6-Dipp}_2$, $\text{Dipp} = \text{C}_6\text{H}_3\text{-2,6-}i\text{Pr}_2$) toward Alkynes:

Isolation of a Stable Digermacyclobutadiene. *J. Am. Chem. Soc.* **2004**, *126*, 5062–5063.

(10) (a) Lee, V. Ya.; Yasuda, H.; Ichinohe, M.; Sekiguchi, A. SiGe₂ and Ge₃: Cyclic Digermenes that Undergo Unexpected Ring-Expansion Reactions. *Angew. Chem., Int. Ed.* **2005**, *44*, 6378–6381. (b) Sugahara, T.; Sasamori, T.; Tokitoh, N. 2,5-Digermaselenophenes: Germanium Analogues of Selenophenes. *J. Am. Chem. Soc.* **2018**, *140*, 11206–11209. (c) Sugahara, T.; Sasamori, T.; Tokitoh, N. Highly Bent 1,3-Digermasilaallene. *Angew. Chem., Int. Ed.* **2017**, *56*, 9920–9923. (d) Sugahara, T.; Tokitoh, N.; Sasamori, T. Synthesis of a Dichlorodigermasilane: Double Si–Cl Activation by a Ge=Ge Unit. *Inorganics* **2017**, *5*, 79–86. (e) Sugahara, T.; Sasamori, T.; Tokitoh, N. Chalcogenation Reaction of Cyclic Digermenes. *Chem. Lett.* **2018**, *47*, 719–722.

(11) (a) Fischer, R. C.; Power, P. P. π -Bonding and the Lone Pair Effect in Multiple Bonds Involving Heavier Main Group Elements: Developments in the New Millennium. *Chem. Rev.* **2010**, *110*, 3877–3923. (b) Asay, M.; Sekiguchi, A. Recent Developments in the Reactivity of Stable Disilynes. *Bull. Chem. Soc. Jpn.* **2012**, *85*, 1245–1261. (c) Sasamori, T.; Tokitoh, N. A New Family of Multiple-Bond Compounds between Heavier Group 14 Elements. *Bull. Chem. Soc. Jpn.* **2013**, *86*, 1005–1021. (d) Guo, J.-D.; Sasamori, T. Activation of Small Molecules by Compounds that Contain Triple Bonds Between Heavier Group-14 elements. *Chem. - Asian J.* **2018**, *13*, 3800–3817.

(12) (a) Maier, G.; Schöttler, K.; Reisenauer, H. P. 1,4-Disilabenzol. - Dimethoxysilylen als idealer synthesebaustein. *Tetrahedron Lett.* **1985**, *26*, 4079–4082. (b) Nakata, N.; Oikawa, T.; Matsumoto, T.; Kabe, Y.; Sekiguchi, A. Silyl-Substituted 1,4-Disila(Dewar benzene): New Synthesis and Unexpected Insertion of CO into the Si–Si Bond To Form a Disilyl Ketone. *Organometallics* **2005**, *24*, 3368–3370. (c) Sekiguchi, A.; Gillette, G. R.; West, R. A new route to 1,4-disilabenzene and 1,4-disilabarrelenes. *Organometallics* **1988**, *7*, 1226–1227. (d) Welsh, K. M.; Rich, J. D.; West, R. The generation of hexamethyl-1,4-disilabenzene and its novel thermal chemistry. *J. Organomet. Chem.* **1987**, *325*, 105–115.

(13) A 1,4-disilabenzene derivative supported by amidinato ligands with tetra-coordinated silicon atoms has been reported. For details, see: Sen, S. S.; Roesky, H. W.; Meindl, K.; Stern, D.; Henn, J. Synthesis, structure, and theoretical investigation of amidinato supported 1,4-disilabenzene. *Chem. Commun.* **2010**, *46*, 5873–5875.

(14) Kabe, Y.; Ohkubo, K.; Ishikawa, H.; Ando, W. 1,4-Disila(Dewarbenzene) and 1,4-Disilabenzene: Valence Isomerization of Bis-(alkylsilylcyclopropenyl)s. *J. Am. Chem. Soc.* **2000**, *122*, 3775–3776.

(15) (a) Priyakumar, U. D.; Saravanan, D.; Sastry, G. N. Isomers of Disilabenzene (C₄Si₂H₆): A Computational Study. *Organometallics* **2002**, *21*, 4823–4832. (b) Priyakumar, U. D.; Sastry, G. N. A Theoretical Study of the Structures, Energetics, Stabilities, Reactivities, and Out-of-Plane Distortive Tendencies of Skeletally Substituted Benzenes (CH)₃XH and (CH)₄(XH)₂ (X = B⁺, N⁺, Al⁺, Si, P⁺, Ga⁺, Ge, and As⁺). *J. Org. Chem.* **2002**, *67*, 271–281.

(16) Although **6** was quantitatively converted into **7**, the isolated yield of **7** was reduced to ca. 20% on account of the careful recrystallization processes that was applied in order to remove the residual excess of tolan.

(17) For XRD analyses, see the [Supporting Information](#) (CCDC-1879595–1879604).

(18) (a) Meyer, H.; Baum, G.; Massa, W.; Berndt, A. Stable Germaethenes. *Angew. Chem., Int. Ed. Engl.* **1987**, *26*, 798–799. (b) Couret, C.; Escudie, J.; Satge, J.; Lazraq, M. The first stable germene: a compound with a germanium-carbon double bond. *J. Am. Chem. Soc.* **1987**, *109*, 4411–4412. (c) Tokitoh, N.; Kishikawa, K.; Okazaki, R. Synthesis and Structure of the First Germaketenedithioacetal. *J. Chem. Soc., Chem. Commun.* **1995**, 1425–1426.

(19) The details of the theoretical calculations are shown in the [Supporting Information](#).

(20) Yamaguchi, K. The electronic structures of biradicals in the unrestricted Hartree-Fock approximation. *Chem. Phys. Lett.* **1975**, *33*, 330–335.

(21) (a) Schleyer, P. v. R.; Maerker, C.; Dransfeld, A.; Jiao, H.; Hommes, N. J. R. v. E. Nucleus-Independent Chemical Shifts: A Simple and Efficient Aromaticity Probe. *J. Am. Chem. Soc.* **1996**, *118*, 6317–

6318. (b) Stanger, A. Nucleus-Independent Chemical Shifts (NICS): Distance Dependence and Revised Criteria for Aromaticity and Antiaromaticity. *J. Org. Chem.* **2006**, *71*, 883–893.

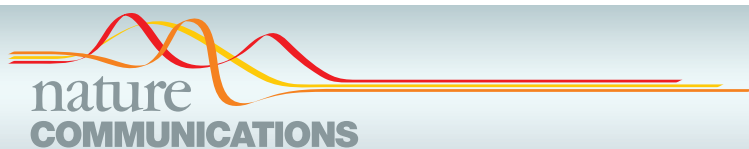
(22) Horspool, W. M. Equipment and Techniques. In *Synthetic Organic Photochemistry*; Springer: Boston, MA, 1984; pp 489–509. The filter solution was prepared using (1) NaNO₂ aq (1.0 M), (2) CuSO₄ aq (1.5 M), (3) NH₃ aq (4.0 equiv).

(23) Attempted trapping reactions of the expected biradical intermediates in the presence of 9,10-dihydroanthracene under otherwise identical conditions were unsuccessful.

(24) (a) Spikes, G. H.; Fetting, J. C.; Power, P. P. Facile Activation of Dihydrogen by an Unsaturated Heavier Main Group Compound. *J. Am. Chem. Soc.* **2005**, *127*, 12232–12233. (b) Chu, T.; Nikonov, G. I. Oxidative Addition and Reductive Elimination at Main-Group Element Centers. *Chem. Rev.* **2018**, *118*, 3608–3680. (c) Weetman, C.; Inoue, S. The Road Travelled: After Main-Group Elements as Transition Metals. *ChemCatChem* **2018**, *10*, 4213–4228.

(25) For activation reactions of H₂ and/or CO₂ using previously reported 1,4-dimetallabenzene derivatives, see: (a) Wu, D.; Kong, L.; Li, Y.; Ganguly, R.; Kinjo, R. 1,3,2,5-Diazadiborinine featuring nucleophilic and electrophilic boron centres. *Nat. Commun.* **2015**, *6*, 7340. (b) von Grothuss, E.; Diefenbach, M.; Bolte, M.; Lerner, H.-W.; Holthausen, M. C.; Wagner, M. Reversible Dihydrogen Activation by Reduced Aryl Boranes as Main-Group Ambiphiles. *Angew. Chem., Int. Ed.* **2016**, *55*, 14067–14071. (c) Wang, B.; Li, Y.; Ganguly, R.; Hirao, H.; Kinjo, R. Ambiphilic boron in 1,4,2,5-diazadiborinine. *Nat. Commun.* **2016**, *7*, 11871. (d) Taylor, J. W.; McSkimming, A.; Guzman, C. F.; Harman, W. H. N-Heterocyclic Carbene-Stabilized Boranthrene as a Metal-Free Platform for the Activation of Small Molecules. *J. Am. Chem. Soc.* **2017**, *139*, 11032–11035. (e) von Grothuss, E.; Prey, S. E.; Bolte, M.; Lerner, H.-W.; Wagner, M. Selective CO₂ Splitting by Doubly Reduced Aryl Boranes to Give CO and [CO₃]²⁻. *Angew. Chem., Int. Ed.* **2018**, *57*, 16491–16495.

(26) Detailed DFT calculations revealed the mechanisms for the reactions of **8** with CO₂ and H₂; both reactions proceed with very small free energy barriers of 5.4 and 7.8 kcal/mol, respectively. The barrier for the retro-reaction of **17** (22.3 kcal/mol) is much higher than that of **16** (14.9 kcal/mol); cf. [Supporting Information](#).






ARTICLE

<https://doi.org/10.1038/s41467-019-10616-z>

OPEN

Probabilistic controllability approach to metabolic fluxes in normal and cancer tissues

Jean-Marc Schwartz ¹, Hiroaki Otokuni², Tatsuya Akutsu ³ & Jose C. Nacher ²

Recent research has shown that many types of cancers take control of specific metabolic processes. We compiled metabolic networks corresponding to four healthy and cancer tissues, and analysed the healthy–cancer transition from the metabolic flux change perspective. We used a Probabilistic Minimum Dominating Set (PMDS) model, which identifies a minimum set of nodes that act as driver nodes and control the entire network. The combination of control theory with flux correlation analysis shows that flux correlations substantially increase in cancer states of breast, kidney and urothelial tissues, but not in lung. No change in the network topology between healthy and cancer networks was observed, but PMDS analysis shows that cancer states require fewer controllers than their corresponding healthy states. These results indicate that cancer metabolism is characterised by more streamlined flux distributions, which may be focused towards a reduced set of objectives and controlled by fewer regulatory elements.

¹Faculty of Biology, Medicine and Health, University of Manchester, Manchester M13 9PT, UK. ²Department of Information Science, Faculty of Science, Toho University, Funabashi 274-8510, Japan. ³Bioinformatics Center, Institute for Chemical Research, Kyoto University, Uji 611-0011, Japan. Correspondence and requests for materials should be addressed to J.-M.S. (email: jean-marc.schwartz@manchester.ac.uk) or to J.C.N. (email: nacher@is.sci.toho-u.ac.jp)

Metabolic pathways are essential chemical processes that catalyse complex reactions indispensable for development and life. Recent research has shown that many types of cancers take control of specific metabolic processes¹. In particular, cancer pathogenesis has recently been closely associated to serine, glycine and one-carbon metabolism². Preclinical analyses have shown that by adopting a specific diet that limits the amount of serine and glycine, tumour growth was severely inhibited.

Understanding how metabolic networks are controlled is a challenging question though. Metabolic control analysis was originally developed to evaluate how metabolic fluxes depend on kinetic parameters of enzymatic reactions or metabolite concentrations. The level of control is quantified by calculating control or elasticity coefficients^{3,4}. However, these approaches are not easily applicable to large systems since they rely on a kinetic model of the metabolic pathways. More recently, an approach was developed that uses flux couplings between metabolic reactions⁵. Flux couplings identify constrained relations between fluxes of different reactions, which arise from the network topology and mass conservation⁶. Five types of couplings were identified, namely directional, partial, full, anti and inhibitive couplings. The networks were analysed using a minimum dominating set (MDS) approach to identify potential driver nodes reactions⁵. The MDS approach was proposed by Nacher and Akutsu⁷ and has been used to analyse many biological systems and identify proteins associated to cancer^{8–12}. However, the flux coupling approach uses a discrete definition of coupling between reactions and does not take into account the full range of possible flux distributions that the metabolic system is able to support. For example, two reactions are defined as anti-coupled if when one of them is inactive then the other carries a non-zero flux (in a non-zero steady state), but this definition does not take into account the relation between both fluxes in situations where both reactions are active.

Here, we argue that in order to investigate the distributed control of metabolic flux in large-scale metabolic networks, a

different approach is needed. Coupling should be measured by a continuous value characterising the relations between reaction fluxes over all feasible steady states, instead of a set of binary values that represent particular subsets of steady states. In order to distinguish this continuous measure from previously used definitions of coupling, we hereon use the term correlation. Such a measure already exists: as demonstrated by Poolman et al.¹³, it can be obtained from the angles between the vectors forming an orthonormal basis of the null-space (or kernel) of the stoichiometric matrix defining the metabolic network. The cosine of this angle precisely represents Pearson's correlation coefficient between the fluxes carried by a pair of reactions over all possible steady states of the system, and was therefore named reaction correlation coefficient. Hence, the reaction correlation coefficient ϕ_{ij} of a pair of reactions i and j is a continuous value comprised between -1 and 1 , where $\phi_{ij} = 0$ indicates that the fluxes of both reactions are completely independent, $\phi_{ij} = 1$ indicates that they are perfectly correlated and $\phi_{ij} = -1$ indicates that they are perfectly anti-correlated.

In this work, we compiled metabolic networks corresponding to four healthy and cancer tissues, namely breast, lung, kidney and urothelial cancer. This data allows us to analyse the transition from healthy to cancer states from the metabolic flux perspective (Fig. 1). We first assembled a metabolic flux correlation network obtained from biochemical metabolic pathways in healthy and cancer tissues. Indeed, the above-mentioned flux correlation coefficient can be interpreted as a failure probability, which suggests that a probabilistic model can be suitable to address flux control. For example, a positive correlation interaction with value 1 could be understood as an interaction with failure probability of zero. Similarly, an absence of correlation with value 0 would suggest a failure probability of 1 . These concepts pave the way to the applicability of a probabilistic control theory for complex metabolic networks. Here, we used a Probabilistic Minimum Dominating Set (PMDS) model that can identify a minimum set of nodes that act as driver nodes and control the entire network in a context of probabilistic

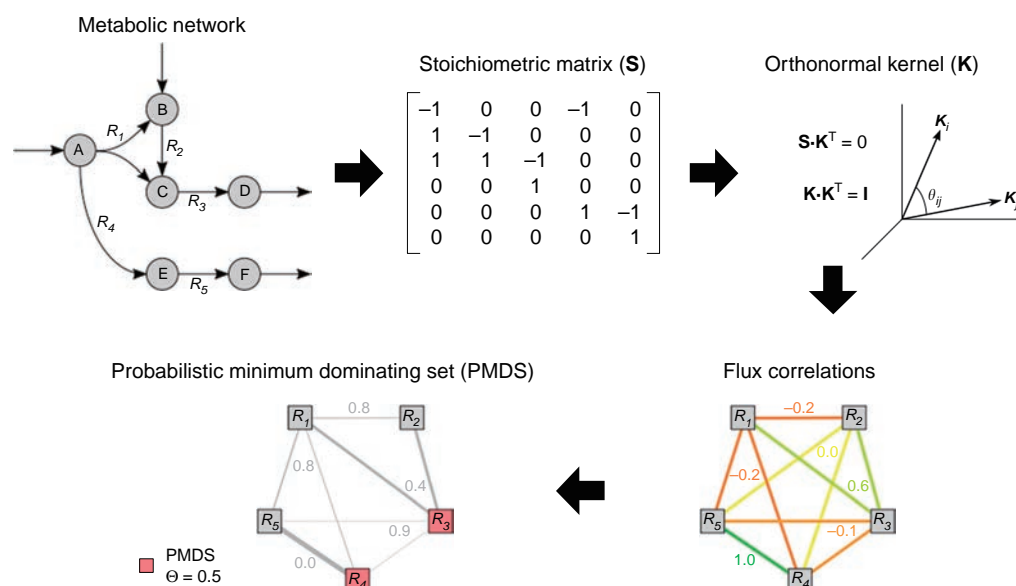


Fig. 1 Method for the application of probabilistic control theory to metabolic flux analysis. The stoichiometric matrix of the metabolic network is constructed and used to compute the orthonormal kernel matrix. The reaction correlation coefficient ϕ_{ij} is the cosine of the angle between the reaction rows in the kernel and represents the strength of control between both reactions. The failure probability ρ_{ij} is defined as $1 - |\phi_{ij}|$, which is used to determine the probabilistic minimum dominating set. We require that each node (reaction) is covered by multiple nodes in PMDS so that the probability that at least one edge (incoming flux) is active is greater than the threshold θ

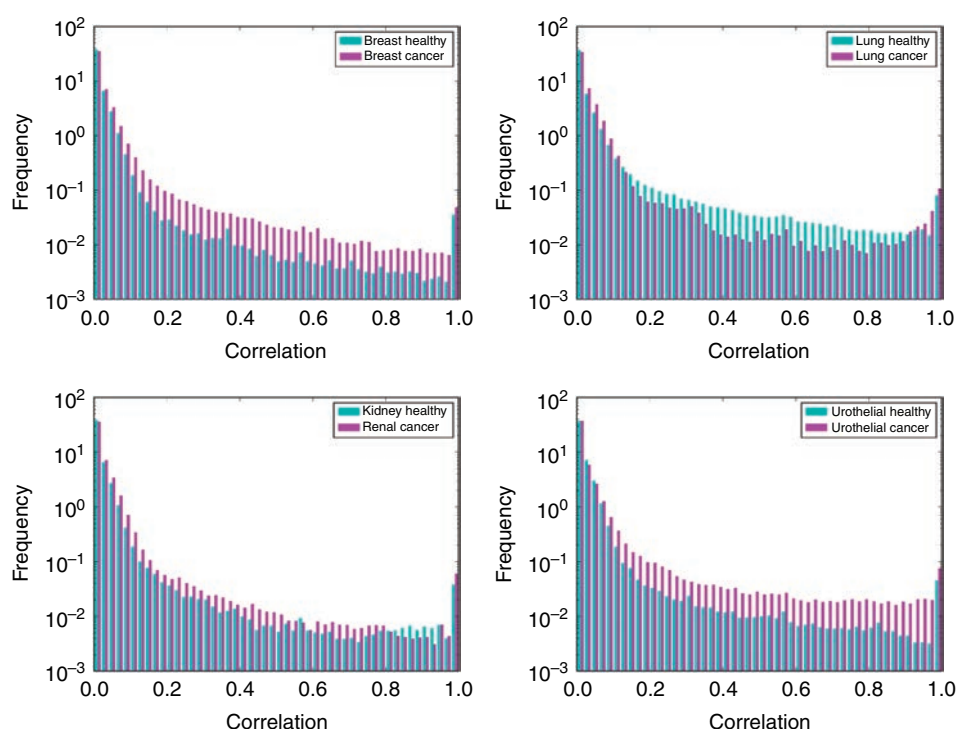


Fig. 2 Probability distribution of reaction correlations. Probability distribution of reaction correlations in healthy (blue) and cancer (purple) states of four human tissues

interaction failures¹⁴. In this network representation, the nodes are interpreted as metabolic reactions and the weighted edges correspond to the probabilistic flux exchanged among reactions. The application of PMDS in the context of metabolic fluxes makes it possible to connect controllability theory with flux correlations.

Results

Cancer metabolic reaction fluxes show higher correlations. Frequency distributions of all correlations in models of healthy and cancer cells corresponding to four different tissues were computed and the results are shown in Fig. 2. In general, we observed that the correlations are stronger in the cancer state than the healthy state for breast, kidney and urothelial tissues. However, for lung cancer the results show an opposite tendency with a weaker correlation distribution for the cancer state.

Statistical analysis of genome-scale metabolic flux networks. The clustering degree in all networks shows, however, a similar local structure (Table 1). This indicates that the differences observed in cancer states are not due to changes in the network structure, but to changes in the relations between fluxes.

We also determined the degree distributions in all these networks and found that they are similar and adhere to the classical scale-free distribution observed in most biological networks, including metabolic networks (Fig. 3). It is interesting that in spite of large metabolic flux changes, the global statistical pattern of the network remains conserved.

However, the specificity of lung cancer appears in the fraction of nodes connected to the giant connected component (Table 2 and Fig. 4). Breast, urothelial and renal cancers show larger giant components than the corresponding healthy states. In contrast, healthy lung tissue shows a larger giant component than the

Table 1 Topological properties of the complete metabolic networks

Network	Clustering coefficient	Connected components
Breast healthy	0.780	4
Breast cancer	0.766	7
Lung healthy	0.772	5
Lung cancer	0.771	8
Kidney healthy	0.770	6
Renal cancer	0.764	5
Urothelial healthy	0.780	6
Urothelial cancer	0.769	8

cancer state. This may imply a higher correlation between fluxes in the cancer state for 3 out of 4 cancer types.

Cancer states require fewer controllers except in lung cancer.

Based on the PMDS model described in the Methods section, we computed the number of reactions necessary to achieve full control of each network in a probabilistic context of flux correlations. We calculated the PMDS for each network using different values of Θ (threshold probability). The results (Fig. 5) show that the fraction of driver nodes is smaller in all cancer tissues compared to their corresponding healthy states, suggesting that it may be theoretically easier to control these cancer states. This change is consistent with an increase in flux correlations observed in three out of four cancer states. In lung the PMDS fraction is still smaller in the cancer state, even though the healthy state shows higher flux correlations than the cancer state. The size of the largest component is higher in the healthy state for lung, which may explain the observed higher correlations.

To account for possible inaccuracies in the original models, we verified that these results are stable with respect to small

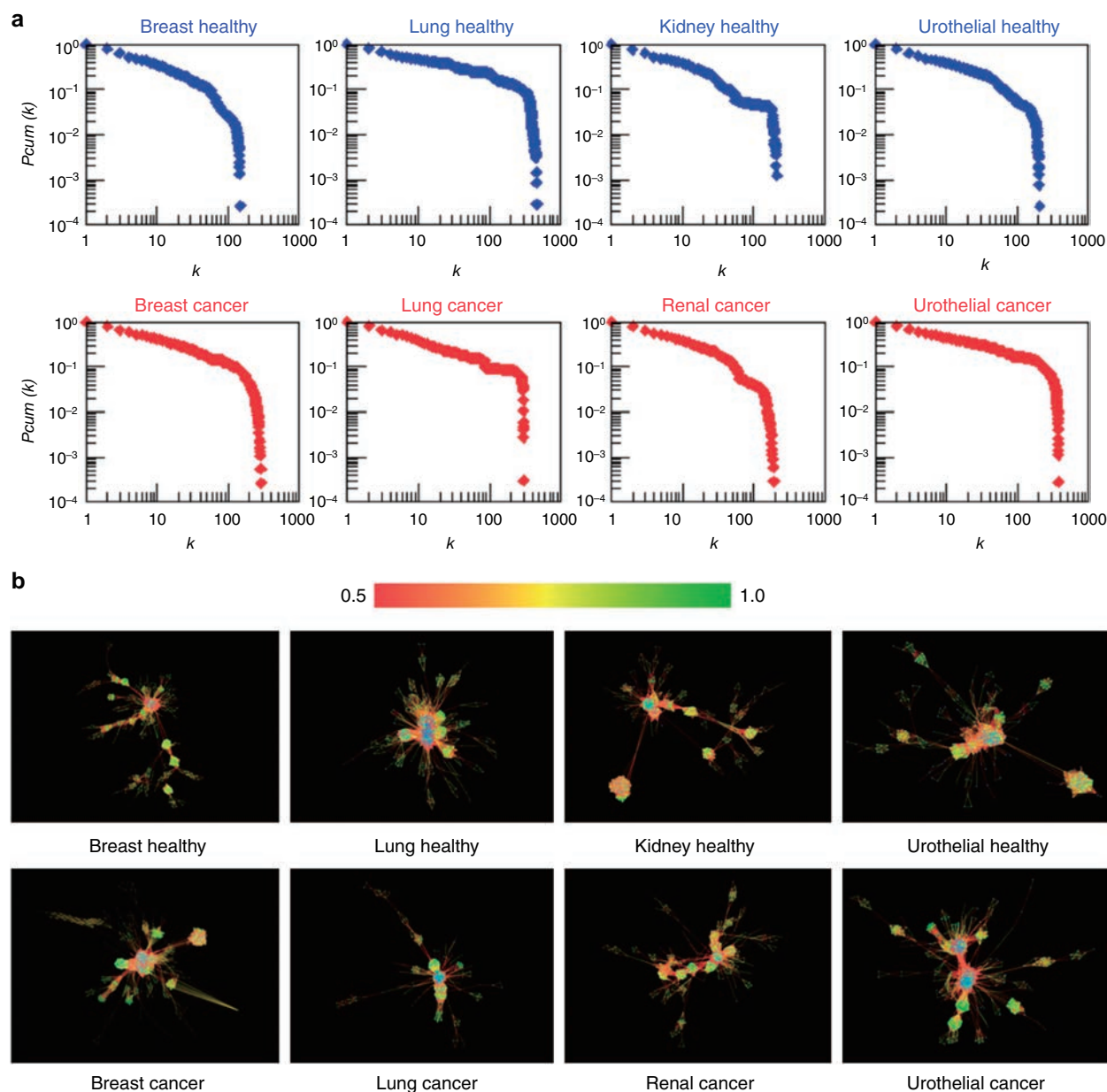


Fig. 3 Topology of healthy and cancer networks. **a** Cumulative degree distributions of healthy and cancer high flux correlation networks. **b** Visual representation of high flux correlation networks; the edge colour represents the flux correlation ranging from 0.5 (red) to 1.0 (green)

Table 2 Properties of high flux correlation networks in healthy and cancer states of human tissues			
Network	Total network size	Size of giant component	Fraction of giant component
Breast healthy	3729	611	0.164
Breast cancer	3741	1103	0.295
Lung healthy	3510	1091	0.311
Lung cancer	3350	598	0.179
Kidney healthy	3986	711	0.178
Renal cancer	3444	677	0.197
Urothelial healthy	3890	660	0.170
Urothelial cancer	3618	1078	0.298

alterations in the topologies of the four healthy and cancer networks. For each tissue type and for each value of Θ , we constructed 10 randomised networks by rewiring 1%, 5% and 10% of the edges, respectively. In order to conserve the topological properties of the networks during randomisation, we applied an edge rewiring algorithm that preserves the degree distribution (see Methods). Even with a moderate perturbation of 10%, the average PMDS fraction only marginally increased and the PMDS fraction in the healthy state always remained larger than in the corresponding cancer state (Supplementary Figs 1, 2 and 3).

Distribution of controllers in metabolic pathways. In order to compare the controller and non-controller nodes from a perspective of biological significance, we analysed the distribution of

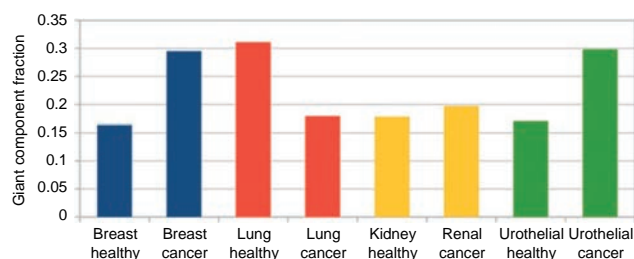


Fig. 4 Fraction of giant component in healthy and cancer tissues. In these networks, nodes represent reactions and two reactions are connected if the absolute flux correlation between them is higher than 0.5, as described in Methods. The giant component is the largest connected component in each network; the fraction was calculated by dividing the number of nodes in the giant component through the total number of nodes in each network

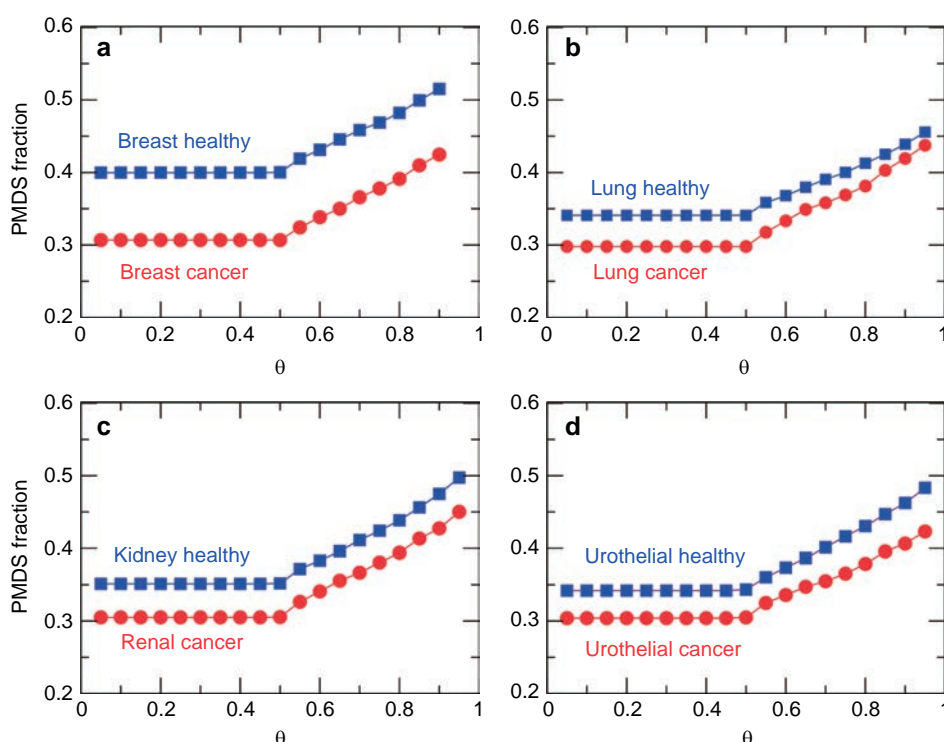


Fig. 5 Fraction of PMDS in healthy and cancer tissues. **a–d** The PMDS fraction in four healthy (blue) and cancer (red) tissues is displayed for different values of the threshold θ

PMDS and non-PMDS nodes among metabolic pathways from the KEGG database. Since we are using metabolic models, a comparison to metabolic pathways is more appropriate than for example the Gene Ontology, which contains other types of biological functions not included in the data. We found that some central metabolic pathways are enriched in PMDS nodes across cancer and non-cancer networks: these pathways include glycolysis (p -values from 0.009 to 0.06; all p -values derived from two-tailed Fisher exact tests) and pyruvate metabolism (p -values from 0.003 to 0.06, except renal cancer $p = 0.12$). The citrate cycle is significantly enriched in PMDS nodes in breast and renal tissues (p -values from 0.01 to 0.05) but not in urothelial and lung; inositol phosphate metabolism was enriched in healthy breast ($p = 0.03$). Conversely, aminoacyl-tRNA biosynthesis was significantly depleted in PMDS nodes in all cancer and non-cancer networks (p -values from $3e-5$ to 0.05), as well as N-glycan biosynthesis (p -values from $3e-5$ to 0.03). Overall, the fact that a higher proportion of controller nodes are found in central

metabolic pathways is consistent with expectations, since these pathways distribute fluxes towards other parts of the metabolic network, and this property is maintained between healthy and cancer cells. Additionally, these results confirm that each cancer type has distinctive characteristics in terms of pathways enriched in PMDS nodes, with lung cancer being more distinct than the three other types.

Folate cycle subnetwork. There is growing evidence of relations between metabolic perturbations and cancer. In particular, serine and glycine pathways were found to be associated with oncogenesis². These amino acids feed into the folate cycle, whose outputs feed into the synthesis of nucleotides and phospholipids. To illustrate how control analysis can shed light on changes occurring in metabolic pathways, we show the results obtained on a subnetwork centred on the folate cycle (Fig. 6).

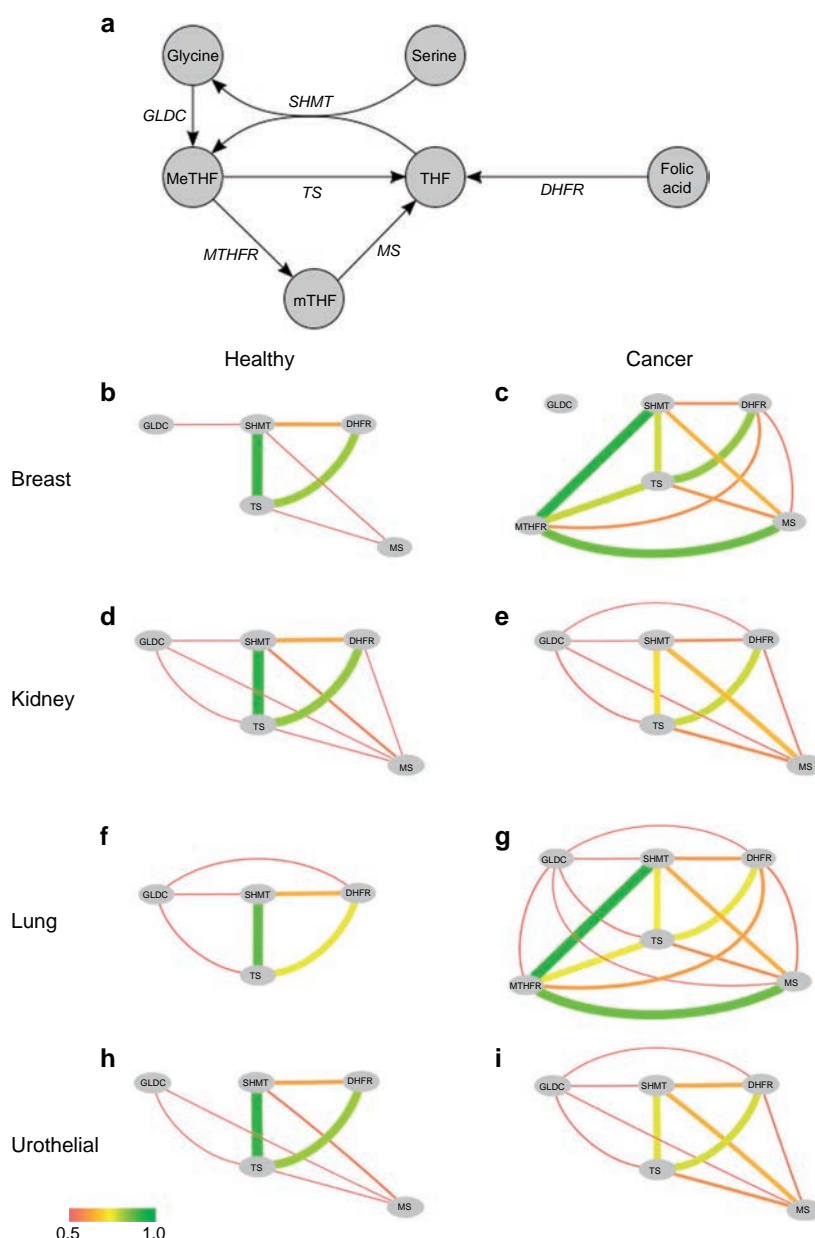


Fig. 6 Flux correlation changes in the folate cycle. **a** Simplified representation of the folate cycle. In this representation, nodes represent metabolites and edges represent metabolic reactions. **b–i** Reaction correlation coefficients in the metabolic system depicted in A for four types of healthy and cancer tissues. In these representations, nodes represent metabolic reactions and the edge colour represents the flux correlation value between the reactions connected by the edge; the colour bar represents the correlations value from red (0.5) to green (1.0). Abbreviations: THF, tetrahydrofolate; MeTHF, 5-10-methylene-tetrahydrofolate; mTHF, 5-methyl-tetrahydrofolate; DHFR, dihydrofolate reductase; GLDC, glycine decarboxylase; MS, methionine synthase; MTHFR, methylene-tetrahydrofolate reductase; SHMT, serine hydroxymethyl transferase; TS, thymidylate synthase

In the healthy states, we observe that SHMT and TS are strongly coupled (Fig. 6b, d, f, h) indicating that the production of THF is strongly coupled to its methylation into MeTHF. In addition, there is a strong positive correlation between TS and DHFR, which means that THF production from folic acid is also coupled to the THF cycle. In the cancer states though, these correlations become weaker (Fig. 6c, e, g, i) and several new connections appear. In breast and lung cancer, MTHFR becomes strongly coupled to SHMT and MS, suggesting that the folate cycle uses mTHF as an intermediate rather than direct transformation of MeTHF to THF. Overall, the cancer states induce more flux interactions between reactions of the THF

system. This increases the complexity of the relations and at the same time opens more possibilities to control the fluxes in the system.

Discussion

Links between metabolism and cancer have been known for a long time, as sustained aerobic glycolysis is well known to occur in cancer cells¹⁵. How these changes are connected to cell proliferation and accumulation is not well understood though. It was also widely observed that obesity increases cancer risk, which raises questions about the existence of causal links between

increased metabolic activity and tumour progression. Conversely, large animals with low metabolic rate are generally found to have lower incidence of cancer than smaller animals with faster metabolic rate, which strengthens the view that metabolic activity could be a factor favouring cancer, at least as important as mutations¹⁶. Several oncogenes are known to stimulate metabolic pathways, in particular glucose and glutamine metabolism¹⁷. Alternative carbon sources such as acetate were found to be better utilised by tumour cells than normal tissue¹⁸. Metabolic flux distributions in tumour cells were observed to correlate with increased lactate production¹⁹ and to maintain levels of NADPH, allowing cells to better resist to oxidative stress^{20,21}.

Our results show that, in the four tissue types for which comparative models of healthy and cancer metabolic networks are available, namely breast, lung, kidney and urothelial, controllability in cancer metabolism is easier than that in healthy metabolism. A generic interpretation of this result can be found by combining knowledge from Fig. 3. The network visualization shows significant flux correlation changes. However, the cumulative degree distribution shows that, in spite that many reactions change flux correlations, the global statistical degree pattern of the network does not change and still follows a power-law for the degree of nodes. This is important technically because in general the PMDS can be computed faster in networks that have a power-law distribution, i.e. scale-free networks. However, the new flux distribution in cancer state seems to be more highly correlated (lower failure probabilities) as shown in Fig. 2, which makes cancer states easier to control from a PMDS view point since key flux routes have lower probability of failure. Indeed, these results are based on comparative analyses of metabolic reconstructions of cancer and healthy tissues and remain dependent on the quality of the models used. Nevertheless, we verified that these results are preserved under moderate alterations of the networks, and as the quality of metabolic models increases and new models become available for other tissue types, these properties can be further tested in the future. It is worth mentioning that other types of analyses not related to controllability may be able to identify differences between cancer and healthy metabolism. For example null-space analysis can characterise properties of genome-scale metabolic networks based on stoichiometry alone¹³ and other types of constraints such as thermodynamics may be taken into consideration.

Nevertheless, specific differences in metabolic flux correlations were observed in lung cancer. These differences were also reflected in the number of reactions assembled in the main connected component of the network. Heterogeneity in metabolic pathway activity has been reported before, not only between different types of cancers²² but also between different types of lung tumours^{23,24}. In spite of the heterogeneous metabolic flux response observed in cancers and in particular a large fluctuation of active correlations (i.e. number of links) among reactions in lung cancer, the number of necessary reactions to be controlled in cancer does not largely change. More importantly, the metabolic flux space in cancer remains easier to control than that in healthy state.

The number of active correlations in lung cancer is twice as large as that number in breast cancer. Counterintuitively, the PMDS size of both lung and breast cancer is lower than that in the corresponding healthy state. This indicates that the size of the reaction control backbone of both lung and breast cancer is very similar. The increase in correlations observed in lung cancer, consistent with the already reported variability on cancer metabolism, might only perform peripheral metabolic functions without critical control roles. Glutamine metabolism is altered in many types of cancer cells, but the consumption of glutamine by lung cancer cells is higher than in other cancer types²⁵.

The glutamine metabolic pathway is tightly interconnected with the mTOR signalling pathway, which promotes cell survival and is activated by glutamine efflux; this particular feature is being investigated for potential therapeutic applications²⁶. The tyrosine kinase epidermal growth factor receptor (EGFR) is frequently mutated in non-small cell lung cancer and has strong interrelations to several metabolic pathways. It was shown that EGFR signalling promotes not only glucose consumption and lactate production, but also de novo pyrimidine synthesis, therefore it plays a major regulatory role on global metabolism²⁷. Different KRAS mutations are also found in lung cancer, which do not have the same cellular activity. It was shown that they affect different metabolic pathways, with distinguishing effects in particular in the glutaminolysis and glutathione pathways²⁸. These examples show that, in addition to strong metabolic effects shared with other types cancers such as aerobic glycolysis, lung cancers can also be characterised by original relations with metabolic pathways. The full extent of these relations is still poorly understood but is an active area of research towards new therapies²⁵.

Methods

Computation of reaction correlation coefficients. The computation starts by constructing the stoichiometric matrix of the network, S , whose elements are the stoichiometric coefficients of each metabolite in each reaction. The kernel matrix K is defined by vectors constituting a basis of the null-space of S , such that $S K^T = 0$.

In most cases, K is not unique. However, if the vectors of K form an orthonormal basis, which means $K K^T = I$, then the angles θ_{ij} between the row vectors of K are invariant. The reaction correlation coefficient ϕ_{ij} is defined as the cosine of θ_{ij} :

$$\phi_{ij} = \frac{k_i k_j^T}{\sqrt{(k_i k_i^T)(k_j k_j^T)}} = \cos(\theta_{ij}) \quad (1)$$

where k_i and k_j are the row vectors of K corresponding to reactions i and j respectively. As demonstrated in Poolman et al.¹³, ϕ_{ij} represents the Pearson correlation coefficient between the fluxes carried by reactions i and j over all possible steady states of the system. The mathematical demonstration is based on introducing a random matrix R that contains all possible steady states, s being the number of steady states which can be arbitrarily large. Then the Pearson correlation r of this distribution is defined, and when s tends towards infinite it is shown that r tends towards a product of k vectors, which represents the cosine of the angle.

We calculated K using the *null* function in Matlab and verified that it meets the orthonormality condition for each metabolic network. After obtaining ϕ_{ij} for each pair of reactions, the probability of failure between reactions i and j was defined as $\rho_{ij} = 1 - \text{abs}(\phi_{ij})$.

Probabilistic control model. Natural and engineered complex networks are composed of thousands of nodes and tens of thousands of links. These links representing regulatory interactions or transmission lines suffer from probabilistic failures. The flux correlation coefficient allows us to define the probability of failure between reactions i and j (ρ_{ij}) and integrate it into a probabilistic control model. We want each node (reaction) to be covered by multiple nodes in MDS so the probability that at least one edge (incoming flux) is active is at least Θ . This problem can be formulated as a probabilistic minimum dominated (PMDS) as follows. Let S be a dominating set, then we require S to satisfy:

$$\left(1 - \prod_{i \in S} \rho_{ij}\right) \geq \Theta, \forall j \in V \quad (2)$$

which can be rewritten as:

$$\sum_{i \in S} -\ln(\rho_{ij}) \geq -\ln(1 - \Theta) \quad (3)$$

where ρ_{ij} indicates the probability of failure between reactions (i, j) .

The standard MDS problem is formalized by the following integer linear programming (ILP) problem:

$$\text{Minimise } \sum_{i \in V} x_i$$

subject to:

$$x_i + \sum_{(j,i) \in E} x_j \geq 1, \quad (4)$$

$$x_i \in \{0, 1\}, \forall i \in V,$$

where an MDS is obtained by the set $\{x|x_i = 1\}$, V indicates the set of reaction nodes in the network and E denotes the set of undirected edges between reaction nodes. Then, inserting the probabilistic condition shown in Eqs 2 into 3 leads to the PMDS formalized as the following ILP:

$$\begin{aligned} & \text{Minimise } \sum_{i \in V} x_i, \\ & \text{subject to: } x_j \geq 1, \forall j \in V \text{ such that } \deg(j) = 0, \\ & -\ln(1 - \Theta)x_j + \sum_{(i,j) \in E} (-\ln(\rho_{ij})x_i) \geq -\ln(1 - \Theta), \forall j \in V \text{ such that } \deg(j) > 0, \end{aligned} \quad (5)$$

$$x_i \in \{0, 1\}, \forall i \in V$$

where $\deg(j)$ denotes the degree of reaction node j . In the above expression, the first term $-\ln(1 - \Theta)x_j$ is added because if node j is included in the PMDS, the inequality needs to be hold. In the implementation of the ILP-based method, a small number (10^{-6}) is added to ρ_{ij} to avoid infinity occurrence at $\rho_{ij} = 0$. The ILP problem was solved using the IBM ILOG CPLEX Optimiser package version 12.0.

Construction of cancer networks. Genome-scale models representing human metabolic pathways in healthy and cancer states were compiled from Basler et al.⁵ and Gatto et al.²⁹ Supplementary data. Then, flux correlation networks were constructed by computing the reaction correlation coefficients. To create healthy and cancer networks a threshold of 0.5 was used, which means that absolute correlations smaller than 0.5 were deleted, or conversely that failure probabilities higher than 0.5 were deleted; in the resulting networks, nodes represent reactions and two reactions are connected if their correlation is higher than 0.5. This means that we are considering the high flux correlation networks in our analysis.

Construction of randomised networks. For each tissue type and for each value of Θ , we constructed 10 randomised networks by rewiring 1%, 5% and 10% of the edges, respectively. We used the `rewire` function from the R `igraph` package, together with the `keeping_degseq` function that preserves the original network's degree distribution, in order to conserve the topological properties of the networks.

Pathway enrichment analysis. We analysed the distribution of PMDS and non-PMDS nodes across all metabolic pathways of the KEGG database in order to determine whether some pathways are significantly enriched or depleted in controller nodes. Enzyme Commission numbers associated to reactions were extracted from the raw metabolic models, then were mapped to PMDS and non-PMDS node lists in the same conditions as described above. These node lists were searched against KEGG pathways using the KEGG Mapper tool³⁰ in order to obtain the number of PMDS and non-PMDS nodes in each pathway, then two-tailed Fisher exact tests were conducted using R in order to determine significant enrichment or depletion.

Reporting summary. Further information on research design is available in the Nature Research Reporting Summary linked to this article.

Data availability

The models used in this study are available from <https://doi.org/10.1101/gr.202648.115>, Supplemental Material section. Data that support the tables and figures of this study are available from the corresponding authors upon request.

Code availability

Custom code used in this study is available from the corresponding authors upon request.

Received: 8 June 2018 Accepted: 17 May 2019

Published online: 20 June 2019

References

- Yang, W. et al. Potentiating the antitumour response of CD8⁺ T cells by modulating cholesterol metabolism. *Nature* **531**, 651–655 (2016).
- Locasale, J. W. Serine, glycine and one-carbon units: cancer metabolism in full circle. *Nat. Rev. Cancer* **13**, 572–583 (2013).
- Kacser, H. & Burns, J. A. The control of flux. *Biochem. Soc. Trans.* **23**, 341–366 (1995).
- Fell, D. *Understanding the Control of Metabolism*. (Portland Press, 1997).
- Basler, G., Nikoloski, Z., Larhlmi, A., Barabási, A.-L. L. & Liu, Y.-Y. Control of fluxes in metabolic networks. *Genome Res.* **26**, 956–968 (2016).

- Burgard, A. P., Nikolaev, E. V., Schilling, C. H. & Maranas, C. D. Flux coupling analysis of genome-scale metabolic network reconstructions. *Genome Res.* **14**, 301–312 (2004).
- Nacher, J. C. & Akutsu, T. Dominating scale-free networks with variable scaling exponent: heterogeneous networks are not difficult to control. *New J. Phys.* **14**, 073005 (2012).
- Molnár, F., Sreenivasan, S., Szymanski, B. K. & Korniss, G. Minimum dominating sets in scale-free network ensembles. *Sci. Rep.* **3**, 1736 (2013).
- Wuchty, S. Controllability in protein interaction networks. *Proc. Natl Acad. Sci. USA* **111**, 7156–7160 (2014).
- Zhang, X.-F., Ou-Yang, L., Zhu, Y., Wu, M.-Y. & Dai, D.-Q. Determining minimum set of driver nodes in protein-protein interaction networks. *BMC Bioinforma.* **16**, 146 (2015).
- Kagami, H., Akutsu, T., Maegawa, S., Hosokawa, H. & Nacher, J. C. Determining associations between human diseases and non-coding RNAs with critical roles in network control. *Sci. Rep.* **5**, 14577 (2015).
- Sun, P. G. Co-controllability of drug-disease-gene network. *New J. Phys.* **17**, 085009 (2015).
- Poolman, M. G., Sebu, C., Pidcock, M. K. & Fell, D. A. Modular decomposition of metabolic systems via null-space analysis. *J. Theor. Biol.* **249**, 691–705 (2007).
- Nacher, J. C. & Akutsu, T. Structurally robust control of complex networks. *Phys. Rev. E* **91**, 01282(2015).
- Warburg, O. On the origin of cancer cells. *Science* **123**, 309–314 (1956).
- Dang, C. V. Links between metabolism and cancer. *Genes Dev.* **26**, 877–890 (2012).
- Borouh, L. K. & DeBerardinis, R. J. Metabolic pathways promoting cancer cell survival and growth. *Nat. Cell Biol.* **17**, 351–359 (2015).
- Mashimo, T. et al. Acetate is a bioenergetic substrate for human glioblastoma and brain metastases. *Cell* **159**, 1603–1614 (2014).
- Schwartz, J.-M., Barber, M. & Soons, Z. Metabolic flux prediction in cancer cells with altered substrate uptake. *Biochem. Soc. Trans.* **43**, 1177–1181 (2015).
- Jeon, S.-M. M., Chandel, N. S. & Hay, N. AMPK regulates NADPH homeostasis to promote tumour cell survival during energy stress. *Nature* **485**, 661–665 (2012).
- Zielinski, D. C. et al. Systems biology analysis of drivers underlying hallmarks of cancer cell metabolism. *Sci. Rep.* **7**, 41241 (2017).
- Mehrmohamadi, M., Liu, X., Shestov, A. A. & Locasale, J. W. Characterization of the usage of the serine metabolic network in human cancer. *Cell Rep.* **9**, 1507–1519 (2014).
- Hensley, C. T. et al. Metabolic heterogeneity in human lung tumors. *Cell* **164**, 681–694 (2016).
- Goodwin, J. et al. The distinct metabolic phenotype of lung squamous cell carcinoma defines selective vulnerability to glycolytic inhibition. *Nat. Commun.* **8**, 15503 (2017).
- Mohamed, A., Deng, X., Khuri, F. R. & Owonikoko, T. K. Altered glutamine metabolism and therapeutic opportunities for lung cancer. *Clin. Lung Cancer* **15**, 7–15 (2014).
- Fumarola, C., Bonelli, M. A., Petroni, P. G. & Alfieri, R. R. Targeting PI3K/AKT/mTOR pathway in non small cell lung cancer. *Biochem. Pharmacol.* **90**, 197–207 (2014).
- Makinoshima, H. et al. Epidermal growth factor receptor (EGFR) signaling regulates global metabolic pathways in EGFR-mutated lung adenocarcinoma. *J. Biol. Chem.* **289**, 20813–20823 (2014).
- Brunelli, L., Caiola, E., Marabese, M., Broggin, M. & Pastorelli, R. Capturing the metabolomic diversity of KRAS mutants in non-small-cell lung cancer cells. *Oncotarget* **5**, 4722–4731 (2014).
- Gatto, F., Nookaew, I. & Nielsen, J. Chromosome 3p loss of heterozygosity is associated with a unique metabolic network in clear cell renal carcinoma. *Proc. Natl. Acad. Sci.* **111**, E866–E875 (2014).
- Kanehisa, M. Enzyme annotation and metabolic reconstruction using KEGG. *Methods Mol. Biol.* **1611**, 135–145 (2017).

Acknowledgements

J.C.N. thanks the Royal Society for an International Exchange grant (IE160248). J.C.N. was partially supported by JSPS KAKENHI Grant Number 18K11535. T.A. was partially supported by JSPS KAKENHI Grant Number 18H04113. This research was also supported in part by Research Collaboration Projects of the Institute for Chemical Research, Kyoto University.

Author contributions

J.M.S. and J.C.N. designed the study, performed the analysis and wrote the manuscript. J.M.S., H.O. and J.C.N. analysed the data. T.A. contributed to the theoretical discussion and data analysis interpretation. All authors read and approved the final manuscript.

Additional information

Supplementary Information accompanies this paper at <https://doi.org/10.1038/s41467-019-10616-z>.

Competing interests: The authors declare no competing interests.

Reprints and permission information is available online at <http://npg.nature.com/reprintsandpermissions/>

Peer review information: *Nature Communications* thanks Jürgen Zanghellini and the other anonymous reviewer(s) for their contribution to the peer review of this work. Peer reviewer reports are available.

Publisher's note: Springer Nature remains neutral with regard to jurisdictional claims in published maps and institutional affiliations.



Open Access This article is licensed under a Creative Commons Attribution 4.0 International License, which permits use, sharing, adaptation, distribution and reproduction in any medium or format, as long as you give appropriate credit to the original author(s) and the source, provide a link to the Creative Commons license, and indicate if changes were made. The images or other third party material in this article are included in the article's Creative Commons license, unless indicated otherwise in a credit line to the material. If material is not included in the article's Creative Commons license and your intended use is not permitted by statutory regulation or exceeds the permitted use, you will need to obtain permission directly from the copyright holder. To view a copy of this license, visit <http://creativecommons.org/licenses/by/4.0/>.

© The Author(s) 2019

4. 參考資料

京都大学化学研究所
化学関連分野の深化・連携を基軸とする先端・学際グローバル研究拠点
令和元年度国際共同利用・共同研究公募要領

京都大学化学研究所は、「化学に関する特殊事項の学理及び応用の研究を掌る」ために、化学を中心とする分野で基礎研究に重点を置いた先端研究に邁進してまいりました。平成22～30年度の期間には、文部科学大臣から国立大学共同利用・共同研究拠点としての認定を受け、化学研究所の活性を基盤とする「化学関連分野の深化・連携を基軸とする先端・学際研究拠点」として国内外の化学関連分野の研究者との共同利用・共同研究を推し進めてまいりました。この拠点活動におけるグローバル共同利用・共同研究が評価され、平成30年化学研究所は文部科学省から国際共同利用・共同研究拠点に認定されました。これを受けて、令和元年度からの国際共同利用・共同研究拠点活動においては、多様でグローバルな化学分野の共同研究を一層強力に推進すべく、さらなる事業展開を図っております。

つきましては、化学に関わる分野でご活躍の皆様のご意見・ご要望を尊重しつつ、世界の化学の基礎・応用研究を皆様とともに一層推進することを念頭に置き、下記の要領で令和元年度の拠点共同利用・共同研究の課題公募をさせていただきます。

この公募に当たりましては、分野選択型（計画研究型）、課題提案型、連携・融合促進型および施設・機器利用型の四つに分けて研究課題を募集いたします。これらの課題の実施に際しては当研究所の専任教員または客員教員との共同研究を基調といたしますが、いずれの課題でも後述の共通設備・機器・資料等のご利用が可能です。なお、各課題とも、海外研究者を研究代表者あるいは研究協力者とする国際共同研究（この場合、英語フォームで申請下さい）と、国内研究者を研究代表者とする国内共同研究を実施致します。これらの点も勘案いただき、本公募要領の詳細について十分ご確認の上、期日（平成31年1月31日）までにご申請下さいますようお願いいたします。

京都大学化学研究所長 辻井敬亘
共同研究ステーション長 寺西利治

1. 研究期間

1年間（平成31年4月1日から令和2年3月31日まで）。

2. 研究課題分類

下記のような分類（型）ごとに研究課題を募集いたします。いずれの課題についても、分類ないし分野の担当者もしくは当研究所で対応する共同研究者にご一報の上、ご申請下さい。また、研究経費に関しては、p.3の表をご覧ください。

2-1. 分野選択型（計画研究型）研究課題

分野選択型（計画研究型）研究課題は、あらかじめ設定された分野に関して化学研究所内の研究者と共同で遂行する課題です。令和元年度は下記の5分野について課題を公募いたします。5分野を合わせて、萌芽的な課題と発展的な課題をそれぞれ20件程度、採択の予定です。

ビーム科学分野（担当者：阪部 周二; sakabe@laser.kuicr.kyoto-u.ac.jp）

基本テーマ：先進量子ビームの開発と新奇診断分析手法の創出

趣旨：レーザー、X線、電子線、イオンビームなどの量子ビームの高度化とその先端的診断分析法への応用を進めます。また、これらの量子ビームを複合的に用いて、極微細領域での超高速化学・物理現象の解明を目指します。

元素科学分野（担当者：中村 正治; masaharu@scl.kyoto-u.ac.jp）

基本テーマ：元素科学に基づく物質創製・機能創出

趣旨：元素の新たな特性を引き出し、この特性をもとに優れた機能を有する新物質を創製します。元素と社会との関わりを俯瞰した元素戦略研究も推進します。物質の機能は、構成元素の特性を相乗的に反映して発現します。この発現機構を明らかとし、望みの機能を意のままに創出することを目指します。

バイオ情報学分野（担当者：緒方 博之; ogata@kuicr.kyoto-u.ac.jp）

基本テーマ：バイオ情報を含む複合情報の融合解析

趣旨：ゲノムやメタゲノムに代表される最新バイオ情報に立脚して、バイオ情報がいかに生体内や自然環境における化学現象と関わっているかを明らかにし、生命システムについての化学的理解の深化を図ります。さらに、その成果を応用して、ゲノム創薬やパーソナライズド医療などへの展開も目指します。

物質合成分野（担当者：村田 靖次郎; yasujiro@scl.kyoto-u.ac.jp）

基本テーマ：複合機能材料の戦略的創製

趣旨：異種材料のハイブリッド化・複合化ならびにナノサイズ化に重点を置き、新規な機能をもつ新世代材料の創製を目指すとともに、生体の認識、応答、反応などの諸機能を担う例えば生体膜等も複合機能材料と捉え、機能物質と生命現象の化学的相関の解明も目指します。

現象解析分野（担当者：寺西 利治; teranisi@scl.kyoto-u.ac.jp）

基本テーマ：複合測定に基づく物質解析

趣旨：化学を基盤とする多種の分光学的手法・解析的手法を複合的に駆使して、天然および人工物質の構造・性質を分子レベルから巨視的レベルまで階層的に理解・記述することを目指し、一方、その結果を還元することによって新たな物質科学の枠組みを構築する取り組みも目指します。

2-2. 課題提案型研究課題（担当者：梶 弘典; kaji@scl.kyoto-u.ac.jp）

課題提案型研究課題は、前項 1 で設定した一つの分野に留まらない分野、あるいはそれ以外の分野について、化学関連分野の研究者から自由にご提案いただく課題です。萌芽的な課題と発展的な課題を、それぞれ 20 件程度、採択の予定です。新分野の開拓につながるような課題を特に歓迎いたします。なお、緊急性・重要性が極めて高いと判断した課題については、前記の応募期日にかかわらず、直ちに採択することもあります。

2-3. 連携・融合促進型研究課題（担当者：渡辺 宏; hiroshi@scl.kyoto-u.ac.jp）

連携・融合促進型研究課題は、化学関連分野における国内外の研究連携の強化を主目的とする共同研究課題です。国外も念頭に置く場合は、化学研究所の部局間国際学術交流締結先 (http://www.kuicr.kyoto-u.ac.jp/sites/international_exchange/agreement/ 参照) との共同研究を開始する場を求めていることも可能です。また、この目的に沿った研究集会の開催も本課題として応募いただけます。5 件程度を採択する予定です。

2-4. 施設・機器利用型研究課題（担当者：倉田 博基; kurata@eels.kuicr.kyoto-u.ac.jp）

施設・機器利用型研究課題は、http://www.kuicr.kyoto-u.ac.jp/sites/research_activities/joint_research/kaken_kyodo_instr/ (拠点ホームページ) に記載の共通設備・機器・資料等の利用を主とする共同研究課題です。15 件程度を採択する予定です。

令和元年度国際共同利用・共同研究経費概算値

	経費上限／件 [*] （千円）	
	国際共同研究	国内共同研究
分野選択型萌芽的研究	1,000	800
分野選択型発展的研究	2,000	1,500
課題提案型萌芽的研究	1,000	800
課題提案型発展的研究	2,000	1,500
連携・融合促進型研究	1,000	800
施設・機器利用型研究	1,000	800

^{*}表中の金額は目安です。予算の状況に応じた減額もありえますことをご了解下さい。
経費内での備品費、消耗品費、旅費の配分は、申請者と化学研究所の共同研究者が協議して決定下さい。特に、旅費については、地域性を勘案してご決定下さい。

3. 共同研究応募方法

3-1. 申請資格

国公立大学、国公立研究機関、独立行政法人等の専任研究者、または、これに準ずる者。

3-2. 申請書記入要領

申請に当たっては、該当する募集分類・分野の担当者もしくは当研究所で対応する共同研究者と、事前に研究課題、研究内容、研究経費に関して、必ずご協議下さい。対応する共同研究者は、当研究所の専任教員または令和元年度客員教員からお選び下さい。なお、教員のリストは下記の化学研究所ホームページをご参照下さい。

教員リスト http://www.kuicr.kyoto-u.ac.jp/sites/research_activities/chemist/

また、対応する共同研究者をお決めになれない場合は、各分類・分野の担当者に、まず、ご相談ください。
上記の表の経費上限は目安です。特に、経費内での備品費、消耗品費、旅費の配分については、当研究所で対応する共同研究者と十分にご協議の上で申請下さい。特に、旅費については、地域性を勘案してご申請下さい。

課題申請は、本要領に添付の分野選択型共同利用・共同研究申請書（様式1）、課題提案型共同利用・共同研究申請書（様式2）、連携・融合促進型共同利用・共同研究申請書（様式3）、施設・機器利用型共同利用・共同研究申請書（様式4）に必要事項を記入し、下記の要領で、化学研究所共同研究推進室にご提出下さい。

なお、各課題とも、海外研究者を研究代表者あるいは研究協力者とする国際共同研究も実施可能です。この場合、英語フォーム（Forms 1~4）の左肩の欄にチェックを入れて、ご申請下さい。

<記入上の注意事項>

1. ※を付した事項は当研究所で記入します。
2. 当研究所で対応する共同研究者は必ずご記入下さい。
3. 申請者（研究代表者）と共同研究者の役割分担を明記して下さい。事前に共同研究者の承諾を得ていただくことが必要です。

3-3. 提出期限および提出先

応募に当たっては、前記の申請書にご記入の上、平成31年1月31（木）までに、下記宛に電子メール添付書類（Word書類）としてお送り下さい。

書類提出先および問い合わせ先

京都大学化学研究所共同研究推進室 国際共同利用・共同研究係

E-mail: icr-hub@scl.kyoto-u.ac.jp, 電話: (0774)38-3121

4. 課題選考と採択通知

応募課題の採否は、当研究所の共同研究委員会で審査し、運営評議会の承認を経て決定されます。審査に際しては、共同研究の申請内容だけでなく、予算枠や、共通設備・機器・資料の使用時間等も考慮いたします。採否の結果（内定）については、平成31年3月に当研究所の所長から研究代表者に通知いたします。

5. 研究の実施および研究成果報告

5-1. 研究経費等

研究代表者と当研究所で対応する共同研究者には、予算の範囲内で、研究経費（備品費および消耗品費）と旅費が支給されます。また、研究協力者（学生も含めることが可能です*）にも予算の範囲内で旅費が支給されます。共同研究の実施に当たっては、まず対応する共同研究者にご連絡下さい。なお、当研究所には、共同研究者のための宿泊施設はありません。

* 研究協力者について、学生の場合は原則として大学院生といたします。なお、傷害保険等に参加していることが必要です。

5-2. 研究成果報告

採択された研究課題については、研究成果報告書を次に記す作成要領に従って記載・提出していただきます。その報告書は、まとめて当研究所の国際共同利用・共同研究報告書集として公開させていただく予定です。また、その内容を研究成果報告会でご報告いただくことがあります。なお、報告会についての詳細は、採択課題の研究代表者に後日お知らせいたします。

5-3. 研究成果報告書の作成要領

分野選択型研究、課題提案型研究、施設・機器利用型研究については1頁、連携・融合促進型研究については2頁の報告書を（様式5）を用いて作成下さい。A4版の用紙には1頁あたり1,200字程度が記載できます。図表などカラーを用いても構いませんが、報告書集刊行の際はモノクロ印刷になることもありますので、その点をお含み置き下さい。

1頁の1行目の中央に研究課題名、3行目に右詰めで研究代表者の氏名と所属、5行目から本文を記載して下さい。なお、当研究所で対応した共同研究者は報告書の共著者とはせず、必要に応じて本文中に明記して下さい。また、国際共同研究の場合、報告書は必ず英文でご作成ください。

5-4. 報告書の内容

形式は自由ですが、例えば、実験的研究では、目的、実験方法、実験結果、考察、成果報告（論文、学会発表等）をお書き下さい。なお、連携・融合促進型研究で研究集会を開催した場合には、研究集会のプログラム、参加者名簿（所属機関・部局・職名を明記）、および、作成された場合は要旨集またはプロシーディングスを添付して下さい。

5-5. 報告書の提出

提出締切日は、令和2年2月末日とします。電子ファイル（PDFファイル）を、下記へ電子メール添付書類としてお送り下さい。なお、添付ファイル名は「課題番号+代表者名（姓）」として下さい（例：2019-1 田中.doc、2019-1 田中.pdf）。

報告書提出先

京都大学化学研究所共同研究推進室 国際共同利用・共同研究係

E-mail: icr-hub@scl.kyoto-u.ac.jp, 電話: (0774)38-3121

5-6. 研究成果の公開

学術論文などによる研究成果の公開に際しては、京都大学化学研究所の国際共同利用・共同研究として行われたことを明記して下さい。英文での謝辞例を次に示します。

謝辞例: This work was supported by the International Collaborative Research Program of Institute for Chemical Research, Kyoto University (grant # XXXX).

日本語での謝辞は、この英文表記に準ずるものとして下さい。

化学研究所共同利用・共同研究拠点令和元年度採択課題(応募179件、採択122件)

課題番号	研究代表者	研究代表者所属	化研内 研究協力者	型	選択 分野	実施 状況	国際	課題名(和文・英文)
2019-1	Takeshi Nagashima	Faculty of Science and Engineering, Setsunan University	橋田 昌樹	分野選択型	1	発展的	国際	高輝度テラヘルツ波ハルズによる材料表面への新規機能性付与 Advanced functionality on materials induced by Intense THz pulse irradiation
2019-2	Yasunobu Arikawa	Institute of Laser Engineering, Osaka University	井上 俊介	分野選択型	1	萌芽的	国際	レーザー駆動X線とスピン偏極重水素標的による超高指向性中性子ビームの発生 Ultra directional neutron beam generation by using laser driven x-ray and spin polarized deuterium target
2019-3	Takayuki Saeki	Accelerator division VI, KEK	岩下 芳久	分野選択型	1	発展的	国際	超電導空洞の内面処理による高性能化とコスト削減の研究 Research on the high-performance superconducting cavity and the cost reduction by noble inner-surface processes
2019-4	Koichi Kino	Research Institute for Measurement and Analytical Instrumentation, Advanced Industrial Science and Technology (AIST)	岩下 芳久	分野選択型	1	発展的	国際	リチウムイオン二次電池の電極材内の充放電反応可視化を目的とした、六極磁石によるハルズ中性子透過イメージ拡大の研究 Study on magnification of the pulsed-neutron transmission image using the sextupole magnet, aimed at visualization of charge and discharge in the electrode materials of Li-ion batteries
2019-5	河合 武司	東京理科大学・工学部	倉田 博基	分野選択型	1	発展的		競像体過剰率による金ナノワイヤーのらせん構造制御 Controlling chiral structure of Au nanowires by enantiomeric excess
2019-6	老川 典夫	関西大学・化学生命工学部	藤井 知実	分野選択型	1	発展的		根粒菌由来GraEタンパク質の結晶構造解析 Crystal structure analysis of GraE protein from root-nodule-forming bacterium
2019-7	藤岡 慎介	大阪大学・レーザー科学研究所	井上 俊介	分野選択型	1	萌芽的		マルチピコ秒の相対論的放射圧で駆動される臨界面の超高速度運動の観測 Probing ultrafast motion of critical surface pushed by multi-pico-second relativistic radiation pressure
2019-8	砂原 淳	大阪大学・レーザー科学研究所	井上 俊介	分野選択型	1	発展的		ブリルバリス付与による高変換TNSAイオン加速 Enhanced production of fast ions by TNSA with pre-pulse Laser
2019-9	車場 光博	大阪産業大学・工学部・電子情報通信工学科	橋田 昌樹	分野選択型	1	発展的		レーザー吸収制御によるシリコンの微細加工に関する基礎研究 Fundamental study on micro-fabrication of Si with controlling laser absorption
2019-10	大西 哲哉	理化学研究所・仁科加速器科学研究センター	若杉 昌徳	分野選択型	1	萌芽的		カーボンナノチューブを用いたISOL用標的の開発 Development of new target material using CNT
2019-11	榎園 昭智	理化学研究所・仁科加速器科学研究センター	若杉 昌徳	分野選択型	1	発展的		Rf超前方電子散乱実験のための高速・高感度中性子トリガー検出器の開発 Development of a fast and efficient neutron trigger device for electron-Rf scattering experiments
2019-12	羽島 良一	量子科学技術研究開発機構	岩下 芳久	分野選択型	1	発展的		化学反応の量子制御を目指したCEP安定化自由電子レーザーのための省電力型超伝導加速空洞の製作方法の高度化 Optimization of fabrication process of a superconducting electron accelerating cavity operated by small electricity power for a CEP-stabilized free-electron laser
2019-13	近藤 康太郎	量子科学技術研究開発機構 関西光科学研究所	橋田 昌樹	分野選択型	1	萌芽的		グラファイト化薄膜テープ標的を用いたレーザー駆動イオン加速実験 Laser driven ion acceleration experiment using carbonized thin tape target
2019-14	Wei-Tin Chen	Center for Condensed Matter Sciences, National Taiwan University	島川 祐一	分野選択型	2	発展的	国際	High pressure approach to the synthesis of novel ferroelectric photovoltaic transition metal oxides
2019-15	Haichuan Guo	Ningbo Institute of Industrial Technology (GNITECH) of the Chinese Academy of Sciences	島川 祐一	分野選択型	2	萌芽的	国際	遷移金属酸化物における触媒性能研究 Catalysis research of transition metal oxides
2019-16	Rainer Streubel	Institute for Inorganic Chemistry, University of Bonn	時任 宣博	分野選択型	2	発展的	国際	「新規なアニオン性FLPを用いた小分子活性化」 “Small molecule activation using anionic crypto-FLPs”

2019-17	Takeaki Iwamoto	Department of Chemistry, Tohoku University	時任 宣博	分野選択型	2	発展的	国際	非対称型高周期典型元素 π 電子系の開拓と物性解明 Development of unsymmetrical π -electron systems of heavier main group elements and elucidation of their property
2019-18	Naohiko Yoshikai	Division of Chemistry and Biological Chemistry, School of Physical and Mathematical Sciences, Nanyang Technological University	中村 正治	分野選択型	2	発展的	国際	3d 金属触媒によるC-H 結合変換反応の反応機構研究 Mechanistic studies of C-H bond functionalization reactions catalyzed by 3d transition metals
2019-19	Alakananda Hajra	Department of Chemistry, Visva-Bharati University	中村 正治	分野選択型	2	萌芽的	国際	Development of iron-catalyzed strategies for diversity oriented synthesis of heterocycles and carbocycles
2019-20	Shingo Ito	School of Physical and Mathematical Sciences, Nanyang Technological University	中村 正治	分野選択型	2	萌芽的	国際	ヘテロビシクロアルケンの鉄触媒カルボメタリル化: 不斉反応の開発と多環芳香族炭化水素合成への応用 Iron-catalyzed carbometallation of heterobicyclic alkenes: development of asymmetric reactions and application to synthesis of polycyclic aromatic hydrocarbons
2019-21	Shih-Ching Chuang	Department of Applied Chemistry, National Chiao Tung University	村田 靖次郎	分野選択型	2	萌芽的	国際	高分子太陽電池応用のための n 型複合材料としての水素を組み込んだ開放かご型フラーレン Open-cage fullerenes incorporating hydrogen as n-type composite materials for polymer solar cell applications
2019-22	板谷 治郎	東京大学・物性研究所	金光 義彦	分野選択型	2	萌芽的		中赤外線レーザー光源の開発とナノ物質科学への応用 Development of mid-infrared laser and applications to nano-material sciences
2019-23	立津 慶幸	名桜大学・リバラルアーツ機構	寺西 利治	分野選択型	2	萌芽的		微量In 元素添加型新奇Fe-Pd 相の安定機構に関する研究 Study on the mechanism for the stability of an In-doped novel Fe-Pd phase
2019-24	橘 洋一	京都市産業技術研究所 高分子系チーム	中村 正治	分野選択型	2	萌芽的		ウルシオール金属錯体を構成要素とする新規機能性塗料の開発 Development of the novel functional paint using metallic urushiol complexes
2019-25	山口 佳隆	横浜国立大学・大学院工学研究院	中村 正治	分野選択型	2	発展的		モノアニオン性3座ピンサー型配位子を有するニッケラート錯体の研究 Study on nickelate complexes constructed by a monoanionic tridentate pincer-type ligand
2019-26	中村 泰之	物質・材料研究機構・統合型材料開発・情報基盤部門	山子 茂	分野選択型	2	発展的		アクリロニトリル系ポリマー末端ラジカルの反応機構研究とその合成応用 Mechanistic and synthetic studies of poly((meth)acrylonitrile) chain end radicals
2019-27	笹森 貴裕	名古屋市立大学・大学院システム自然科学研究科	若宮 淳志	分野選択型	2	発展的		高性能ペロブスカイト太陽電池作成を指向した高活性酸化スカベンジャーの開発 Creation of effective oxidation scavenger for efficient perovskite-based solar cells
2019-28	小川 佳宏	上越教育大学・学校教育研究科	金光 義彦	分野選択型	2	萌芽的		ヘテロダイナミクス分光法を用いた鉛ペロブスカイト太陽電池の光電流の研究 Photocurrent of Pb perovskite solar cells by heterodyne interference spectroscopy
2019-29	Samuel Chaffron	CNRS UMR6004	Blanc-Mathia	分野選択型	3	萌芽的	国際	微生物生態学におけるデータ駆動型探索と仮説検証のためのネットワーク解析の利用 Network analyses for data-driven exploration and hypothesis testing in microbial ecology
2019-30	Nigel Grimsley	Sorbonne University	遠藤 寿	分野選択型	3	萌芽的	国際	全球海洋におけるプラシノウィルスの分布および宿主予測に関する研究 Distribution of prasinoviruses and their association with natural hosts in the global ocean
2019-31	Jiim-Moon Yang	Department of Biological Science and Technology/ Institute of Bioinformatics & Systems Biology, National Chiao Tung University	阿久津 達也	分野選択型	3	発展的	国際	深層学習を用いたオミクスデータとモジュールに基づくネットワークデータの統合解析による腫瘍細胞分類 Integrating omics data and module-based network with deep learning to develop cancer type predictive models
2019-32	Jiangning Song	Biomedicine Discovery Institute, Monash University	阿久津 達也	分野選択型	3	発展的	国際	タンパク質分解酵素による切断部位の高精度予測のための次世代ハイオインフォマティクス技術 Next-generation bioinformatics approaches for the accurate identification of protease-specific substrate cleavage sites
2019-33	長崎 慶三	高知大学・農林海洋科学部	遠藤 寿	分野選択型	3	萌芽的		赤潮顕発性閉鎖海域の微生物生態系にウイルスが及ぼす影響の解明 Viral impacts on microbial ecosystems in the highly-enclosed inlet, Uranouchi Bay, Kochi

2019-34	武村 政春	東京理科大学・理学部	緒方 博之	分野選択型	3 萌芽的	新規巨大ウイルスの単離とゲノム・トランスクリプトーム解析 Isolation of new giant viruses and their genomic and transcriptomic characterization
2019-35	吉田 天士	京都大学・大学院農学研究科・応用生物科学専攻	緒方 博之	分野選択型	3 萌芽的	環境サンプルからの赤潮藻類の濃縮とその藻類に感染するウイルスの同定 Concentration of bloom forming algae from environmental samples and identification of the viruses infecting the alga
2019-36	志賀 元紀	岐阜大学・工学部・電気電子・情報工学科	馬見塚 拓	分野選択型	3 萌芽的	生物ネットワーク構造の局所構造変化の網羅的解析 Exhaustive analysis of local structural changes of biological networks
2019-37	茅野 光範	帯広畜産大学・グローバルアグリメディシン研究センター	馬見塚 拓	分野選択型	3 発展的	分子ネットワーク解析のための統計的機械学習法の開発と応用 Statistical machine learning methods for molecular network analysis
2019-38	ホセ ナサエル	東邦大学・理学部・情報科学科	阿久津 達也	分野選択型	3 萌芽的	最小支配集合による複雑ネットワークの制御と解析 Control and analysis of complex networks via minimum dominating sets
2019-39	Davor Margetic	Division of organic chemistry and biochemistry, Laboratory for physical organic chemistry	村田 靖次郎	分野選択型	4 萌芽的	s-トラジンを利用したフラレーレンのグアジニン官能基化 Application of s-tetrazines in guanidine functionalization of fullerenes
2019-40	Akimitsu Narita	Max Planck Institute for Polymer Research	廣瀬 崇至	分野選択型	4 発展的	平面π系と湾曲π系の組み合わせによる新規機能性材料の創出 Coupling of planar and curved π-systems for the development of novel functional materials
2019-41	Akinori Saeki	Department of Applied Chemistry, Graduate School of Engineering, Osaka University	若宮 淳志	分野選択型	4 発展的	非鉛ペロブスカイトに特化した電荷輸送材料の設計・合成・評価 Design, synthesis, and characterization of charge transport materials for non-lead perovskite
2019-42	尾坂 格	広島大学・大学院工学研究科	脇岡 正幸	分野選択型	4 発展的	新規π共役系ポリマーの開発と有機薄膜太陽電池への応用 Development of novel π-conjugated polymers and their application to organic photovoltaics
2019-43	平井 智康	大阪工業大学・応用化学科	竹中 幹人	分野選択型	4 萌芽的	分岐型立体規則性ブロック共重合体の合成とその分子鎖凝集構造解析 Preparation of novel branched block copolymer with well-controlled stereoregularity and evaluation of its molecular aggregation state
2019-44	赤木 和夫	立命館大学・総合科学技術研究機構	辻井 敬亘	分野選択型	4 萌芽的	キラルメタリック液晶のアンカリング挙動に関する研究 Study of anchoring behavior of chiral nematic liquid crystal
2019-45	鈴木 充朗	大阪大学・工学研究科	村田 靖次郎	分野選択型	4 発展的	薄膜構造制御を志向した有機半導体の分子エンジニアリング:熱前駆体法によるアプローチ Molecular engineering of organic semiconductors toward the control of molecular packing in thin films via a thermal precursor approach
2019-46	清水 章弘	大阪大学・大学院基礎工学研究科	廣瀬 崇至	分野選択型	4 発展的	電子ドナー性アニオンと電子アクセプター性カチオンを連結したπ共役双性イオンの合成と物性 Synthesis and properties of π-conjugated zwitterions composed of an electron-donating anion and an electron-accepting cation
2019-47	Tung-Yuan Ho	Research Center for Environmental Changes, Academia Sinica	宗林 由樹	分野選択型	5 発展的	亜寒帯太平洋における粒子状態微量金属の元素・同位体組成:起源と内部循環 The elemental and isotopic composition of particulate trace metals in the subarctic Pacific Ocean: sources and internal cycling
2019-48	Gurumurthy Gundiga Puttoji Rao	Geochemistry Research lab, Birbal Sahni Institute of Palaeosciences	宗林 由樹	分野選択型	5 萌芽的	後期中新世アラビア海の環境推定への $\delta^{38/36}\text{Mo}$ および $\delta^{182/184}\text{W}$ 同位体比の応用 Application of $\delta^{38/36}\text{Mo}$ and $\delta^{182/184}\text{W}$ isotopes ratios for the reconstruction of late miocene oxygenation in the Arabian sea
2019-49	Abderrazzak Douhal A	Physical Chemistry, University of Castilla-La Mancha (UCLM, Spain)	坂本 雅典	分野選択型	5 萌芽的	ヘビードープ半導体ナノ粒子における熱キャリアの緩和過程の調査 Investigation on the decay process of hot carriers in heavily doped semiconductor nanocrystals
2019-50	Yasuhiro Tachibana	School of Engineering, RMIT University	寺西 利治	分野選択型	5 発展的	キャリアダイナミクスと構造の定量的解析による光触媒材料の開発 Development of photocatalytic materials by quantitative charge carrier dynamics and structural analysis
2019-51	Sathish K. Sukumaran	Graduate School of Organic Materials Science, Yamagata University	渡辺 宏	分野選択型	5 発展的	高分子液体の高周波シオロジ—および誘電応答 High frequency rheological and dielectric response of polymeric liquids

2019-52	Quan Chen	Changchun Institute of Applied Chemistry, Chinese Academy of Sciences (CAS)	松宮 由美	分野選択型	5	萌芽的	国際	テレレリック型イオマーの伸長レオロジー Elongational rheology of telechelic-type ionomers
2019-53	中口 謙	近畿大学・理工学部	宗林 由樹	分野選択型	5	発展的		都市大気エアロゾルの起源および発生メカニズム解明に関する研究 Study on the origin and generation mechanism of urban atmospheric aerosol
2019-54	向井 浩	京都教育大学・教育学部理学科	宗林 由樹	分野選択型	5	萌芽的		イオン液体を液膜とした金属イオンの液膜輸送と分離に関する研究 Study on transportation and separation of metal ions through a liquid membrane using ionic liquid
2019-55	大坂 景	岡山理科大学・大学院理学研究科	竹中 幹人	分野選択型	5	萌芽的		高分子オレオゲルのゲル化機構の解明 Study on gelation behaviors of polymer oleogels
2019-56	玉井 尚登	関西学院大学・理工学部	坂本 雅典	分野選択型	5	萌芽的		機能性配位子保護量子ドットの緩和過程の解明 Investigation on the carrier relaxation processes of quantum dots protected with functional organic molecules
2019-57	圓山 正史	群馬大学・大学院理工学部	長谷川 健	分野選択型	5	発展的		新規部分フッ素化リン脂質分子群の膜物性・構造のキャラクタリゼーション Characterization of physical properties and structure of partially fluorinated phospholipid membrane
2019-58	野呂 篤史	名古屋大学・大学院工学研究科	渡辺 宏	分野選択型	5	萌芽的		スチレン系ブロック共重合体をベースとした非共有結合性エラストマーの調製と力学特性 Preparation and mechanical properties of noncovalent bonded elastomers based on styrenic block copolymers
2019-59	Li-Jia Qu	School of Life Sciences, Peking University	青山 卓史	課題提案型		発展的	国際	植物細胞形態形成における遺伝子発現制御ネットワーク Regulatory network of gene expression for plant cell morphogenesis
2019-60	Yohei Ohashi	MRC Laboratory of Molecular Biology, University of Cambridge	青山 卓史	課題提案型		萌芽的	国際	植物細胞内の膜交通におけるPX-PHタイプホスホリバーゼDの役割 Role of PX-PH-type phospholipase Ds in plant intracellular membrane traffic
2019-61	Liu Zhou	School of Pharmacy, Fudan University	上杉 志成	課題提案型		発展的	国際	小分子化合物による選択的タンパク質アセチル化 Site-selective protein acetylation by a small molecule
2019-62	Xiaoguang Lei	College of Chemistry and Molecular Engineering, Peking University	上杉 志成	課題提案型		萌芽的	国際	プロテオーム解析による胆汁酸結合酵素の阻害剤探索 Proteomic approach to discovering specific inhibitors for bile-acid interacting enzymes
2019-63	Kab-Jin Kim	Department of Physics, Korea Advanced Institute of Science and Technology	小野 輝男	課題提案型		発展的	国際	フェリ磁性体でのマグノン特性研究 Study of magnonic properties of ferrimagnets
2019-64	Dongdong Zhang	Department of Chemistry, Tsinghua University	梶 弘典	課題提案型		発展的	国際	Development of highly efficient and stable blue organic light emitting diodes using thermally activated delayed fluorescent materials as sensitizer
2019-65	Jang Hyuk Kwon	Department of Information Display, Kyung Hee University	梶 弘典	課題提案型		発展的	国際	Highly efficient blue thermally activated delayed fluorescence emitters using sterically hindered donor skeleton
2019-66	小林 武史	Ames National Laboratory, U.S. Department of Energy	梶 弘典	課題提案型		発展的	国際	固体効果による動的核分極NMRを用いた有機デバイス非晶膜の局所構造解析 Structural analysis of organic amorphous thin films using solid effect dynamic nuclear polarization NMR
2019-67	Thomas Wirth	School of Chemistry, Cardiff University	川端 猛夫	課題提案型		発展的	国際	フローケミストリーを用いる不斉記憶型反応 Memory of chirality using flow electrochemistry
2019-68	Jonathan Clayden	School of Chemistry, University of Bristol	川端 猛夫	課題提案型		発展的	国際	水素結合ネットワークに基づく機能性分子の創製 Creation of functional molecules based on hydrogen bond networks

2019-69	Torranin Chairuangsrri	Industrial Chemistry, Chiang Mai University	倉田 博基	課題提案型	萌芽的	国際	Micro- and nano-structural characterization by advanced transmission electron microscopy of novel functional materials for battery development
2019-70	Maria Michela Corsaro	Department of Chemical Sciences, University of Naples Federico II	栗原 達夫	課題提案型	発展的	国際	細菌外膜小胞表面成分の構造機能解析
2019-71	Xianzhu Dai	College of Resources and Environment, Southwest University	栗原 達夫	課題提案型	萌芽的	国際	Structural and functional analysis of the surface components of bacterial outer membrane vesicles
2019-72	Kensuke Homma	Physics, Hiroshima University	阪部 周二	課題提案型	発展的	国際	低温適応微生物を用いたタンパク質低温発現システムの構築
2019-73	Ying Ma	Department of Chemistry and Chemical Engineering, South China University of Technology	大野 工司	課題提案型	発展的	国際	Construction of low-temperature protein expression system by using cold-adapted microorganisms
2019-74	Robert C. Ferrier, Jr.	Chemical Engineering and Materials Science, Michigan State University	大野 工司	課題提案型	発展的	国際	宇宙暗黒成分解明へ向けた真空内四光波混合の探索
2019-75	Vincent Ladmiral	University of Montpellier	大野 工司	課題提案型	発展的	国際	Search for four-wave-mixing in the vacuum - Unveiling dark components in the Universe -
2019-76	Chengshan Wang	Middle Tennessee State University	長谷川 健	課題提案型	萌芽的	国際	刺激応答性ポリマーブラシと電気化学解析を駆使したバイオセンサーの開発
2019-77	Tim Stasevich	Dept. of Biochemistry and Molecular Biology, Colorado State University	今西 未来	課題提案型	発展的	国際	Development of biosensors by combining stimuli-responsive polymer brushes with electrochemical analysis
2019-78	Anne S. Ulrich	Institute of Organic Chemistry (IOC) and Institute of Biological Interfaces (IBG-2), Karlsruhe Institute of Technology (KIT)	二木 史朗	課題提案型	発展的	国際	リチウムイオン電池の性能向上に向けたポリエーテル系ナノコンポジット電解質の開発
2019-79	Marcus W. Doherty	Research School of Physics and Engineering, Australian National University	水落 憲和	課題提案型	発展的	国際	Exploring new polyether nanocomposite electrolytes to enhance energy storage of lithium ion batteries
2019-80	Gopalakrishnan Balasubramanian	Max-Planck Institute for Biophysical Chemistry, Göttingen, Germany, Max-Planck Independent Research	水落 憲和	課題提案型	発展的	国際	Fluorinated polymer-brush-grafted nanoparticles: Precise synthesis and applications to membrane technology
2019-81	Youngdon Kwon	School of Chemical Engineering, Sungkyunkwan University (Korea)	松宮 由実	課題提案型	萌芽的	国際	Determine the three-dimensional structure of ¹³ C labeled α -synuclein(61-95) in the Langmuir-Blodgett film and supported phospholipids bilayers by p-MAIRS FT-IR
2019-82	雷永 るみ	広島大学 生物圏科学研究科	青山 卓史	課題提案型	萌芽的		Real-time imaging of single-molecule mRNA with different methylation states
2019-83	伊藤 昭博	東京薬科大学・生命科学部	上杉 志成	課題提案型	発展的		曲率誘導ペプチドの構造活性相関
2019-84	長澤 和夫	東京農工大学・工学部・生命工学科	上杉 志成	課題提案型	発展的		Structural and functional analysis of curvature-inducing peptides
2019-85	田中 雅章	名古屋工業大学・物理工学科	小野 輝男	課題提案型	萌芽的		ダイアモンド多量子ビット量子プロセッサの研究
							Research of multi-qubit diamond quantum processors
							表面近傍のNV 中心の研究
							Research on shallow NV center in diamond
							末端会合/解離平衡下におけるA型高分子鎖の誘電緩和に対する双極子配置の効果
							Effect of dipole alignment along chain backbone on dielectric relaxation of type-A polymers at association/dissociation equilibrium
							植物表皮細胞の分化における制御ネットワークの研究
							Study on the regulatory network of plant epidermal cell differentiation
							アンリド・ハミンの新機能
							New cellular functions of acylodopamine
							ビタミンDの新機能の調節
							Modulation of new cellular functions of vitamin D
							高スピン偏極電流源の開発のためのコバルトフェライト薄膜の磁気・電気的性質の評価
							Investigation of magnetic and electric properties of cobalt ferrite films for development of high spin-polarized current source

2019-88	長浜 太郎	北海道大学 工学研究院	小野 翔男	課題提案型	発展的	ワイル半金属Mn ₃ Sn エピタキシャル薄膜の開発 Develop of the epitaxial thin film of Weyl semimetal Mn ₃ Sn
2019-87	山田 啓介	岐阜大学 工学部・化学・生命工学科	小野 翔男	課題提案型	発展的	ゾル・ゲル法により作製した多結晶Bi-YIG薄膜の微細構造と損失定数の相関説明 Effect of microstructure on damping constant in polycrystalline Bi-YIG thin films prepared by sol-gel method
2019-88	松本 貴裕	名古屋大学 工学部 芸術工学研究科	金光 義彦	課題提案型	萌芽的	ナノ結晶シリコン表面に終端した重水素元素が有する巨大同位体効果の分光学的解明とその応用 Giant isotope effects of deuterium atoms terminating on nanocrystalline silicon and their use
2019-89	山中 正浩	立教大学 理学部 化学科	川端 猛夫	課題提案型	発展的	4-ピロリジン-ピリジン型分子触媒による化学選択的アシル化反応の理論的解析 Theoretical study on chemoselective acylation catalyzed by 4-pyrrolidinopyridine derivatives
2019-90	永澤 秀子	岐阜薬科大学 薬学部	川端 猛夫	課題提案型	萌芽的	α -フッ素化アミノ酸を含む抗腫瘍性環状オクタデセンペプチドの合成と生物学的評価 Synthesis and biological evaluation of antitumor cyclic octadecapeptide containing α -fluorinated amino acid
2019-91	吉村 智之	金沢大学 医薬保健学域薬学系 機能性分子合成学	川端 猛夫	課題提案型	萌芽的	Gonytolide 類の全合成研究 Studies on total synthesis of gonytolides
2019-92	倉田 淳志	近畿大学 農学部 応用生命化学科	栗原 達夫	課題提案型	発展的	腸内細菌および発酵食品由来細菌が生産する膜小胞の生理機能解析と応用 Analysis of the physiological functions of membrane vesicles produced by intestinal bacteria and fermented food-derived bacteria and their application
2019-93	大森 勇門	大阪工業大学 工学部 生命工学科	栗原 達夫	課題提案型	萌芽的	Geobacillus kaustophilusにおける2種類のアラニン脱水素酵素の生理的意義の解析 Studies on the physiological significance of two alanine dehydrogenases in Geobacillus kaustophilus
2019-94	齊藤 高志	高エネルギー加速器研究機構 物質構造科学研究所	島川 祐一	課題提案型	萌芽的	異常高原子価イオンを含む機能性酸化物合成とその構造物性研究 Synthesis and study of oxides with unusually high-valent cation
2019-95	倉橋 健介	大阪府立大学 工業高等専門学校	宗林 由樹	課題提案型	萌芽的	溶媒含浸樹脂を用いた白金族元素抽出における界面活性剤の利用 Application of surfactant for extraction of platinum group elements using solvent impregnated resin
2019-96	内田 幸明	大阪大学 大学院基礎工学研究科	大野 工司	課題提案型	発展的	ポリマーブラシ付与強磁性ナブレートの精密合成による強磁性フォトニック液晶の実現 Fine synthesis of polymer brush on ferromagnetic nano-platelet for ferromagnetic photonic LC
2019-97	村瀬 浩貴	共立女子大学 家政学部被服学科	辻井 敬亘	課題提案型	萌芽的	Additive Manufacturing による多孔性高分子複合材料の3次元構造制御 Manipulation of three dimensional structure of porous polymer composites controlled by additive manufacturing
2019-98	重島 豊	東京工業大学 フロンティア材料研究所	寺西 利治	課題提案型	発展的	強磁性単電子トランジスタ Ferromagnetic single-electron transistor
2019-99	山田 哲弘	千葉大学 教育学部	長谷川 健	課題提案型	萌芽的	パーフルオロアルキル鎖とアミノ酸頭部基を有する新規な界面活性性リ型防錆剤の探索 Investigation of new anti-lust surfactant containing a perfluoro-alkyl chain and an amino acid head group
2019-100	野村 歩	東京医科歯科大学 生体材料工学研究科	二木 史朗	課題提案型	発展的	NanoBRET 型CXCR4 結合解析によるペプチドリガンド評価系の構築 Development of NanoBRET-based screening system for peptidic CXCR4 ligands
2019-101	大橋 若奈	富山大学 大学院医学薬学研究部	二木 史朗	課題提案型	発展的	がん深部到達型修飾透過ペプチドの創出と太陽がん幹細胞効率的除去への展開 Establishment of cell penetrating peptide (CPP)-based delivery system into resident cancer stem cells in deep cancer tissue
2019-102	徳田 親夫	金沢大学 ナノマテリアル研究所	水落 憲和	課題提案型	発展的	ダイヤモンド表面近傍のNV 中心作製 Manufacture of shallow NV centers in diamond

2019-103	牧野 俊晴	産業技術総合研究所 先進パワーエレクトロニクス研究センター	水落 憲和	課題提案型	発展的	ダイヤモンド中のNV 中心量子ビットの電氣的制御と電氣的検出 Electrical control and detection of qubit of NV center
2019-104	藤塚 守	大阪大学・産業科学研究所	山子 茂	課題提案型	萌芽的	シクロパラフェニレンの励起ダイミクスの環サイズ依存性 Ring-size-dependent excitation dynamics of cycloparaphenylenes
2019-105	井上 正志	大阪大学・大学院理学研究科	松宮 由実	課題提案型	萌芽的	半屈曲性高分子溶液の非線形レオロジー Nonlinear rheology of semiflexible polymer solutions
2019-106	島田 良子	日本女子大学・理学部・数物科学科	渡辺 宏	課題提案型	萌芽的	分子スケールの温度勾配下におけるDNAの Soret 効果の解析 Analysis of Soret effect for DNA in molecular-scale temperature gradient
2019-107	Maya K. Endoh	Department of Material Science and Chemical Engineering, Stony Brook University	竹中 幹人	連携・融合促進型	国際	殺菌性を有する高分子ナノ表面設計 Fabrication of nanotopographical polymer surfaces with bactericidal properties
2019-108	Jye-Shane Yang	Department of Chemistry, National Taiwan University	山子 茂	連携・融合促進型	国際	Synthesis of structurally controlled polymers having green fluorescence protein chromophore and their photophysical properties in solution
2019-109	Shunsuke Chiba	School of Physical and Mathematical Sciences, Division of Chemistry and Biological Chemistry, Nanyang Technological University	山子 茂	連携・融合促進型	国際	Vinyl azides as new monomers of radical polymerization for the fabrication of green polymers having chemically- and biodegradable properties
2019-110	Tadashi Inoue	Department of Macromolecular Science, Osaka University	松宮 由実	連携・融合促進型	国際	東アジア圏の若手レオロジストのための第15回ワークショップ The 15th International workshop for East Asian Young Rheologists
2019-111	濱島 義隆	静岡県立大学・薬学部	川端 猛夫	連携・融合促進型		第8回日本-中国有機化学シンポジウム The 8th Japanese-Sino Symposium on Organic Chemistry for Young Scientists
2019-112	松野 丈夫	大阪大学・大学院理学研究科	菅 大介	連携・融合促進型		第26回酸化物エレクトロニクスに関する国際会議 26th International workshop on oxide electronics
2019-113	Juan Qiao	Department of Chemistry, Tsinghua University	堀 弘典	施設・機器利用型	国際	Atomic level analysis and fabrication of highly stable perovskite films and light emitting diodes
2019-114	J. Paul Attfield	Centre for Science at Extreme Conditions and School of Chemistry, University of Edinburgh	島川 祐一	施設・機器利用型	国際	High-pressure synthesis of potential multiferroic oxides
2019-115	Mao Minoura	College of Science, Department of Chemistry, Rikkyo University	時任 宣博	施設・機器利用型	国際	新規有機セレンおよびテルル化合物の合成と性質解明 Synthesis and characterization of novel organoselenium and -tellurium compounds
2019-116	宮本 光貴	島根大学・総合理工学部	倉田 博基	施設・機器利用型		核融合プラズマ対向材中の水素・ヘリウム挙動に関する電子分光学的研究 Nano-electron spectroscopic study on hydrogen and helium behavior in plasma facing materials for nuclear fusion devices
2019-117	斉藤 光	九州大学・大学院総合理工学研究科	倉田 博基	施設・機器利用型		プラズマモニタリング結晶上のプラズマモン-エキシトン結合 Plasmon-exciton coupling on a plasmonic crystal
2019-118	高橋 まさえ	東北大学・大学院農学研究科	時任 宣博	施設・機器利用型		完璧な π 共役二次元シートを持つフラットシリセンの設計 Design of flat silicene with perfect pair-conjugate 2D sheet
2019-119	長岡 紀嘉	福岡大学・理学部化学科	時任 宣博	施設・機器利用型		カルコゲン/シリウム部位を含むアセン型分子の合成と構造解析 Synthesis and structures of acene molecules bearing chalcogenopyrylium units

2019-120	松尾 司	近畿大学・理工学部	時任 宣博	施設・機器利用型		高周期14族元素二価化学種の合成と分子構造の解明 Synthesis and structural characterization of divalent species of heavier group 14 elements
2019-121	吾郷 友宏	茨城大学・工学部・物質科学工学科	時任 宣博 水畑 吉行	施設・機器利用型		単結晶X線構造解析を用いた、含フッ素共役分子の結晶構造におけるフルオラス相互作用の解明 Elucidation of the fluorocyclic interactions in the crystal structures of fluorine-containing conjugated molecules by the single-crystal X-ray structural analysis
2019-122	秦野 修	奈良県立医科大学・医学部	磯崎 勝弘	施設・機器利用型		生体組織由来のカルボニル化合物を標的とする高感度質量分析イメージング解析 High sensitive imaging mass spectrometry targeting the carbonyl compounds derived from biological tissues

